

QUALITATIVE ANALYSIS OF FLOW PATTERNS: TWO-PHASE FLOW CONDENSATION AT LOW MASS FLUXES AND DIFFERENT INCLINATION ANGLES

by

Rainah Kombo

Submitted in partial fulfilment of the requirements for the degree

MASTER OF APPLIED SCIENCE

Department of Mechanical and Aeronautical Engineering

University of Pretoria

2016

Supervisor: Prof J. P. Meyer



To God be the glory, for the things he has done

His love endures forever

&

To my family

Abstract

Title: Qualitative analysis of flow patterns: Two-phase flow condensation at low mass fluxes and different inclination angles

Supervisor: Prof. J.P. Meyer

Department: Mechanical and Aeronautical Engineering

Degree: Master of Applied Science

A great deal of work has been conducted on in-tube condensation in horizontal and vertical smooth tubes. The available literature points to mechanisms governing two-phase condensation heat transfer coefficients and pressure drops, which are directly linked to the local flow pattern for both horizontal and inclined configurations. However, the work has been limited to flow pattern observations, heat transfer, pressure drops and void fractions for both horizontal and inclined tubes at high mass fluxes. No work has been conducted on the analysis of the observed flow patterns and the effect of temperature difference between the average wall temperature and average saturation temperature for different inclination angles at mass fluxes of $100 \text{ kg/m}^2\cdot\text{s}$ and below. The purpose of this study is to carry out a qualitative analysis of flow patterns, and show the effect of temperature difference on the heat transfer coefficient for inclination angles from $+90^\circ$ (upward flow) to -90° (downward flow) at mass fluxes below $100 \text{ kg/m}^2\cdot\text{s}$. An experimental set-up provided the measurements for the two-phase condensation of R-143a in a smooth tube with an inside diameter of 8.38 mm and a length of 1.5 m. The mass fluxes were $25 \text{ kg/m}^2\cdot\text{s}$ to $100 \text{ kg/m}^2\cdot\text{s}$, the saturation temperature was 40°C and the mean qualities were 0.1 to 0.9. A high-speed camera was used to visually analyse and determine the flow patterns for both the inlet and the outlet of the test section. Through the results, eight flow patterns were observed: stratified-wavy, stratified, wavy, wavy-churn, intermittent, churn, annular and wavy-annular. The maximum heat transfer was observed for downward flow between inclination angles of -15° and -30° . The Thome-Hajal flow pattern map correctly predicted horizontal flow patterns, but failed to predict most of the inclined flow patterns. Various flow pattern transitions were identified and proposed for all the investigated inclination angles in this study. Finally, the heat transfer coefficient was found to be dependent on quality, mass flux, temperature difference and inclination angle.

Key words: *Two-phase flow, condensation, flow pattern, inclination, heat transfer coefficient, smooth tube, low mass flux.*

Acknowledgements

- Prof J.P. Meyer: I am grateful to my supervisor for his patient supervision and guidance throughout the experimental and write-up phases of my dissertation and for offering great expertise, knowledge and wisdom;
- Daniel Ekyes Ewim a PhD student: I am grateful for his day to day assistance and guidance with running the experimental test bench, and with setting up and conducting the experimental work;
- Charles Moon, Danie Gouws, Koos Mtombeni and Tersia Evans: I am grateful to the technical and administrative support team. I extend my appreciation to them for their assistance particularly regarding the lab work, the experimental work and the administrative work;
- Westplex Pvt (Ltd) and staff (Michael Westwood, Peter Westwood, Khotso Majoe and Charmaine Wecke): I am grateful to this team of people for their support through the donation of two 601f Basler cameras for my experimental set-up as well as for the other technical assistance they offered throughout the course of the experimental set-up and the running of the experiments;
- I offer my heartfelt thanks to my family. In particular, I thank my sister Lindiwe Chibanda for assisting me tremendously with my work by being there whenever I needed physical, emotional, spiritual or psychological assistance;
- I thank my friends who offered emotional support, Jaqueline Mtungwazi, Spiwe Muchemedzi, Pastor Hendrick Motsoeneng, Nelly Dhladhla, and Ruth Nyamambi (nee Makuchete);
- I would like to extend special thanks to Rudolf Bester for assisting me intellectually and financially when I was in need and also to Marilize Everts who has always been a source of inspiration and encouragement;
- Finally, I would like to extend a special word of thanks to my pastor Dr Thomas Swift for his emotional and spiritual support.



Table of contents

Abstract	ii
Acknowledgements	iii
Table of contents	iv
List of figures	viii
List of tables	xiii
Nomenclature	xiv
1. Introduction	1
1.1. Background.....	1
1.1.1. Two-phase flow analytical tools.....	2
1.1.2. The work of the Thome research group	3
1.1.3. The work of the Meyer research group	3
1.2. Gaps in literature and problem statement	4
1.3. Purpose.....	5
1.3.1. Aim	5
1.3.2. Objectives.....	5
1.3.3. Scope	6
1.4. Structure of the dissertation	6
2. Literature review	8
2.1. Introduction.....	8
2.2. Non-dimensional parameters and other two-phase flow terminologies	8
2.2.1. Reynolds number (Re).....	8
2.2.2. Prandtl number (Pr)	8
2.2.3. Nusselt number (Nu)	9
2.2.4. Two-phase flow terminology	9
2.2.4.1 Quality (x).....	9
2.2.4.2 Void fraction (ϵ)	10
2.2.4.3 Mass flux (G)	10
2.3. Condensation	10
2.3.1. Gravity-driven two-phase flow condensation.....	11
2.4. Flow patterns	11
2.4.1. Annular flow pattern	12
2.4.2. Mist flow pattern.....	12
2.4.3. Wavy flow pattern.....	13
2.4.4. Stratified flow pattern.....	13
2.4.5. Intermittent flow pattern.....	13
2.4.5.1 Slug flow	13
2.4.5.2 Plug flow.....	14
2.4.6. Dispersed to bubbly flow pattern	14
2.4.7. Churn flow pattern	14
2.5. Two-phase flow pattern maps, transitions and heat transfer correlations.....	15
2.5.1. Soliman flow pattern map.....	16
2.5.2. Hajal-Thome-Cavallini condensation flow pattern map	16
2.5.3. Flow pattern transitions.....	17



2.5.4.	The Thome-Hajal-Cavallini flow pattern-based heat transfer model	19
2.5.5.	Other heat transfer coefficient models	21
2.6.	Previous work on two-phase flow condensation.....	21
2.6.1.	Condensing two-phase flow patterns at low mass flux in horizontal tubes.....	22
2.6.2.	Condensing flow patterns at high mass fluxes at different inclinations.....	23
2.6.3.	Condensing two-phase flow patterns at low mass flux in inclined tubes.....	24
2.7.	Conclusion	25
3.	Experimental set-up	26
3.1.	Introduction.....	26
3.2.	Experimental set-up	26
3.2.1.	Vapour compression cycle	26
3.2.2.	Water cycle.....	27
3.3.	Test section	28
3.3.1.	Flow visualisation	28
3.4.	Instrumentation	29
3.4.1.	Pressure transducers.....	29
3.5.	Data reduction.....	29
3.6.	Experimental data range	32
3.7.	Uncertainty.....	33
3.8.	Experimental procedure and data acquisition.....	33
3.9.	Conclusion	33
4.	Experimental data validation.....	34
4.1.	Introduction.....	34
4.2.	Test matrix.....	34
4.3.	Flow pattern map	35
4.3.1.	The Hajal-Thome-Cavallini flow pattern map	35
4.4.	Heat transfer data comparison in horizontal tubes.....	36
4.4.1.	Data comparison	37
4.5.	Heat transfer data comparison in inclined tubes.....	38
4.5.1.	Heat transfer comparison for different qualities and inclination angles.....	39
4.6.	Flow pattern transition	40
4.7.	Flow patterns	41
4.8.	Summary and conclusion	42
5.	Results: flow patterns and heat transfer coefficients.....	44
5.1.	Introduction.....	44
5.2.	Observed flow patterns in this study	44
5.3.	Horizontal configuration: flow patterns and heat transfer coefficient	46
5.3.1.	Effect of quality	46
5.3.2.	Effect of mass flux	48
5.3.3.	Effect of ΔT	50
5.4.	Inclined configuration – flow patterns and heat transfer coefficient.....	52
5.4.1.	Effect of quality	52
5.4.2.	Effect of mass flux	54
5.4.3.	Effect of ΔT	56



5.5.	Summary of the heat transfer coefficient for inclined flow	59
5.5.1.	Summary on the effect of quality on heat transfer coefficient	59
5.5.2.	Summary of the effect of mass flux on the heat transfer coefficient.....	60
5.5.3.	Summary of effect of temperature difference on the heat transfer coefficient.....	62
5.5.4.	Graphical representation of heat transfer coefficient for each inclination angle	64
5.5.4.1	Positive inclination	64
5.5.4.2	Negative inclination	65
5.6.	Conclusion	66
6.	Results: flow patterns and flow pattern transitions	69
6.1.	Introduction.....	69
6.2.	Vertical configuration – analysis of flow patterns	69
6.2.1.	Vertically upward (+90°).....	69
6.2.2.	Vertically down (-90°).....	70
6.3.	Inclined configuration – analysis of flow patterns	71
6.3.1.	Positive inclinations for a quality of 0.25	71
6.3.2.	Positive inclinations for a quality of 0.75	73
6.3.3.	Negative inclinations for a quality of 0.25	75
6.3.4.	Negative inclinations for a quality of 0.75	77
6.4.	Graphic presentation of flow patterns and flow pattern transitions	78
6.4.1.	Present data on the El Hajal-Thome-Cavallini flow pattern map	78
6.4.1.1	Positive inclinations	79
6.4.1.2	Negative inclination	80
6.4.2.	Flow pattern transitions – present data	81
6.4.2.1	Positive inclination	81
6.4.2.2	Negative inclinations.....	83
6.5.	Conclusion	83
7.	Summary, conclusions and recommendations.....	86
7.1.	Summary	86
7.2.	Conclusion	87
7.3.	Recommendations	88
References	90
Appendix A. Uncertainty analysis.....		A-1
A.1.	Introduction.....	A-1
A.2.	Uncertainty analysis methods.....	A-1
A.3.	Uncertainty of the test section tube length.....	A-2
A.4.	Uncertainty in the test tube inner diameter.....	A-2
A.5.	Heat transfer area uncertainty.....	A-2
A.6.	Refrigerant mass flow rate uncertainty	A-2
A.7.	Mass flux uncertainty	A-2
A.8.	The uncertainty in saturation temperature (T_{sat})	A-3
A.9.	Uncertainty of the wall temperature	A-3
A.10.	Uncertainty in temperature difference.....	A-3
A.11.	Uncertainty in heat input	A-3
A.12.	Heat transfer coefficient uncertainty.....	A-4

A.13.	Uncertainty in quality.....	A-4
A.13.1.	Uncertainty in inlet vapour quality	A-4
A.13.2.	Uncertainty in outlet vapour quality.....	A-6
A.14.	Sample calculations of uncertainties	A-8
A.14.1.	Heat transfer area uncertainty.....	A-9
A.14.2.	Mass flux uncertainty.....	A-10
A.14.3.	Uncertainty in saturation temperature (T_{sat}).....	A-10
A.14.4.	Uncertainty of the wall temperature	A-10
A.14.5.	Uncertainty in temperature difference.....	A-11
A.14.6.	Uncertainty in heat input	A-11
A.14.7.	Heat transfer coefficient uncertainty.....	A-11
A.15.	Summary of the uncertainties for this study	A-12
A.15.1.	Results of uncertainties.....	A-12
A.16.	Conclusion	A-18
Appendix B. Heat transfer coefficients and flow patterns		B-1
B.1.	Introduction.....	B-1
B.2.	Effect of quality	B-1
B.3.	Effect of mass flux	B-10
B.4.	Effect of temperature difference	B-18
B.5.	Summary	B-23
Appendix C. Flow pattern transitions for a ΔT of 3 °C.....		C-1
C.1.	Introduction.....	C-1
C.2.	Flow pattern transitions for the horizontal inclination 0°	C-1
C.3.	Flow pattern transitions for the inclination angle of $\pm 5^\circ$	C-3
C.4.	Flow pattern transitions for the inclination angle of $\pm 10^\circ$	C-6
C.5.	Flow pattern transitions for the inclination angle of $\pm 15^\circ$	C-9
C.6.	Flow pattern transitions for the inclination angle of $\pm 30^\circ$	C-12
C.7.	Flow pattern transitions for the inclination angle of $\pm 45^\circ$	C-15
C.8.	Flow pattern transitions for the inclination angle of 60°	C-18
C.9.	Flow pattern transitions for the inclination angle of $\pm 90^\circ$	C-21
C.10.	Summary	C-24
C.10.1.	Comparing flow pattern transitions for negative and positive inclination angles	C-25
C.10.2.	Comparing test condenser inlet and outlet flow pattern transitions.....	C-25

List of figures

Figure 2.1:	Annular flow pattern.....	12
Figure 2.2:	Mist flow pattern	12
Figure 2.3:	Wavy flow pattern.....	13
Figure 2.4:	Stratified flow pattern.....	13
Figure 2.5:	Slug flow pattern	14
Figure 2.6:	Plug flow pattern.....	14
Figure 2.7:	Bubbly flow pattern.....	14
Figure 2.8:	Churn flow pattern	15
Figure 2.9:	Soliman flow pattern map.....	16
Figure 2.10:	The condensing flow pattern map of Hajal <i>et al.</i> [29]	17
Figure 3.1:	Experimental set-up	26
Figure 4.1:	Current data on the Hajal-Thome-Cavallini flow pattern map	36
Figure 4.2:	Heat transfer coefficient comparison at $G = 100 \text{ kg/m}^2 \cdot \text{s}$ and $40 \text{ }^\circ\text{C}$ saturation temperature	37
Figure 4.3:	Comparison of heat transfer coefficients at (a) $x = .25$, (b) $x = 0.5$ and (c) $x = 0.75$	39
Figure 4.4:	Hajal-Thome-Cavallini flow pattern map and flow pattern transitions.....	40
Figure 4.5:	Flow pattern visualisation for a mass flux of $100 \text{ kg/m}^2 \cdot \text{s}$, and temperature difference of $3 \text{ }^\circ\text{C}$	42
Figure 5.1:	Observed flow patterns.....	45
Figure 5.2:	Effect of quality for the horizontal inclination at a mass flux of $100 \text{ kg/m}^2 \cdot \text{s}$ and temperature difference of $5 \text{ }^\circ\text{C}$ on: (a) the heat transfer coefficient; and (b) the flow patterns	47
Figure 5.3:	Effect of mass flux and observed flow patterns in: (a) the heat transfer coefficient; (b) the quality of 0.75; and (c) the quality of 0.25 for the horizontally inclined tube.....	49
Figure 5.4:	Effect of ΔT on: (a) the heat transfer coefficient for mass flux $100 \text{ kg/m}^2 \cdot \text{s}$; and qualities of (b) 0.6 ;(c) 0.5; and (d) 0.25 for a horizontally inclined tube	51
Figure 5.5:	Effect of quality for different inclinations for a mass flux of $100 \text{ kg/m}^2 \cdot \text{s}$ and a temperature difference of $5 \text{ }^\circ\text{C}$	53
Figure 5.6:	Effect of mass flux on (a) the heat transfer coefficient; and (b) flow patterns for different inclinations for a quality of 0.75.....	55
Figure 5.7:	Effect of ΔT on: (a) the heat transfer coefficient; and (b) the flow patterns for different inclinations at a quality of 0.5	58
Figure 5.8:	Total effect of quality on heat transfer coefficient.....	60

Figure 5.9:	Total effect of mass flux on the heat transfer coefficient	61
Figure 5.10:	Total effect of ΔT on the heat transfer coefficient	63
Figure 5.11:	Heat transfer coefficients for positive inclination angles	64
Figure 5.12:	Heat transfer coefficients for negative inclination angles	66
Figure 6.1:	Flow patterns observed for 90° vertically upward flows	70
Figure 6.2:	Flow patterns observed for -90° downward flows	71
Figure 6.3:	Flow pattern transitions for $x = 0.25$ upward flows of 0° to 90°	72
Figure 6.4:	Flow pattern transitions for $x = 0.75$ upward flows of 0° to 90°	74
Figure 6.5:	Flow pattern transitions for $x = 0.25$ downward flows of 0° to -90°	76
Figure 6.6:	Flow pattern transitions for $x = 0.75$ downward flows of 0° to -90°	77
Figure 6.7:	Present data for positive inclinations on the Hajal-Thome-Cavallini flow pattern map.....	79
Figure 6.8:	Present data for negative inclinations on the Hajal-Thome-Cavallini. flow pattern map.....	80
Figure 6.9:	Effect of inclination on flow patterns for positive inclinations.....	82
Figure 6.10:	Effect of inclination on flow patterns for negative inclinations.....	83
Figure A.1:	Uncertainty in the heat transfer coefficients at a temperature difference of 3 °C	A-16
Figure A.2:	Uncertainty of quality for a mass flux of 100 kg/m ² .s and a temperature difference of 3 °C.....	A-16
Figure A.3:	Uncertainty in quality at different mass fluxes and temperature difference of 5 °C	A-17
Figure A.4:	Uncertainty in temperature difference at different mass fluxes.....	A-17
Figure B.1:	Effect of quality for a mass flux 100 kg/m ² .s and a temperature difference of 3 °C	B-2
Figure B.2:	Effect of quality for a mass flux 100 kg/m ² .s and a temperature difference of 5 °C	B-3
Figure B.3:	Effect of quality for a mass flux 100 kg/m ² .s and a temperature difference of 8 °C	B-4
Figure B.4:	Effect of quality for a mass flux 75 kg/m ² .s and a temperature difference of 3 °C	B-5
Figure B.5:	Effect of quality for a mass flux 75 kg/m ² .s and a temperature difference of 5 °C	B-6
Figure B.6:	Effect of quality for a mass flux 75 kg/m ² .s and a temperature difference of 8 °C	B-7
Figure B.7:	Effect of quality for a mass flux 50 kg/m ² .s and a temperature difference of 1 °C	B-8

Figure B.8:	Effect of quality for a mass flux $50 \text{ kg/m}^2\cdot\text{s}$ and a temperature difference of $3 \text{ }^\circ\text{C}$	B-9
Figure B.9:	Effect of mass flux for a temperature difference of $1 \text{ }^\circ\text{C}$ and a quality of 0.75....	B-10
Figure B.10:	Effect of mass flux for a temperature difference of $3 \text{ }^\circ\text{C}$ and a quality of 0.25....	B-11
Figure B.11:	Effect of mass flux for a temperature difference of $3 \text{ }^\circ\text{C}$ and a quality of 0.5.....	B-12
Figure B.12:	Effect of mass flux for a temperature difference of $3 \text{ }^\circ\text{C}$ and a quality of 0.75....	B-13
Figure B.13:	Effect of mass flux for a temperature difference of $5 \text{ }^\circ\text{C}$ and a quality of 0.25....	B-14
Figure B.14:	Effect of mass flux for a temperature difference of $5 \text{ }^\circ\text{C}$ and a quality of 0.5.....	B-15
Figure B.15:	Effect of mass flux for a temperature difference of $8 \text{ }^\circ\text{C}$ and a quality of 0.35....	B-16
Figure B.16:	Effect of mass flux for a temperature difference of $8 \text{ }^\circ\text{C}$ and a quality of 0.5.....	B-17
Figure B.17:	Effect of temperature difference for a mass flux of $100 \text{ kg/m}^2\cdot\text{s}$ and a quality of 0.25.....	B-18
Figure B.18:	Effect of temperature difference for a mass flux of $100 \text{ kg/m}^2\cdot\text{s}$ and a quality of 0.5.....	B-19
Figure B.19:	Effect of temperature difference for a mass flux of $100 \text{ kg/m}^2\cdot\text{s}$ and a quality of 0.75.....	B-20
Figure B.20:	Effect of temperature difference for a mass flux of $75 \text{ kg/m}^2\cdot\text{s}$ and a quality of 0.5.....	B-21
Figure B.21:	Effect of temperature difference for a mass flux of $50 \text{ kg/m}^2\cdot\text{s}$ and a quality of 0.5.....	B-22
Figure B.22:	Effect of temperature difference for a mass flux of $50 \text{ kg/m}^2\cdot\text{s}$ and a quality of 0.75.....	B-23
Figure B.23:	Summary of flow pattern transitions.....	B-24
Figure C.1:	Flow pattern transition at 0° inclination angle and a quality of 0.25	C-1
Figure C.2:	Flow pattern transition at 0° inclination angle and a quality of 0.5	C-2
Figure C.3:	Flow pattern transition at 0° inclination angle and a quality of 0.75	C-2
Figure C.4:	Flow pattern transition at -5° inclination angle and a quality of 0.25	C-3
Figure C.5:	Flow pattern transition at $+5^\circ$ inclination angle and a quality of 0.25	C-3
Figure C.6:	Flow pattern transition at -5° inclination angle and a quality of 0.5	C-4
Figure C.7:	Flow pattern transition at $+5^\circ$ inclination angle and a quality of 0.5	C-4

Figure C.8: Flow pattern transition at -5° inclination angle and a quality of 0.75 C-5

Figure C.9: Flow pattern transition at $+5^\circ$ inclination angle and a quality of 0.75 C-5

Figure C.10: Flow pattern transition at -10° inclination angle and a quality of 0.25 C-6

Figure C.11: Flow pattern transition at $+10^\circ$ inclination angle and a quality of 0.25 C-6

Figure C.12: Flow pattern transition at -10° inclination angle and a quality of 0.5 C-7

Figure C.13: Flow pattern transition at $+10^\circ$ inclination angle and a quality of 0.5 C-7

Figure C.14: Flow pattern transition at -10° inclination angle and a quality of 0.75 C-8

Figure C.15: Flow pattern transition at $+10^\circ$ inclination angle and a quality of 0.75 C-8

Figure C.16: Flow pattern transition at -15° inclination angle and a quality of 0.25 C-9

Figure C.17: Flow pattern transition at $+15^\circ$ inclination angle and a quality of 0.25 C-9

Figure C.18: Flow pattern transition at -15° inclination angle and a quality of 0.5 C-10

Figure C.19: Flow pattern transition at $+15^\circ$ inclination angle and a quality of 0.5 C-10

Figure C.20: Flow pattern transition at -15° inclination angle and a quality of 0.75 C-11

Figure C.21: Flow pattern transition at $+15^\circ$ inclination angle and a quality of 0.75 C-11

Figure C.22: Flow pattern transition at -30° inclination angle and a quality of 0.25 C-12

Figure C.23: Flow pattern transition at $+30^\circ$ inclination angle and a quality of 0.25 C-12

Figure C.24: Flow pattern transition at -30° inclination angle and a quality of 0.5 C-13

Figure C.25: Flow pattern transition at $+30^\circ$ inclination angle and a quality of 0.5 C-13

Figure C.26: Flow pattern transition at -30° inclination angle and a quality of 0.75 C-14

Figure C.27: Flow pattern transition at $+30^\circ$ inclination angle and a quality of 0.75 C-14

Figure 7.28: Flow pattern transition at -45° inclination angle and a quality of 0.25 C-15

Figure C.29: Flow pattern transition at $+45^\circ$ inclination angle and a quality of 0.25 C-15

Figure C.30: Flow pattern transition at -45° inclination angle and a quality of 0.5 C-16

Figure C.31: Flow pattern transition at $+45^\circ$ inclination angle and a quality of 0.5 C-16

Figure C.32: Flow pattern transition at -45° inclination angle and a quality of 0.75 C-17

Figure C.33: Flow pattern transition at $+45^\circ$ inclination angle and a quality of 0.75 C-17

Figure C.34: Flow pattern transition at -60° inclination angle and a quality of 0.25 C-18

Figure C.35: Flow pattern transition at $+60^\circ$ inclination angle and a quality of 0.25 C-18

Figure C.36: Flow pattern transition at -60° inclination angle and a quality of 0.5 C-19

Figure C.37: Flow pattern transition at $+60^\circ$ inclination angle and a quality of 0.5 C-19

Figure C.38: Flow pattern transition at -60° inclination angle and a quality of 0.75 C-20

Figure C.39: Flow pattern transition at $+60^\circ$ inclination angle and a quality of 0.75 C-20

Figure C.40: Flow pattern transition at -90° inclination angle and a quality of 0.25 C-21

Figure C.41: Flow pattern transition at $+90^\circ$ inclination angle and a quality of 0.25 C-21

Figure C.42: Flow pattern transition at -90° inclination angle and a quality of 0.5 C-22

Figure C.43: Flow pattern transition at $+90^\circ$ inclination angle and a quality of 0.5 C-22

Figure C.44: Flow pattern transition at -90° inclination angle and a quality of 0.75 C-23

Figure C.45: Flow pattern transition at $+90^\circ$ inclination angle and a quality of 0.75 C-23

Figure C.46: Summary of flow pattern transitions C-24

List of tables

Table 2.1:	Flow pattern transitions.....	18
Table 2.2:	Heat transfer correlations and models	19
Table 3.1:	Experimental criteria.....	32
Table 4.1:	Test matrix for the horizontal configuration.....	34
Table 4.2:	Test matrix for the inclined configuration	35
Table 4.3:	Flow pattern prediction using Thome-El Hajal flow pattern model	40
Table A.1:	Parameters and values used in the sample calculation of uncertainty.....	A-9



Nomenclature

A	Area	[m ²]
A_f	Cross sectional area occupied by liquid	[m ²]
A_g	Cross sectional area occupied by gas	[m ²]
c_p	Special heat	[J/kg.K]
D	Tube diameter	[m]
d	Diameter	[m]
D_L	Characteristic length/diameter	[m]
g	Gravitational acceleration	[m/s ²]
G	Mass flux	[kg/m ² .s]
h	Specific enthalpy	[J/kg]
h_{fg}	Latent heat of vaporisation	[J/kg]
j	Superficial velocity	[m/s]
k	Thermal conductivity	[W/m.k]
L	Length	[m]
\dot{m}	Mass flow rate	[kg/s]
P	Perimeter	[m]
\dot{q}	Heat flux	[W/m ²]
\dot{Q}	Heat transfer rate	[W]
R	Radius of tube	[m]
T	Temperature	[°C]
u	Velocity	[m/s]
x	Vapour quality	[-]

Non- dimensional numbers

A_{fd}	Area occupied by the liquid
A_{gd}	Area occupied by the gas
Bo	Bond number
EO	Eötvös number
f	Roughness factor
Fr	Froude number
Fr_f	Liquid Froude number
Fr_{so}	Soliman Froude transition number
h_{Ld}	Liquid height



Nu	Nusselt number
P_{ld}	Perimeter of interface
Pr	Prandtl number
Re	Reynolds number
We	Weber number
X_{tt}	Martinelli parameter

Greek

α	Heat transfer coefficient	[W/m ² .K]
ε	Void fraction	[-]
ρ	Density	[kg/m ³]
δ	Film thickness	[m]
σ	Surface tension	[N/m]
α	Heat transfer coefficient	[W/m ² .K]
ν	Kinematic viscosity	[m ² /s]
μ	Dynamic viscosity	[kg/m.s]
θ	Upper angle of the tube not wetted by stratified flow liquid	[Rad]
θ	Angle	[Rad]
τ	Shear	[N/m ²]

Subscripts

A	Air
avg	Average
c	Convective
bot	Bottom part of the tube that is occupied by stratified flow
$bubbly$	Bubbly flow transition
cu	Copper
d	Dimensionless
f	Liquid/ fluid
g	Gas
h	Homogeneous
i	Internal/ interfacial
IA	Transition from annular to intermittent
in	Inlet
m	Mixture



<i>max</i>	Maximum
<i>min</i>	Minimum
<i>out</i>	Outlet
<i>pre</i>	Pre-condenser
<i>post</i>	Post-condenser
<i>ra</i>	Rouhani-Axelsson
<i>so</i>	Soliman definition
<i>ref</i>	Refrigerant
<i>strat</i>	Stratified transition
<i>test</i>	Test condenser
<i>tot</i>	Total
<i>top</i>	Top part of the tube not occupied by stratified flow
<i>TP / tp</i>	Two-phase
<i>water</i>	Water for cooling or heating
<i>wall</i>	Tube wall
<i>wavy</i>	Wavy transition

1. Introduction

1.1. Background

In-tube condensation has various applications in refrigeration, air conditioning systems, chemical processing plants, power generation and pharmaceuticals. Failure of the condenser to dissipate heat can result in the built-up of pressure thus increasing the compressor power. To rectify this, the size of the condenser has to be increased. This however is not cost effective as more refrigerant needs to be charged to the system apart from the added material and maintenance costs. Therefore, accurate and unified methods to design heat transfer systems that are energy efficient, that save space, and that reduce the greenhouse effect through the use of environmentally friendly refrigerants are essential.

Heat pumps, water heaters and coolers, the cooling of food in storages and cargo, domestic and industrial air conditioning, electronic heat removal, power plants, desalination plants and condensers that achieve high heat transfer rates due to enthalpy phase change processes, are some of the applications of two-phase flow systems. The complexity of the analysis of these systems is brought about by the influence of vapour velocity and the rate at which liquid builds up on internal walls of the tube. Cheng, Ribatski and Thome [1] state that the determination of flow patterns is an essential aspect of two-phase flow pressure drops and heat transfer because without knowledge of the local flow pattern, one cannot predict the hydraulic and thermal design parameters precisely. It is necessary to identify and understand the flow patterns involved in condensing systems for thermal and hydraulic design purposes as stated by Cavallini, Doretti, Matkovic and Rossetto [2].

Two-phase flow systems for both condensing and adiabatic conditions are governed by different characteristics due to the energy and momentum of the two-phases; the gas phase and the liquid phase. The complex nature of the two-phase flow patterns varies due to the differences in geometry, channel size, channel orientation, internal roughness, mass flux, saturation temperature and the properties of the fluid among other factors. Most of the work that has been carried out was in gas liquid adiabatic flows, and some of the pioneers are, Barnea, Shoham and Taitel. [3], Spedding and Spence [4], Taitel and Dukler [5], Weisman, Duncan, Gibson and Crowfords [6], and Baker [7]. With regards to diabatic two-phase flow patterns, condensation and boiling are mainly encountered in heat pumps, condensers, air conditioning, flow boiling and refrigeration systems. Previous flow pattern maps for adiabatic conditions have been extrapolated for diabatic flow conditions, but the results were incorrect and unreliable as they had no effect on heat transfer [1].

The earliest flow pattern maps were presented by Baker [7], Taitel and Dukler [5], Mandhane, Gregory and Aziz [8] and Spedding and Nguyen [9]. However, they were all for

gas-liquid two-phase flow. The two-phase flow pattern map of Kattan-Thome-Favrat [10] (the Kattan-Thome-Favrat flow pattern map) was one of the first maps to be developed for diabatic condition (evaporation). Later, studies for the development and modifications of the flow pattern map two-phase flow condensation were conducted by Hajal-Thome-Cavallini, [11]. These maps were developed based on the flow patterns observed, and this allows the designer to identify which flow patterns are likely to be observed in the design and avoid transitions to other flow patterns that might be undesirable [12]. The challenge faced nowadays is the incorporation of the flow pattern effect and two-phase flow structures with the prediction of the model.

Ghiaasiaan [13] stated that the current methods used for predicting two-phase flow patterns are far from perfect. This is as a result of the variations in flow characteristics due to the differences in density between the two phases that led to the phases responding differently to forces of gravity, and churn forces. Quite a number of models that have so far been proposed have outlined stratified and non-stratified flows, based on the collective analysis of heat transfer databases instead of flow pattern observations, as mentioned by Thome [12]. Most of the models and correlations have been developed for horizontal channels and for annular and stratified flow patterns only.

1.1.1. Two-phase flow analytical tools

The complex nature of the two-phase flow led to limitations in the development of successful mathematical formulas and models for the flow patterns. However a number of predictive tools used to determine two-phase condensation heat transfer eased the design process of heat exchangers or heat transfer systems. Some of the previous methods that have been used include empirical, theoretical and universal methods. Recently computational fluid dynamics (CFD) has been used to model two-phase flow patterns, heat transfer coefficients and pressure drops. However, some of the tools have failed to predict flow patterns correctly, as they are only valid for specific diameters, fluids and operating conditions [14].

Empirical models use quantifiable properties of the two-phase flow, whereby the gas and liquid characteristics of the fluid are taken into account. The two-dimensional flow pattern maps of Baker [7], Hewitt and Roberts [15] and Mandhane *et al.* [8] are empirical maps for concurrent horizontal gas-liquid flow. Empirical models are derived from the experimental data. An example of this is the map of Baker [7]. However, the map does not correctly predict horizontal flow patterns in various situations as stated by Rouhani and Sohal [16]. Hewitt and Roberts [15] also developed an empirical two-phase flow pattern map with superficial gas-liquid velocities as coordinates. However this map cannot be used as a universal flow pattern map for two-phase flow.

Theoretical flow pattern maps were developed according to the structure of the flow and are linked to the diabatic flow characteristics. The map of Taitel and Dukler [5] is a semi-theoretical map that makes use of different dimensionless parameters that have proven to be very effective in the prediction of a wider range of conditions. The work used the Lockhart-Martinelli correlation for a stratified flow to derive different flow pattern transitions for horizontal and slightly inclined channels. The semi-theoretical method of Taitel and Dukler [17] to determine flow pattern transition was criticised by Weisman *et al.* [6] as being too general.

On the other hand, universal models are based on the consolidated database for a variety of fluids, as well as operating conditions [18]. Spedding, Cooper and McBride [19] developed a universal flow pattern map for horizontal two-phase flow in pipes, but the map only covered very large diameters above 25 mm and only gas-liquid two-phase flow.

1.1.2. The work of the Thome research group

The research group of Thome and co-workers (Hajal, Thome and Cavallini [11], Thome [12, 20], Thome, Hajal and Cavallini [21] and Olivier, Liebenberg, Thome and Meyer [22]) came up with a more accurate model and flow pattern map for two-phase condensing flows based on flow patterns. The flow pattern map and model could correctly predict flow patterns and heat transfer coefficient for horizontal flows for a large database of refrigerants (including R-134a), mass fluxes between 24 kg/m².s and 1 022 kg/m².s, qualities from 0.03 to 0.97 and diameters from 3.1 mm to 21.4 mm. Unlike the previous flow pattern maps and models that were developed for air-water mixtures, the model of Thome and co-workers for condensing flows showed greater improvement in heat transfer coefficient predictions as it was based on the following: the prevailing flow pattern, the large data base used, the inclusion of the effect of temperature difference in the model for stratified flows for the falling-film heat transfer equation, and the effect of vapour shear that increases the interfacial waves on the vapour liquid interface causing high amplitudes and an increase in the magnitude of the waves. The model could predict five flow patterns: annular, intermittent, stratified-wavy, stratified and mist flow patterns. The flow pattern map and model could give much better results, but they were only developed for horizontal flow.

1.1.3. The work of the Meyer research group

Very few studies have tackled the issue of inclination with regards to flow patterns and heat transfer coefficients. The first comprehensive condensing studies in smooth tubes for different inclinations were conducted by Meyer and co-workers (Meyer, Dirker and Adelaja [23], Olivier, Meyer, Paepe and Kerpel [24], and Lips and Meyer [25]). The studies included a consideration of the effect of inclination on flow patterns and heat transfer coefficients and pressure drop in a smooth tube at high mass fluxes above 100 kg/m².s. They also considered the effect of saturation temperature that has been studied recently [23]. The flow patterns

identified were intermittent, stratified-wavy, smooth stratified and annular flow patterns. Images were also shown for the different inclination angles under investigation. For these studies, the diameter of the tube was 8.38 mm, the refrigerant was R-134a, the vapour qualities were between 0.9 and 0.1, the saturation temperature was 40 °C and the test section length was 1 488 mm. The studies concluded that maximum heat transfer coefficients were between -10° and -30° (downward) flow and the inclination effect was more evident at lower mass fluxes. The effect of temperature difference was however not discussed.

1.2. Gaps in literature and problem statement

As mentioned earlier, the heat transfer coefficients and pressure drops can be accurately predicted by identifying the local flow pattern. Adiabatic two-phase flow patterns are not relevant for diabatic conditions, as the heat transfer has no effect on the local flow pattern or the transition from one flow pattern to another [1]. The studies mentioned in Section 1.1.2 and Section 1.1.3 were mainly conducted at high mass fluxes of 100 kg/m².s and above. Some flow patterns at high mass fluxes (above 100 kg/m².s) differ from those at low mass fluxes. Annular, mist, and wavy flow patterns are dominant at high mass fluxes in horizontal and inclined channels. However, stratified and stratified-wavy flow patterns are evident at mass fluxes of 100 kg/m².s and below in horizontal channels.

In industry, the main common orientations of condensers are 60° A-frame condensers, for which no work has been conducted to justify this angle [24]. However studies of inclination angles are very limited.

Coleman and Garimella [26] noted that there is a greater need to identify two-phase flow patterns, as they precede the development of pressure drops and heat transfer correlations. Thome [12] proposed a marriage between two-phase flow for predicting adiabatic flow transitions, and two-phase flow heat transfer for predicting condensing or evaporative heat transfer coefficients by the inclusion of flow patterns and phase flow structures on both the process and prediction of the model.

From this, it can be concluded that there is still a need for more studies to be carried out for different inclination angles and mass fluxes of 100 kg/m².s and below. This should be done in order to achieve the following:-

- Properly identify observed flow patterns for different inclination angles;
- Correctly predict the heat transfer coefficient at low mass fluxes;
- Determine the optimum angle that yields a higher heat transfer coefficient at mass fluxes of 100 kg/m².s and below, as some industrial condensers have inclined tube settings, and to use this for future design recommendations;

- To combine heat transfer coefficients with local flow patterns observed, as proposed by Thome [12], to determine which flow patterns give rise to a higher heat transfer coefficient for different inclination angles;
- Validate the results with the flow pattern map for condensation of Hajal *et al.* [11];
- Determine the effects of quality, mass flux and inclination angle on the heat transfer coefficient for both the horizontal and inclined orientations at mass fluxes of $100 \text{ kg/m}^2\cdot\text{s}$ and below;
- Investigate the effect of temperature difference on the heat transfer coefficient at low mass fluxes for all the inclination angles;
- Determine all flow pattern transitions from the inlet to the outlet of the test section for inclined orientations;
- Investigate the flow pattern transitions with changes in inclination, mass flux, quality and temperature difference;
- Show flow pattern transitions on a flow pattern map for each inclination angle.

1.3. Purpose

The purpose of the study is to qualitatively identify condensing flow patterns at mass fluxes of $100 \text{ kg/m}^2\cdot\text{s}$ and below in a smooth tube of 8.38 mm at different inclination angles, and thereby determine the effect of quality, mass flux, inclination angle and temperature difference (ΔT) on the heat transfer coefficient, and as well as the effect of inclination on the flow patterns.

1.3.1. Aim

The aim of the study is to qualitatively analyse flow patterns and flow pattern transitions for in-tube condensation for inclined tubes at mass fluxes of $100 \text{ kg/m}^2\cdot\text{s}$ and below for design purposes. An experimental set-up was used, and images were captured for both the inlet and the outlet of the test section. The images and the heat transfer data for different qualities, mass fluxes, temperature difference and inclination angles were analysed and conclusions derived that would assist in predicting the heat transfer coefficient for in-tube condensation in gravity driven flows.

1.3.2. Objectives

The objectives of the study comprise the following:-

- Show flow patterns for in-tube condensation at mass fluxes of $100 \text{ kg/m}^2\cdot\text{s}$ and below and different inclination angles;
- Observe flow pattern transitions for different inclination angles;
- Examine changes in heat transfer coefficients during in-tube condensation at low mass fluxes;

- Examine flow patterns at different operating conditions (different; qualities and mass fluxes) and thereby determine changes in heat transfer coefficients;
- Investigate the effect of temperature difference on the heat transfer coefficient and the flow pattern for different inclination angles;
- Display flow pattern transitions from the inlet to the outlet of the test section for different operating conditions;
- Determine the inclination angle that gives optimum heat transfer coefficients;
- Ascertain the effect of temperature difference between the tube wall and the saturation temperature on the heat transfer coefficient.

1.3.3. Scope

Two Besler high-speed cameras were used to capture images of the flow patterns. The refrigerant under investigation was R-134a, condensing in a smooth tube with an inner diameter of 8.38 mm and a tube length of 1.5 m. The mass fluxes varied between 25 kg/m².s and 100 kg/m².s, and saturation temperatures were between 30°C and 40 °C. Vapour quality was between 0.1 and 0.9 for horizontal and inclination angles from +90° to -90°.

1.4. Structure of the dissertation

The remainder of this dissertation is summarised in six chapters. Chapter 2 focuses on the literature review, where the basic two-phase flow condensation principles are discussed. These include two-phase flow formulas and equations, as well as non-dimensional numbers, correlations and models, and descriptions of flow patterns and flow pattern maps. In addition, two-phase condensing work in horizontal and inclined tubes in both low and high mass fluxes is briefly described.

Chapter 3 sets out the experimental test set-up and test procedure. The set-up is displayed in a simple diagram with a brief explanation of the water and refrigeration cycles, the test section and the flow visualisation model. The experimental set-up validation, the uncertainties of the test bench set-up and the equipment, as well as how the data is acquired are also discussed.

Chapter 4 considers validation of the results in relation to other research. The work of Hajal *et al.* [11] has been used as the validation criteria, since this model and flow pattern map for horizontal two-phase flow condensation has proven to be very reliable compared to the work of previous authors. The flow pattern data is plotted on the flow pattern map of Thome *et al.* [21] and this model is used to validate the flow pattern transitions. Heat transfer coefficients are validated for both horizontal and inclined orientations in accordance with the work of Meyer *et al.*[23] and Olivier *at al.*[24].

Chapter 5 and Chapter 6 give a review of the experimental results. Flow patterns observed in this study are identified and defined from images. Chapter 5 concentrates mainly on

analysing the effect of quality, mass flux and temperature difference on the heat transfer coefficient, and the flow pattern for both the horizontal and other inclination angles. The chapter concludes with the effect of inclination on the heat transfer coefficient and a summary of all the aspects mentioned above. Chapter 6, on the other hand, shows a detailed analysis of the flow patterns and the flow pattern transitions for the vertically upward flows $+90^\circ$ and vertically downwards -90° , as well as other inclination angles. The emphasis is on the transition from one inclination angle to another, and for different qualities. Flow patterns are represented on the flow pattern map of Hajal *et al.* [11], where-after *the* observed flow pattern transitions for this study are represented graphically. Chapter 7 presents a brief summary of the research, a conclusion and some recommendations.

2. Literature review

2.1. Introduction

The literature review presented here focuses on the two-phase condensation of refrigerants. Firstly, a short review of dimensionless parameters and definitions of basic two-phase flow terminologies is represented; followed by an overview of condensation and gravity-driven flows, flow patterns, flow pattern maps, correlations and models in two-phase flow condensation. Some of the work regarding horizontal in-tube condensation at mass fluxes of $100 \text{ kg/m}^2\cdot\text{s}$ and below and inclined orientations at both low and high mass fluxes was explored, and a summary is presented here. Finally, a short summary and discussion of the elements that have been presented concludes this chapter.

2.2. Non-dimensional parameters and other two-phase flow terminologies

For different fluids and operating conditions encountered, it is important to have basic relationships between system variables through the use of dimensionless groups. Theoretical and empirical correlations of different parameters in two-phase flow can be obtained through dimensionless groups.

2.2.1. Reynolds number (Re)

The Reynolds number predicts corresponding flow regimes in different fluid flow conditions and is basically defined as a ratio of inertia forces to viscous forces. Osborne Reynolds made use of this concept in 1883. According to White [27], estimating the Reynolds number first would indicate whether the flow is laminar, turbulent or viscous creeping. This basically means that at small Reynolds numbers, fluid fluctuations are suppressed by the large viscous forces, which implies that the flow tends to be laminar.

$$Re = \frac{uD}{\nu} = \frac{\rho uD}{\mu} \quad 2.1$$

2.2.2. Prandtl number (Pr)

The Prandtl number defines the characteristic of heat transfer in a fluid and is given as the rate of momentum diffusion to the rate of diffusivity of heat. In 1994, Ludwig Prandtl introduced the boundary layer theory and the Prandtl number depends only on the fluid state and the fluid itself. Conductive heat transfer is pronounced for low Prandtl numbers while convective heat transfer is associated with high Prandtl numbers [28]. The thermal boundary layer is much thicker than the velocity boundary for low Prandtl numbers for viscous fluids.

$$Pr = \frac{\mu C_p}{k} \quad 2.2$$

2.2.3. Nusselt number (Nu)

The Nusselt number, named after Wilhelm Nusselt, represents the ratio of the convective heat transfer rate to the conduction heat transfer rate. The smaller the Nusselt number, the more the heat transfer is by conduction. Therefore, a Nusselt number of 1 shows that the heat transfer through a boundary layer is by pure conduction, [29]. The Nusselt number non-dimensionalises the heat transfer coefficient in Equation 2.3.

$$Nu = \frac{\alpha D_l}{k} \quad 2.3$$

The Nu was later developed by Colburn [30] for smooth and rough tubes, and thereafter applied to smooth tubes for fully developed flow.

$$Nu = 0.023 Re^{0.8} Pr^{1/3} \quad \text{for } \begin{cases} 0.7 \leq Pr \leq 160 \\ Re > 10\,000 \end{cases} \quad 2.4$$

Dittus and Boelter [31] improved the Colburn's equation by a constant n for the heating or cooling of the fluid. The equation is most accurate for minimum temperature differences between the wall and the fluid [29].

$$Nu = 0.023 Re^{0.8} Pr^n \quad \text{where } n = 0.3 \text{ for cooling} \quad 2.5$$

2.2.4. Two-phase flow terminology

Correlations and basic models have been formulated by a combination of different terminologies. Two-phase flow terminologies used in this study are discussed and defined according to Awad [28].

2.2.4.1 Quality (x)

Quality is the ratio of the mass flow rate of a gas phase to the total mass flow rate, where the total mass flow rate is the sum of the liquid and the gas mass flow rates. Quality is one important flow parameter in two-phase flow as flow patterns are dependent on both quality and the mass flow rate.

$$x = \frac{\dot{m}_g}{\dot{m}_g + \dot{m}_f} ; \quad 1 - x = \frac{\dot{m}_f}{\dot{m}_g + \dot{m}_f} \quad 2.6$$

2.2.4.2 Void fraction (ε)

Void fraction is the ratio of the cross-sectional area of the tube that the gas occupies to the total cross-sectional area of the tube. Many void fraction models have been used over the years. These include empirical, homogeneous, one-dimensional and drift flux models. The important parameter that is mostly used to determine the two-phase flow heat transfer coefficient and flow patterns is the void fraction, as mentioned by Thome *et al.* [21]. The drift flux model of Rouhani and Axelsson [32] was the one used by Thome *et al.* [21] for their new flow pattern based on the heat transfer model for condensing flows in horizontal tubes.

$$\varepsilon = \frac{A_g}{A_g + A_f} \quad 2.7$$

For a cross-sectional area of the tube, A , the cross-sectional area that is occupied by the gas or liquid is given as:

$$\varepsilon = \frac{A_g}{A} ; (1 - \varepsilon) = \frac{A_f}{A} \quad 2.8$$

2.2.4.3 Mass flux (G)

Mass flux or mass velocity is the ratio of the mass flow rate to the cross-sectional area of the tube, as described by Collier and Thome [33]. The flow patterns of Thome *et al.* [21] Collier and Thome [33] and Soliman [34] use mass flux on the vertical axis and quality on the abscissa to depict flow pattern transitions.

$$G = \frac{\dot{m}}{A} = \rho u = \frac{u}{v} \quad 2.9$$

2.3. Condensation

Condensation can be defined as the changing process of a substance from a gaseous state to a liquid state and is simply defined by Collier and Thome [33] as the conversion of vapour into liquid by heat removal from the system. This process takes place when vapour cools below the saturation temperature onto a surface. Drops form on top of the surface and due to vapour shear or gravity, the drops are drained from the surface leaving a clean non-wetted surface, where-after the cycle continues. This is termed drop-wise condensation and is the most desirable and efficient form of condensation with high heat transfer rates. However in most engineering systems, it is very hard to maintain the non-wetted surface. Film condensation on the other hand, is the most practical and common mode of heat transfer used in most systems. Although not as efficient as drop-wise, film condensation occurs when the vapour condenses forming tiny droplets that coalesce and wets the surface. The liquid then flows due to vapour shear or gravity [13]. The formation and coalescence of vapour droplets and flow of either or both, results in the development of

flow patterns. For in-tube condensation, the flow patterns can be wavy, annular, bubbly or slug.

2.3.1. Gravity-driven two-phase flow condensation

Gravity-driven two-phase flow condensation is characterised by conduction (being the main mode of heat transfer) and gravity as the driving force. Due to the low velocities of the fluid, the liquid condensate is dragged down from the inner periphery or tube sides to the bottom of the tube forming pools of liquid at the bottom of the tube by gravity forces which overweigh shear forces. The main flow patterns observed for gravity-driven condensations in horizontal tubes are stratified, stratified-wavy and intermittent flow patterns. Nusselt pioneered the theory of condensation on a flat plate driven downwards by gravity [29] and derived the Nusselt numbers. Chato [35] developed the Nusselt theory, concentrating on low vapour velocity flows (stratified flows), of which a model of the thickness of the liquid condensate at the bottom of the tube was developed. Rosson and Myers [36] concluded from their experiments that the heat transfer coefficient is greater at the top of the tube. This is the effect of the condensate thickness, which is thinner at the top compared to the sides and the bottom where the condensate layer increases as the condensate moves from the top to the bottom of the tube. As a result, the bottom of the tube (having the thickest layer of condensate) has the lowest heat transfer coefficients.

2.4. Flow patterns

The interactions of the liquid and vapour phases in in-tube condensation during heat and mass transfer promote the development of flow patterns. As mentioned earlier, flow patterns are dependent upon tube geometry, tube size, mass flux, pressure, heat flux and orientation of the tube (inclination), quality of the vapour mixture and fluid properties. Dobson and Chato [37] mentioned that the correct identification of flow patterns provides accurate predictions of heat transfer coefficients and pressure drops. The development of flow pattern-based correlations suitable for general use is based on the correct identification of the locally observed flow pattern [38]. There are many methods of flow pattern observation, and Rooyen [39] elaborates on most of these methods. In this study, however, a visual observation was used. A set-back, however, is that the identification of the flow patterns is subjective. Nevertheless, this is one of the most common methods used by researchers to identify flow patterns to date.

Although a variety of names have been assigned to different flow patterns by different researchers, it is important to define the main flow patterns observed for horizontal and vertical tubes. The flow patterns will be named according to definitions provided by pioneers like Thome and co-workers [10-12, 21, 33, 38, 40-42], Barnea, Shoham and Taitel [3, 43] and Weisman *et al.* [6] and Weisman and Kang [44]. Subsections 2.4.1 to 2.4.7 contain

definitions of condensing two-phase flow patterns that can be observed for both horizontal and inclined angles.

2.4.1. Annular flow pattern

As super-heated vapour enters the inlet of the tube in in-tube condensation, the vapour starts to condense on to the inner surfaces of the tube. This is the onset of the annular flow pattern. It consists of a very thin liquid film around the annulus of the tube and vapour at the core [45]. The flow pattern is normally observed at high vapour qualities and at both horizontal and vertical tube inclinations. Vapour velocity at this stage is much higher than that of the condensate. Annular flow has been observed mainly at higher mass fluxes although it can still be observed in lower mass fluxes at very high qualities. The liquid vapour interface of annular flow may consist of interfacial waves resulting from the high velocity of vapour at the core. The waves can grow visibly in amplitude. This has been observed by Barnea *et al.* [43] as wavy-annular flow. The annular flow pattern has also been observed in inclined tubes, especially at vertical inclinations of $+90^\circ$ and -90° , as described by Arslan [46].



Figure 2.1: Annular flow pattern

2.4.2. Mist flow pattern

The mist flow pattern is observed at a high quality and very high gas flow rates with minute liquid droplets that can only be observed under some form of magnification and special lighting. Unlike bubbly flow, whereby the gas bubbles are dispersed within the liquid condensate, mist flow is characterised by liquid droplets that are drawn along the continuous gas phase [47]. These liquid droplets may intermittently wet the tube walls.

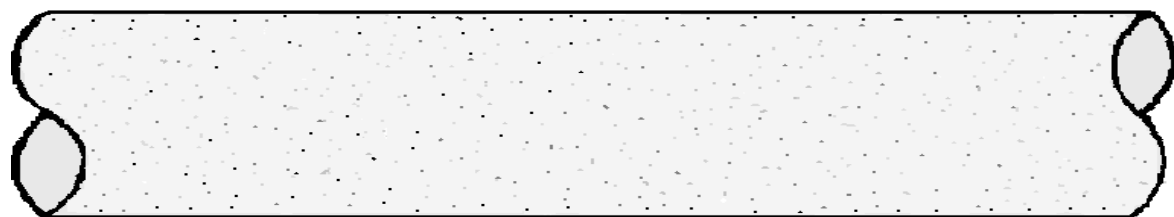


Figure 2.2: Mist flow pattern

2.4.3. Wavy flow pattern

The wavy flow pattern has a vapour layer flowing on the upper part of the channel with a liquid layer that is confined to the bottom of the tube. The vapour-liquid interface is characterised by surface waves, resulting from the increase in vapour velocity. This flow pattern is mostly observed in large diameter tubes and then disappears as the tube diameter decreases. The flow is also observed at very low qualities and high mass fluxes as well as at low to medium quality and low mass fluxes as stated by Coleman and Garimella [48]. Some authors have defined the stratified-wavy flow pattern as just wavy flow [37, 49].

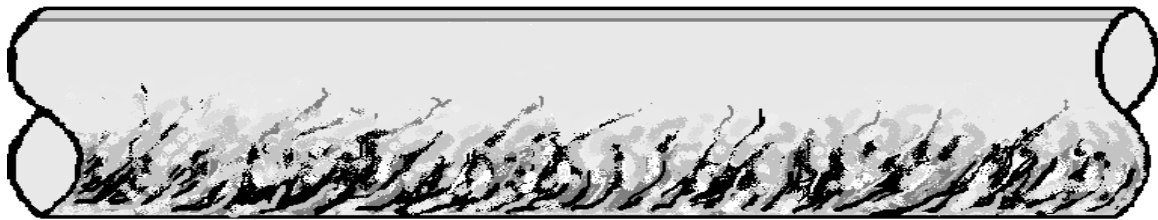


Figure 2.3: Wavy flow pattern

2.4.4. Stratified flow pattern

The stratified flow pattern is a gravity-driven flow pattern that occurs at very low vapour velocities. The condensate that forms on the top surface of the tube flows downwards to the bottom of the tube due to gravity. The velocity on the top of the tube is downwards. A liquid pool forms at the bottom of the tube and flows to the direction of the flow along the tube length due to the vapour shear. A smooth vapour-liquid interface is the result of very low vapour velocities [37].

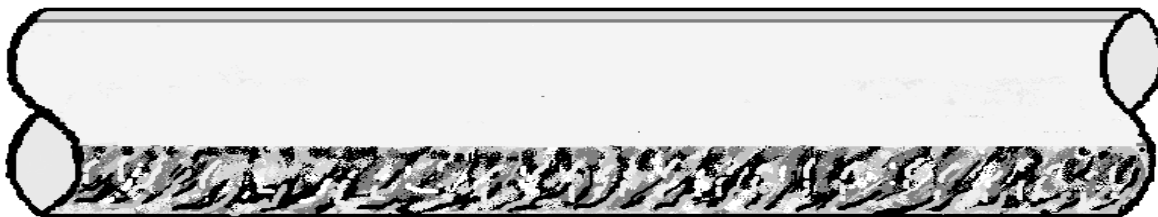


Figure 2.4: Stratified flow pattern

2.4.5. Intermittent flow pattern

This type of flow pattern consists of slug and plug flows.

2.4.5.1 Slug flow

The slug flow pattern has a long bubble that moves in between the liquid slugs and some scattered bubbles following behind this bubble. Liquid slugs are formed as a result of the growth in amplitude of the interfacial waves that blocks the cross-section of the tube at

particular sections along the tube. The slugs are a result of the liquid condensate flowing down the tube. In large diameter tubes, the slugs can be seen confined to the upper part of the tube, while in small-diameter tubes, the slugs are in the middle of the tube.



Figure 2.5: Slug flow pattern

2.4.5.2 Plug flow

The plug flow pattern unlike the slug flow pattern does not have scattered bubbles trailing behind the elongated bubbles.



Figure 2.6: Plug flow pattern

2.4.6. Dispersed to bubbly flow pattern

This flow pattern consists of bubbles that are dispersed within the liquid. The bubbles can be dispersed, clustered, churning or turbulent within the liquid. Garimella [50] describes this as bubbly flow due to the suspension of the bubbles in the liquid. The instability in the liquid results in the break-up of the plugs, forming small bubbles that are dispersed within the liquid. The bubbly flow pattern is observed at low quality and high mass fluxes.

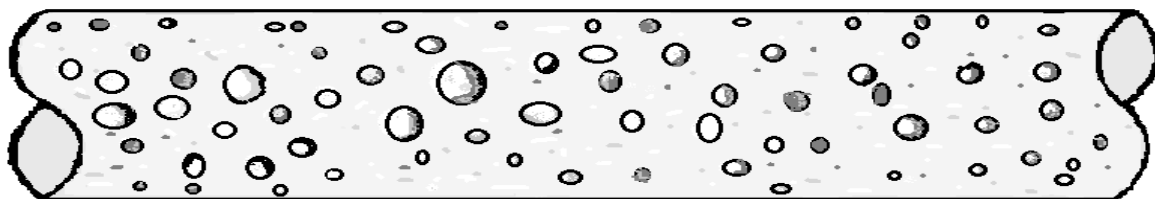


Figure 2.7: Bubbly flow pattern

2.4.7. Churn flow pattern

In churn flow, the bubbles increase due to the increase in gas velocity. As these bubbles collapse, the flow becomes unstable causing an oscillating motion of the liquid moving

upwards and downwards in the tube. This flow pattern is mainly observed in vertically upward flows.



Figure 2.8: Churn flow pattern

2.5. Two-phase flow pattern maps, transitions and heat transfer correlations

Section 2.5.1 to Section 2.5.3 summarise two-phase flow pattern maps, flow pattern transitions and correlations for condensing flows. Most of the flow patterns that were developed in the past have been unable to predict the flow pattern transitions correctly, as they were initially developed for air-water mixtures, and could therefore not be used to accurately predict condensing flow patterns and flow pattern transitions. Some of these flow pattern maps include the flow pattern maps of Baker [7], Hewitt and Roberts [15], Hashizume [51], and Taitel and Dukler [5]. Nonetheless, some of the flow pattern maps that have been developed take note of the diabatic conditions in the heat exchanger. Some of these are the flow pattern maps of Soliman [34], Breber, Palen and Taborek [52], Kattan *et al.* [10] and Tandon, Varma and Gupta [53]. In this study, the only flow patterns that are discussed are for condensing flows, which are the flow pattern maps of Soliman [34] and the state-of-the-art flow pattern map of Hajal *et al.* [11]. Despite the wide range of flow patterns that have been developed, there is still not enough information on which flow pattern map to use for a particular application as identified by Hajal *et al.* [11]. In addition, transition regions are quite large, thereby posing the risk that both flow patterns would occur sporadically in the same region. The flow pattern observation, along with its transition to neighbouring flow patterns, has also rarely been available, making it difficult to determine the transition. The subjective nature of flow patterns, as mentioned earlier, poses a threat to the proper identification of flow patterns and flow pattern transitions. Some flow pattern maps distinguish between steady flow patterns, while others do not. This

makes it difficult to compare the flow patterns. As a result, it is important that a unified flow pattern map be developed. However, the development can only start through the proper identification of flow patterns and the analysis of their transitions.

2.5.1. Soliman flow pattern map

The flow pattern map of Soliman [34] was developed for condensing flow in horizontal tubes Figure 2.9. The flow map transitions are for wavy, annular and mist flow patterns. The wavy flow pattern, which is a gravity-driven flow pattern, occurs in all the mass flux and vapour quality ranges, but, the prevalence of wavy flow increases with the decrease in both mass flux and quality. The flow pattern map cannot predict stratified flow and intermittent flow, as these are not specified in the flow pattern map.

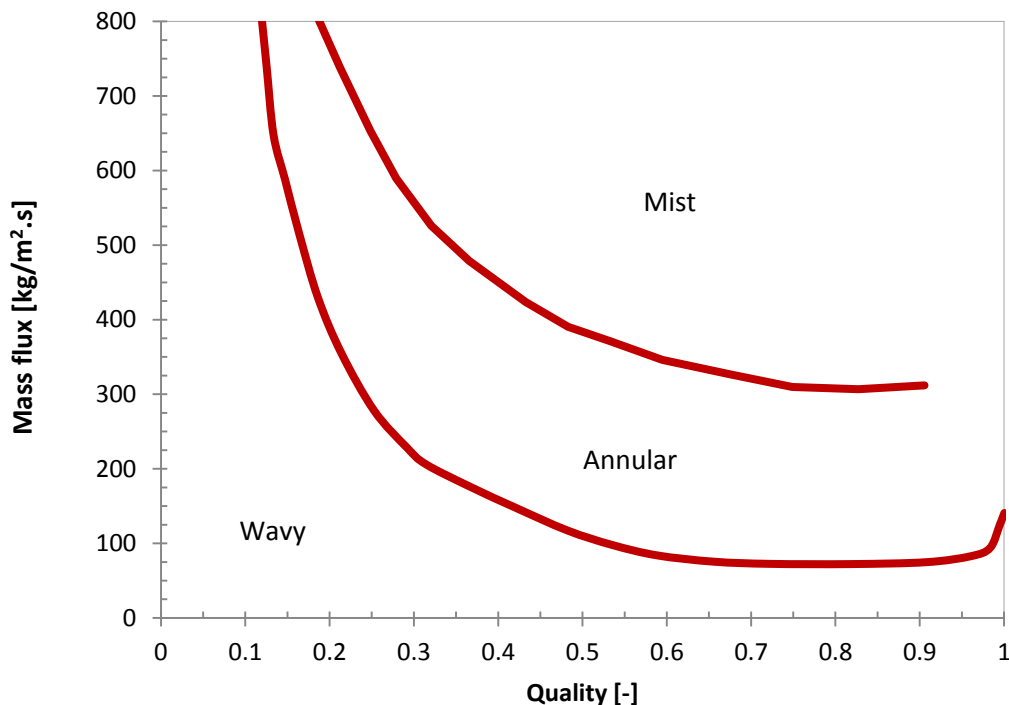


Figure 2.9: Soliman flow pattern map

2.5.2. Hajal-Thome-Cavallini condensation flow pattern map

The flow pattern map of Hajal *et al.* [11] (the Hajal-Thome-Cavallini flow pattern map) is an extension of the flow pattern map of Kattan *et al.* [10]. The map improved in accuracy from the Kattan evaporating flow pattern map. The condensing flow map is reliable for a range of parameters ($16 < G < 1532 \text{ kg/m}^2.\text{s}$, $3.14 < D < 21.4 \text{ mm}$ and $0.02 < Pr < 0.8$), as well as a wider range of refrigerants. The flow pattern map has proven to be easy to use and accurate [54]. Unlike the Soliman flow pattern map, the flow pattern map of Hajal *et al.*[11], predicts a wider range of flow patterns, including stratified, annular, intermittent,

stratified-wavy and mist flow patterns. Although mist flow is not shown in the map in Figure 2.10 it is typically observed at high qualities and high mass fluxes.

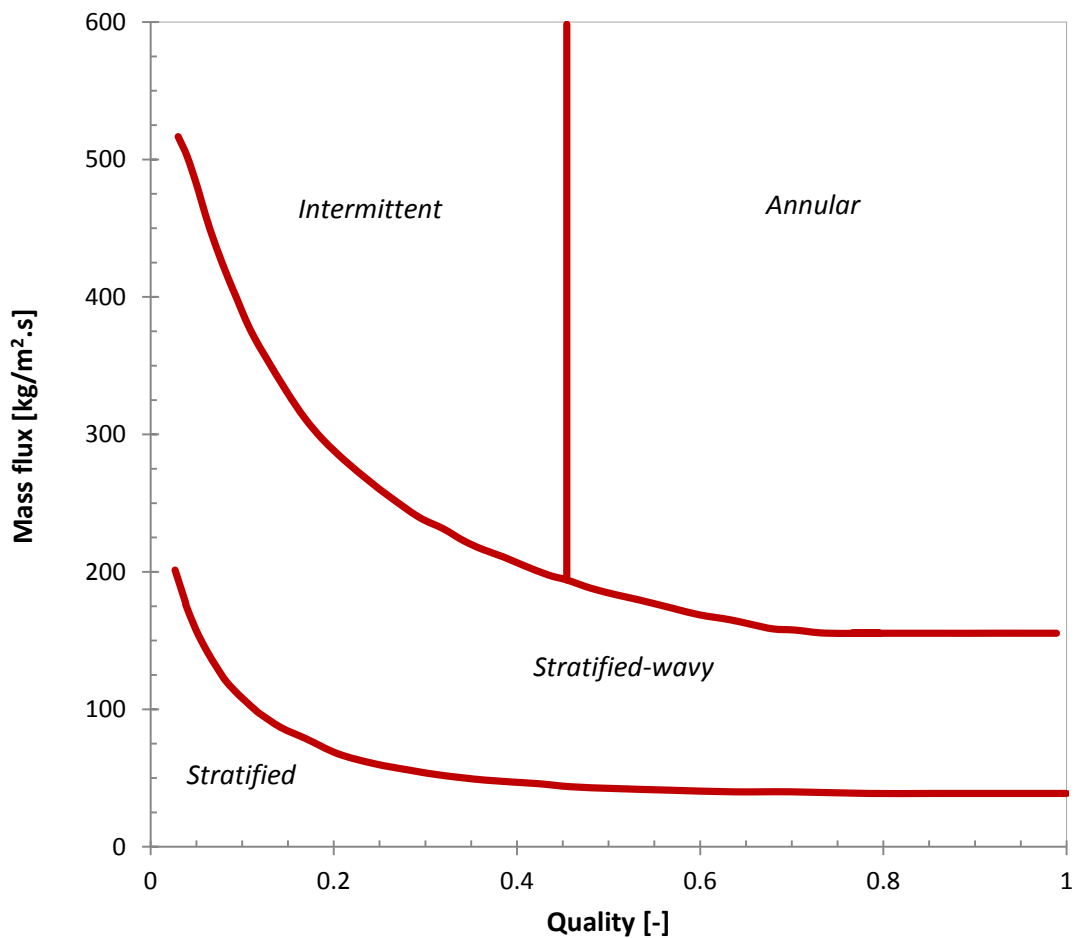


Figure 2.10: The condensing flow pattern map of Hajal *et al.* [11]

2.5.3. Flow pattern transitions

Flow pattern transitions are dependent upon factors that include inclination angle, mass flux, quality and type of fluid. Models have been developed for different flow pattern transitions, and these are shown in Table 2.1. These models have been developed for flow pattern maps. The pay-off of determining the flow pattern is now recognised in accurate predictions of heat transfer coefficients, leading to flow pattern-based heat transfer correlations developed by Thome *et al.* [21] (the Thome-Hajal-Cavallini flow pattern map), as shown in Table 2.2. The heat transfer model is further expounded in Equations 2.18 to 2.18.

Table 2.1: Flow pattern transitions

Thome [12]

Annular to intermittent (slug/plug flow)

$$X_{IA} = \left\{ \left[C \left(\frac{\rho_f}{\rho_g} \right)^{0.5} \left(\frac{\mu_g}{\mu_f} \right)^{0.1} \right]^{1/0.9} + 1 \right\}^{-1} \quad 2.10$$

where $C = 0.3218$ for smooth tubes

Hajal [11]

Stratified to stratified-wavy flow transition

$$G_{strat} = \left(\frac{226.2 \cdot A_{gd}^2 \cdot A_{fd}^2 \rho_g \cdot (\rho_f - \rho_g) \mu_f g \cos \varphi}{x^2 (1-x) \pi} \right)^{1/3} \quad 2.11$$

where: $A_{fd} = \frac{A(1-\varepsilon)}{D^2}$; and $A_{gd} = \frac{A \cdot \varepsilon}{D^2}$

Stratified to intermittent flow/ annular flow transition

$$G_{wavy} = \left(\left(\frac{16 \cdot A_{gd} \cdot g D \rho_f \rho_g}{x^2 \pi^2 (1 - (2h_{fd} - 1)^2)^{0.5}} \right) \left[\frac{\pi^2}{25 \cdot h_{fd}^2} (1-x)^{-F_1} \left(\frac{We}{Fr} \right)^{-F_2} + \frac{1}{\cos \varphi} \right] \right)^{0.5} + 50 \quad 2.12$$

Transition for Annular flow to intermittent flow

$$X = \left[\left(0.34^{1/0.875} \left(\frac{\rho_g}{\rho_f} \right)^{-1/1.75} \left(\frac{\mu_g}{\mu_f} \right)^{-1/7} \right) + 1 \right]^{-1} \quad 2.13$$

Table 2.2: Heat transfer correlations and models

Thome *et al.* [21]

Condensation flow model

$$\alpha_p = \frac{\alpha_f R \theta + (2\pi - \theta) R \alpha_c}{2\pi R} \quad 2.14$$

Jaster and Kosky [55]

Condensation heat transfer correlation

$$\frac{\alpha D_i}{k_f} = 0.725 \left[\frac{\rho_f (\rho_f - \rho_g) h_{fg} g D^3 \epsilon_g^3}{k_f \mu_f (T_{sat} - T_{wall})} \right]^{1/4} \quad 2.15$$

Rosson and Myers [36]

Empirical correlation

$$Nu_{top} = 0.31 Re_g^{0.12} \left[\frac{\rho_f (\rho_f - \rho_g) g h_{fg}^* D^3}{k_f \mu_f (T_{sat} - T_{wall})} \right]^{1/4}; \text{ and } Nu_{bot} = \frac{\varphi_f \sqrt{8Re_f}}{5 \left[1 + \frac{\ln(1 + 5Pr_f)}{Pr_f} \right]} \quad 2.16$$

$$\text{But } \varphi_f = \sqrt{1 + \frac{1}{X_{tt}} + \frac{12}{X_{tt}}}$$

Mohseni, Akhavan-Behabadi and Saeedinia [56]

Empirical correlation

$$Nu = 1.371 Pr^{1/3} (GD/\mu_f)^{0.69} \left[\frac{(\rho_f/\rho_m)_{in}^{0.5} + (\rho_f/\rho_m)_{out}^{0.5}}{2} \right]^{0.91} (\Delta x D/L)^{0.29} \quad 2.17$$

$$\left(1 + (1-x)^{0.1} \cos(\theta_{ia} - 10^\circ) \right)^{0.2}$$

$$\text{where: } \rho_f/\rho_m = 1 + x(\rho_f - \rho_g)/\rho_g$$

2.5.4. The Thome-Hajal-Cavallini flow pattern-based heat transfer model.

The model of Thome *et al.* [21] assumes convective and film condensation as the two heat transfer mechanisms unlike the model used by Dobson and Chato [37]. The Dobson-Chato model is based on stratified and un-stratified flows, while the Thome-Hajal-Cavallini model assumes annular, stratified-wavy, stratified, mist and bubbly and intermittent flow patterns. However, intermittent and mist flow patterns have been treated as annular flow and bubbly

flow because they could not be modelled due to a lack of data. The effect of temperature difference is included, as its effect on the heat transfer coefficient for stratified flow is known experimentally.

Equation 2.14 shows the Thome-Hajal-Cavallini condensation flow model. Here, α_{tp} , α_f and α_c are the local condensing heat transfer coefficients, the Nusselt film-condensing coefficient on the top section of the tube and the convective condensation heat transfer coefficient respectively. R is the radius of the tube, and C , n and m being the imperial constants; δ and f_i are the film thickness and interfacial roughness correction factor respectively. Since the model was developed by observing the flow pattern, it is applied in the same way by identifying the flow pattern first.

$$\alpha_c = CRe_f^n Pr_f^m \frac{k_f}{\delta} f_i \quad 2.18$$

$$\alpha_f = 0.728 \left[\frac{\rho_f (\rho_f - \rho_g) g h_{fg} k_f^3}{\mu_f D_i (T_{sat} - T_w)} \right]^{1/4} \quad 2.19$$

$$A_f = \frac{2\pi - \theta}{8} \left[D^2 - (D - 2\delta)^2 \right] \quad 2.20$$

$$f_i = 1 + \left(\frac{u_g}{u_f} \right)^{0.5} \left(\frac{(\rho_f - \rho_g) g \delta^2}{\sigma} \right)^{1/4} \quad 2.21$$

$$\theta_{strat} = 2\pi - 2 \left\{ \frac{\pi(1 - \varepsilon) + \left(\frac{3\pi}{2} \right)^{1/3} \left[1 - 2(1 - \varepsilon) + (1 - \varepsilon)^{1/3} - \varepsilon^{1/3} \right] - \frac{1}{200} (1 - \varepsilon) \varepsilon [1 - 2(1 - \varepsilon)]}{\left[1 + 4 \left((1 - \varepsilon)^2 + \varepsilon^2 \right) \right]} \right\} \quad 2.22$$

$$\theta = \theta_{strat} \left[\frac{(G_{wavy} - G)}{(G_{wavy} - G_{strat})} \right]^{0.5} \quad 2.23$$

$$\alpha_f = 0.728 \left[\frac{\rho_f (\rho_f - \rho_g) g h_{fg} k_f^3}{\mu_f D (T_{sat} - T_w)} \right]^{1/3} \quad 2.24$$

For predicting the heat transfer coefficient for annular, mist and intermittent flow patterns, the model assumes that $\alpha_{tp} = \alpha_c$, hence the film thickness at the bottom of the tube is calculated by Equation 2.20; f_i and α_c are then obtained by Equation 2.21 and Equation 2.18 respectively, where-after Equation 2.22 is used to calculate θ , since for annular flow, $\theta = \theta_{strat}$.

For the stratified-wavy flow pattern, the prediction model for the heat transfer coefficient is calculated by determining the stratification angle θ_{strat} , and θ through Equations 2.22 and 2.23 first. Then, α_c and α_f are determined using Equations 2.18 and Equations 2.19. For determining the film thickness (δ) and the interfacial roughness correction factor (f_i), Equation 2.20 and Equation 2.21 are used. Lastly, the local heat transfer condensation, α_{tp} , can be calculated using Equation 2.14.

The final step is using the model to determine the heat transfer coefficient for a stratified flow. The stratification angle, θ_{strat} , is calculated by using Equation 2.22 and for the stratified flow pattern, $\theta_{strat} = \theta$. The film thickness, δ , and the interfacial correction factor, f_i , are calculated where-after Equations 2.18 and 2.19 for the convective condensation heat transfer coefficient (α_c) and α_f are determined. Finally Equation 2.14 for α_{tp} is determined for the stratified flow pattern. Although the effects of factors including diameter, temperature difference, void fraction mass flux, surface tension, film thickness, and flow pattern are considered in the model, the effect of the inclination of the tube is not considered.

2.5.5. Other heat transfer coefficient models

The correlation of Jaster and Kosky [55] assumes that heat transfer through the bottom, where the condensate layer is thicker, is negligible; hence, their correlation is based on the top part of the tube. Their model considers the effects of factors that include diameter, temperature difference, and void fraction, but the effect of fluid thickness, surface tension and inclination angle are not considered.

Mohseni et al. [56] use a Nusselt correlation, whereby the effect of vapour quality, mass flux and inclination angle are considered. The correlation manages to consider most of the parameters that are a function of the heat transfer coefficient. These are diameter, mass flux, quality and inclination angle. However, the effect of temperature difference is not considered.

2.6. Previous work on two-phase flow condensation

This section considers work regarding two-phase condensing flows carried out by Dobson and Chato [37], Dobson, Chato, Hinde and Wang [57], Aprea, Greco and Vanoli [58], Thome [12, 20, 42], Thome et al.[21] Thome and Hajal [59] Suliman Liebenberg and Meyer [60], Suliman, Kyembe and Meyer [61] and Park, Lee and Mudawar. [14]. The work includes condensation at low mass flux for horizontally inclined tubes, condensation at high mass fluxes at different inclination angles and condensation at low mass fluxes and different

inclination angles. However, the latter has little information as it has rarely been studied. The discussion highlights the experimental research outcomes of in-tube condensing flows.

2.6.1. Condensing two-phase flow patterns at low mass flux in horizontal tubes

Most of the work carried out in two-phase flow condensation has been for horizontal inclinations and high mass fluxes above $200 \text{ kg/m}^2\cdot\text{s}$, [22, 62-67]. According to Cheng *et al.* [1], few authors have ventured into the study of condensing two-phase flow pattern identification and analysis to date.

Flow patterns at mass fluxes of $100 \text{ kg/m}^2\cdot\text{s}$ and below in horizontal tubes differ from those at high mass fluxes, as gravity is the dominant driving force for low mass fluxes. In studies conducted by the few authors who have studied two-phase flow condensations at low mass fluxes in horizontal tubes, the mass fluxes ranged from $26 \text{ kg/m}^2\cdot\text{s}$ and above [14, 60, 61, 68-71].

Dobson and Chato [37] conducted an extensive study of condensation in smooth horizontal tubes. The study was carried out for a wider range of fluids with mass fluxes $25 \text{ kg/m}^2\cdot\text{s}$ and $800 \text{ kg/m}^2\cdot\text{s}$, an average quality of between 0.1 and 0.9, Saturation temperatures between $35 \text{ }^\circ\text{C}$ and $60 \text{ }^\circ\text{C}$, and a temperature difference of between $1.8 \text{ }^\circ\text{C}$ and $4 \text{ }^\circ\text{C}$. The study concluded that, mass flux and quality are the major factors that affect flow patterns. From mass fluxes of $25 \text{ kg/m}^2\cdot\text{s}$ up to $75 \text{ kg/m}^2\cdot\text{s}$, only stratified to stratified-wavy patterns were observed. A mass flux of $25 \text{ kg/m}^2\cdot\text{s}$ was confined to the stratified flow pattern for all the ranges of quality. Their data was plotted on the flow pattern map of Soliman [34, 72]. The flow pattern map does not have a stratified flow pattern, but only predicts wavy flow for the low mass flux range. For heat transfer coefficients at low mass fluxes, they reported a gradual or slight increase with the increase in quality. For low qualities and low mass fluxes, the Nusselt numbers are slightly higher compared to higher mass fluxes and low qualities. The heat transfer coefficient was reported to be slightly constant for the low mass flux range. The study also investigated the effect of temperature difference on the heat transfer coefficient. It was shown that the temperature difference has a significant impact on stratified and wavy flow patterns, which are gravity-driven flow patterns. As temperature difference increase, Nusselt numbers decrease for the full range of quality. A significant effect of temperature difference on the wavy flow pattern was recorded. The observed flow pattern for the lowest mass flux was stratified flow without interfacial waves. Heat transfer was reported to be dependent on the flow pattern. Film condensation was the governing means of heat transfer for the gravity-driven flows.

Apra *et al.* [58] investigated condensing heat transfer coefficients for R-22 and R-407C in smooth tubes. The refrigerating vapour compression plant ran at mass fluxes between $45.5 \text{ kg/m}^2\cdot\text{s}$ and $120 \text{ kg/m}^2\cdot\text{s}$. They mentioned that the gravity driven flow patterns were stratified, wavy, and intermittent and that heat transfer coefficients were enhanced at

higher vapour qualities and lower at low vapour qualities. As the condensate layer at the bottom of the tube reduced in thickness (increasing the interfacial area), the void fraction increased as quality increased. They also noted that the heat transfer coefficient dependence on vapour quality is stronger at high mass fluxes.

Hajal *et al.* [11] and Thome *et al.* [21] proposed and developed a flow pattern map and a heat transfer model for mass fluxes between $24 \text{ kg/m}^2\cdot\text{s}$ and $1\,022 \text{ kg/m}^2\cdot\text{s}$, vapour qualities between 0.03 and 0.97 and diameters between 3.1 mm and 21.4 mm. The map has mass flux and quality as co-ordinates and can be reliable and correct for the following range of parameters: $16 < G < 1\,532 \text{ kg/m}^2\cdot\text{s}$, $3.14 < D < 21.4 \text{ mm}$, $0.02 < Pr < 0.8$, and

$76 < \left(\frac{We}{Fr}\right) < 884$. where We is the Weber number and Fr is the Froude number. The map was an extension of Kattan *et al.* [10]. See further discussion in Section 1.1.2.

Suliman *et al.* [60] conducted a study of an improved flow pattern map and accurate prediction of heat transfer coefficients during condensation of R-134a in smooth horizontal tubes at mass fluxes of between $75 \text{ kg/m}^2\cdot\text{s}$ and $300 \text{ kg/m}^2\cdot\text{s}$. The study went on to incorporate the transition regions of annular, intermittent and stratified flow patterns into the Thome-Hajal flow map. Only two points are captured for heat transfer coefficients for the $75 \text{ kg/m}^2\cdot\text{s}$ mass flux. The study showed the improved flow pattern map of Kattan *et al.* [10], but experimental data was not shown on the new map. Another study by Suliman *et al.* [61], with mass flux between $67 \text{ kg/m}^2\cdot\text{s}$ and $162 \text{ kg/m}^2\cdot\text{s}$ for R-134a revealed temperature dependent results. The temperature difference between the wall temperature and the saturation temperature was found to be directly linked to the heat flux. The observed flow patterns were intermittent (slug and plug), stratified-wavy and stratified.

Park *et al.* [14] conducted experimental investigations to determine flow patterns and heat transfer coefficients for the condensation of FC-72 in horizontal tubes. The flow patterns that were identified were stratified, stratified-wavy and wavy-annular. The study used four different flow pattern maps to determine flow pattern transitions, comparing them to predictions of previous correlations [37, 73-77]. They concluded that gravity for refrigerant FC-72 played a big role for lower mass fluxes as evidenced by the observed stratified and stratified-wavy flow patterns.

2.6.2. Condensing flow patterns at high mass fluxes at different inclinations

Meyer *et al.* [23], and Lips and Meyer [25, 78] conducted two-phase flow condensation studies for tubes at inclination angles from -90° to $+90^\circ$, and the flow patterns observed were annular, wavy-annular, stratified-wavy, intermittent and churn flow. The studies highlighted a lack of experimental investigations into the prediction of heat transfer coefficient changes, with a change in inclination angle during phase change in condensing two-phase flow systems with most models and correlations having been derived for

horizontal tubes. Their study produced important and useful findings that include the following:-

- The inclination angle has an effect on the heat transfer coefficients and pressure drops, depending on the flow pattern being observed at a specified inclination angle;
- The optimum heat transfer coefficients can be observed at some condition and specific inclination angle;
- There is a need for two-phase flow modelling in terms of heat transfer, pressure drops, flow patterns maps and void fractions at different inclined angles;
- For high mass fluxes, the flow pattern remained annular at high vapour qualities whatever the inclination angle. On the other hand, at low mass fluxes and low vapour qualities, the flow pattern depends strongly on inclination angle;
- The liquid layer thickness at the bottom for a stratified flow pattern strongly affects the heat transfer coefficient;
- New predictive tools are to be developed for flow pattern maps and heat transfer correlations in order to enhance heat transfer by just inclining the tubes for industrial processes;
- Two models in literature [2, 21] could not correctly predict flow pattern transitions for R-134a condensing in an inclined smooth tube with an inner diameter of 8.34 mm [25];
- There was a 20% increase in heat transfer coefficients at -15° downward flow.

2.6.3. Condensing two-phase flow patterns at low mass flux in inclined tubes

Two-phase flow condensation experiments at different inclination angles by Meyer *et al.* [23], and Lips and Meyer [25] were at higher mass fluxes above $100 \text{ kg/m}^2\cdot\text{s}$. However Mohseni *et al.* [56] investigated two-phase flow condensation in a smooth tube with an internal diameter of 8.38 mm at different inclination angles and mass fluxes between $53 \text{ kg/m}^2\cdot\text{s}$ and $212 \text{ kg/m}^2\cdot\text{s}$. They discovered that, despite the quality and flow rate, for vertically downwards -90° , the flow is always annular due to the shear and gravity forces acting along the flow direction and at this inclination, which is where the heat transfer coefficient was the lowest. The study also specified that varying tube inclination meant a significant change in heat transfer coefficients, especially at low mass fluxes. The highest heat transfer coefficients were observed at low vapour qualities at an inclination angle of $+30^\circ$ (upward flow). This, however, is contrary to the results of Meyer *et al.* [23, 24].

Arslan and Eskin [46] conducted an experimental investigation into heat transfer characteristics for the condensing of R-134a in a vertical smooth tube at mass fluxes of between $20 \text{ kg/m}^2\cdot\text{s}$ and $75 \text{ kg/m}^2\cdot\text{s}$ in a copper tube with a diameter of 7.52 mm. However, the work only covered the heat transfer coefficient correlations and the only observed flow

pattern was annular. The study concluded that the rate of heat removal is directly proportional to the temperature difference.

2.7. Conclusion

This chapter highlights the work carried out in two-phase flow condensation systems. It discussed dimensionless parameters and other two-phase flow terminology relevant to the study, and provided a brief overview of two-phase flow condensation and gravity-driven flows. A general visual representation of flow patterns relevant to this study was shown and discussed. The relevant flow patterns include annular, stratified, wavy, intermittent (plug and slug flow), bubbly and churn flow patterns. The prediction of condensing flow patterns was given by two flow patterns: that of Soliman [34] and the that of Hajal *et al.* [11]. Finally, the work of Dobson and Chato [37], Hajal *et al.* [11] and other researchers was discussed in detail, emphasising the research out-comes relevant to this study. The flow pattern transition model of Hajal *et al.* [11] was also presented, as it made reference to Section 4.6. The literature review has highlighted investigations of condensing flow at low mass fluxes and different inclination angles, as it was observed that inclination affects the flow patterns and flow pattern transitions, and that heat transfer coefficients vary with inclination angle and flow patterns. The study and analysis of flow patterns and flow pattern transitions necessitates the accurate developments of flow pattern maps and heat transfer coefficient models.

3. Experimental set-up

3.1. Introduction

This chapter presents a description of the experimental set-up and test procedure for the vapour compression cycle used for the experimental investigations of condensing R-134a in a smooth circular tube. The main function of the test set-up is to allow data for in-tube condensation to be collected for a wide range of operating conditions. The experimental set-up has been used by various researchers [23, 60-62, 79, 80] in the Thermoflow Laboratories of the University of Pretoria's Department of Mechanical Engineering. The instrumentation, data acquisition, experimental uncertainties and data reduction methods are also discussed in this chapter.

3.2. Experimental set-up

Figure 3.1 shows the experimental set-up that consisted of two main cycles: the water cycle and the vapour-compression cycle. Below is a schematic diagram of the system set-up.

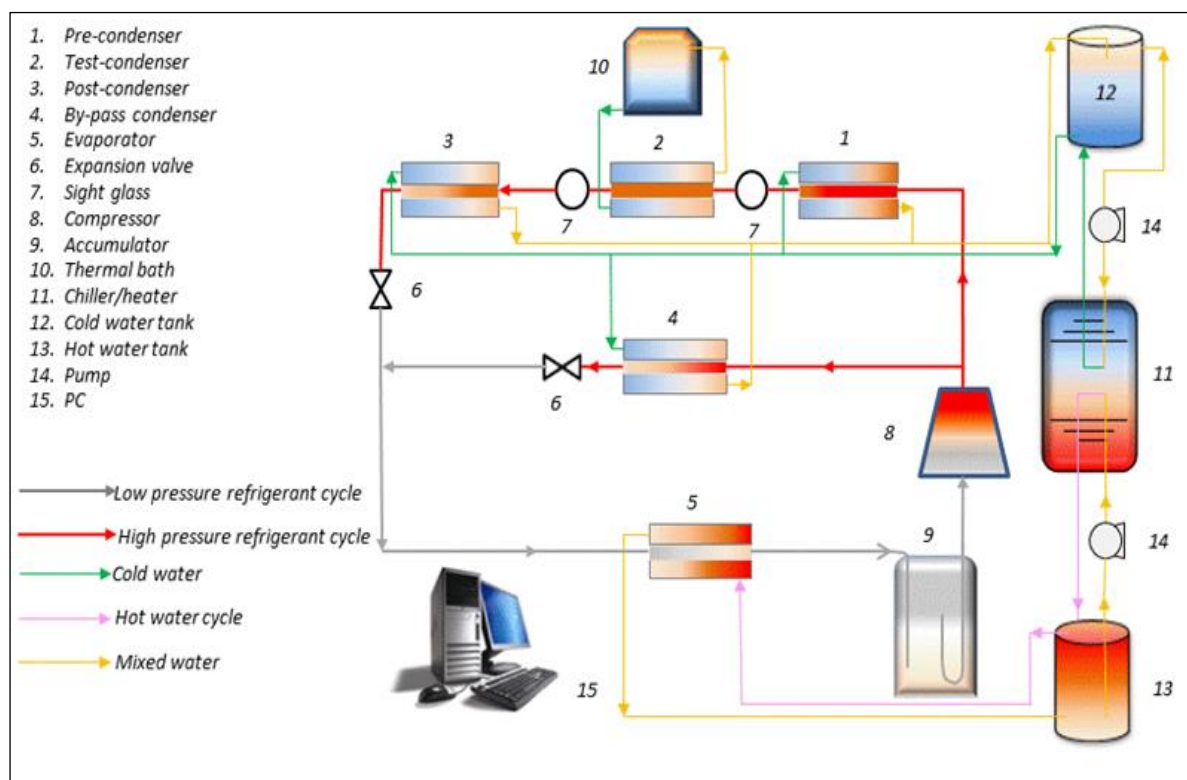


Figure 3.1: Experimental set-up

3.2.1. Vapour compression cycle

The vapour compression cycle consists of four main components: the compressor, suction accumulator, water-cooled heat exchangers, and expansion valves. The compressor is a

hermetically sealed Copeland scroll compressor with a cooling capacity of 10 kW. The suction accumulator was installed as a safety measure to protect the compressor from pumping excess liquid by storing the excess liquid and allowing only vapour and lubricating oil to the compressor. Four Carel electronic expansion valves (EEV) were installed with only two working at the same time. Two expansion valves were installed in the bypass line to control test pressure, while the other two were installed in the test line to control the mass flow through the test line. The heat exchangers consisted of four condensers, the fluted tube coil post-condenser, the in-tube test condenser, the fluted tube coil pre-condenser and the fluted tube coil bypass condenser in the high-pressure line and a fluted tube coil evaporator in the low pressure-line. The pre-condenser was used to regulate the inlet quality into the test condenser where the test data was collected, and the post-condenser ensured total condensation of the vapour into liquid before the expansion valves. The pre-condenser had two parallel heat exchangers, the smaller pre-condenser for low mass fluxes with a heating capacity of 2.5 kW and a large pre-condenser with a heating capacity of 10 kW. Hence, if working with mass fluxes of $100 \text{ kg/m}^2 \cdot \text{s}$ and below, the smaller pre-condenser was selected, and vice versa for the large pre-condenser. However, for the experiment in this study, a smaller pre-condenser was used. The by-pass condenser was used to regulate the pressure, temperature and mass flow rate through the test section. Six needle valve pressure gauges were also installed on the test inlet and outlet, as well as the outlet of the compressor before the expansion valves, post-condenser inlet and outlet, and pre-condenser inlet.

For safety, there were low-pressure (LP) and high-pressure (HP) switches installed to prevent damage to the system. The low-pressure switch switched off once the suction line pressure dropped to 3 bars, while the high-pressure switch switched off when the compressor discharge pressure was more than 25 bars. Another safety high-pressure switch (SHP) ensured that the system could not be switched on if the suction pressure rose to 12 bars due to the increase in the ambient temperature. The system could only be switched on once the pressure reduced to below 9 bars, which was achieved by running 15°C of cold water through the system.

3.2.2. Water cycle

The water cycle consists of the hot and the cold water loops, water pumps, mixing valves, dual heat pump, thermal bath and flow meters. The hot water loop exchanges heat with the refrigerant in the evaporator, while the cold water loop acts as a heat sink in the condenser. The cold water loop was set at between 15°C and 20°C , with cold water for the pre-condenser and post-condenser supplied by a 70 kW cooling dual heat pump that also supplied the evaporator and had a heating capacity of 50 kW. The hot and cold water was stored individually in an insulated 5 000 litre tank. The test section, however, was supplied with cold water by a luada thermal bath. The water temperature from the thermal bath could be reduced to as low as 10°C and increased to more than 25°C , depending on the

required testing conditions. The water for the pre-condenser and post-condenser was pumped by Ebara CMA-050M water pumps, with a head of 6 m above the test set-up. Ebara CMB-100M with a high-volume flow rate and constant head were selected for the evaporator and bypass condenser. Honeywell DN16 KVS 4.0 and DN20 KVS 6.3; three-way mixing valves were used to vary the mass flow rate in the heat exchangers. The set-up included six mixing valves, three small ones working with the CMA-050M water pumps and three bigger ones working with the CMB-100M water pumps. The valves receive a signal input of 0-10 V for valve control. The Burkert DN 15 flow meters, with a range of between 0.017 kg/s and 0.5 kg/s were used for the post-condenser to measure the flow rate, where-after the data was sent to the National Instruments data acquisition system. This data was then used by the three-way mixing valves to regulate the flow required for the desired testing conditions. Like-wise, the Burkert DN 25 flow meters, with a cooling capacity of between 0.1 kg/s and 2.0 kg/s, were also used for the bypass and the evaporator.

3.3. Test section

The test section consisted of an in-tube counter-flow heat exchanger, with the cooling water from the Lauda thermal bath on the annulus and the refrigerant in the inner tube. The inner tube was 1 500 mm long with an inside hydraulic diameter of 8.38 mm and a tube thickness of approximately 0.575 mm. The tube was copper with a thermal conductivity of 0.034 W/m.K. The annulus internal diameter was 14.5 mm and the test section was insulated to minimise the heat loss with an insulation of thermal conductivity of 0.041.W/m.K. There were 28 T-type thermocouples at each station along the circumference of the outer test tube, to measure the wall temperatures. Four thermocouples were placed at the same axial position around the circumference of the outer tube. The thermocouples were placed on the top, bottom and sides of the tube wall, equidistance from each other, to make seven thermocouple stations along the test section. The test section could be inclined from +90° to -90°. Two calming sections, one at the inlet and the other at the outlet 50 diameters long, were placed so that fully developed flow would be maintained at the inlet, which meant that the flow was not disturbed in the test section or the outlet sight glass.

3.3.1. Flow visualisation

Flow visualisation was accomplished by two high-speed Basler A601f monochrome cameras fitted on the inlet and outlet to the test section. Two sight glasses were installed on the inlet and the outlet to view the flow. The sight glass consisted of two boron-silicate tubes, the inner refrigerant tube and the outer safety tube. The assembly of the sight glasses is fully described by Christians [54]. The inlet Basler camera was fitted with a Myutron 25 mm zoom lens and a 60 x 60 CCS QL red backlight. The outlet, on the other hand, had a Basler camera fitted with a 25 mm Myutron lens and a Phlox 50 x 50 red backlight. Pylon viewer software was used for flow visualisation and video capturing. The maximum frame rate of the camera

at a very low resolution was 200 frames per second (fps), however, for clarity and high resolution, a maximum of 60 fps was used, and up to 500 frames were captured for each instance. The frame sizes were 500 x 270 and 494 x 200 due to the slight differences in the lenses used.

3.4. Instrumentation

The signal from the mass flow meters, mixing valves, thermocouples, expansion valves and pressure transducers was collected with a National Instrument data acquisition system and was controlled using a computer. The user can regulate the mixing valves, expansion valves and mass flow meters via the National instruments dashboard. The following six parameters were controlled and kept constant: mass flow rate, quality, saturation temperature, condensing temperature difference (ΔT_{ref}) of the inlet and the outlet of the refrigerant in the test section, energy balance and temperature difference (ΔT) between the wall and the saturation temperatures. Data was always captured when the energy balance was below 5% and the temperature difference between the wall and saturation temperature was kept constant to about ± 0.1 °C or 0.2 °C tolerance. The temperature difference of the refrigerant was also kept constant at 0.2 °C. Except for other conditions where the system was not stable, the temperature difference could go as far as 0.6 °C.

3.4.1. Pressure transducers

Two differential transducers were used for the test section to measure pressure drop across the test section, 0.86 kPa and 8.6 kPa. This was incorporated to ensure greater accuracy for the low pressure drops below 0.8 kPa and for higher pressure drops. High pressure drops were mainly observed at vertically upward inclinations.

3.5. Data reduction

In order to get the thermo-physical properties of the refrigerant condensate, the properties of the refrigerant were measured on the inlet of the pre-condenser, as well as the outlet of the post-condenser, and data for the refrigerant properties was obtained from REFPROP [81]. Hence, other properties of the refrigerant, such as quality, enthalpies for the inlet and outlet to the test section, and the heat transfer coefficient across the test section, were calculated.

The quality of the inlet vapour to the test section and the outlet vapour were calculated from the enthalpies as in Equations 3.1 and 3.2. However, the enthalpy on the inlet to the test section had to be calculated first. The mean vapour quality is given in Equation 3.3.

$$X_{in} = \frac{h_{test,in} - h_f}{h_v - h_f} \quad 3.1$$

$$X_{out} = \frac{h_{test,out} - h_f}{h_v - h_f} \quad 3.2$$

$$X_{avg} = \frac{X_{in} + X_{out}}{2} \quad 3.3$$

The vapour enthalpy (h_v) and liquid enthalpy (h_f) were evaluated from the saturation temperature and pressure measured at the inlet to the test section by REFPROP. In addition, properties of the working fluid on the inlet and the outlet of the pre-condenser and the outlet of the post-condenser were determined from the pressure and temperature measurements. Thus, the enthalpy at the inlet to the test condenser ($h_{test,in}$) lay somewhere within the two-phase. For this reason, it was calculated by the enthalpy at the inlet to the pre-condenser, the mass flow rate of the refrigerant and the heat transferred on the water-side, as can be seen in Equation 3.4. The inlet enthalpy to the pre-condenser was evaluated from the temperature and pressure, as it lay in the superheated region.

$$h_{test,in} = h_{pre,in} - \frac{|\dot{Q}_{pre,water}|}{\dot{m}_{ref}} \quad 3.4$$

Assumptions made for the rate of heat transfer on the refrigerant side in the pre-condenser was that, the rate of heat transfer on the water-side in the annulus of the pre-condenser was equal to the rate of heat transfer on the refrigerant side of the pre-condenser, when losses were neglected. The same assumption for the heat transfer rate was also applied for the test and post-condensers on the refrigerant side. Hence, the heat that was transferred on the water-side was calculated by the product of the measured mass flow rate of water, the specific heat of the water and the temperature difference in and out of the pre-condenser as shown in Equation, 3.5.

$$\dot{Q}_{pre,water} \approx \dot{m}_{water} C_p (T_{pre,out} - T_{pre,in}) \quad 3.5$$

$$\dot{Q}_{test,water} \approx \dot{m}_{water} C_p (T_{test,out} - T_{test,in}) \quad 3.6$$

$$\dot{Q}_{post,water} \approx \dot{m}_{water} C_p (T_{post,out} - T_{post,in}) \quad 3.7$$

The rate of heat transfer (on the water-side) or annulus for the test section was calculated in the same way as in Equation 3.5, except that the temperature difference will be the temperature to the inlet and the outlet of the test section, as can be seen in Equation 3.6. Likewise, the rate of heat transfer for the post-condenser was determined in the same way, as illustrated by Equation 3.7. Therefore, the outlet enthalpy at the test section outlet could be deduced from the inlet enthalpy to the test section and the rate of heat transfer on the

water-side in the test section and the mass flow rate of the refrigerant, as can be seen in Equation 3.8.

$$h_{test_out} = h_{test_in} - \frac{|\dot{Q}_{test_water}|}{\dot{m}_{ref}} \quad 3.8$$

The total heat lost by the refrigerant to the water \dot{Q}_{ref_tot} was calculated as follows:

$$\dot{Q}_{ref_tot} = \dot{m}_{ref} (h_{ref_pre_in} - h_{post_out}) \quad 3.9$$

But the total heat gained by the water in the annulus is the sum of the heat gained by the water in the pre-condenser, in the test section and in the post-condenser.

$$\dot{Q}_{water_tot} = \dot{Q}_{pre_water} + \dot{Q}_{test_water} + \dot{Q}_{post_water} \quad 3.10$$

Heat that was lost by the refrigerant in the test section was calculated by the differences in the inlet and the outlet enthalpies times the mass flow rate of the refrigerant, as is illustrated by Equation 3.11.

$$\dot{Q}_{test_ref} = \dot{m}_{ref} (h_{test_ref_in} - h_{test_ref_out}) \quad 3.11$$

The heat lost by the refrigerant could also be calculated by the heat balance, so that heat gained by the water in the annulus is equal to the heat lost by the refrigerant, thus assuming negligible heat losses. For this conclusion to be made, the energy balance was calculated by Equation 3.12. A very good energy balance of 5% and below ensured little heat loss to the surroundings, and also that the temperature measurements on the water side and the refrigerant side were correct.

$$EB = \frac{|\dot{Q}_{ref_tot} - \dot{Q}_{water_tot}|}{\dot{Q}_{ref_tot}} \quad 3.12$$

The heat transfer coefficient could then be calculated from Equation 3.14, with A being the internal surface area of the test tube, where $A = \pi D_i L$. T_{sat} is the average saturation temperature on the inlet and outlet of the test section, and is given by the following equation:

$$\bar{T}_{sat} = \frac{(T_{sat_in} + T_{sat_out})}{2} \quad 3.13$$

$$\alpha_{cond} = \left| \frac{\dot{Q}_{test, water}}{A(\bar{T}_{wall, in} - T_{sat})} \right| = \left| \frac{\dot{Q}_{test, ref}}{A(\bar{T}_{wall, in} - T_{sat})} \right| \quad 3.14$$

However, the average internal wall temperatures of the inlet and outlet had to be determined. These are presented in equations 3.15 and 3.17. The thermal resistance of the wall was evaluated from equation 3.16. Its functions are the inner and outer diameter of the test tube, the thermal conductivity of the copper and its length, although this was found to be too small and therefore was neglected.

$$\bar{T}_{wall, in} = \bar{T}_{wall, out} + |\dot{Q}_{test} R_{wall}| \quad 3.15$$

$$R_{wall} = \ln \left(\frac{d_o/d_i}{2\pi k_{cu} L} \right) \quad 3.16$$

$$\bar{T}_{wall, out} = \frac{1}{L} \sum_{j=1}^Z [(T_{wall, out}^{j+1} + T_{wall, out}^j)(z_{j+1} - z_j)] \quad 3.17$$

The average outlet wall temperature was determined by the trapezoidal numerical integration method, and is displayed in Equation 3.17. Finally, the heat transfer coefficient was calculated using Equation 3.14, and the heat transfer rate (\dot{Q}) was determined from the heat gained by the water in the test section as presented in Equation 3.6.

3.6. Experimental data range

Due to the instabilities and constant fluctuations on the refrigerant side, some deviations in mass flux, wall temperature, saturation temperature and quality were expected. Each experimental data point had 121 samples that were averaged. Uncertainty for the data points are calculated and presented in Appendix A, which shows a detailed calculation of the uncertainty. Spread-sheet for other mentioned values from the raw data can be provided. Table 2.1 shows experimental measurements, ranges and deviations from the desired measurement.

Table 3.1: Experimental criteria

Measurement	Range	Deviations	Units
Mass flow rate of refrigerant (G)	20 - 100	±5	kg/m ² .s
Temperature of the refrigerant (T _{sat})	35 - 40	±0.5	°C
Quality (x)	0.01 - 0.99	±0.01	-
Temperature difference (ΔT)	1 - 10	±0.2	°C

3.7. Uncertainty

The average uncertainty in the heat transfer coefficient for the experimental results was 3% for all the mass fluxes tested in this study. A complete summary of the uncertainty is given in Appendix A.15.

3.8. Experimental procedure and data acquisition

The day-to-day experimental procedure ran according to the experimental matrix drawn-up and is summarised in Section 4.2. The first test matrix Table 4.1, was for the horizontal inclination only, and, while other parameters (i.e. the Mass flux, temperature difference, saturation temperature, and inclination angle) were kept constant, Only the quality was varied from (0.05 to 0.9) per test set. The heat transfer coefficients could thus be compared for different qualities, and also for different mass fluxes. However, for the second test matrix, presented in Table 4.2, the tests were carried out for different inclination angles, while the other mentioned parameters were kept constant. Data was captured, and heat transfer coefficients calculated for different inclination angles. The study captured 121 samples for each data point, and these were averaged to get one data point.

3.9. Conclusion

This chapter gives a brief summary of the experimental set-up of the system used for the experimental investigations carried out in this study. A schematic diagram was presented, showing major components and cycles that make up the system. Two major cycles that made-up the system were the vapour compression cycle and the water cooling cycle. The main part of the system was the test section, where all test results were obtained. Apart from the in-tube heat exchanger, the test section included two clear sight glasses at the inlet and the outlet of the test section, which were used for flow visualisation. In order to capture the images, two high-speed cameras with red backlights were used. A brief discussion of the instrumentation used (i.e. pressure transducers), the way in which the data was deduced and the experimental uncertainties and ranges was also presented. Finally, the general outline of the experimental procedure was discussed.

4. Experimental data validation

4.1. Introduction

This chapter presents a validation of the experimental data by comparing it with work on the condensation of refrigerants by various authors. A comparison of other experimental data within the same range of operation (e.g. similar operating fluid, flow rates and saturation temperatures) is also presented. Current data is validated on the flow pattern map of Hajal *et al.* [11]., using experimental data. Heat transfer coefficients are validated with experimental data from various researchers in the two-phase flow condensation of refrigerants for both horizontal and inclined tubes.

4.2. Test matrix

All the experiments that were conducted for this study are summarised in Table 4.2. The tests were conducted at different mass fluxes, qualities, temperature difference between the wall temperature and the saturation temperature, and inclination angles at a saturation temperature of 40 °C. Videos were also captured on the inlet to the test section and on the outlet from the test section in order to monitor the flow patterns. The first test to be conducted was for the horizontal inclination (0°) for validation purposes. Tests for different inclinations were done. A test matrix for the horizontal configuration is given in Table 4.1.

Table 4.1: Test matrix for the horizontal configuration

Mass flux [kg/m ² .s]	Inclination angles [°]	Mean quality [-]	Temperature difference [°C]	Saturation temperature [°C]	Total	Videos inlet and outlet
100	0	0.096 to 0.81	3,5,8,10	40	35	35
75	0	0.1 to 0.74	3, 5,	40	13	13
50	0	0.1 to 0.75	1, 3, 5	40	14	14
20	0	0.1 to 0.55	1	40	3	16
Total					65	78

The inclination angles from positive to negative (+90° to -90°) include the following angles; (0, 5, 10, 15, 30, 45, 60, 90, 0; -5, -10, -15, -30, -45, -60 and -90)°. The angle 0° is the horizontal inclination. It is repeated because tests were conducted from the horizontal inclination, then to upward inclinations (positive) up to 90°, then back to the horizontal, and then to the downward inclinations (negative) to -90°. The list of inclination angles stated above is therefore in the sequence of the experimental tests conducted for the inclined angles.

Table 4.2: Test matrix for the inclined configuration

Mass flux [kg/m ² .s]	Inclination angles [°]	Mean quality [-]	Temperature difference [°C]	Saturation temperature [°C]	Total	Videos inlet and outlet
100	-90 to +90	0.25, 0.35, 0.5, 0.62, 0.75	3, 5, 8, 10	40	223	223
75	-90 to +90	0.25, 0.35, 0.5, 0.62, 0.75	3, 5, 8	40	141	141
50	-90 to +90	0.35, 0.5, 0.62, 0.75	1, 3	40	110	110
25	-90 to +90	0.75	1	40	16	16
Total					490	490

4.3. Flow pattern map

As stated in chapters 1 and Chapter 2 a number of different flow pattern maps have been developed. As the flow pattern has an effect on the heat transfer coefficient, flow pattern maps have become useful for designers, because they can predict heat transfer coefficients through knowledge of the fluid properties, diameter of the tube, quality and flow rate. The flow pattern map of Hajal *et al.* [11] is compared with the data collected in this study to see if the flow patterns can be predicted correctly as observed in the experiments.

4.3.1. The Hajal-Thome-Cavallini flow pattern map

The study's experimental data is overlaid on the Hajal-Thome-Cavallini [11] flow pattern map, in Figure 4.1. The study's data shows stratified-wavy and stratified flow patterns as the dominant flow patterns for condensing flow in a smooth horizontal tube. The stratified flow pattern, as defined by Collier and Thome [33], is characterised by two phases that flow separately with a smooth interface: the liquid phase, occupying the bottom section of the tube, and the gas phase in the upper part of the tube. Thome *at al.* [21] define the stratified-wavy flow pattern as having waves that are small in amplitude and do not rise to touch the top of the tube. As can be seen in Figure 4.1, as the mass flow rate is reduced, stratification increases with an increase in quality, so much so that at mass fluxes below 35kg/m².s, the flow is fully stratified for all vapour qualities. However, there are slight differences when it comes to very low qualities for 100 kg/m².s mass velocity. The differences can be attributed to the transition from stratified to stratified-wavy flow patterns. All points closer to the transition line could be on either side of the flow pattern. The flow pattern that is observed can either be stratified or stratified-wavy, as the waves begin to form slightly at some interval. The point could thus lie in the transition region.

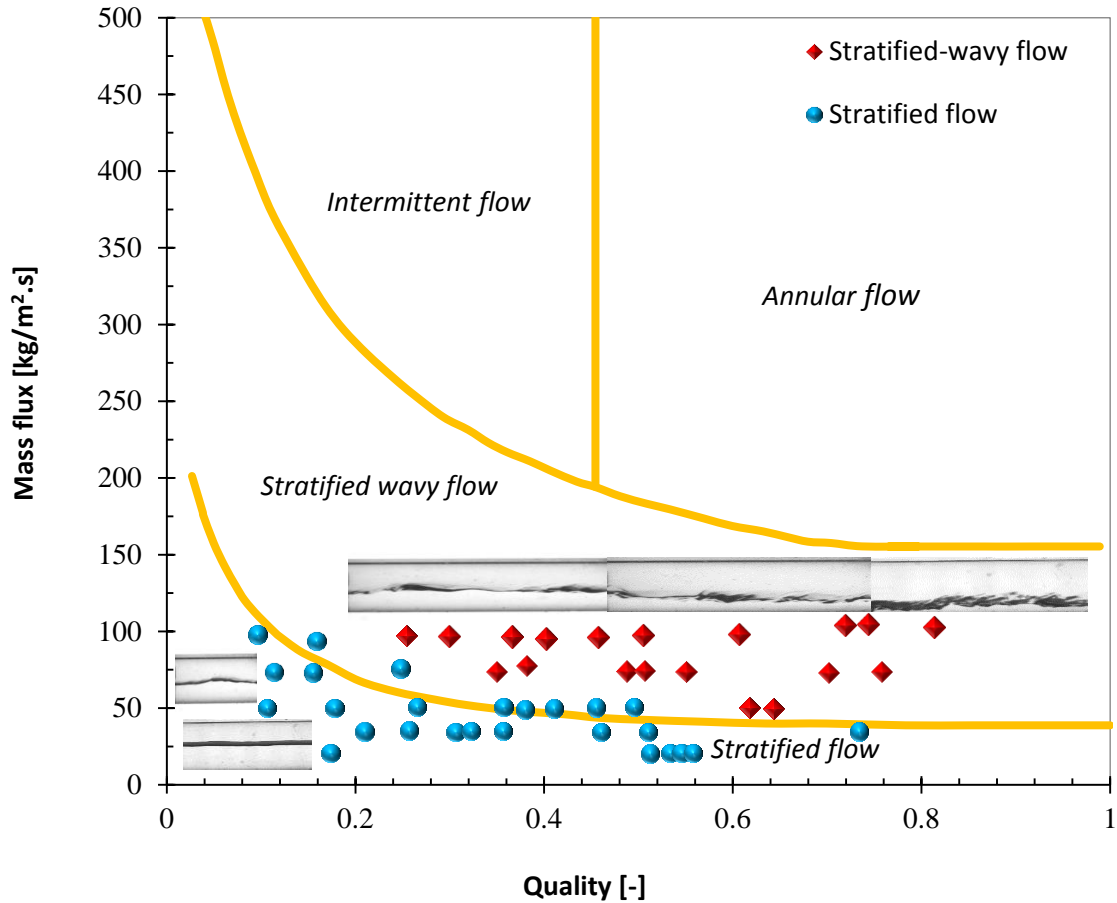


Figure 4.1: Current data on the Hajal-Thome-Cavallini flow pattern map

4.4. Heat transfer data comparison in horizontal tubes

A comparison of heat transfer coefficients for the horizontal inclination was carried out using data from various researchers. Due to slight differences in parameters like working fluid properties, tube diameter, saturation temperatures, mass velocity, and test set-ups, there are expected differences in heat transfer coefficients. However, almost similar experimental parameters to other researchers were used to validate this study's experimental data. Most comparisons shown in this section are for R-134a, with saturation temperatures of 40 °C, mass fluxes of 100 kg/m².s or less, and tube diameters close to 8 mm, ±1.5 mm.

4.4.1. Data comparison

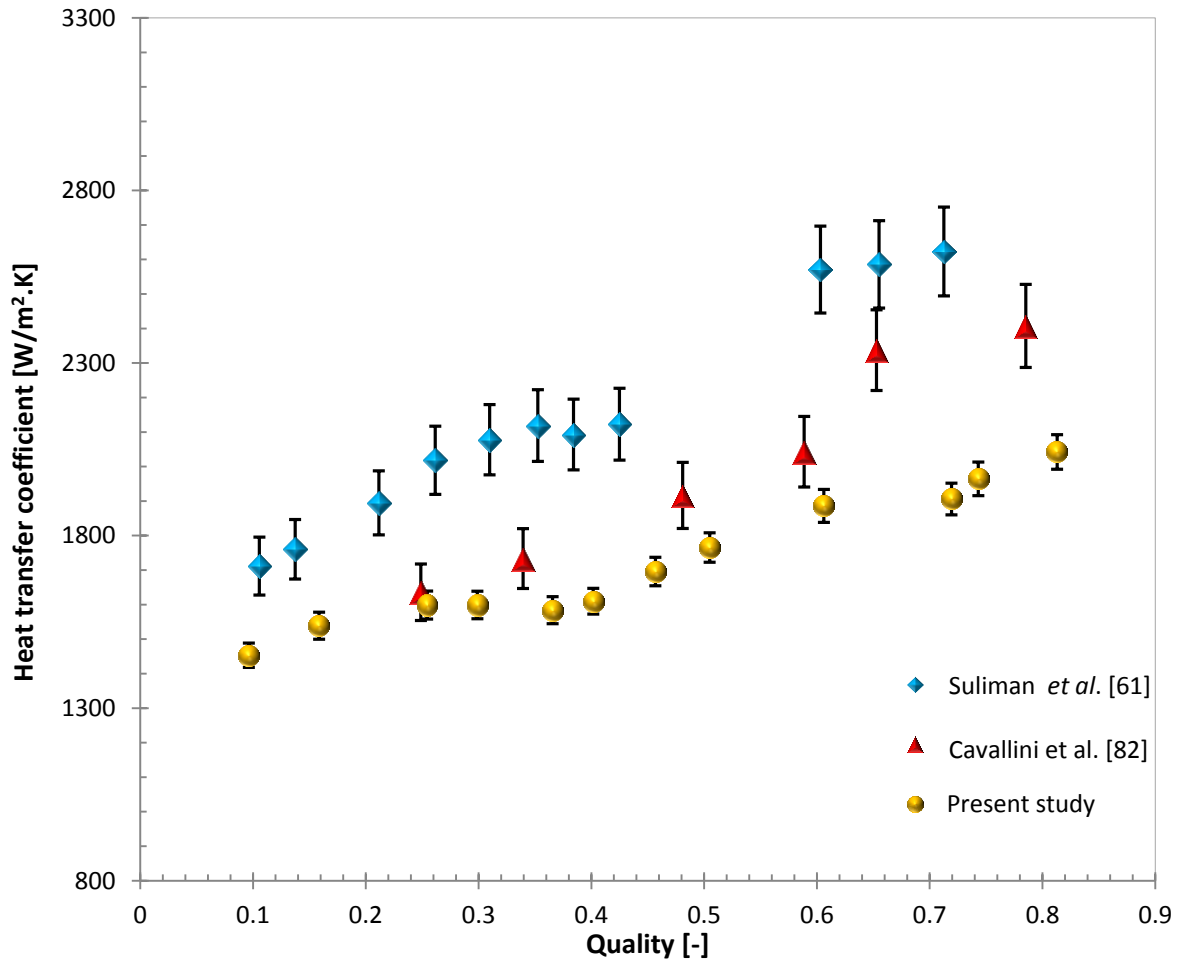


Figure 4.2: Heat transfer coefficient comparison at $G = 100 \text{ kg/m}^2\cdot\text{s}$ and 40°C saturation temperature

Experimental data of heat transfer coefficients for Suliman *et al.* [61] and Cavallini *et al.* [82] at a mass flux of $100 \text{ kg/m}^2\cdot\text{s}$ is shown in Figure 4.2. Suliman heat transfer coefficients are between 10% and 15% higher than Cavallini *et al.*[82] and even the present experimental data. The reason for the differences is the difference in the driving temperature which is due to the difference in the wall temperature as the saturation temperature was the same at 40°C for Suliman experimental data and the present study. The other difference was the differences in the boundary conditions for the experimental data of Cavallini, the heat transfer rate was kept constant at 200 W through the experiment while the heat transfer rate for the present study varied from 171 W at low qualities to 237W at higher qualities hence the driving temperature difference was kept constant at $3^\circ\text{C} \pm 0.2^\circ\text{C}$ for the experimental data in Figure 4.2. For the data of Suliman, temperature difference was as low as 0.6°C to 1.8°C , while for the present data; the temperature difference was maintained at $3^\circ\text{C} \pm 0.2^\circ\text{C}$. The experimental data of Cavallini had the driving temperature difference approximately 3°C for a quality of 0.25 and decreasing as quality increased. If the rate of

heat transfer rate \dot{Q} was kept constant at 200 W then at a higher quality of 0.79, where the heat transfer coefficient is approximately 2408 W/m².K, and the tube length is 1.6 m and tube diameter, 8 mm then the driving temperature at this point would be approximately 2.07 °C. The saturation temperature for the experiments was 40 °C and the wall temperatures for this experiment for the current study Figure 4.2 ranged between 35.9 °C and 37.2 °C. This concludes that for the driving temperature difference below 3 C then the wall temperature was higher than the above wall temperature range. Hence the differences in the heat transfer coefficients of approximately 13% at lower qualities and 32% for higher qualities.

4.5. Heat transfer data comparison in inclined tubes

With the limited number of studies for inclined tubes at low mass fluxes, the present data for the heat transfer coefficients was compared to Olivier *et al.*, [24] and Meyer *et al.*, [23] for a mass flux of 100 kg/m².s. The data comparison was conducted from the same test set-up, but under different operating conditions and boundary conditions. Although the boundary conditions were different and no other work could be used to validate the experimental data, Meyer and Olivier's studies were used just to show the behaviour of the heat transfer coefficient when inclination angle was varied.

Figure 4.3 (a), Figure 4.3 (b) and Figure 4.3 (c) show the experimental data of Meyer *et al.*, [23], Olivier *et al.*, [24] and the present study of the heat transfer coefficients for a mass flux of 100 kg/m².s, a saturation temperature of 40 °C and the R-134a refrigerant. The diameter of the tube was 8.38 mm for all the studies whilst the tube length was 1.488 m for both Olivier and Meyer. The major difference in these tests was the boundary conditions. Meyer controlled the heat transfer rate between 230 W and 270 W, while Olivier kept the heat transfer rate constant at 200 W. If the heat transfer rate of Olivier was kept constant at 200 W then the temperature difference at -15° would be around 2°C hence the higher heat transfer coefficient than the current data. For this data set however the temperature difference was kept constant at 3 °C ±0.2 °C. The differences in the heat transfer rate for all the studies was due to the differences in the wall temperature as saturation temperature was kept constant at 40 °C. The wall temperature for the present study was kept constant whilst for those of Meyer and Olivier the wall temperatures would vary.

From the graphs, it can be concluded that the maximum angle for the highest heat transfer is between -10° and -30° (downward flow). The present study shows maximum heat transfer coefficient to be at angles between -15° and -30°. This corresponds with the results of Meyer *et al.*, [23], which also indicate maximum heat transfer coefficients between the angles of -15° and -30° for qualities of 0.75 and 0.5. The graphs show the same trend for the negative inclination (which is the downward flow), whereby the heat transfer increases steadily from the horizontal up to either -10° or -15°, and then decreases sharply from -60°

to -90° . The heat transfer coefficient was lowest at the inclination angle of -90° for all the studies.

4.5.1. Heat transfer comparison for different qualities and inclination angles

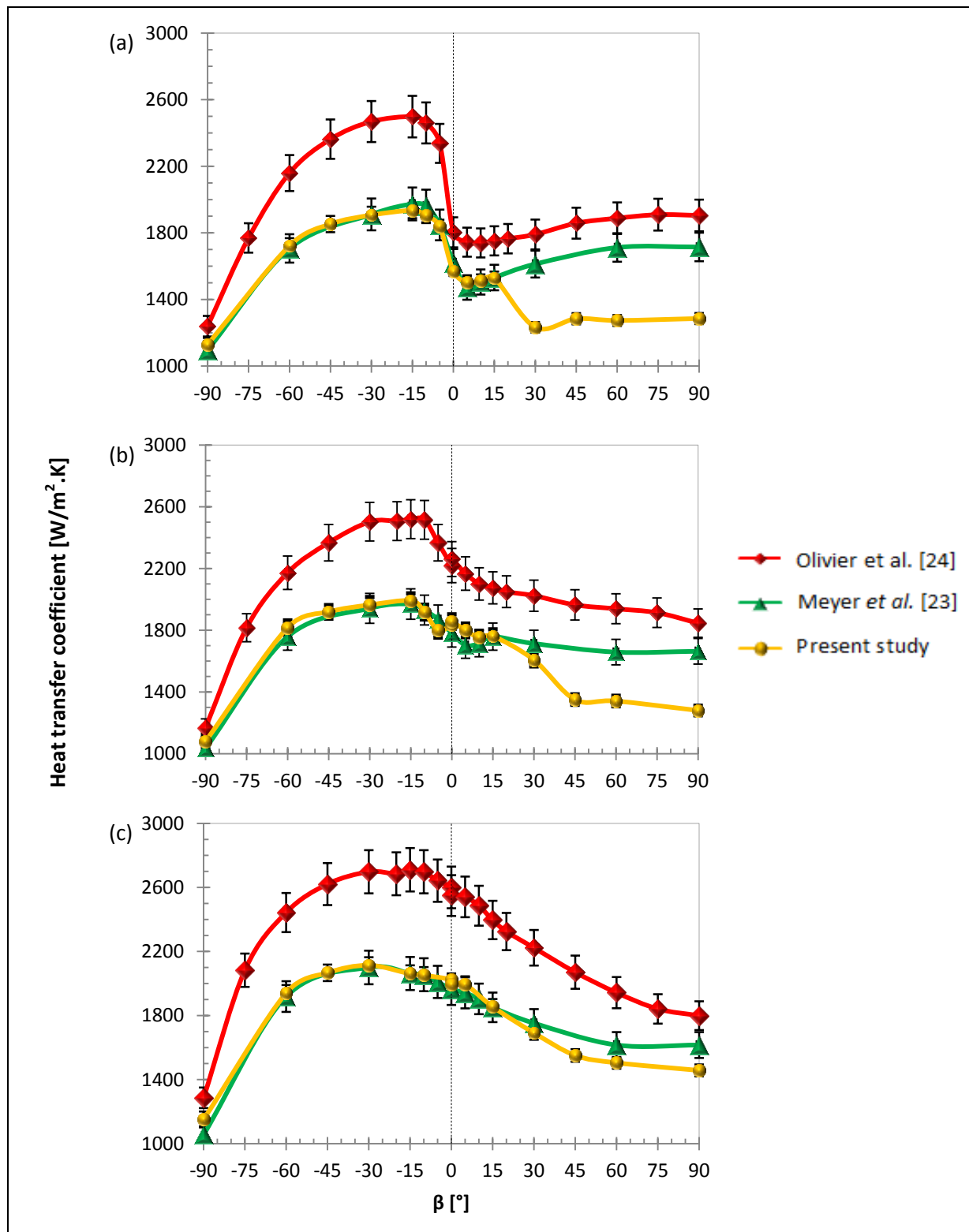


Figure 4.3: Comparison of heat transfer coefficients at (a) $x = 0.25$, (b) $x = 0.5$ and (c) $x = 0.75$

4.6. Flow pattern transition

Table 4.3: Flow pattern prediction using Thome-El Hajal flow pattern model

Quality [-]	Mass flow rate [kg/m ² .s]	G_{strat} [kg/m ² .s]	G_{wavy} [kg/m ² .s]	Flow pattern Stratified = $G < G_{strat}$ Stratified-wavy = $G_{strat} < G < G_{wavy}$
0.1	98	140	338	Stratified
0.16	94	100	284	Stratified
0.25	98	72	236	Stratified-wavy
0.3	97	65	220	Stratified-wavy
0.37	97	58	201	Stratified-wavy
0.4	95	55	192	Stratified-wavy
0.46	97	51	182	Stratified-wavy
0.51	98	49	173	Stratified-wavy
0.61	98	46	158	Stratified-wavy
0.72	105	44	147	Stratified-wavy
0.74	105	43	145	Stratified-wavy
0.81	103	43	144	Stratified-wavy

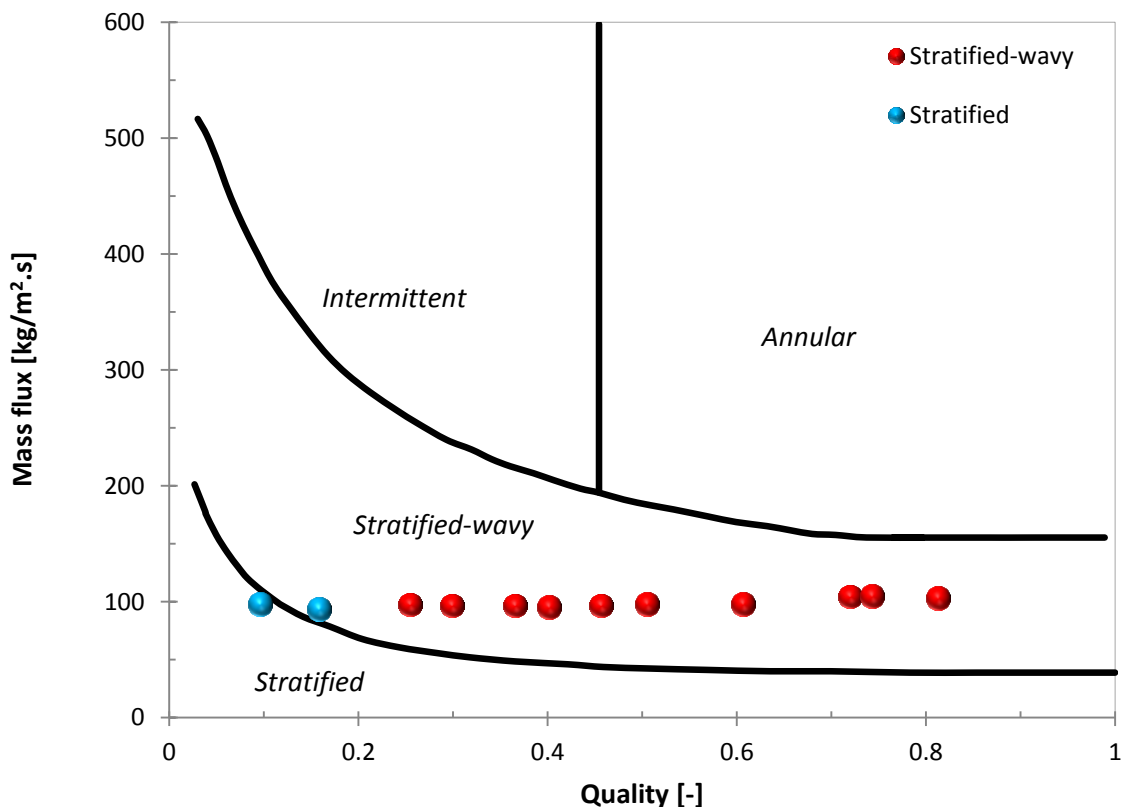


Figure 4.4: Hajal-Thome-Cavallini flow pattern map and flow pattern transitions

Table 4.3 and Figure 4.4 show the experimental data for the current studies for a mass flux of 100 kg/m².s at different qualities. Using the transition model of Hajal *et al.* [11], it can be noted that most of the data points are predicted as stratified-wavy, except for two data

points at the lowest quality, which are predicted as stratified flow (see Equations 2.11 and 2.13). With the same data plotted on their flow pattern map, only two data points of qualities of 0.09 and 0.15 are predicted as stratified flow. The second point of 0.15 is very close to the transition region from Stratified to stratified-wavy flow patterns.

4.7. Flow patterns

The visualised flow patterns from the inlet to the test section and the outlet from the test section are depicted in Figure 4.5 for the given vapour qualities. The flow pattern transition correlation for stratified-wavy of Hajal *et al.* [11] can predict the flow patterns observed during condensation as shown in Figure 4.5 and Table 4.3. There is a clear evolution in the wave structure as the vapour condenses from the inlet to the outlet of the test section. At higher liquid velocities vapour shear on the liquid interface causes significant wave formation on the liquid vapour interface that travel in the direction of the flow. As can be seen in Figure 4.5, for qualities of 0.3 upwards, on the inlet to the test condenser, the wave amplitude is quiet distinct depending on the velocities of the two phases (liquid and gas). Due to further heat removal along the test condenser, vapour velocity is reduced causing a reduction in the vapour shear on the liquid film. The liquid condensate from the top of the tube falls down to the bottom increasing the liquid pool at the bottom of the tube. There is an increase in liquid film thickness at the bottom of the tube from the inlet to the test condenser to the outlet. The condensate liquid height also increases with a decrease in quality with the flow transitioning from stratified-wavy to stratified flow pattern as the liquid film from the top of the tubes falls to the bottom due to the increase in the gravity effects [42]. This results in the complete separation of the two-phases with the liquid vapour interface becoming smooth without waves as vapour shear forces become negligible at low qualities. This constitutes a reduction in the heat transfer coefficient at lower qualities as the liquid height or condensate thickness increases.



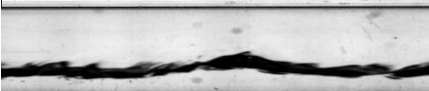
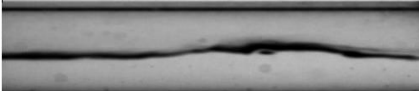
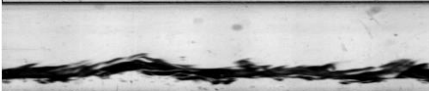









Quality	Inlet	Outlet	Observed flow pattern
0.1			<i>Stratified</i>
0.3			<i>Stratified-wavy</i>
0.4			<i>Stratified-wavy</i>
0.5			<i>Stratified-wavy</i>
0.6			<i>Stratified-wavy</i>
0.75			<i>Stratified-wavy</i>
0.83			<i>Stratified-wavy</i>

Figure 4.5: Flow pattern visualisation for a mass flux of $100 \text{ kg/m}^2\cdot\text{s}$, and temperature difference of $3 \text{ }^\circ\text{C}$

4.8. Summary and conclusion

This chapter presented the experimental validation for the tests carried out in the study. Firstly, two test matrices were presented in tabular form for condensation in a horizontal tube and other inclination angles. The first set of tests carried-out was only for the horizontal orientation at mass fluxes from $100 \text{ kg/m}^2\cdot\text{s}$ and below. For the horizontal inclinations, quality was varied, while the other parameters (i.e. mass flux, temperature difference and saturation temperature) were held constant. For each set of experiments (for inclined angles), all the other parameters (i.e. quality, temperature difference, mass flux and saturation temperature) were kept constant, but the inclination angle was varied from 0° to $+90^\circ$, and from 0° to -90° . Experimental data of Suliman *et al.* [61] and Cavallini *et al.* [82], was used to validate the experimental data of the present study. It was not possible to find data that could validate well with the current study as no experimental data with the same boundary conditions of keeping the driving temperature difference constant at 3° for all the tests at a mass flux of $100 \text{ kg/m}^2\cdot\text{s}$ could be used. Although Dobson and Chato [37] did conduct tests at a temperature difference of 3°C , the fluid under study was R-32/R-125 in a 7.04 mm diameter tube and at a saturation temperature of 35°C . The data of Suliman was however used as the effect of temperature difference was employed but the range was very low at temperature differences between 0.6 and $1.8 \text{ }^\circ\text{C}$. This study was used in order to just depict the effect of temperature difference on the heat transfer

coefficient. On the other hand, the data of Cavallini was used for the horizontal inclinations as all the other parameters were very similar with the difference being on the heat transfer rate for Cavallini which was kept constant which means the driving temperature difference would vary, increasing with a reduction in quality. This resulted in the data only validating well at a quality of 0.25 whereby the driving temperature difference was almost the same. The same goes for the inclined experimental studies; no work has been conducted so far where temperature difference was kept constant. However the work of Meyer and Olivier was used so that similarities in the behavior of the heat transfer coefficient with inclination can be shown. What corresponded well was the inclination angles that yield higher heat transfer coefficients and the one that yield the lowest. It was observed that the inclination angle between -10° and -30° had the highest heat transfer coefficients and that the inclination angle of -90° yielded the lowest heat transfer coefficients.

Overly, heat transfer coefficient increased as quality was increased for most data points. The flow pattern transition model of Thome and Hajal [59] was used to validate the flow patterns that were observed. The model predicted well the flow patterns well except for one point that was close to the transition line. This was because the transition region from one flow pattern to another occur across a mass velocity of about $50 \text{ kg/m}^2\cdot\text{s}$, Thome *et al.* [21].

5. Results: flow patterns and heat transfer coefficients

5.1. Introduction

This chapter presents a discussion of the flow patterns and heat transfer coefficients for a mass flux of $100 \text{ kg/m}^2\cdot\text{s}$ and below. The main focus is on the effect of quality, mass flux and temperature difference between the wall temperature and the saturation temperature on the heat transfer coefficient. This is discussed for horizontal configurations, as well as various inclination angles. Firstly, various flow patterns that were observed in this study are presented, followed by the effects of quality, mass flux and temperature difference on the heat transfer coefficient for the horizontal configuration and other inclined configurations. Thereafter, a summary of the heat transfer coefficient, as a function of quality, mass flux and temperature difference, and a graphical representation of the heat transfer coefficient, as a function of inclination angle and quality, are presented and discussed. A summary of the flow patterns for different configurations and how the flow patterns are linked to the heat transfer coefficient are also presented. This includes the variation in film thickness, wave formation and different forms of the observed flow patterns.

All the data presented in this chapter is derived from the test matrix for the horizontal configuration presented in Table 4.1, and the inclined configurations for mass fluxes of $100 \text{ kg/m}^2\cdot\text{s}$, $75 \text{ kg/m}^2\cdot\text{s}$, $50 \text{ kg/m}^2\cdot\text{s}$ and $25 \text{ kg/m}^2\cdot\text{s}$, mean qualities 0.75 to 0.25, temperature difference of 1°C ; 3°C ; 5°C ; 8°C and 10°C , and saturation temperature of 40°C presented in Table 4.2. The flow patterns were captured at 60 fps. However, certain frames were selected to show the flow patterns. All the flow patterns not specified as “inlet” or “outlet” in this chapter was for the outlet from the test section and the qualities are averaged qualities from the inlet to the outlet of the test condenser.

5.2. Observed flow patterns in this study

Figure 5.1 shows different flow patterns that were observed in this study. A substantial number of names have been given to flow patterns to describe them, and these have generally been subjective. However, a clear consensus regarding the description of major flow patterns has been arrived at by a number of authors [25, 33, 42, 83-85]. These descriptions include, annular, wavy, stratified, intermittent and churn flow patterns. Hajal et al [11], Collier and Thome [33] and Thome *et al.* [42] have not shown any distinction between wavy and stratified-wavy flow patterns, but have rather used the terms interchangeably. Eight flow patterns were observed. These comprised the following: stratified-wavy, stratified, wavy, wavy-churn, intermittent, churn, annular and wavy-annular flow patterns. Five of these flow patterns (stratified, wavy, intermittent, churn and annular) are the main flow patterns, while the other three are transitional.

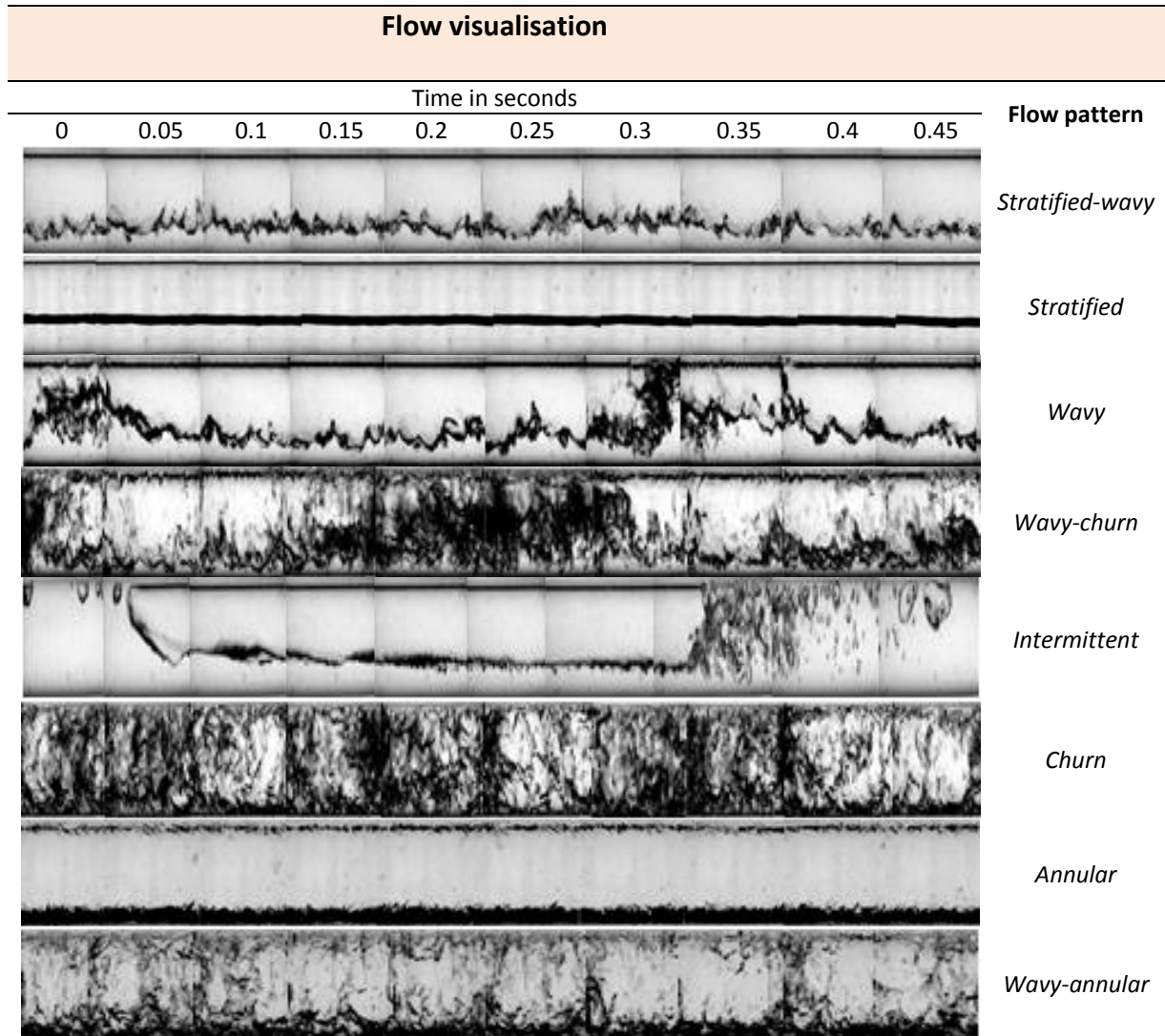


Figure 5.1: Observed flow patterns

The main flow patterns are identified in accordance with those defined by Collier and Thome [33]. The transitional flow patterns are a mixture of the main flow patterns like stratified-wavy, wavy-annular and wavy-churn. Wavy and stratified-wavy flow patterns have been observed as the same flow pattern. In this study however, the two flow patterns, wavy and stratified-wavy are treated separately; with stratified-wavy consisting of stratified flow with interfacial waves that have a reduced frequency and do not reach the diameter of the tube, and wavy consisting of waves with a higher frequency momentarily sweeping the inside roof of the tube as a continuous wave. Coleman and Garimella [48] separated these waves from discrete to dispersed wave flows. They defined the discrete waves as having large wave lengths and amplitudes, while the dispersed waves occur at higher mass fluxes. Waves of different structures make the liquid vapour interface indistinguishable. Nema, Garimella and Fronk [45] also makes reference to the wavy flow pattern. They specified that the waves regularly touch the top of the tube. Wavy-annular was defined by

Barnea *et al.* [43] as annular flow with some unstable waves that momentarily sweep through to the top of the tube.

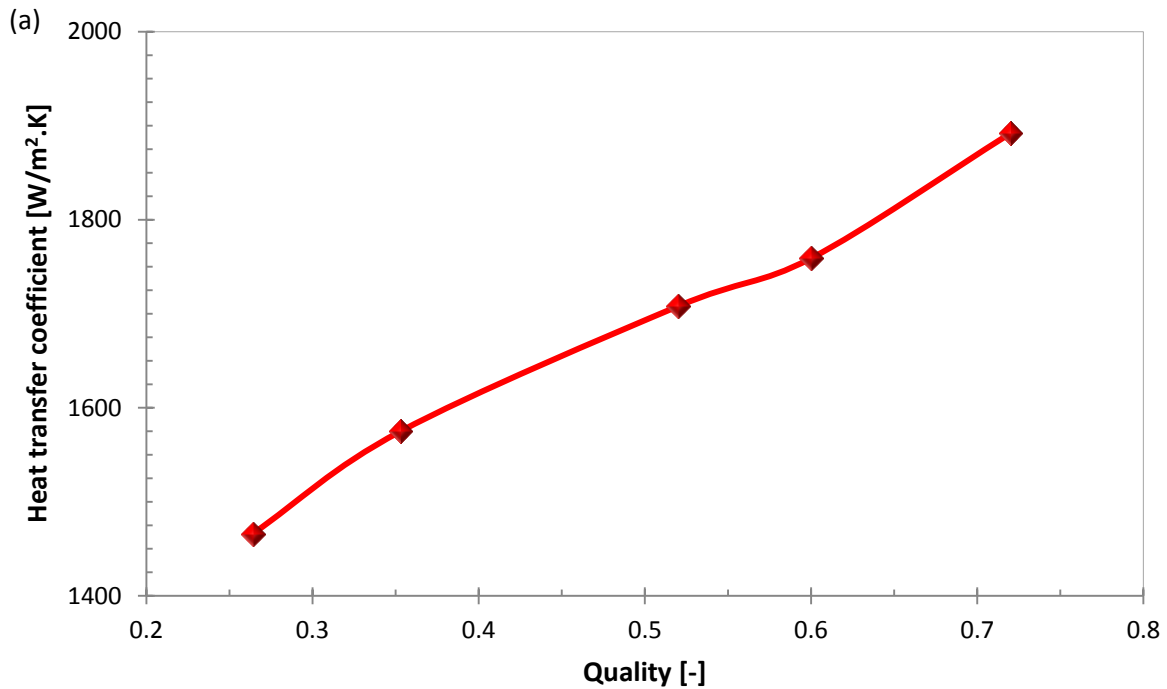
For wavy-churn flow, the waves have a much higher frequency and now and again the waves would sweep the periphery of the tube constantly with a slight churning effect and a stratifying effect at the bottom of the tube. In churn flow, the increase in the velocity of the flow destabilises the flow, causing the flow to have an oscillatory motion as the liquid condensate moves upwards and downwards due to the gravity and shear forces acting in opposite directions. The need to describe the flow patterns is fully supported by the images that are presented in Figure 5.1, and the rest of this chapter. The flow direction for all the images presented in this study is from right to left, and each frame represented in Figure 5.1 is 0.05 seconds apart. This means that, given the frame rate of 60 fps, every third image is used to show each flow pattern, so a total of ten frames are used. The flow patterns that were observed for the study were observed for different mass fluxes, qualities and inclinations.

5.3. Horizontal configuration: flow patterns and heat transfer coefficient

The observed flow patterns and the resultant heat transfer coefficients for the horizontal configuration are discussed in this section. The effects of quality, mass flux and temperature difference on the heat transfer coefficient are summarised and the prevailing flow patterns are also discussed. For the horizontal flow, only stratified and stratified-wavy flow patterns were observed. Stratification effects differed with quality, mass flux and temperature differences and this had a significant influence on the heat transfer coefficient. Only a mass flux of $100 \text{ kg/m}^2\cdot\text{s}$ was observed for Section 5.3.1 and Section 5.3.3, while all the other mass fluxes in this study are compared in Section 5.3.2.

5.3.1. Effect of quality

Figure 5.2 (a) and Figure 5.2 (b) show the heat transfer coefficients at different qualities and the observed flow patterns respectively. The analysis was done for a mass flux of $100 \text{ kg/m}^2\cdot\text{s}$ and a temperature difference of $5 \text{ }^\circ\text{C}$. The increase in the heat transfer coefficient was about 7% to 8% as quality increased.




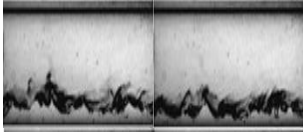

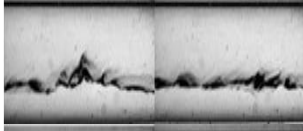
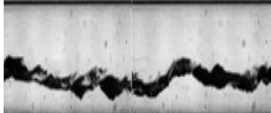
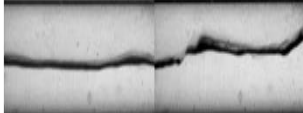
(b) Quality [-]	Inlet	Observed flow pattern	Outlet	Observed flow pattern
0.75		<i>Stratified-wavy</i>		<i>Stratified-wavy</i>
0.5		<i>Stratified-wavy</i>		<i>Stratified-wavy</i>
0.25		<i>Stratified-wavy</i>		<i>Stratified-wavy</i>

Figure 5.2: Effect of quality for the horizontal inclination at a mass flux of $100 \text{ kg/m}^2\cdot\text{s}$ and temperature difference of $5 \text{ }^\circ\text{C}$ on: (a) the heat transfer coefficient; and (b) the flow patterns

The increase in the heat transfer coefficient with an increase in quality was due to the interfacial wave instability and the decrease in the liquid film thickness at higher qualities. Dobson and Chato [37] mentioned that an increase in the vapour velocity causes a rise in the interfacial waves as the liquid-vapour interface becomes Helmholtz unstable, the flow pattern becomes wavy flow which in this case is stratified-wavy. The stratified flow pattern was only observed below a quality of 0.15 for a mass flux of $100 \text{ kg/m}^2\cdot\text{s}$. Above that, only a stratified-wavy flow pattern was observed. However, there are significant variations in the waves with quality for the same mass velocity, as can be seen in Figure 5.2 (b). The thickness of the condensate increases with a decrease in quality as seen from the inlet to the outlet, as well as across different qualities from 0.75 to 0.25. As the vapour condenses from the inlet along the tube length in the test section, the amount of condensate increases, forming

a thick layer of condensate on the outlet. The wave formation across the quality range shows that, for high qualities, wave instability increases greatly with very short wavelengths and amplitude on the vapour-liquid interface. However, as the quality decreases, the wavelengths increase due to the decrease in the velocity of the vapour. Finally, when gravity becomes the dominating stabilising mechanism on the interface, the flow becomes stratified.

5.3.2. Effect of mass flux

Figure 5.3 (a), Figure 5.3 (b) and Figure 5.3 (c), show the dependency of the heat transfer coefficient on mass flux for qualities of 0.75 and 0.25 respectively, and a temperature difference of 3 °C. The results show the same trend as that of various researchers, indicating that the heat transfer coefficient increases with increase in mass flux for all the observed qualities [23, 25, 37, 46, 82]. However, as stated by Cavallini *et al.* [82], when mass flux decreases, there is less dependency of the heat transfer coefficient on quality. This is evident for a mass flux of 25 kg/m².s. The percentage increase in the heat transfer coefficient is approximately 8% for a quality of 0.25 to 0.75 for the lowest mass flux of 25 kg/m².s. For the other mass fluxes, the percentage increase ranged from approximately 24% to 33%.

The increase in the heat transfer coefficient is evident due to the variation in the stratification effect for different mass fluxes. Although the flow patterns observed for the horizontal flow vary from stratified-wavy to stratified flow, the stratification is not the same for different mass fluxes and qualities. Figure 5.3 (b) and Figure 5.3 (c) show the differences in the film condensate from the highest mass flux of 100 kg/m².s to the lowest mass flux of 25 kg/m².s, and from the mean quality of 0.75 to the mean quality of 0.25. The differences reveal that the flow pattern is influenced greatly by the vapour flow rate. The vapour tends to move much faster than the liquid film that causes agitation at the vapour-liquid interface. This results in the formation of waves. The wave length increases with a reduction in the vapour flow rate, while the frequency of the waves reduces with a reduction in the vapour flow rate, causing the flow to transition from stratified-wavy to stratified flow at very low mass fluxes and for low qualities.

The layer of condensate at the bottom of the tube causes resistance to heat transfer; hence the thicker the condensate, the higher the resistance, resulting in a reduction of the rate of heat transfer. Figure 5.3 (a) reveals this effect, in that the mass flux of 25 kg/m².s has the lowest heat transfer coefficient.

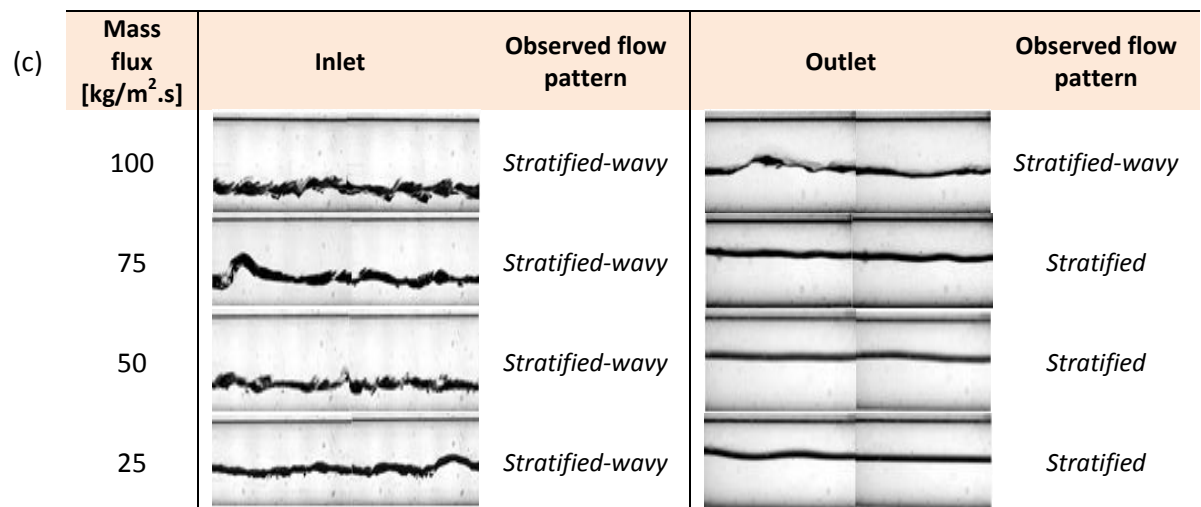
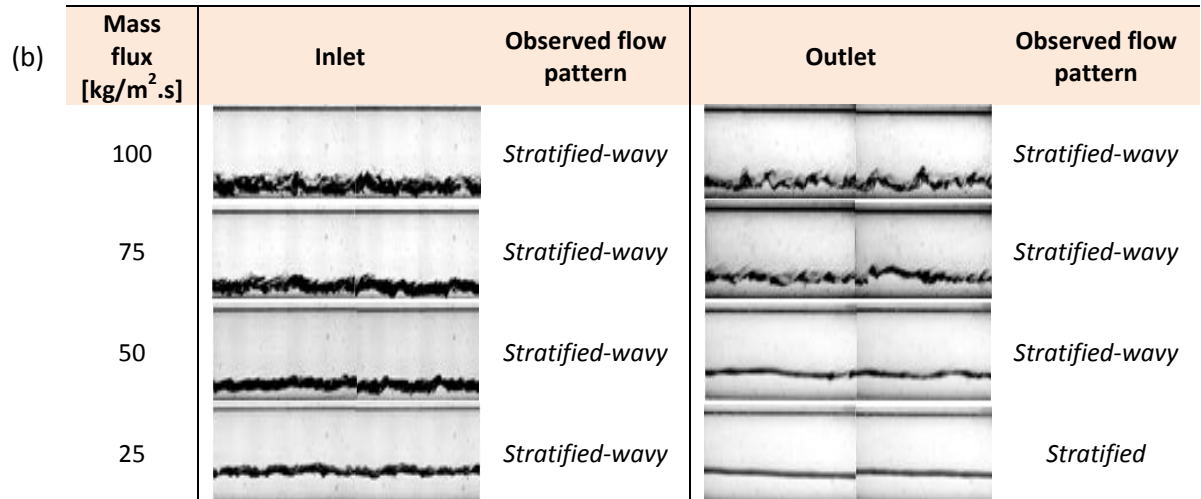
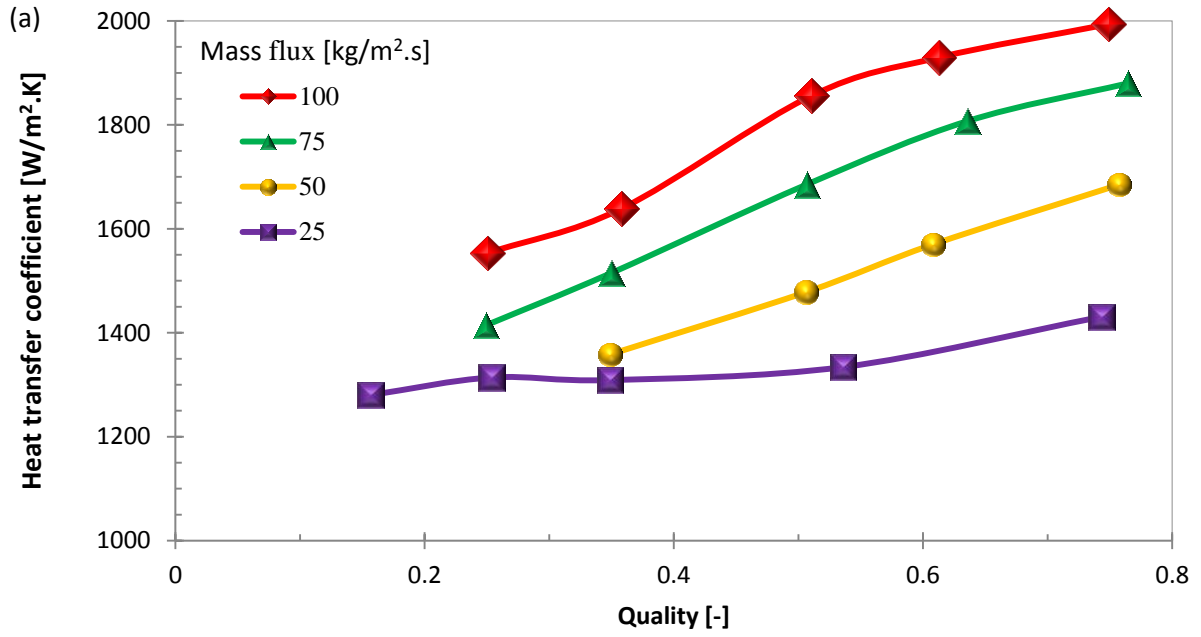


Figure 5.3: Effect of mass flux and observed flow patterns in: (a) the heat transfer coefficient; (b) the quality of 0.75; and (c) the quality of 0.25 for the horizontally inclined tube

5.3.3. Effect of ΔT

The dependence of the heat transfer coefficient on temperature difference is shown in Figure 5.4 for a mass flux of $100 \text{ kg/m}^2\cdot\text{s}$. A comparison of the heat transfer coefficient is presented in Figure 5.4 (a), and a comparison of the observed flow patterns is shown for qualities of 0.6 in Figure 5.4 (b), 0.5 in Figure 5.4 (c) 0.25 in Figure 5.4 (d). Cavallini *et al.* [82] mention that there is no dependency of the heat transfer coefficient on the driving temperature difference for higher mass fluxes above or equal to $400 \text{ kg/m}^2\cdot\text{s}$. However, for mass fluxes of $100 \text{ kg/m}^2\cdot\text{s}$ and less, the heat transfer coefficient is dependent upon temperature difference. Figure 5.4 (a), shows that a decrease in the temperature difference constitutes an increase in the heat transfer coefficient, with a much more pronounced increase for lower temperature differences from 5°C and below. The percentage increase was approximately 2.3% between the temperature difference of 10°C and temperature difference of 8°C and approximately 8.6% between the temperature difference of 5°C and temperature difference of 3°C for a quality of 0.5. Comparing the effect of temperature difference with increases in quality, it can be seen that the increase in heat transfer coefficient with an increase in quality is evident especially for lower temperature differences of 5°C and below.

For all the inlets for different temperature differences, it was observed that the film thickness was higher for the lowest temperature difference, decreasing as temperature difference increases. The flow pattern (stratified-wavy) does not change for all the temperature differences on the inlet to the test section. However, on the outlet to the test section, the flow pattern transitions from stratified-wavy to stratified as the temperature difference increases. Thome [42] stated that in heat exchangers, the most attractive mode of condensing heat transfer is the falling film condensation as it provides good heat transfer performances. Falling film is comprised of a base film that has small amplitude waves on top instead of moving axially it flows down the tube walls due to the increase in gravity forces over the vapour velocities that moves the liquid along the flow direction. The level of condensate at the bottom of the tube is due to the falling liquid film from the top crest of the tube as vapour shear decreases and the force of gravity increase. Since the residence time of the liquid film on the top surface of the tube is small, the heat transfer rates are high. The results of this as stated by Suliman [61] conform to the Nusselt falling film theory that predicts the heat transfer coefficient to be inversely proportional to a temperature difference to the power $1/4$ during film-wise condensation The wall temperature has a significant impact on the heat transfer coefficient for a stratified-wavy flow pattern hence the larger the driving temperature difference the thicker the liquid condensate at the bottom of the tube and the lower the heat transfer coefficient [37]. A further decrease in the quality causes the liquid inventory to increase at the bottom of the tube

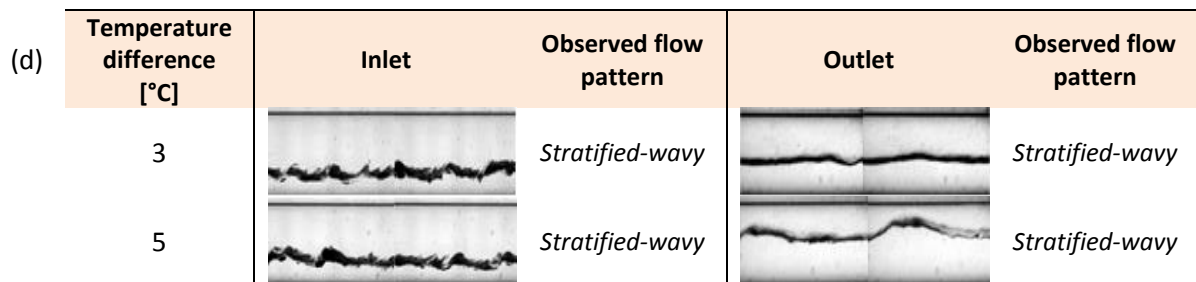
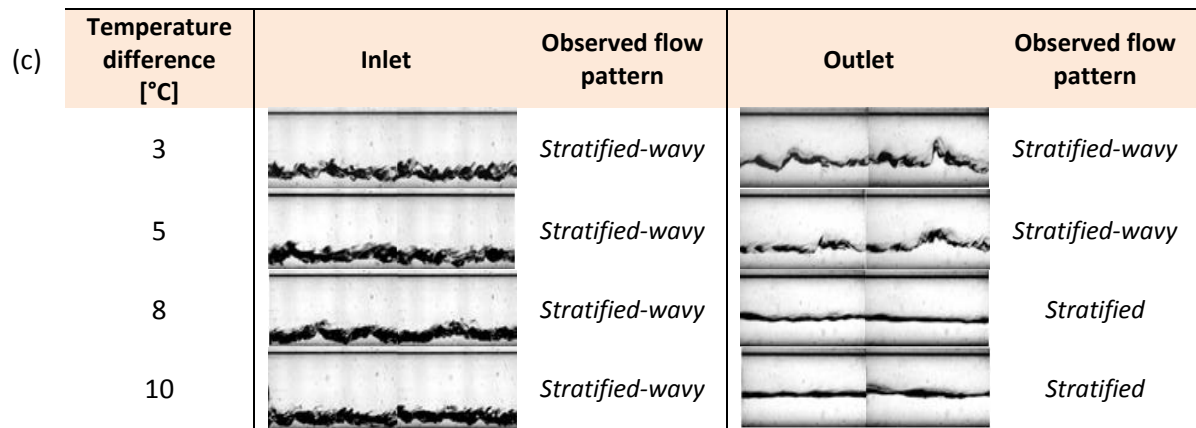
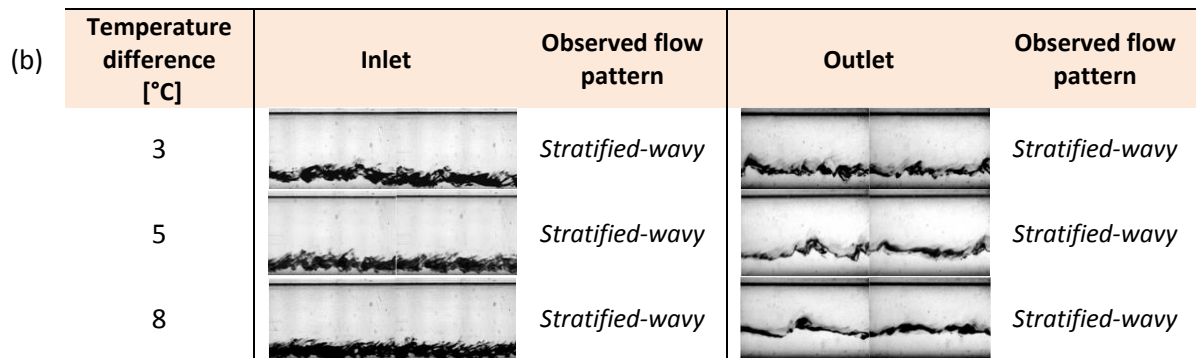
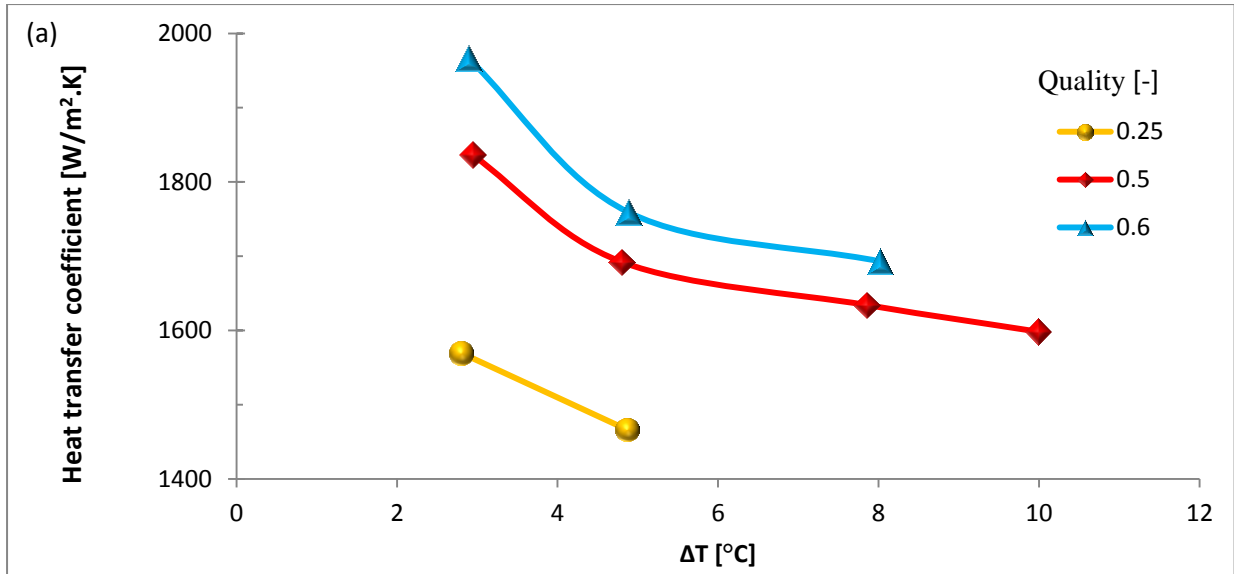


Figure 5.4: Effect of ΔT on: (a) the heat transfer coefficient for mass flux $100 \text{ kg/m}^2\cdot\text{s}$; and qualities of (b) 0.6 ;(c) 0.5; and (d) 0.25 for a horizontally inclined tube

5.4. Inclined configuration – flow patterns and heat transfer coefficient

Section 5.4 shows the effect of quality, mass flux and temperature difference on the heat transfer coefficient and the flow patterns for inclined configurations. The experiment was conducted for mass flux ranges from $25 \text{ kg/m}^2\cdot\text{s}$ to $100 \text{ kg/m}^2\cdot\text{s}$, qualities between 0.25 and 0.75, and temperature differences between $3 \text{ }^\circ\text{C}$ and $10 \text{ }^\circ\text{C}$. The flow patterns that were observed for inclined configurations were different to those of horizontal configurations for gravity-controlled flows. However, a stratified-wavy flow pattern was common for both the horizontal and the negative inclinations (downward flow).

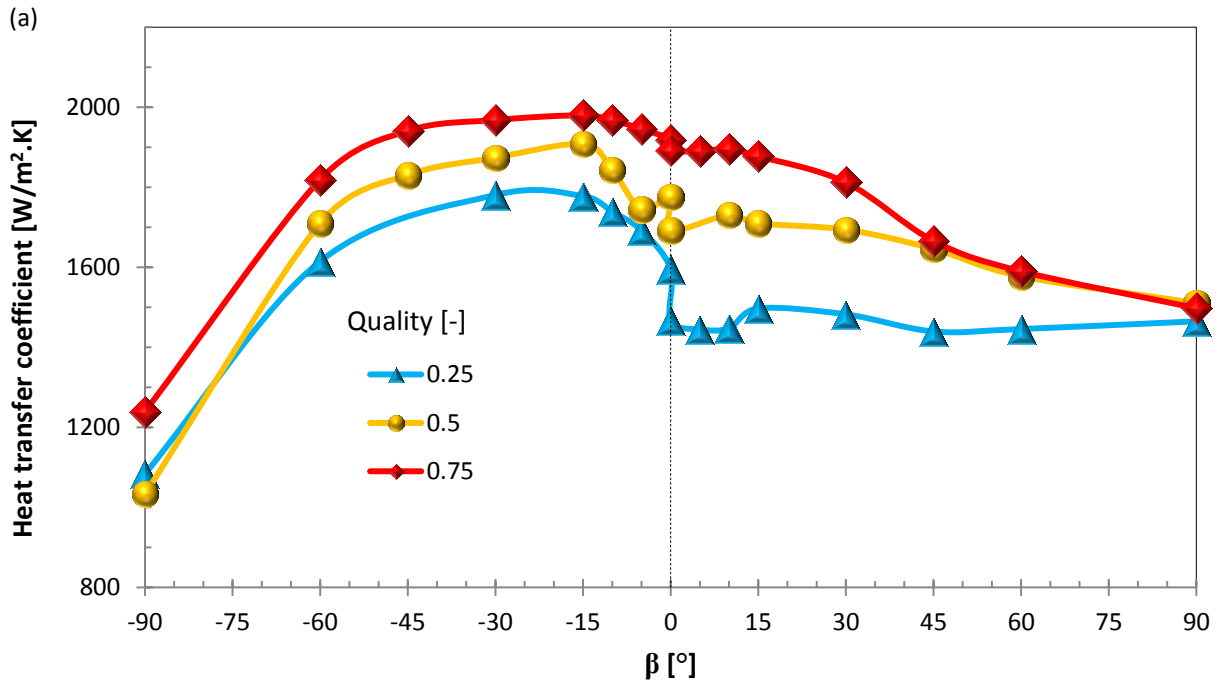
5.4.1. Effect of quality

Figure 5.5 (a) and Figure 5.5 (b) show the effect of quality on the heat transfer coefficient and the resultant flow patterns on the outlet to the test section for a mass flux of $100 \text{ kg/m}^2\cdot\text{s}$ and a temperature difference of $5 \text{ }^\circ\text{C}$. Averaging the data points at 0° , the approximate heat transfer coefficient increase from the lowest quality of 0.25 to 0.75 is 22% for the horizontal inclination. However for small downward inclination angles of -5° and -10° , the increase is much more than the horizontal inclination at 5%. This means that, at smaller inclination angles, the differences in heat transfer coefficient are more significant than at other inclination angles. The trend that the heat transfer coefficient increased with an increase in quality, which has always been evident in the studies of different researchers, is also true for most inclination angles, with an exception for vertically up ($+90^\circ$) and vertically down (-90°) angles. The maximum heat transfer coefficient for this study was between -15° and -30° downward flow. The general trend for different qualities for a mass flux of $100 \text{ kg/m}^2\cdot\text{s}$ is that, for downward flow, the heat transfer coefficient increases from 0° up to -15° , and then gradually starts to decrease up to -60° , followed by a linear decrease in the heat transfer coefficient from -60° to -90° .

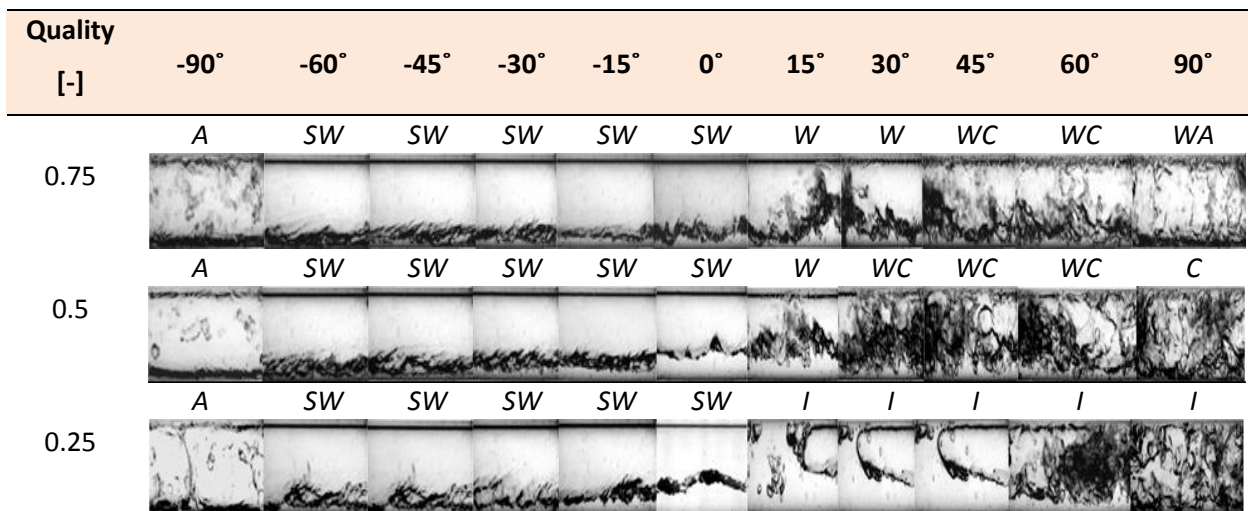
The trend is slightly different for the upward inclination ($+90^\circ$). From the horizontal inclination 0° , the heat transfer coefficient decreases slightly at $+5^\circ$, and then increases up to $+15^\circ$, where-after it gradually decreases from $+30^\circ$ to $+90^\circ$ at higher qualities of 0.62 and 0.75. However, for a quality of 0.25, the heat transfer coefficient decreases from 0° to $+5^\circ$, and then increases slightly from $+60^\circ$ to $+90^\circ$.

The cause of a difference in the heat transfer coefficient can be observed from the flow patterns in Figure 5.5 (b). The increase in the heat transfer coefficient for inclinations of -5° to -15° can be seen by the condensate thickness and the reduction in the amplitude of the interfacial waves at -15° . At this inclination angle, the liquid condensate is suppressed reducing the thickness of the condensate. The flow pattern observed is stratified-wavy with the stratification effect differing with each inclination and change in quality. The slight decrease in the heat transfer coefficient for inclination angles of -30° to -60° is due to the increase in the amplitude of the interfacial waves. A sharp decrease in the heat transfer

coefficient for a vertically downward flow -90° is due to the annular flow pattern with film thickness both on the upper part of the tube and the bottom part. This shows that the two film thicknesses form a resistant barrier for heat transfer, resulting in the sharp decrease.



(b)



A: annular SW: stratified-wavy I: intermittent C: churn WA: wavy-annular
 W: wavy WC: wavy-churn

Figure 5.5: Effect of quality for different inclinations for a mass flux of $100 \text{ kg/m}^2\cdot\text{s}$ and a temperature difference of 5°C .

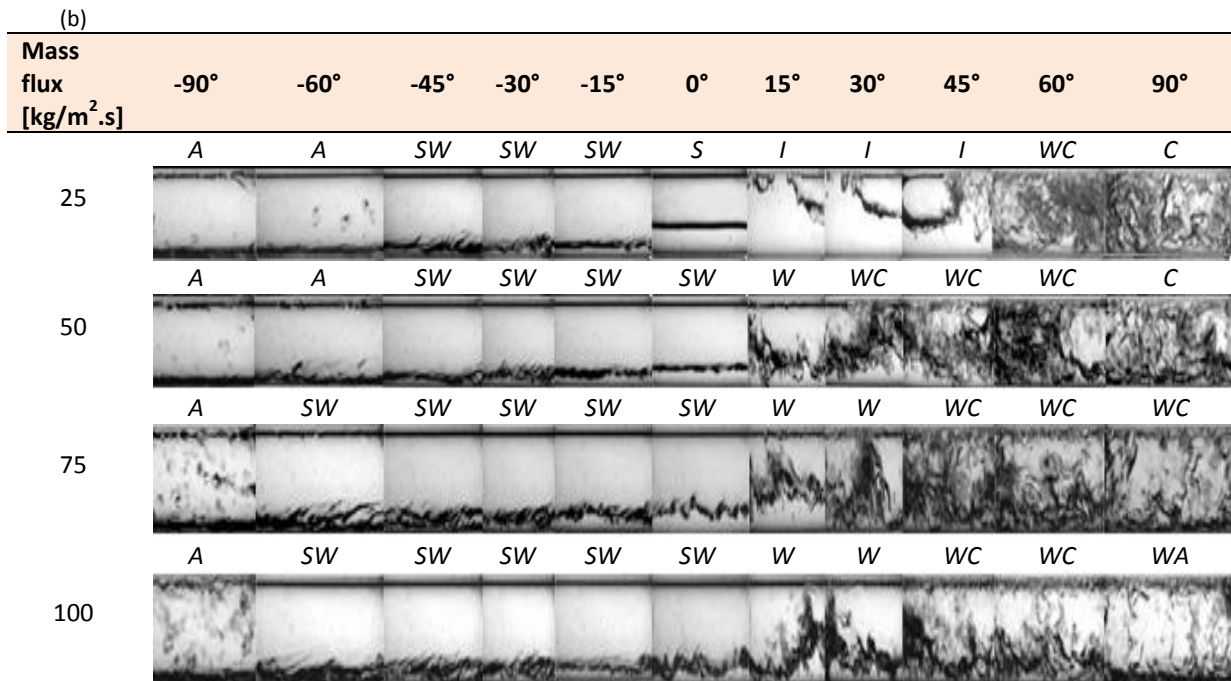
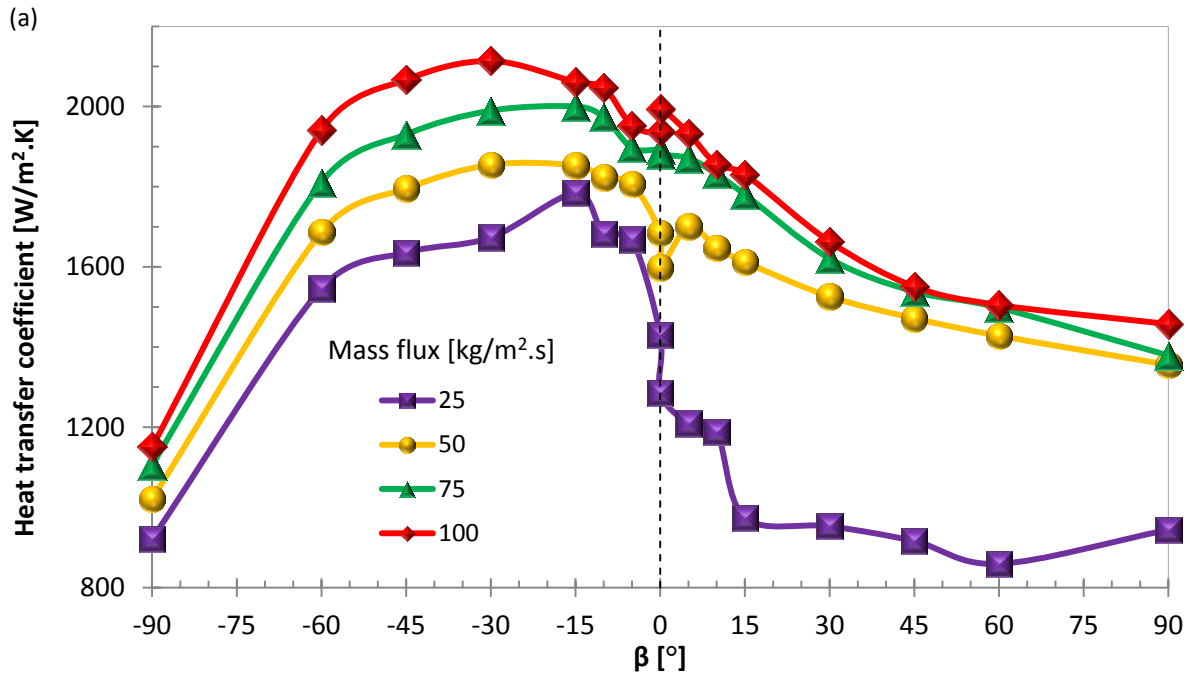
The positive inclinations, unlike the negative inclination, which only yielded stratified-wavy and annular flow patterns, differ with quality and inclination effect. This is evident in the

flow patterns observed and the heat transfer coefficient changes. The flow patterns observed for the positive inclinations were wavy, churn, wavy-churn, wavy-annular and Intermittent flow patterns. The wavy flow pattern was prevalent for smaller inclination angles from $+5^\circ$ to $+30^\circ$ at higher qualities. As the angle of inclination increases, gravity forces acting against the flow increase and the flow transitions from wavy to wavy-churn at $+30^\circ$ and $+45^\circ$. With a further increase in inclination, the shear and gravity forces acting on the vapour cause the flow to transition from wavy-churn to churn or wavy-annular. At a lower quality of 0.25, slug flow patterns are common for lower inclination angles of $+5^\circ$ to $+45^\circ$ due to the high condensate levels and effect of gravity acting against the flow.

In conclusion, for inclined configurations at mass fluxes between $25 \text{ kg/m}^2\cdot\text{s}$ and $100 \text{ kg/m}^2\cdot\text{s}$ and a temperature difference of 5°C , the heat transfer coefficient is a function of quality and inclination. As quality increases, the heat transfer coefficient also increases with the exception of the vertically up ($+90^\circ$) and vertically down (-90°) inclinations. For all the qualities, it is observed that the highest heat transfer coefficient is always at around -15° and the lowest at -90° . From the horizontal inclination, the percentage increase of the heat transfer coefficient is approximately 11%, 7% and 3% for qualities of 0.25, 0.5 and 0.75 respectively. This shows that, as quality increases, the rate of the effect of quality on the heat transfer coefficient decreases.

5.4.2. Effect of mass flux

Figure 5.6 (a) and Figure 5.6 (b) summarise the effect of mass flux on the heat transfer coefficient and the resultant flow patterns that were observed. The mass fluxes are $50 \text{ kg/m}^2\cdot\text{s}$, $75 \text{ kg/m}^2\cdot\text{s}$ and $100 \text{ kg/m}^2\cdot\text{s}$ at a temperature difference of 3°C . A mass flux of $25 \text{ kg/m}^2\cdot\text{s}$ was at a temperature difference of 1°C was presented together with the other mass fluxes at a temperature difference of 3°C because at that low mass flux, the system became unstable. The gravity forces tend to overcome the flow due to the low velocities. The condensing temperature difference from the inlet to the outlet of the test section was maintained at 0.2°C to 0.6°C for the inclined configurations. But, for instances where the systems was unstable, especially for mass fluxes of $50 \text{ kg/m}^2\cdot\text{s}$ and below and at higher inclination angles the condensing temperature difference would therefore go beyond the range, despite it being limited to 0.6° and less. This was evident at higher inclination angles of 30° and above. The low heat transfer coefficients observed in Figure 5.6 for positive inclinations at a mass flux of $25 \text{ kg/m}^2\cdot\text{s}$ could be tied to the above-mentioned instability and high condensing temperature differences that were experienced. Since the other test parameters were the same like saturation temperature and quality for all the mass fluxes, a driving temperature difference of 1°C at a mass flux of $25 \text{ kg/m}^2\cdot\text{s}$ was plotted together with a temperature difference of 3°C for the other mass fluxes to just show the effect of mass flux and inclination on the heat transfer coefficient at a mass flux of $20 \text{ kg/m}^2\cdot\text{s}$.



A: annular *S: stratified* *SW: stratified-wavy* *I: intermittent* *C: churn* *WA: wavy-annular*
W: wavy *WC: wavy churn*

Figure 5.6: Effect of mass flux on (a) the heat transfer coefficient; and (b) flow patterns for different inclinations for a quality of 0.75

Figure 5.6 (a) shows a general trend, which has also been observed in horizontal inclinations, that as mass flux increases, the heat transfer coefficient increases as well [11, 14, 37, 57, 61, 82]. The increase in mass flux at a higher quality causes the vapour shear forces to increase as well, overcoming the forces of gravity. The flow therefore moved from the dominance of gravity to shear dominance, which resulted in a higher heat transfer

coefficient. The maximum heat transfer coefficient was observed between -15° and -30° as observed by Meyer *et al.* [23] for higher mass fluxes. The percentage rate of the increase of the heat transfer coefficient decreases with the increase in mass flux from approximately 30% to 7% for mass fluxes of $25 \text{ kg/m}^2 \cdot \text{s}$ and $100 \text{ kg/m}^2 \cdot \text{s}$ respectively.

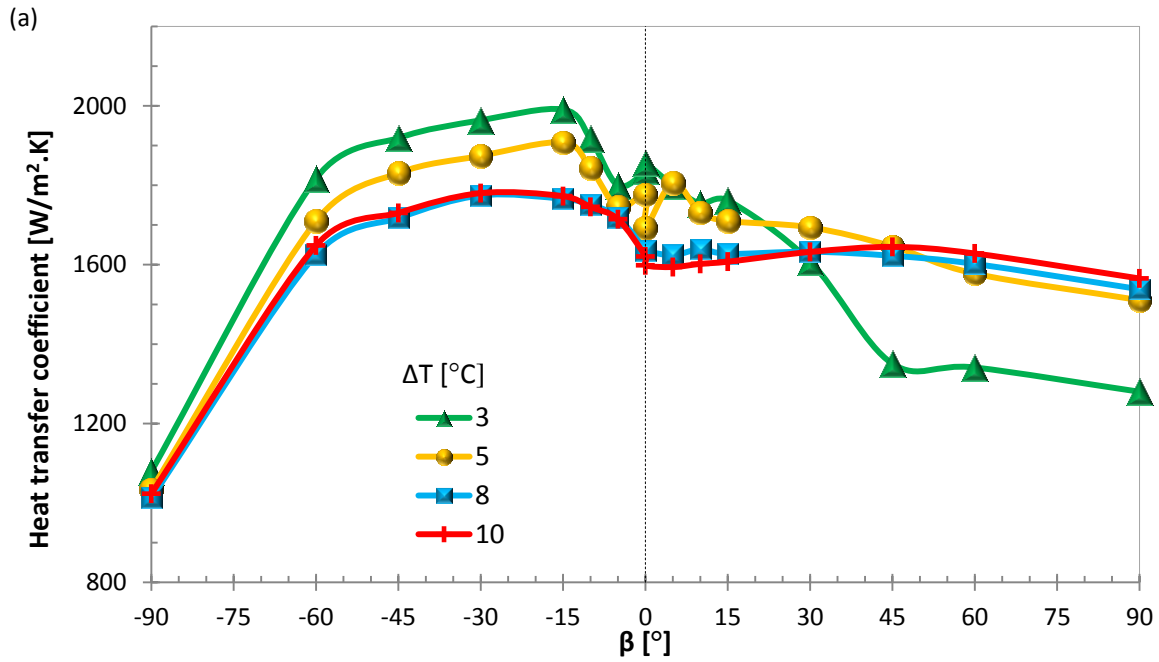
Figure 5.6 (b) shows the observed flow patterns for the same operating parameters stated above. When considering a mass flux of $50 \text{ kg/m}^2 \cdot \text{s}$, only flow patterns for angles -15° , -45° , -60° and 90° were not captured, hence flow patterns for a quality of 0.62 were used to assume the predicted flow patterns for a quality 0.75. Two flow patterns were observed for the downward flow: annular and stratified-wavy. At low mass fluxes, a stratified flow pattern is observed at 0° , while a stratified-wavy flow pattern was prevalent at higher mass fluxes. Intermittent, wavy, wavy-churn, wavy-annular and churn flow patterns are observed for the upward inclination. The increase in the heat transfer coefficient for the angles of -15° to -30° was due to the thinning of the condensate height for all the mass fluxes. However, as inclination increases for -30° upwards, the wave height or wave amplitude increases as the liquid condensate is carried by the waves along the flow direction.

5.4.3. Effect of ΔT

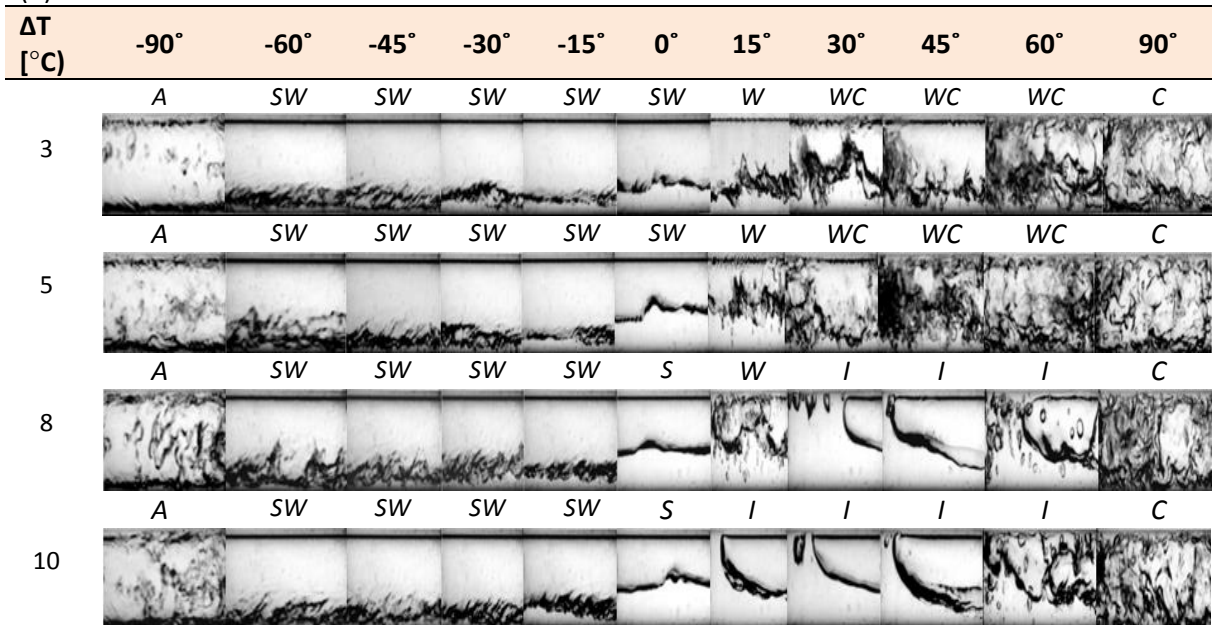
Figure 5.7 (a) depict the effect of the temperature difference on the heat transfer coefficient and Figure 5.7 (b) the resulting flow patterns that were observed. The data provided is for a mass flux of $100 \text{ kg/m}^2 \cdot \text{s}$, a quality of 0.5 and a saturation temperature of 40°C . The observed flow patterns are also for these parameters. The effect of temperature difference for the inclined flow is a bit different to the effect of quality and mass flux on the heat transfer coefficient. As discussed in Section 5.4.1 and Section 5.4.2, the heat transfer coefficient increased with an increase in mass flux and quality. However, the effect is different for temperature difference at different inclination angles. The heat transfer coefficient decreased with an increase in the temperature difference (ΔT), but only for negative angles (0 to -90°), and only for small positive angles from 0° up to $+30^\circ$. However, above 30° , the heat transfer coefficient increased with an increase in temperature difference as can be seen in Figure 5.7 (a). This transition happens between $+15^\circ$ and $+30^\circ$. As discussed in Section 5.3.3, it can be noted that, for horizontal inclinations, the effect of temperature difference on the heat transfer coefficient diminishes for higher temperature differences. It was also observed that the same effect applies to inclined orientations. At a temperature difference of 8°C and 10°C , the heat transfer coefficient is almost the same, with an average percentage difference of approximately 0.02% for the negative angles, 1.4% for angles of 0° up to $+30^\circ$ and 1.6% for angles of $+45^\circ$ to $+90^\circ$. The decrease in the heat transfer coefficient for angles above $+30^\circ$ at a temperature difference of 3°C could be the result of the low heat flux and the increase in the gravitational forces acting against the direction of flow as the angle of inclination increases. For temperature differences of 3°C , 5°C , 8°C and 10°C , the average heat flux is approximately 5 kW/m^2 , 8.3 kW/m^2 , 13 kW/m^2

and 15.7 kW/m^2 respectively. This results in an overall decrease in the heat transfer coefficient with a decrease in the temperature difference. This in turn, proves that, for temperature differences higher than $8 \text{ }^\circ\text{C}$, the change in the heat transfer coefficient is negligible for gravity-driven flows. The maximum values of the heat transfer coefficients are observed between the angles of -15° and -30° .

The flow patterns that were observed for the downward inclination angles were annular and stratified-wavy while a stratified flow pattern was observed at higher temperature differences of $8 \text{ }^\circ\text{C}$ and $10 \text{ }^\circ\text{C}$. For upward inclinations, however, wavy, wavy-churn, churn and intermittent flow patterns were observed. What can be noted in Figure 5.7 (b) is that for stratified-wavy flow patterns for downward flow, the thinning condensate film improving the heat transfer. Nonetheless, the wave structure tends to change as the angle of inclination increases, as a result the forces of gravity and shear both acting along the flow direction. The temperature difference does not have much of an effect on the -90° angle. This is evident through the annular flow pattern that is common for all the temperature differences. From $+5^\circ$ to $+15^\circ$, a wavy flow pattern is prevalent from a temperature difference of $3 \text{ }^\circ\text{C}$ to $8 \text{ }^\circ\text{C}$; then, the flow transitions to wavy-churn or intermittent. The intermittent flow pattern is also common for higher temperature differences, as it is dominant in low qualities and low mass fluxes.



(b)



WA: wavy-annular SW: stratified-wavy W: wavy C: churn S: stratified I: intermittent
 WC: wavy-churn

Figure 5.7: Effect of ΔT on: (a) the heat transfer coefficient; and (b) the flow patterns for different inclinations at a quality of 0.5

In conclusion, the test results of the heat transfer coefficient and resultant flow patterns for a mass flux of $100 \text{ kg/m}^2 \cdot \text{s}$ and a quality of 0.5 show that the heat transfer coefficient is also a function of temperature difference. This only applies to negative inclination angles from 0° to -90° and positive inclination angles from 0° to $+15^\circ$ and from the temperature difference (ΔT) of 8°C and below. In this case, the heat transfer coefficient increases with a decrease in

the temperature difference. From an inclination of $+30^\circ$ to $+90^\circ$, the heat transfer coefficient increases with an increase in the temperature difference.

5.5. Summary of the heat transfer coefficient for inclined flow

Figure 5.8 to Figure 5.12 summarise the effects of quality, mass flux, temperature difference and inclination angle on the heat transfer coefficient. The data is for mean qualities from 0.25 to 0.75, mass fluxes from $25 \text{ kg/m}^2\cdot\text{s}$ to $100 \text{ kg/m}^2\cdot\text{s}$ and temperature difference of 1°C to 10°C . The common trend is that, at higher mass fluxes, a wider range of mean qualities could be captured at a lower temperature difference of 3°C and 5°C . However, as mass flux decreased to $50 \text{ kg/m}^2\cdot\text{s}$ and $25 \text{ kg/m}^2\cdot\text{s}$, only certain qualities could be captured. Due to the low mass flux and the effect of gravity on the flow for a mass flux of $25 \text{ kg/m}^2\cdot\text{s}$, a temperature difference higher than 1°C could not be captured. Each data point represents each test carried-out.

5.5.1. Summary on the effect of quality on heat transfer coefficient

Figure 5.8 gives an overview of the effect of quality on the heat transfer coefficient for different mass fluxes of $100 \text{ kg/m}^2\cdot\text{s}$, $75 \text{ kg/m}^2\cdot\text{s}$ and $50 \text{ kg/m}^2\cdot\text{s}$ at a constant temperature difference of 3°C . Attention is drawn to the differences in temperature difference in Figure 5.8 (a), with a temperature difference of 3°C , and Figure 5.8 (a), with a temperature difference of 5°C . For inclined configurations, the effect of quality is still significant, even for gravity-driven flows. The increase of the heat transfer coefficient with the increase in quality is also evident in Figure 5.3 (a), for the horizontal inclination, and Figure 5.8 (a), Figure 5.8 (b) and Figure 5.8 (c) at 0° . Although a change in quality has a pronounced effect on the heat transfer coefficient for the horizontal inclination, it is not so for other inclination angles like $+90^\circ$ and -90° . For lower qualities, the change is insignificant. For $+90^\circ$, however, the heat transfer coefficient decreases with an increase in quality for lower qualities and mass flux. This can be seen in Figure 5.8 (b) for a mass flux of $75 \text{ kg/m}^2\cdot\text{s}$ and Figure 5.8 (a) for qualities between 0.25 and 0.62 at a mass flux of $100 \text{ kg/m}^2\cdot\text{s}$. The decrease was approximately 3% for a downward inclination at -90° , and for all the mass fluxes, the heat transfer coefficient difference is very small. It can therefore be concluded that, for gravity-driven flows, at -90° and $+90^\circ$ inclinations, the effect of quality on the heat transfer coefficient is insignificant for lower qualities of 0.62 and below.

For other inclination angles, there is a significant difference in the increase in the heat transfer coefficient for downward flow at -30° to -60° . However, for smaller angles of -15° to -5° , the increase in the heat transfer coefficient was quite small especially with a decrease in mass flux, see Figure 5.8 (c) for a mass flux of $50 \text{ kg/m}^2\cdot\text{s}$. The opposite is true for upward flow. For smaller inclination angles of -5° to -15° , there is a remarkable increase in the heat transfer coefficient, with an increase in quality for higher mass fluxes. For higher positive inclination angles of $+30^\circ$ to $+60^\circ$, the effect is reversed at lower qualities of 0.62 and below,

whereby a notable difference in the heat transfer coefficient is visible at lower mass fluxes. For an upward angle of 60°, the increase in the heat transfer coefficient is approximately 3.5% to 8% for mass fluxes of 100 kg/m².s and 50 kg/m².s, respectively. The increase in the heat transfer coefficient is therefore notable at lower mass fluxes. See Appendix B.2 for further analysis.

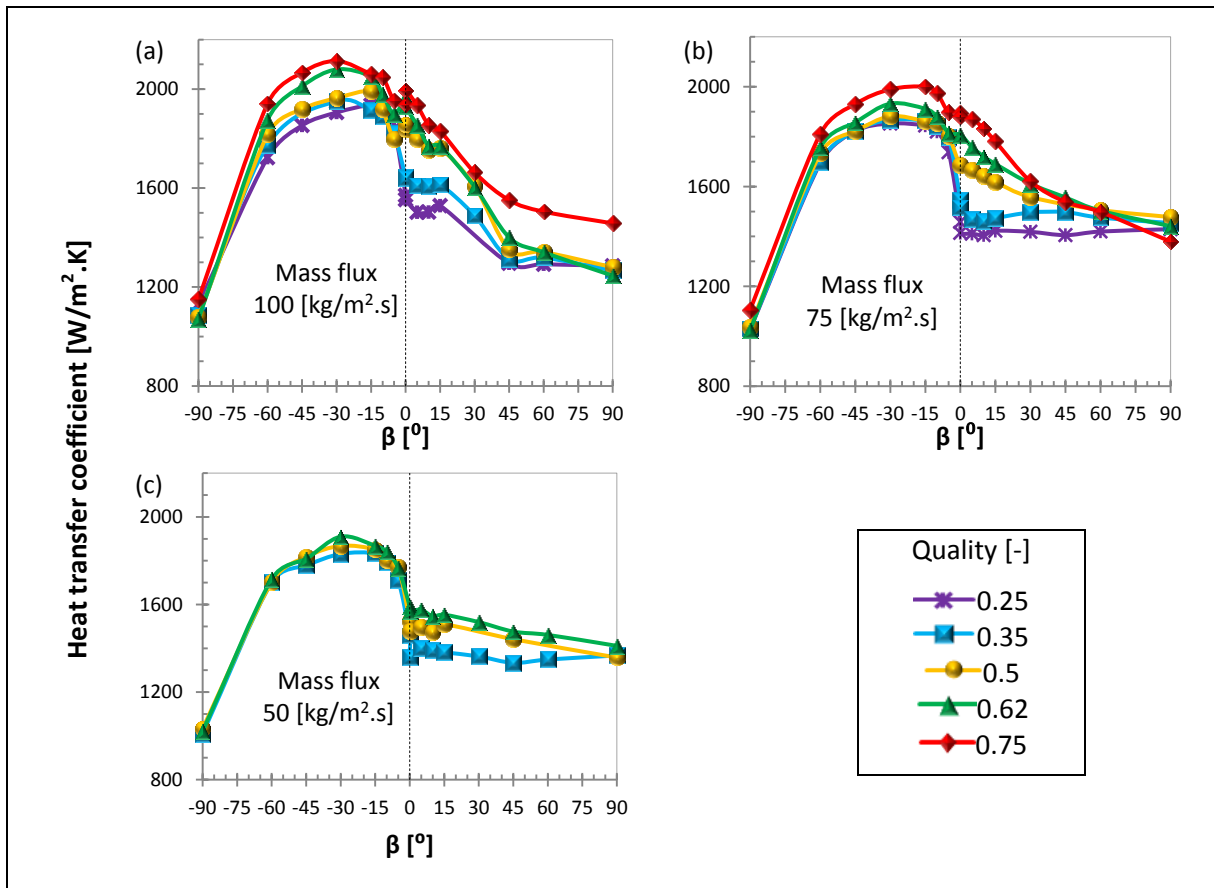


Figure 5.8: Total effect of quality on heat transfer coefficient.

5.5.2. Summary of the effect of mass flux on the heat transfer coefficient

Figure 5.9 (a) to Figure 5.9 (f) show the effect of mass flux on the heat transfer coefficient for different qualities, temperature differences and inclination angles. The results compared are for mass fluxes of 25 kg/m².s to 100 kg/m².s, qualities of 0.25, 0.5, 0.62 and 0.75, and temperature differences of 1 °C, 3 °C, 5 °C and 8 °C. The aim here is to see if the same conclusions drawn in Section 5.4.2 can be drawn here for different qualities and ΔT s.

The first two figures, Figure 5.9 (a) and Figure 5.9 (b), compare of different qualities at a temperature difference of 3 °C and mass fluxes of 100 kg/m².s, 75 kg/m².s and 50 kg/m².s. For the negative inclination angles, the trend follows the one in Section 5.4.2, that the heat transfer coefficient increases with an increase in mass flux. For a temperature difference of 3 °C the same conclusion is drawn for positive inclination angles for a higher quality of 0.75. For qualities lower than 0.75 and a temperature difference of 3 °C, at between +15° and

+30°, the results show that a mass flux of 100 kg/m².s has a drop in the heat transfer coefficient up to +90° (see Appendix B.3). A quality of 0.25, follows the same trend, as can be seen in Figure 5.9 (a). In Figure 5.9 (b) to Figure 5.9 (f), the trend remained the same, so for all inclination angles, the heat transfer coefficient increased with an increase in mass flux.

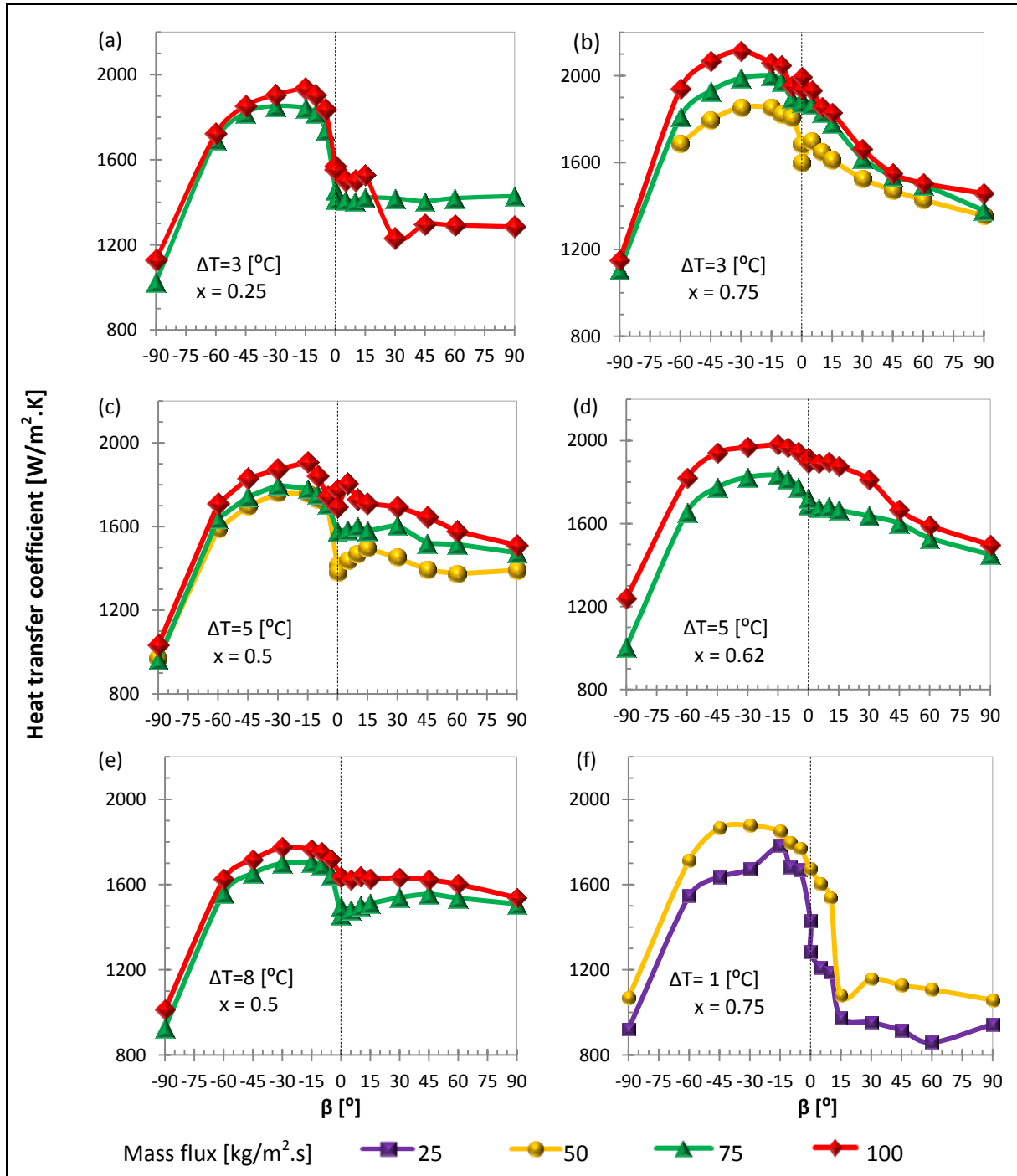


Figure 5.9: Total effect of mass flux on the heat transfer coefficient

In conclusion, the effect of mass flux on the heat transfer coefficient is that, at high qualities, of 0.62 and above, the heat transfer coefficient increases from one mass flux to another for negative inclination angles from -15° to -60° .

5.5.3. Summary of effect of temperature difference on the heat transfer coefficient

Figure 5.10 (a) to Figure 5.10 (j) show a summary of the effect of temperature difference on the heat transfer coefficient. The data depicted is for mass fluxes of $100 \text{ kg/m}^2\cdot\text{s}$, $75 \text{ kg/m}^2\cdot\text{s}$ and $50 \text{ kg/m}^2\cdot\text{s}$, qualities of 0.25 to 0.75 and temperature differences from 1°C to 10°C . What can be observed is that the effect of temperature difference is almost negligible for an angle of -90° . The heat transfer coefficient increases with a decrease in temperature difference for the rest of the negative inclination angles, although the significance of the increase diminishes with a decrease in inclination angle as quality and mass flux increases. The latter effect is also evident for small positive inclination angles, 0° to 15° , except for the mass flux of $50 \text{ kg/m}^2\cdot\text{s}$. As mentioned in Section 5.4.3, there is a negligible difference in the effect of temperature difference on the heat transfer coefficient for higher temperature difference of 8°C and 10°C as can be seen in Figure 5.10 (c). See Appendix B.4 for a further analysis of the effect of temperature difference.

In conclusion, it is observed that temperature difference has little effect for a -90° inclination angle for most of the qualities, with a noticeable difference at higher qualities of 0.75. The heat transfer coefficient always increases with a decrease in temperature difference for other negative inclination angles from 0° to -60° for all qualities. For positive inclination angles, the majority of the results show an increase in the heat transfer coefficient, with an increase in temperature difference for inclination angles $+30^\circ$ to $+90^\circ$. The maximum heat transfer coefficient is observed between inclination angles of -15° and -30° for all mass fluxes.

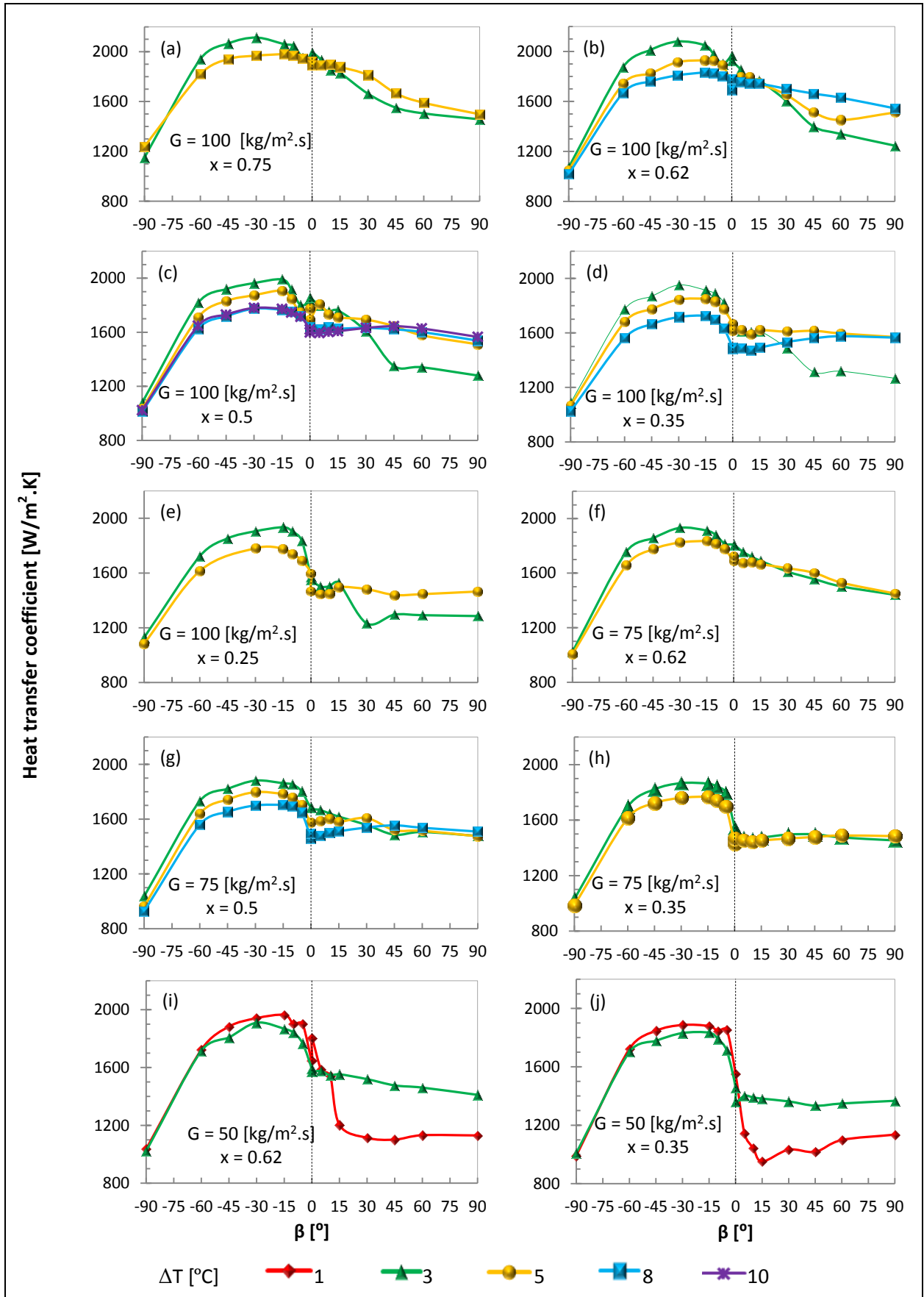


Figure 5.10: Total effect of ΔT on the heat transfer coefficient

5.5.4. Graphical representation of heat transfer coefficient for each inclination angle

Figure 5.11 is a graphic representation of the heat transfer coefficients for a temperature difference of 3 °C for mass fluxes of 100 kg/m².s, 75 kg/m².s and 50 kg/m².s, as well as for a mass flux of 25 kg/m².s, where the temperature difference was 1 °C for positive inclination angles. Figure 5.12 represents negative inclination angles. The data is plotted with quality on the abscissa and heat transfer coefficient on the vertical axis. The aim is to analyse the effect of quality and inclination angle on the heat transfer coefficient, and how the effect of quality varies with inclination angle.

5.5.4.1 Positive inclination

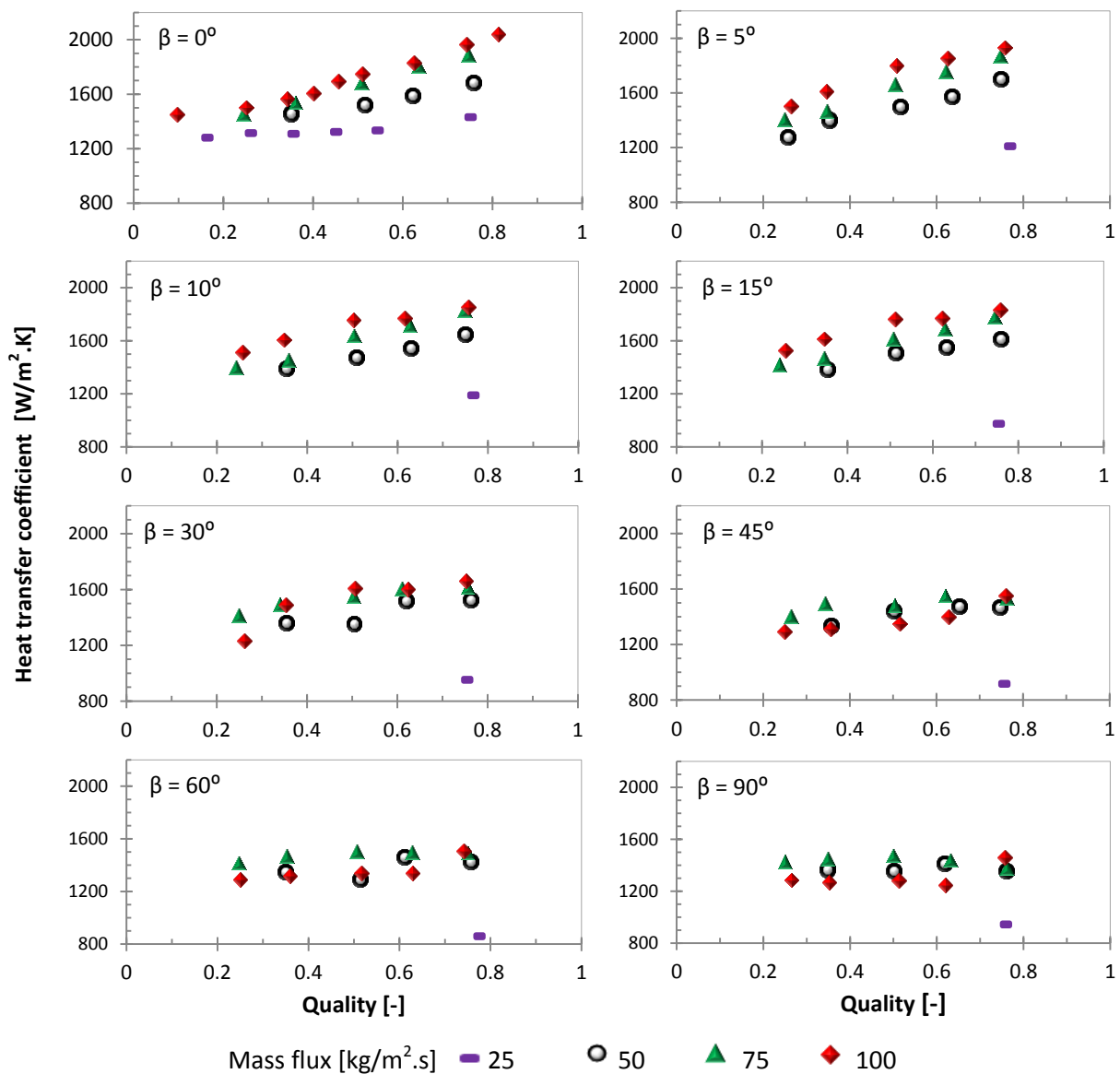


Figure 5.11: Heat transfer coefficients for positive inclination angles

Figure 5.11 show positive inclination angles. At the horizontal inclination (0°), the effect of quality on the heat transfer coefficient is very much evident for all mass fluxes, although this effect decreases with a decrease in mass flux and quality. From 0° to $+15^\circ$, the heat transfer coefficient still increase with an increase in quality for mass fluxes of $100 \text{ kg/m}^2\cdot\text{s}$, $75 \text{ kg/m}^2\cdot\text{s}$ and $50 \text{ kg/m}^2\cdot\text{s}$. However, at the lowest mass flux of $25 \text{ kg/m}^2\cdot\text{s}$, the heat transfer coefficient decreased with each increase in inclination. Apart from a mass flux of $25 \text{ kg/m}^2\cdot\text{s}$, the mass fluxes from an angle of $+30^\circ$ to $+90^\circ$ show that the effect of quality on the heat transfer coefficient diminishes with an increase in quality. On the other hand, the heat transfer coefficient decreases with an increase in mass flux and an inclination angle from $+30^\circ$ to $+90^\circ$. This effect is evident for a mass flux of $100 \text{ kg/m}^2\cdot\text{s}$. The highest heat transfer coefficient for positive inclination angles is for angles between 0° and 5° for all mass fluxes. An annular flow pattern dominated the -90° angle, which is why the heat transfer coefficient is very low at this inclination angle.

5.5.4.2 Negative inclination

Figure 5.12 summarises the negative inclination angles, and the effect of quality and mass flux on the heat transfer coefficient. It can be observed that the same trend for the negative inclinations suffice in that an increase in, the heat transfer coefficient with an increase in mass flux and quality is true for all inclination angles except for -90° . The increase in the heat transfer coefficient is quite significant as quality increases. The lowest heat transfer coefficients are for the inclination angle -90° for all mass fluxes, while the highest are for the inclination angles between -15° and -30° . The amount of stratification and wave formation is the determining factor between the increase and decrease in the heat transfer coefficient.

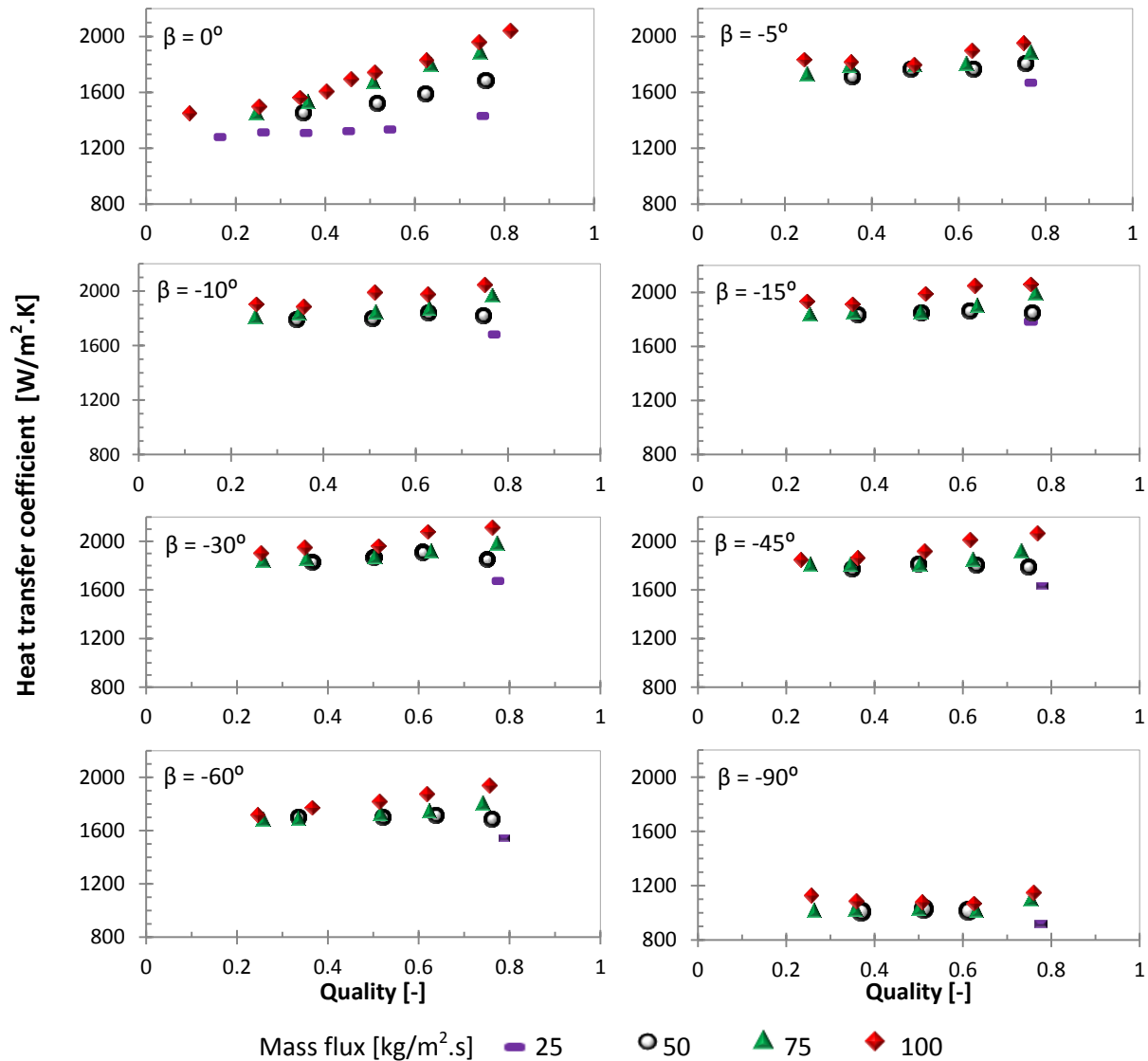


Figure 5.12: Heat transfer coefficients for negative inclination angles

5.6. Conclusion

The effects of quality, mass flux, temperature difference and inclination on the heat transfer coefficient, together with the resultant flow patterns, were discussed in this chapter. The results are in agreement with the findings of other researchers for most of the areas that were investigated in terms of two-phase in-tube condensation. However, new ground has been laid for research into the effects of inclination at mass fluxes of $100 \text{ kg}/\text{m}^2\cdot\text{s}$ and below, which has not been researched to date. The study observed eight flow patterns, including stratified-wavy, stratified, wavy, wavy-churn, intermittent, churn, annular and wavy-annular. The flow patterns have a direct effect on the heat transfer coefficient, and any prediction of the heat transfer coefficient therefore has to be based on the observed flow pattern. For horizontal flow, only stratified and stratified-wavy flow patterns were observed, which are common at mass fluxes of $100 \text{ kg}/\text{m}^2\cdot\text{s}$ and below.

At horizontal configurations, the heat transfer coefficient is a function of quality, mass flux and temperature difference. As quality increases for horizontal flow, the heat transfer coefficient increases as well. The increase in stratification effect, whereby the film thickness increases for stratified and stratified-wavy patterns, work as an insulator against heat transfer, resulting in the notion that the greater the film thickness, the lower the heat transfer coefficient. The increase in mass flux for horizontal configurations also saw an increase in the heat transfer coefficient. However, there is less dependency of the heat transfer coefficient on quality as mass flux is decreased. This is due to the increase in film thickness. The effect of temperature difference on the heat transfer coefficient on horizontal flow is such that, as temperature difference decreases, the heat transfer coefficient increases. The rate at which the heat transfer coefficient increases, is much lower at higher temperature differences of 8 °C and 10 °C and increases as temperature difference is decreased.

For inclined configuration, the flow patterns observed are stratified and stratified-wavy, including wavy, wavy-annular, annular, churn, wavy-churn and intermittent flow patterns. The heat transfer coefficient is a function of quality, mass flux, temperature difference and inclination angle. Throughout the experiment, maximum heat transfer coefficient is always between the angles of -15° and -30°, for downward flow, while the lowest heat transfer coefficient is observed for the vertically downward inclination at an angle of -90°. The heat transfer coefficient increases with an increase in quality for all the inclination angles except for the vertical inclinations of +90° and -90°. The increase in the heat transfer coefficient for different qualities is more evident at smaller inclinations for positive angles between 0° and +30°. This increase is more evident at higher mass fluxes. The percentage increase in the heat transfer coefficient from the horizontal inclination is approximately 11%, 7% and 3% for qualities of 0.25, 0.5 and 0.75 respectively.

As in the horizontal configuration, the increase in mass flux for inclined flows constitutes an increase in the heat transfer coefficient for a quality of 0.75 and temperature difference of 3 °C. For a mass flux of 100 kg/m².s, and a quality of 0.5, the heat transfer coefficient increases with a decrease in temperature difference for all the negative inclination angles and for positive inclination angles from 0° to +15°. However, at about +30°, the heat transfer coefficient increases with an increase in temperature difference. The highest heat transfer coefficient for positive inclination angles (upward flow) is between 0° and +5°.

Eight flow patterns were observed for in-tube condensation for mass fluxes of 100 kg/m².s and below unlike at mass fluxes above 200 kg/m².s. Only stratified and stratified-wavy flow patterns were observed for horizontal flow at mass fluxes of 100 kg/m².s and less. However, after adding the effect of inclination, six more flow patterns were observed, where some have good properties and configurations to enhance heat transfer. These six flow patterns include intermittent, wavy, wavy-churn, churn, annular and wavy-annular. For this study, the maximum angle of inclination that gives the highest heat transfer coefficient is

between -15° and -30° . The same was established in the results produced by Meyer *et al.* [23], although the study was at higher mass fluxes. The study also concluded that the heat transfer coefficient is a function of quality, mass flux, temperature difference, and inclination angle.

6. Results: flow patterns and flow pattern transitions

6.1. Introduction

This chapter focuses on the flow pattern analysis for the vertically up and vertically down inclinations and other inclination angles. The flow patterns could not all be represented in Chapter 5 as some representations only covered the outlet, where one frame depicts the flow pattern. This could not, however show the full configuration of the flow pattern. This necessitates another chapter to analyse the flow pattern transitions from the inlet to the outlet of the test section. How the flow pattern transitions from inlet to outlet also determines the transitional effect on the heat transfer coefficient for various mass fluxes, qualities and temperature differences. Due to the vast amount of data captured, all the data points could not be represented here. What is presented in this chapter will just be enough to show the effect of the flow pattern and flow pattern transitions on the heat transfer coefficient and how inclination plays a larger role on the flow pattern configuration. A more detailed flow pattern presentation is shown in Appendix C to Appendix G.

Various sections of this chapter look at the flow pattern and flow pattern transitions for the horizontally upward and horizontally downward flows. In addition, various inclination angles, flow pattern and flow pattern transitions are analysed. The data is then plotted on the Hajal-Thome-Cavallini flow pattern map and flow pattern transitions are predicted for all the inclination angles that were investigated.

6.2. Vertical configuration – analysis of flow patterns

Sub-sections 6.2.1 and 6.2.2 discuss the flow patterns and flow pattern transitions from the inlet to the outlet for the vertically downward and vertically upward flows. The flow patterns are depicted by three frames, each 0.083334 seconds apart. Only a mass flux of $100 \text{ kg/m}^2\cdot\text{s}$, at qualities of 0.25, 0.5 and 0.75 are presented at a temperature difference of 5°C . For the other temperature differences and mass fluxes, see Appendix C to Appendix G.

6.2.1. Vertically upward ($+90^\circ$)

The flow patterns observed for the horizontal flow are different from those observed when the tube orientation is vertically up or vertically down. This can be observed in Figure 6.1, where the flow patterns vary from annular, to churn, wavy-churn, wavy-annular and intermittent flow patterns. At low vapour qualities, the inlet flow pattern is churn, which is a highly disturbed flow that consists of a thick unstable liquid film that has an oscillating motion up and down the tube. The flow transitions to an intermittent or slug flow pattern along the tube, although a slight churning effect following the slug can be observed with

some bubbles superseding the slugs. As the quality increases, the film layer at the top and the bottom of the tube stabilises slightly, with some interfacial waves between the vapour and the liquid condensate. This flow pattern at the inlet is wavy-annular. The flow pattern transitions to a wavy-churn flow as the vapour continues to condense along the tube. For higher qualities, the flow is annular at the inlet to the test section and transitions to wavy-annular along the tube.

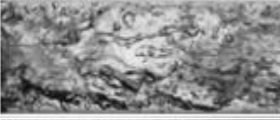

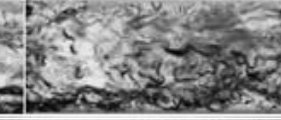




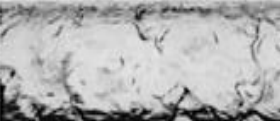

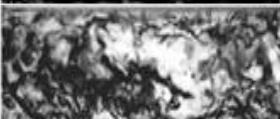




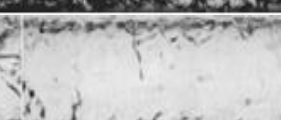
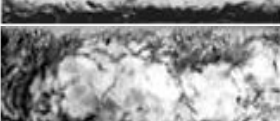

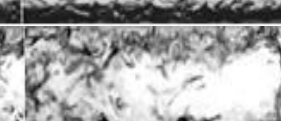
Mass flux of $100 \text{ kg/m}^2 \cdot \text{s}$ and temperature difference of 5°C vertically-upward flows				
Quality position	Time [s]			Observed flow pattern
	0s	0.0833s	0.1667s	
0.25 inlet				<i>Churn</i>
0.25 outlet				<i>Intermittent</i>
0.5 inlet				<i>Wavy-annular</i>
0.5 outlet				<i>Wavy-churn</i>
0.75 inlet				<i>Annular</i>
0.75 outlet				<i>Wavy-annular</i>

Figure 6.1: Flow patterns observed for 90° vertically upward flows

6.2.2. Vertically down (-90°)

Unlike the upward flow where the vapour flows in the opposite direction to the force of gravity, the downward flow has an increased vapour velocity. As the vapour condenses along the tube, the flow is spotted with some liquid droplets increasing from the inlet to the outlet. A vapour-liquid interface is characterised by some slight surface waves. This is due to the increased velocity of the vapour flowing over the interface.

The flow pattern does not change with changes in quality for downward flow. The flow pattern remains annular for all qualities from the inlet to the outlet of the test condenser. The liquid droplets tend to be more for the lower qualities, almost forming small waves in the flow.

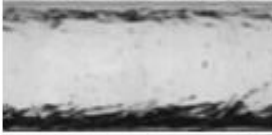


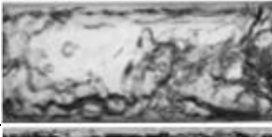
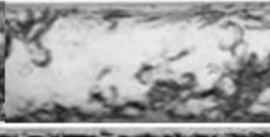



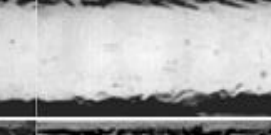






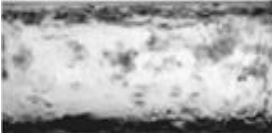


Mass flux of 100 kg/m ² .s and temperature difference of 5°C vertically downward flow				
Quality	Time [s]			Observed flow Pattern
	0s	0.0833s	0.1667s	
0.25 inlet				<i>Annular</i>
0.25 outlet				
0.5 inlet				<i>Annular</i>
0.5 outlet				
0.75 inlet				<i>Annular</i>
0.7 outlet				

Figure 6.2: Flow patterns observed for -90° downward flows

6.3. Inclined configuration – analysis of flow patterns

Section 6.3 summarises the flow pattern transitions from the inlet to the outlet of the tube for different inclinations from +90° to -90°. The flow patterns are captured for a mass flux of 100 kg/m².s, qualities of 0.25 and 0.75 respectively and a temperature difference of 5 °C. A comparison is made between the upward flow and the downward flow pattern transitions. Three frames at 0.25 seconds apart were used to depict the flow pattern as one frame could not fully represent the complete flow pattern.

6.3.1. Positive inclinations for a quality of 0.25

Figure 6.3, depicts different upward flow patterns from the inlet to the outlet for a quality of 0.25. The observed flow patterns from the horizontal up to +90° were stratified-wavy, stratified, wavy intermittent or slug, wavy-churn and churn flow patterns.

Inclination and position	Time [s]			Observed flow pattern
	0	0.25	0.5	
0° inlet				<i>Stratified-wavy</i>
0° Outlet				
5° Inlet				<i>Wavy</i>
5° outlet				<i>Intermittent</i>
10° inlet				<i>Wavy</i>
10° outlet				<i>Intermittent</i>
15° inlet				<i>Wavy</i>
15° outlet				<i>Intermittent</i>
30° inlet				<i>Wavy-churn</i>
30° outlet				<i>Intermittent</i>
45° inlet				<i>Wavy-churn</i>
45° outlet				<i>Intermittent</i>
60° inlet				<i>Churn</i>
60° outlet				<i>Intermittent</i>
90° inlet				<i>Churn</i>
90° outlet				<i>Intermittent</i>

Figure 6.3: Flow pattern transitions for $x = 0.25$ upward flows of 0° to 90°

Apparently, with just a slight increase in the inclination angle up to $+5^\circ$, the flow pattern changes completely. The slight tilt of the tube upward by 5° causes the interfacial waves to grow, thereby momentarily touching the inner surface of the tube without breaking. As the vapour moves along the tube, condensate forming along the tube wall is forced along the length of the tube, with large-amplitude waves forming and being separated by long elongated bubbles that have smaller bubbles trailing behind. These smaller bubbles would coalesce with the larger bubbles that would eventually attach themselves to the elongated bubble. Two flow patterns, wavy at the inlet and intermittent at the outlet, were also observed for $+10^\circ$ and $+15^\circ$ inclination angles of $+10^\circ$ and $+15^\circ$. However, the rate of wave formation and amplitude increased with inclination angle.

From $+30^\circ$ to $+90^\circ$, the flow becomes more disturbed with much increase in wave formation and agitation of the flow due to the gravitational effects. Hence, a combination of wavy and the churning effect, which is the wavy-churn flow pattern, was observed on the inlet, and due to the increase in angle of inclination and gravitational effects, the flow transitioned to intermittent flow for $+30^\circ$ and $+90^\circ$ on the outlet of the test condenser.

6.3.2. Positive inclinations for a quality of 0.75

Figure 6.4, shows upward flow patterns from the inlet to the outlet at a quality of 0.75. At high qualities, unlike at a low quality, some flow patterns observed for the lowest mean quality of 0.25 were not observed at a mean quality of 0.75. The observed flow patterns are stratified-wavy, wavy, wavy-churn, wavy-annular and annular flow patterns. Hence, at higher qualities, there are no stratified, intermittent or churn flow patterns. This is because of the high shear forces that are present for higher qualities. From the flow patterns from 0° to $+15^\circ$, stratified-wavy is common, and the gradual increase from the horizontal upwards should cause the heat transfer coefficient to decrease as film thickness increases.

As the inclination angle is increased, the waves increase and the flow transitions from stratified-wavy to wavy flow at $+15^\circ$. From the inclination angle of $+30^\circ$, the flow transitions from stratified-wavy to wavy-churn flow as a result of the increased gravitational effects acting against the flow. Wavy-annular flow becomes common from $+45^\circ$ to $+60^\circ$ as the inlet flow pattern. However, at the outlet, the flow transitions to wavy-churn, and at the vertical inclination, the flow transitions from annular to wavy-annular.








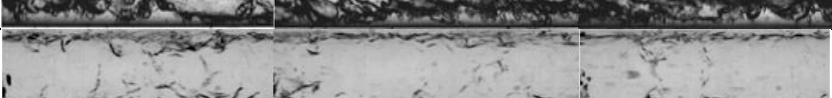
Inclination angle	Time [s]			Observed flow pattern
	0	0.25	0.5	
0° inlet				<i>Stratified-wavy</i>
0° outlet				<i>Stratified-wavy</i>
5° inlet				<i>Stratified-wavy</i>
5° outlet				<i>Stratified-wavy</i>
10° inlet				<i>Stratified-wavy</i>
10° outlet				<i>Stratified-wavy</i>
15° inlet				<i>Stratified-wavy</i>
15° outlet				<i>Wavy</i>
30° inlet				<i>Stratified-wavy</i>
30° outlet				<i>Wavy-churn</i>
45° inlet				<i>Stratified-wavy</i>
45° outlet				<i>Wavy-churn</i>
60° inlet				<i>Stratified-wavy</i>
60° outlet				<i>Wavy-churn</i>
90° inlet				<i>Annular</i>
90° outlet				<i>Wavy-annular</i>

Figure 6.4: Flow pattern transitions for $x = 0.75$ upward flows of 0° to 90°

6.3.3. Negative inclinations for a quality of 0.25

Figure 6.5, represents flow patterns for the downward inclinations for a quality of 0.25. Unlike upward inclinations, downward inclinations have stratified-wavy as the main flow pattern observed for all the inclinations except for -90° , where the annular flow pattern is the only one observed. This explains why the heat transfer coefficient in downward flow is higher than the heat transfer coefficient in the upward flow. The condensate in downward flow is restricted to the bottom part of the tube, with the top part acting as the main source where there is effective heat transfer. For lower qualities, the liquid layer is thicker on the horizontal inclination, gradually thinning up to between -15° and -30° , where, according to this research, the highest heat transfer coefficient is observed. From -45° up to -60° , the film thickness increases as it drives more liquid condensate down the tube, up to -90° , where the flow becomes annular for both the inlet and the outlet. What can be noted as well is the flow pattern for the quality of 0.25 at the outlet from the test condenser, the flow pattern is depicted in the figure as stratified-wavy since in the 501 frames taken, only 3 frames were used and one can argue that it is stratified flow instead of stratified-wavy. The flow as seen by the researcher in all the 501 frames, some frames it would show a stratified flow whilst in others it would show stratified-wavy hence it can be concluded that the flow is lying along the transition line and can either be stratified-wavy or stratified flow pattern. The flow in this case will be labelled stratified-wavy flow pattern

Inclination and position	Time [s]			Observed flow pattern
	0	0.25	0.5	
0° Inlet				Stratified-wavy
0° outlet				
5° inlet				Stratified-wavy
5° outlet				
10° inlet				Stratified-wavy
10° outlet				
15° inlet				Stratified-wavy
15° outlet				
30° inlet				Stratified-wavy
30° outlet				
45° inlet				Stratified-wavy
45° outlet				
60° inlet				Stratified-wavy
60° outlet				
90° inlet				Annular
90° outlet				Annular

Figure 6.5: Flow pattern transitions for $x = 0.25$ downward flows of 0° to -90°

6.3.4. Negative inclinations for a quality of 0.75











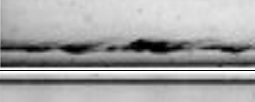



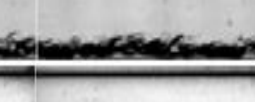
























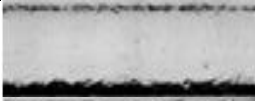






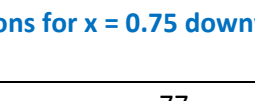
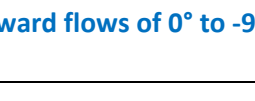
Inclination and position	Time [s]			Observed flow pattern
	0	0.25	0.5	
0° inlet				<i>Stratified-wavy</i>
0° outlet				
5° inlet				<i>Stratified-wavy</i>
5° outlet				
10° inlet				<i>Stratified-wavy</i>
10° outlet				
15° inlet				<i>Stratified-wavy</i>
15° outlet				
30° inlet				<i>Stratified-wavy</i>
30° outlet				
45° inlet				<i>Stratified-wavy</i>
45° outlet				
60° inlet				<i>Stratified-wavy</i>
60° outlet				
90° inlet				<i>Annular</i>
90° outlet				<i>Annular</i>

Figure 6.6: Flow pattern transitions for $x = 0.75$ downward flows of 0° to -90°

In Figure 6.6, the downward flow patterns at a higher quality of 0.75 are shown for different inclination angles. As stated in Section 6.3.3, the flow patterns are just the same as observed, stratified-wavy in other inclinations and annular for the vertically downward (-90°) flow. The only difference between the lower quality and the higher quality is the film thickness. The resulting effect shows that film thickness increases as quality decreases.

In conclusion, for a mass flux of $100 \text{ kg/m}^2\cdot\text{s}$, upward inclinations, stratified and stratified-wavy flow patterns are observed for a lower quality of 0.2 and a horizontal inclination. On the other hand, wavy and intermittent flow patterns are common at lower inclination angles, and wavy-churn, churn and intermittent flow patterns are prevalent at higher inclination angles of $+45^\circ$ to $+90^\circ$ for a quality of 0.2. However, as quality is increased to 0.75, the prevalence of a stratified-wavy flow increases from 0° up to $+30^\circ$. Above $+30^\circ$, wavy-churn, churn and wavy-annular flow patterns are dominant at higher qualities. For the downward flow, only three flow patterns are observed, unlike the eight observed in the upward inclinations. Stratified-wavy flow is very common for all the mean qualities from 0° to -60° , with the film thickness differentiating the level of stratification. For a -90° angle, annular flow is the only flow pattern observed for all the qualities. Hence, the orientation and direction of flow, as well as the quality, influence the different hydraulic set-ups of the two phases for a condensing flow, and this influences the rate at which heat is transferred.

6.4. Graphic presentation of flow patterns and flow pattern transitions

This section presents a graphic representation of the experimental data as a function of mass flux, quality and inclination. The data is for all the mass fluxes investigated from $100 \text{ kg/m}^2\cdot\text{s}$ to $25 \text{ kg/m}^2\cdot\text{s}$, at mean qualities from 0.15 to 0.9 and a temperature difference of 3°C . The data is for all the inclination angles investigated in this study, from $+90^\circ$ to -90° . The data is presented separately for downward flow and for upward flow due to the great differences in the flow structure between the two.

6.4.1. Present data on the El Hajal-Thome-Cavallini flow pattern map

Lips and Meyer [25] conducted studied for R-134a condensing in an 8.38 mm tube at different inclination angles. They plotted their experimental data on the Barnea [85] flow pattern map developed for air-water flows. The flow pattern map failed to predict the flow patterns observed for the condensation of R-134a. They also used the Crawford [6, 86] flow pattern map which was developed for adiabatic flows with R113 refrigerant for tube diameters of 25 mm and 30 mm. The map was in good agreement with their data for the annular flow pattern but it failed to predict the stratified/intermittent flow transition they however concluded that maps that were developed for adiabatic flow could not correctly predict the condensing flow patterns as the condensation phenomenon was not taken into account. The flow pattern map of Hajal *et al.* [11] is used to plot the experimental data for

the positive inclination angles in Figure 6.7 and for the negative inclination angles in Figure 6.8. The flow pattern map used is one of the first comprehensive flow pattern maps for in-tube condensation and it was developed for the horizontal inclined tubes. Although the map would not be expected to predict flow patterns observed for inclined angles, it has been selected as it is the most comprehensive flow pattern map developed so far for the condensing flows and hence could be the starting point for future developments of a flow pattern map for inclined angles. But first one needs to determine where or how the map fails to predict the flow patterns observed for inclined tubes?

6.4.1.1 Positive inclinations

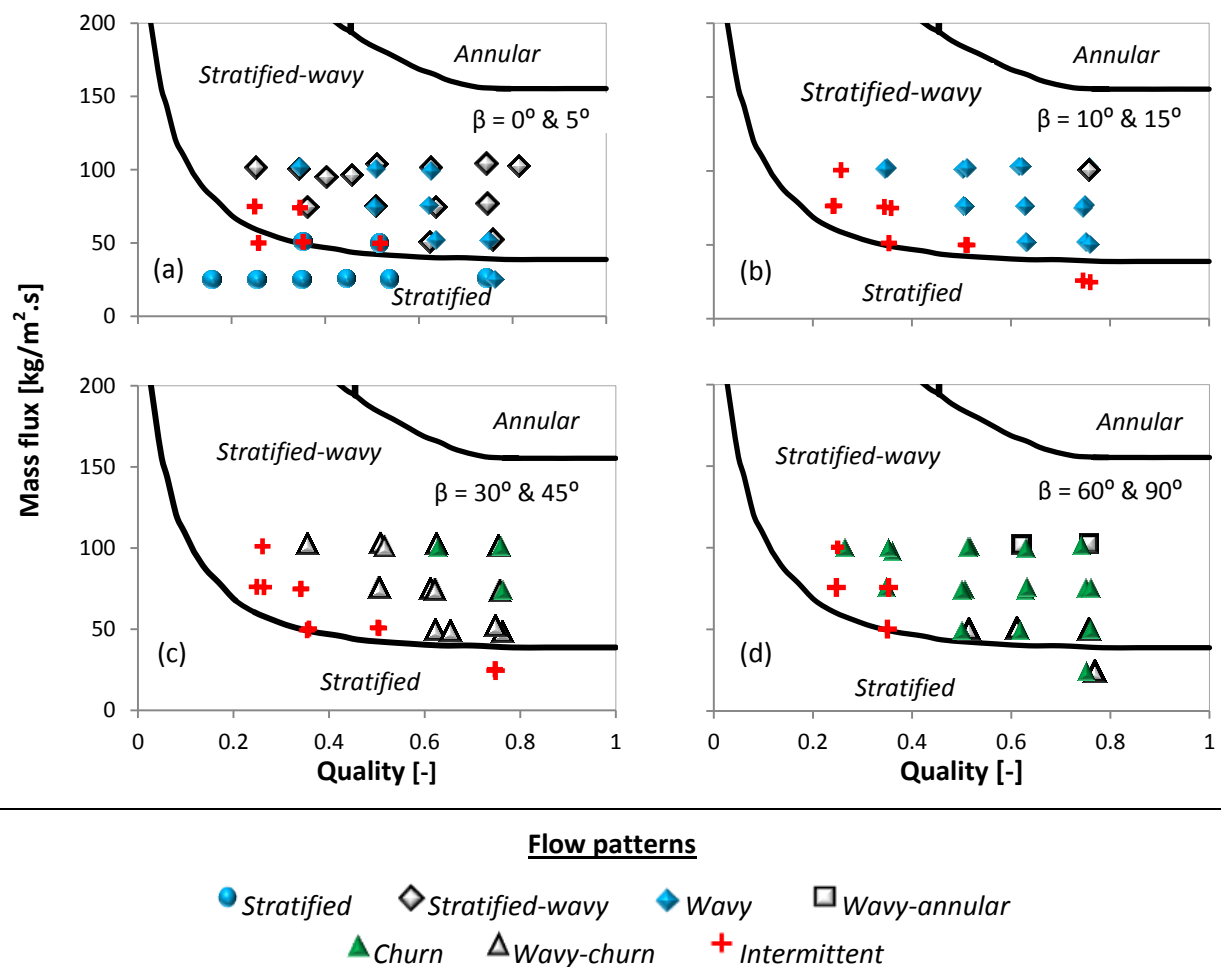


Figure 6.7: Present data for positive inclinations on the Hajal-Thome-Cavallini flow pattern map

In Figure 6.7, it can be seen that, for the upward inclinations, the flow pattern map can only predict the horizontal inclination. From the lowest inclination of +5° up to +90°, the flow pattern map fails to predict the flow pattern correctly, especially for a mass flux of 100 kg/m².s and below. Only stratified and stratified-wavy flow patterns could be predicted for the horizontal inclination. The slip ratio; (gas velocity to liquid velocity) needs to be taken into account since as it varies from flow pattern to flow pattern. It can be observed that at low mass fluxes, the flow patterns are dependent on the inclination hence there may

be significant variation of flow patterns from one inclination angle to another [25]. Lips and Meyer concluded that the inclination effect depends strongly on the vapour quality and mass flux.

6.4.1.2 Negative inclination

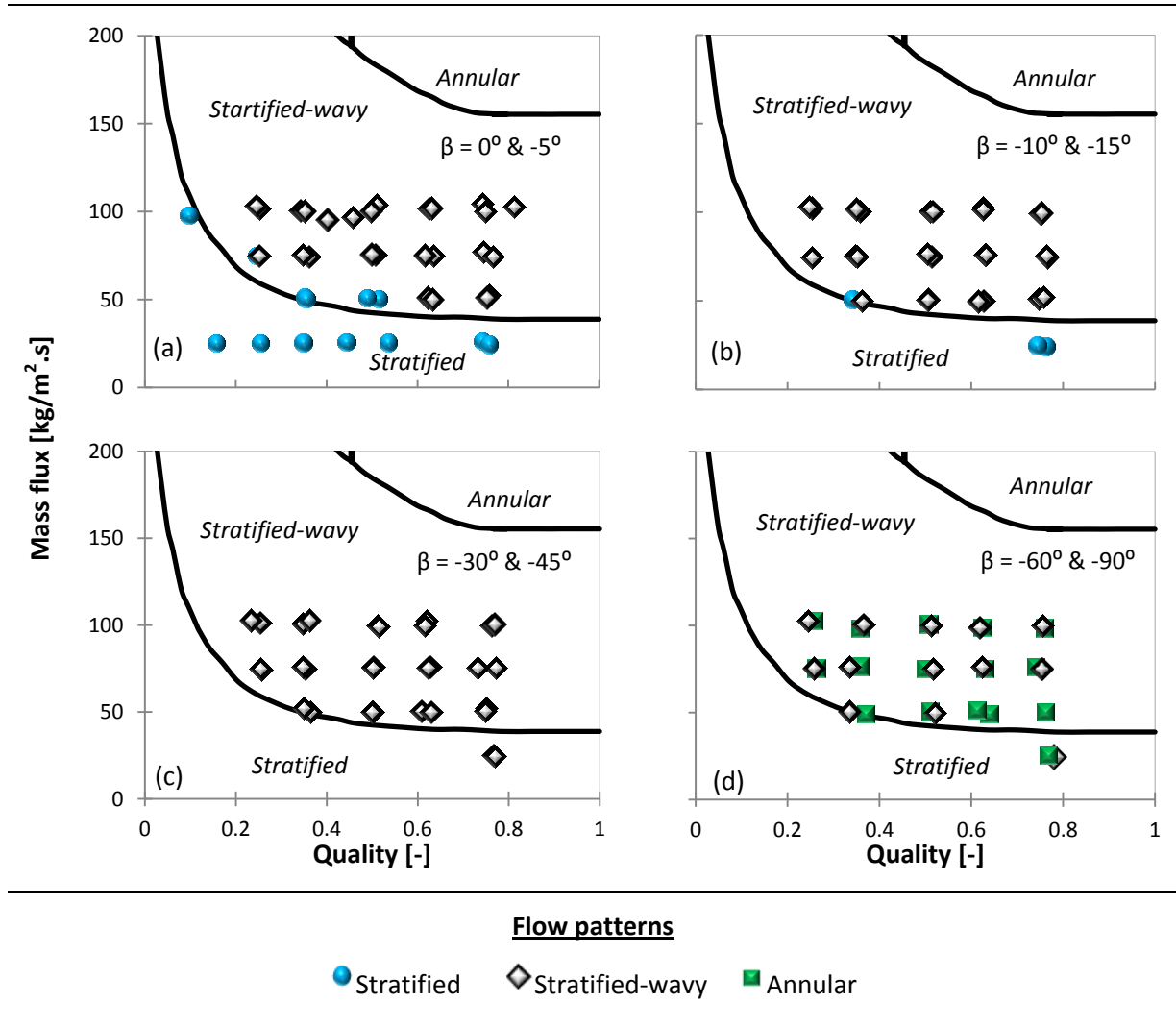


Figure 6.8: Present data for negative inclinations on the Hajal-Thome-Cavallini flow pattern map

Figure 6.8 shows the experimental data for the downward inclination angles plotted on the flow pattern map of Hajal *et al.* [11]. Unlike the downward inclinations, for the upward inclinations, the flow pattern map could almost predict from the horizontal up to -45° for mass fluxes of $50 \text{ kg/m}^2 \cdot \text{s}$ upwards. However, this can only be true for qualities of 0.25 upwards, as the study did not capture data less than 0.25 for inclined angles. Stratified and stratified-wavy flow patterns are observed for inclination angles from 0 to -15° (as can be seen in Figure 6.8 (a) and Figure 6.8 (b)), and these could be predicted well with the flow pattern map. For -30° and -45° , depicted in Figure 6.8 (c), the mass flux of $25 \text{ kg/m}^2 \cdot \text{s}$ could not be predicted by the map. This can already be seen at a quality of 0.75, where the flow pattern is stratified-wavy instead of stratified, indicated on the map. Stratified-wavy could

be predicted well at -60° for mass fluxes of $75 \text{ kg/m}^2\cdot\text{s}$ and $100 \text{ kg/m}^2\cdot\text{s}$, but for a mass flux of $50 \text{ kg/m}^2\cdot\text{s}$, it could be predicted for lower qualities of 0.5 and 0.35. Lower than this, the map is not able to predict. This can be seen in Figure 6.8 (d). The annular flow pattern is the dominant flow pattern for the -90° inclination, and could not be predicted by the map, despite the quality.

6.4.2. Flow pattern transitions – present data

The current data, which is plotted on the Hajal-Thome-Cavallini flow pattern map, is also plotted in Figure 6.9, which depicts positive inclinations, and Figure 6.10, which depicts negative inclinations. Flow pattern transitions are plotted for each inclination angle investigated in the study. Eight different flow pattern transitions are observed for the positive inclination angles. These are shown in Figure 6.9. The stratified flow pattern for the horizontal inclination is only predicted for lower qualities, but increases with a decrease in mass flux. The intermittent flow predicted for all other inclination angles at very low qualities increases with an increase in inclination and a decrease in mass flux up to $+45^\circ$. It decreases with a decrease in quality. The wavy flow pattern is predicted at higher qualities, increasing with an increase in mass flux from $+5^\circ$ up to $+15^\circ$. The flow then transitions to wavy-churn from $+30^\circ$ to $+60^\circ$. From 45° at higher qualities and mass flux, the churn flow pattern is evident, increasing with increase in quality. Finally, the stratified-wavy and wavy-annular flow patterns are only observed at high qualities and mass flux for angles of $+5^\circ$ to $+10^\circ$ and $+90^\circ$ respectively.

6.4.2.1 Positive inclination

There are two flow pattern transitions for the negative inclinations, as can be seen in Figure 6.10. These include stratified-wavy to stratified and annular flow patterns. The stratified flow pattern is observed for low inclinations -5° to -15° , and decreases with an increase in mass flux and quality. The instability of the system could not allow the capture of data below quality of 0.75 for a mass flux of $25 \text{ kg/m}^2\cdot\text{s}$. Hence, at -30° and -45° it is assumed that stratified flow can still be observed at lower qualities at a mass flux of $25 \text{ kg/m}^2\cdot\text{s}$ and below.

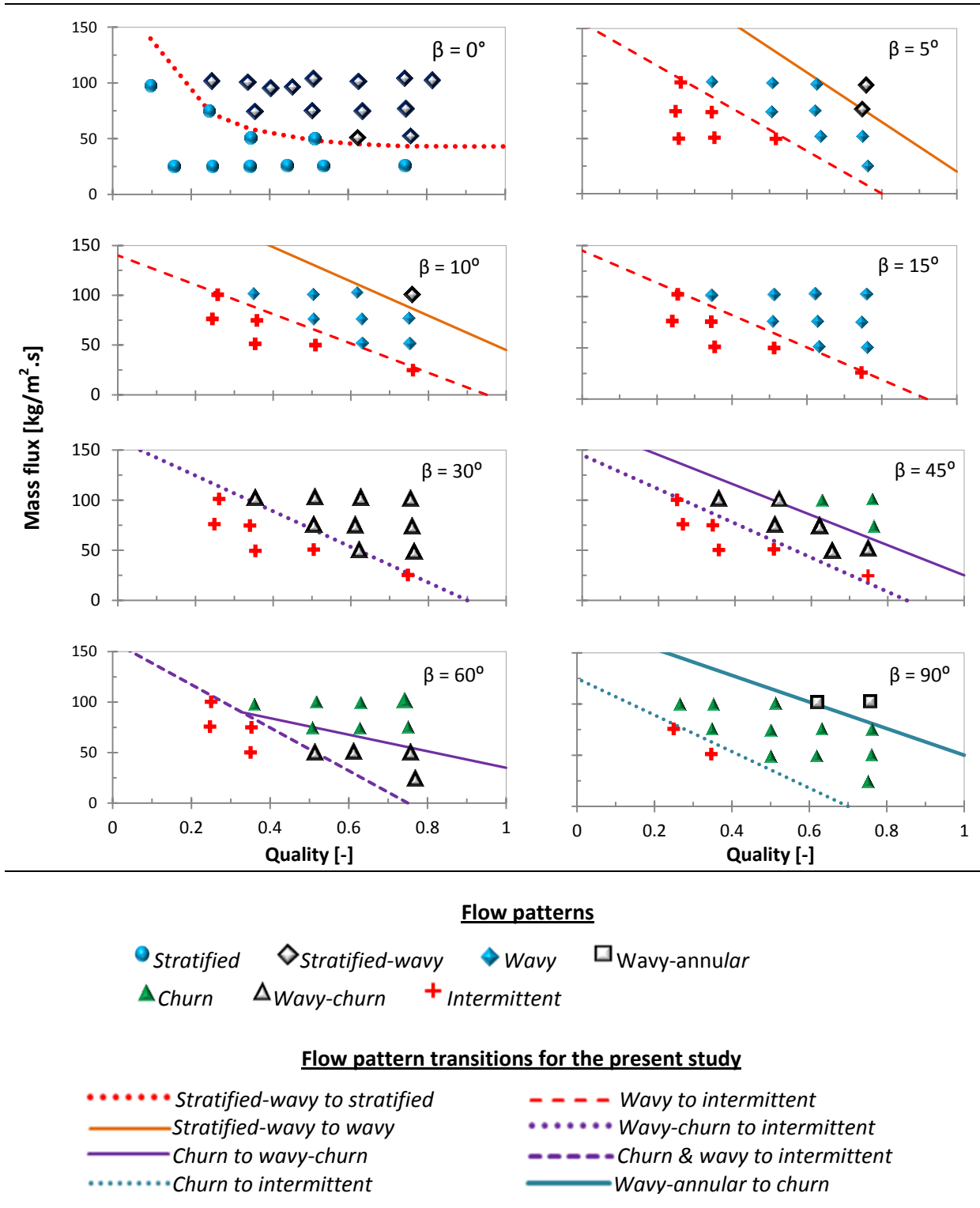


Figure 6.9: Effect of inclination on flow patterns for positive inclinations

6.4.2.2 Negative inclinations

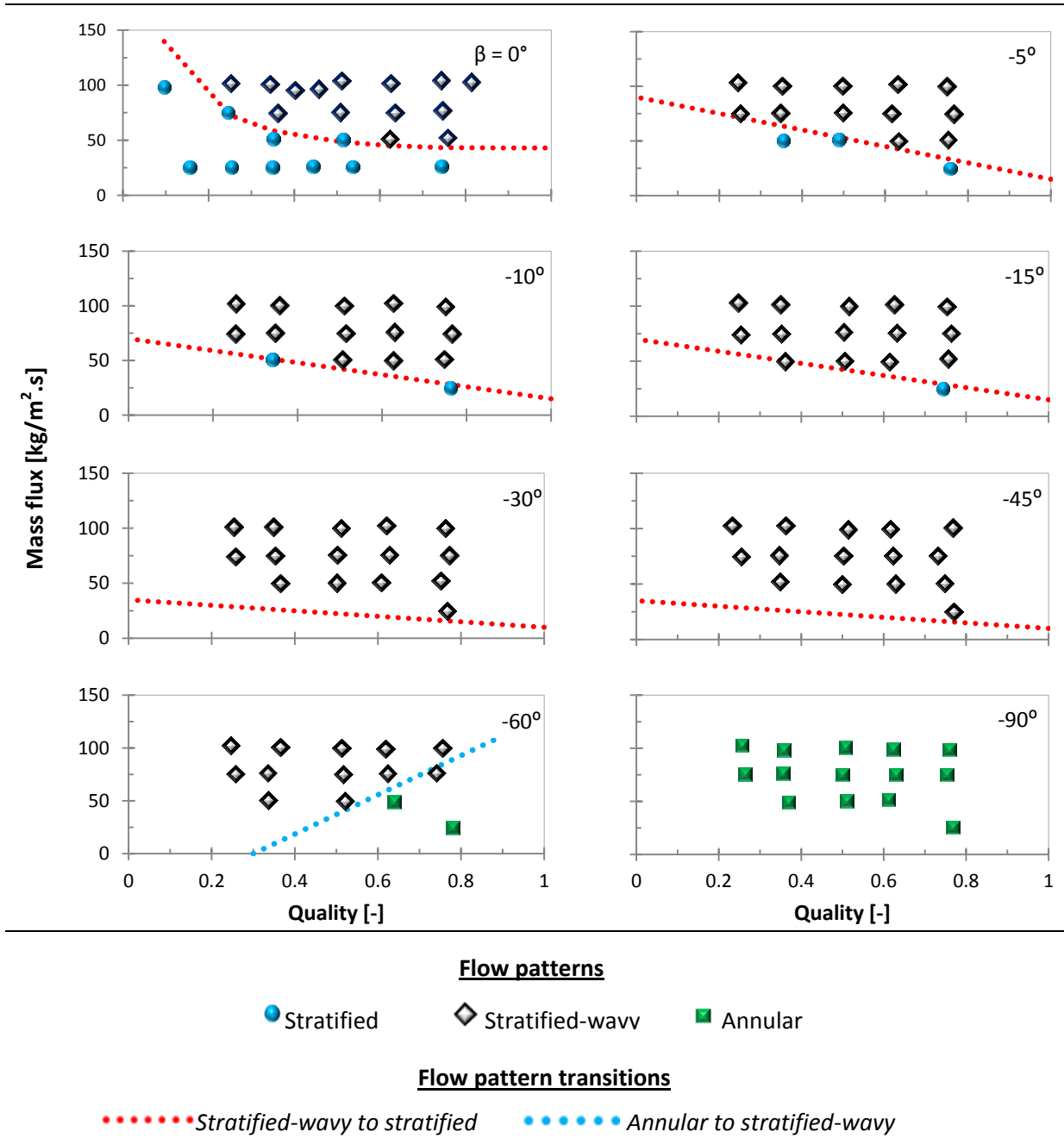


Figure 6.10: Effect of inclination on flow patterns for negative inclinations

Finally, annular flow is predicted for high qualities, and increases with decreasing mass flux, at -90° . The flow remains annular for all qualities and mass flux.

6.5. Conclusion

This chapter summarised the observed flow patterns and flow pattern transitions observed during the experiment. The flow patterns observed were for a mass flux of $100 \text{ kg/m}^2 \cdot \text{s}$, temperature difference of 3°C and qualities of 0.25 and 0.75. For the flow pattern map and graphical representation of the flow patterns, the data used was for all the mass fluxes in

the range at a temperature difference of 3 °C. At a temperature difference of 1 °C, the data was only for a mass flux of 25 kg/m².s. The flow patterns were observed on the inlet to the test section and on the outlet from the test section. This was done to determine the transition of the flow pattern from inlet to outlet, as well as the transition of the flow pattern with an increase or a decrease in quality and inclination angle. The flow patterns with the horizontal, the vertically up or down, and various other inclination were also compared. The data was compared to the Hajal-Thome-Cavallini flow pattern map for the horizontal in-tube condensation. Flow pattern transitions were also suggested for the experimental data.

After the analysis, it was concluded that vertically upward and downward flow patterns differ from those on the horizontal inclination for the same operating parameters and ranges. Vertically upward flow patterns that were observed comprised wavy, churn, wavy-churn, and intermittent flow patterns. For the vertically downward flow, the main observed flow pattern was: annular flow for all qualities and mass fluxes.

The observed flow patterns for the positive inclination angles from 0 to +90° at a quality of 0.25 were stratified-wavy, stratified, wavy, intermittent, wavy-churn; and churn flow patterns. For a quality of 0.75, the following flow patterns were observed: stratified-wavy; wavy, wavy-churn, wavy-annular and annular flow patterns. The rate of wave formation increased with an increase in the inclination angle for positive inclinations.

Eight different flow patterns transitions were observed for the positive inclination angles. These are stratified-wavy to stratified, stratified-wavy to wavy, churn to wavy-churn, churn to intermittent, wavy to intermittent, wavy-churn to intermittent, churn and wavy to intermittent and wavy-annular to churn. The intermittent flow pattern is common at low qualities and low mass fluxes for inclination angles below +60°. The wavy flow pattern is prevalent at higher qualities and increases with an increase in mass flux from +5° to +15°. Two flow pattern transitions for negative inclinations are: stratified-wavy to stratified, and stratified-wavy to annular. The stratified-wavy flow pattern is common for most of the inclination angles from 0° to -60°, whilst the stratified flow pattern is observed for low inclination angles and low qualities at mass fluxes below 100 kg/m².s.

The study revealed that the flow pattern formation and structure has a bearing on the rate at which heat is transferred from the vapour or working fluid to the external source or heat sink. The Hajal-Thome-Cavallini flow pattern map only managed to predict the flow patterns for the horizontal inclination, but failed to predict upward inclinations from +5° to +90°. It managed to predict downward flows from 0° to -15° for mass fluxes above 25 kg/m².s, but failed to predict flow patterns for inclination angles of -30° and -45° and at mass fluxes lower than 25 kg/m².s. The Hajal-Thome-Cavallini flow pattern map only predicted the intermittent flow pattern map at mass flux of 200 kg/m².s and higher and at lower qualities. It can be noted that the inclination effect at lower mass fluxes below 100 kg/m².s resulted in the development of the intermittent flow pattern at lower qualities unlike the stratified and

stratified-wavy flow patterns previously predicted. The proper identification and analysis of the flow pattern will go a long way in assisting researchers to come up with models and correlations that will enable optimum parameters to be used when designing heat exchangers, condensers and refrigerating systems. The flow patterns at mass fluxes below $100 \text{ kg/m}^2\cdot\text{s}$, as observed, differ with inclination. Vertically upward flow patterns differ significantly with vertically downward flows, and the experiments revealed the differences in the heat transfer coefficient of the two. The flow patterns change from one flow pattern to another due to inclination, quality, mass flux and temperature difference. For flow pattern maps to be formulated, flow pattern transitions need to be determined.

In order to correctly predict condensing flow patterns and flow pattern transitions for the inclined configurations at low mass fluxes, the following can be suggested:

- Conduct experimental studies for different refrigerants, tube diameters with flow visualisation on the inlet and outlet of the test section for different inclination angles and identify which flow patterns are observed;
- Develop flow pattern transition models for each inclination angle. The transition models of Hajal-Thome-Cavallini Hajal, Thome and Cavallini [11] can be used by just modifying them to include the effect of inclination and the slip ratio;
- Check if the transition model can predict the observed flow patterns;
- Develop a flow pattern map or maps for the whole data range;
- Do the same for higher mass fluxes;
- A good start will be on the development of the Hajal-Thome-Cavallini condensing flow pattern map although other transitions need to be modelled like churn flow which was not previously included in their model;
- The transition region needs to be specified and kept to a narrow margin other than the $50 \text{ kg/m}^2\cdot\text{s}$ as previously developed.

Figure 6.9 and Figure 6.10 just showed lines drawn to mark the transitions for the experimental data. However flow pattern transition models need to be developed that can precisely predict the flow patterns for a greater range of refrigerants, mass fluxes, diameters and inclination angles.

7. Summary, conclusions and recommendations

7.1. Summary

Energy conservation for two-phase flow systems is best achieved by optimum design levels of energy-efficient systems. Most of the two-phase flow systems are operated by vapour compression cycles and these provide potential for improvement, especially on the main aspect of heat transfer. For this reason the main focus of this study was on the investigation of two-phase flow condensation at mass fluxes below $100 \text{ kg/m}^2\cdot\text{s}$ and different inclination angles. To enable accurate design parameters and the prediction of these systems' design performance, experimental data is needed. Other researchers have proven that mathematical models and correlations have failed to correctly predict the resulting flow patterns and heat transfer coefficients. A number of gravity-driven flow correlations have been developed for stratified flow patterns and annular flow patterns for horizontal flows. However, these cannot correctly predict other flow patterns like wavy, intermittent and churn flow patterns for both horizontal and inclined flows at low mass velocities. Since heat transfer coefficients are directly linked to the prevailing flow pattern, experimental data to investigate the different flow patterns observed for different inclinations at mass fluxes below $100 \text{ kg/m}^2\cdot\text{s}$ is essential. This had not been investigated before.

An experimental set-up previously used for two-phase flow experiments for both horizontal and other inclined flows at high mass fluxes above $100 \text{ kg/m}^2\cdot\text{s}$ was used. The experimental was set-up at the Thermoflow Laboratories of the Clean Energy Research Group of the Department of Mechanical Engineering in the University of Pretoria's Faculty of Engineering, Built Environment and Information Technology. The adaptability of the two-phase flow system enabled condensing and evaporative tests at both high and mass fluxes of $100 \text{ kg/m}^2\cdot\text{s}$ and below to be conducted. Unlike the previous experiments, where only the flow patterns on the outlet to the test section were captured, the experiments for this study managed to capture both the inlet and outlet flow patterns to and from the test section respectively. This necessitated an analysis of flow pattern transitions from the inlet to the outlet of the test section. The test section consisted of a copper in-tube heat exchanger, the annulus with an outer diameter of 15.9 mm with cooling fluid, which in this case, was water. The inner tube with condensing refrigerant R-134a had an inner diameter of 8.38 mm. The length of the test section was 1.5 m, with sight glasses on the inlet to the test section and the other on the outlet to the test section. Two Besler cameras, operating at 60 fps were used to capture the flow patterns of all the tests that were conducted.

7.2. Conclusion

The experimental investigation of two-phase flow in-tube condensation of R-134a at mass fluxes of $100 \text{ kg/m}^2\cdot\text{s}$ and below was carried out in the Thermoflow Laboratory. The study investigated condensing flow patterns for inclined tubes, effect of quality, mass flux, temperature difference and inclination angle on the heat transfer coefficient, and the effect of flow patterns on the heat transfer coefficient for different inclination angles.

The eight flow patterns that were observed for condensing R-134a at different inclination angles were annular, wavy-annular, stratified, stratified-wavy, intermittent, wavy-churn, churn and wavy. Only the stratified flow pattern was observed for the horizontal inclination, which means that inclining the tube had an effect on the hydraulic structure of the condensing fluid. The stratified-wavy flow pattern is common for downward inclinations from 0° to -60° , while the annular flow pattern is prevalent at -90° . Flow patterns transitioned significantly from one flow pattern to another for positive inclination angles. There are three different flow patterns for negative inclinations (including the horizontal orientation), compared to seven flow patterns for the positive inclination angles. The only flow patterns that were not observed for positive inclination angles were the annular flow pattern and that stratified flow pattern, the latter only being observed at the horizontal 0° . When the tube is inclined slightly to $+5^\circ$, the flow pattern transitions from stratified to intermittent flow at low qualities, thereby increasing with a decrease in mass flux. Intermittent flow is very common for all the inclined angles from $+5^\circ$ to $+90^\circ$. The wavy flow pattern is confined to lower inclination angles $+15^\circ$ and below while wavy-churn and churn are common for higher positive inclination angles.

The highest heat transfer coefficient is observed between the inclination angles of -15° to -30° for all mass fluxes, vapour qualities and temperature differences. At these angles, the stratified-wavy flow pattern is observed. The lowest heat transfer coefficient is observed at -90° , where the annular and wavy-annular flow patterns are dominant.

The general trend for most inclination angles is that the heat transfer coefficient increases with an increase in quality. The exception is for higher positive inclination angles especially $+90^\circ$, in which the heat transfer coefficient decreases with an increase in quality for higher mass fluxes of $75 \text{ kg/m}^2\cdot\text{s}$ and $100 \text{ kg/m}^2\cdot\text{s}$. On the other hand, the heat transfer coefficient increases with an increase in mass flux for different inclination angles for temperature differences of 5°C and above. However, for the horizontal inclination, there is a minute increase in the heat transfer coefficient with an increase in quality for mass fluxes of $100 \text{ kg/m}^2\cdot\text{s}$ and below. For a lower temperature difference of 3°C , the heat transfer Coefficient decreases with an increase in mass flux for higher positive inclination angles from $+30^\circ$ to $+90^\circ$. Temperature difference had a remarkable influence on the heat transfer coefficient for most of the inclined angles. The general pattern is that the heat transfer coefficient increases with a decrease in the temperature difference, with a notable increase at lower qualities for the horizontal inclination. At temperature differences above 8°C ,

temperature difference has little influence on the heat transfer coefficient. For other inclined angles, the effect of temperature difference is not the same for the upward and downward flows. For positive inclination angles, there is a striking difference at higher inclination angles above $+15^\circ$ for mass fluxes of $75 \text{ kg/m}^2\cdot\text{s}$ and $100 \text{ kg/m}^2\cdot\text{s}$. The heat transfer coefficient increases with an increase in temperature difference, which is not the same for negative inclination angles.

The variations in inclination angle, mass flux, quality and temperature difference has seen flow pattern characteristics changing. This change in flow patterns constituted a change in the heat transfer coefficient. For condensing R-134a at mass fluxes of $100 \text{ kg/m}^2\cdot\text{s}$ and below, the heat transfer coefficient is a function of quality, mass flux, temperature difference and inclination angle. Any correct and effective modeling of the two-phase flow heat transfer coefficient and the development of correlations for flow pattern transitions should consider the effect of mass flux, quality, temperature difference and inclination angle.

7.3. Recommendations

Condensing two-phase flow models for predicting heat transfer coefficients developed in literature recently are governed by the locally observed flow pattern. Such models have successfully predicted the heat transfer coefficient with a much higher degree of accuracy than those that did not consider the two-phase flow characteristics. Flow patterns relate to the hydraulic and geometric characteristics of the two-phases: vapour and liquid. Moreover, some correlations have been developed to predict flow pattern transitions on flow pattern maps. These maps help to identify flow patterns at various flow conditions. This study lays the foundation for the future modeling of two-phase flow condensing heat transfer coefficients at low mass velocities and flow pattern maps for inclined configurations. The following is therefore recommended:

- Experimental investigations that were conducted for this study can also be extended to other eco-friendly refrigerants like R-410A, R-407C, R152a, R290, and R502;
- Since the minimum average quality obtained for different inclination angles was 0.25, lower average qualities than this, as well as qualities higher than 0.75 can also be investigated;
- The study only focused on smooth tubes, hence enhanced tubes of various roughness and structures can also be investigated;
- Experiments for different diameters and tube geometry can be investigated;
- Since the maximum angle for the highest heat transfer coefficients was between -15° to -30° it is also essential to investigate other angles in between, for example -20° , -25° and -35° . This can be done to see exactly which angle gives the maximum heat transfer coefficients;

- Most models for two-phase flow maps in literature were designed mainly for horizontal configurations. However, the study revealed that inclining the angle changes the structure of the flow hence the effect of inclination has to be included in modeling flow pattern transitions correctly during the development of flow pattern maps;
- Heat transfer models that are based on the prevailing flow pattern can be developed for condensing flow at different inclination angles and low mass velocity.

References

- [1] L. Cheng, G. Ribatski, J.R. Thome, Two-phase flow patterns and flow-pattern maps: fundamentals and applications, 2008.
- [2] A. Cavallini, L. Doretti, M. Matkovic, L. Rossetto, Update on condensation heat transfer and pressure drop inside minichannels, *Heat Transfer Engineering*, 27(4), pp. 74-87 (2006).
- [3] D. Barnea, O. Shoham, Y. Taitel, Flow pattern transition for vertical downward two phase flow, *Chemical Engineering Science*, 37(5), pp. 741-744 (1982).
- [4] P.L. Spedding, D.R. Spence, Flow regimes in two-phase gas-liquid flow, *International Journal of Multiphase flow*, 19(2), pp. 245-280 (1993).
- [5] Y. Taitel, A.E. Dukler, A model for predicting flow regime transitions in horizontal and near-horizontal gas-liquid flow, *ASME Heat Transfer Journal*, 120, pp. 148-155 (1976).
- [6] J. Weisman, D. Duncan, J. Gibson, T. Crowfords, Effects of fluid properties and pipe diameter on two-phase flow patterns in horizontal lines, *International Journal in Multiphase flow*, 5, pp. 437-462 (1979).
- [7] O. Baker, Simultaneous flow of oil and gas, *Oil and Gas Journal*, 53, pp. 185-190 (1954).
- [8] J.M. Mandhane, G.A. Gregory, K. Aziz, A flow map for gas liquid flow in horizontal pipes, *International Journal of multiphase flow*, 1, pp. 537-553 (1974).
- [9] P.L. Spedding, V.T. Nguyen, Regime map for air-water two-phase flow, *Chemical Engineering and Science*, 35, pp. 779-793 (1980).
- [10] N. Kattan, J.R. Thome, D. Favrat, Flow boiling in horizontal tubes - Part 1: development of a diabatic two-phase flow pattern map, *ASME Heat Transfer Journal*, 120, pp. 140-147 (1998).
- [11] J.E. Hajal, J.R. Thome, A. Cavallini, Condensation in horizontal tubes, Part 1: two-phase flow pattern map, *International Journal of Heat and Mass Transfer*, 46, pp. 3349-3363 (2003).
- [12] J.R. Thome, On recent advances in modelling of two-phase in heat transfer, *Heat Transfer Engineering*, 24(6), pp. 46-59 (2003).
- [13] S.M. Ghiaasiaan, Two-phase flow boiling and condensation in conventional and miniature systems, Cambridge University Press, 2008.
- [14] I. Park, H. Lee, I. Mudawar, Determination of flow regimes and heat transfer coefficients for condensation in horizontal tubes, *International Journal of Heat and Mass Transfer*, 80, pp. 698-716 (2015).

- [15] G.F. Hewitt, D.N. Roberts, Studies of two-phase flow patterns by simultaneous x-ray and flash photography, United Kingdom Atomic Energy Research Establishment, 1969.
- [16] S.Z. Rouhani, M.S. Sohal, Two-phase flow patterns: a review of research results, Progress in Nuclear Energy, 11(3), pp. 219-259 (1982).
- [17] Y. Taitel, A.E. Dukler, Brief communication: A theoretical approach to the Lockhart-Martinelli correlation for stratified flow, International Journal of Multiphase flow, 2, pp. 591-595 (1976).
- [18] S.M. Kim, I. Mudawar, Universal approach to predicting heat transfer coefficient for condensing mini/micro-channel flow, International Journal of Heat and Mass Transfer, 56, pp. 238-250 (2013).
- [19] P.L. Spedding, R.K. Cooper, W.J. McBride, A universal flow regime map for horizontal two-phase flow in pipes, Developped Chemical Engineering Mineral Process, 11, pp. 95-103 (2003).
- [20] J.R. Thome, Condensation in plain horizontal tubes: recent advances in modelling of heat transfer to pure fluids and mixtures, Journal of the Brazilian Society of Mechanical Science and Engineering, 27(1), pp. 23-30 (2005).
- [21] J.R. Thome, J.E. Hajal, A. Cavallini, Condensation in horizontal tubes, Part 2: new heat transfer model based on flow regimes, International Journal of Heat and Mass Transfer, 46, pp. 3365-3387 (2003).
- [22] J.A. Olivier, L. Liebenberg, J.R. Thome, J.P. Meyer, Heat transfer, pressure drop and flow pattern recognition during condensation inside smooth, helical micro-fin, and herringbone tubes, International Journal of Refrigeration, 30, pp. 609-623 (2007).
- [23] J.P. Meyer, J. Dirker, A.O. Adelaja, Condensation heat transfer in smooth inclined tubes for R-134a at different saturation temperatures, International Journal of Heat and Mass Transfer, 70, pp. 515-525 (2014).
- [24] S.P. Olivier, J.P. Meyer, M.D. Paepe, K.D. Kerpel, The influence of inclination angle on void fraction and heat transfer during condensation inside a smooth tube, International Journal of Multiphase flow, 80, pp. 1-14 (2016).
- [25] S. Lips, J.P. Meyer, Experimental study of convective condensation in an inclined smooth tube. Part 1: Inclination effect on flow pattern and heat transfer coefficient, International Journal of Heat and Mass Transfer, 55, pp. 395-404 (2012).
- [26] J.W. Coleman, S. Garimella, Characterisation of two-phase flow patterns in small diameter round and rectangular tubes, International Journal of Heat and Mass Transfer, 42, pp. 2869-2881 (1999).
- [27] F.M. White, Fluid mechanics, 7th ed., McGraw-Hill, New York, 2008.

- [28] M.M. Awad, Two-Phase Flow, 2012.
- [29] Y.a.C.a.P. Approach, Heat and mass transfer, McGraw-Hill, New York, 2006.
- [30] A.P. Colburn, 1933.
- [31] F.W. Dittus, L.M.K. Boelter, University of California publications on engineering, 1930.
- [32] S.Z. Rouhani, E. Axelsson, Calculation of void volume fraction in subcooled and quality boiling regions, International Journal of Heat and Mass Transfer, 13, pp. 383-393 (1970).
- [33] J.G. Collier, J.R. Thome, Convective boiling and condensation, 3rd ed., Oxford Science Publications, Oxford University Press, New York, 1994.
- [34] H.M. Soliman, On the annular-to-wavy flow pattern transition during condensation inside horizontal tubes, The Canadian Journal of Chemical Engineering, 60, pp. 475-481 (1982).
- [35] J.C. Chato, Laminar condensation inside horizontal and inclined tubes, ASHRAE Journal, 4, pp. 52 (1962).
- [36] H.F. Rosson, J.A. Myers, Point values of condensing film coefficients inside a horizontal tube, Chemical Engineering Progress symposium Series, 61(59), pp. 190-199 (1965).
- [37] M.K. Dobson, J.C. Chato, Condensation in smooth horizontal tubes, ASME Journal of Heat Transfer, 120, pp. 193-213 (1998).
- [38] L. Wojtan, T. Ursenbacher, J.R. Thome, Investigation of flow boiling in horizontal tubes: Part I - a new diabatic two-phase flow pattern map, International Journal of Heat and Mass Transfer, 48, pp. 2955-2969 (2005).
- [39] E.V. Rooyen, Time-fraction analysis of flow patterns during refrigerant condensation, University of Pretoria, 2007.
- [40] N. Kattan, J.R. Thome, D. Favrat, Flow boiling in horizontal tubes - Part II: new heat transfer data for five refrigerants, ASME Heat Transfer Journal, 120, pp. 148-155 (1998).
- [41] N. Kattan, J.R. Thome, D. Favrat, Flow boiling in horizontal tubes - Part III: development of a new heat transfer model based on flow patterns, ASME Heat Transfer Journal, 120, pp. 156-165 (1998).
- [42] J.R. Thome, Engineering Data Book III, Wolverine Tube, Lausanne, 2004.
- [43] D. Barnea, O. Shoham, Y. Taitel, Flow pattern transition for gas-liquid flow in horizontal and inclined pipe, International Journal in Multiphase flow, 6, pp. 217-225 (1980).

- [44] J. Weisman, S.Y. Kang, Flow pattern transition in vertical and upwardly inclined lines, *International Journal of Multiphase flow*, 7, pp. 271-291 (1981).
- [45] G. Nema, S. Garimella, B.M. Fronk, Flow regime transitions during condensation in microchannels, *International Journal of Refrigeration*, 40, pp. 227-240 (2014).
- [46] G. Arslan, N. Eskin, Heat transfer characteristics for condensation of R-134a in a vertical smooth tube, *Experimental Heat Transfer*, 28, pp. 430-445 (2015).
- [47] J.R. Thome, *Engineering Data Book, Wolverine Tube*, Lausanne, Switzerland, 2010.
- [48] J.W. Coleman, S. Garimella, Two-phase flow regimes in round, square and rectangular tubes during condensation of refrigerant R-134a, *International Journal of Refrigeration*, 26, pp. 117-128 (2003).
- [49] H.M. Soliman, N.Z. Azer, Visual studies of flow patterns during condensation inside horizontal tubes, in: *5th International Heat Transfer Conference*, Japan Society of Mechanical Engineers, Tokyo, pp. 241-245, 1974.
- [50] S. Garimella, Condensation flow mechanisms in microchannels: basis for pressure drop and heat transfer models, *Heat Transfer Engineering*, 25(3), pp. 104-116 (2004).
- [51] K. Hashizume, Flow pattern and void fraction of refrigerant two-phase flow in a horizontal pipe, *Japan Society of Mechanical Engineers*, 26, pp. 1597-1602 (1983).
- [52] G. Breber, J.W. Palen, J. Taborek, Prediction of horizontal tube side condensation of pure components using flow regime criteria, *Journal of Heat Transfer*, 102(3), pp. 471-476 (1980).
- [53] T.N. Tandon, H.K. Varma, C.P. Gupta, A new flow regimes map for condensation inside horizontal tubes, *Journal of Heat Transfer*, 104(4), pp. 763-768 (1982).
- [54] M. Christians, *Flow-pattern-based heat transfer and pressure drop correlations for condensing refrigerants in smooth tubes*, University of Pretoria, Pretoria, 2007.
- [55] H. Jaster, P.G. Kosky, Condensation heat transfer in a mixed flow regime, *International Journal of Heat and Mass Transfer*, 19, pp. 95-99 (1976).
- [56] S.G. Mohseni, M.A. Akhavan-Behabadi, M. Saeedinia, Flow pattern visualisation and heat transfer characteristics of R-134a during condensation inside a smooth tube with different tube inclinations, *International Journal of Heat and Mass Transfer*, 60, pp. 598-602 (2013).
- [57] M.K. Dobson, J.C. Chato, D.K. Hinde, S.P. Wang, *Experimental evaluation of internal condensation of refrigerants R-134a and R-12*, University of Illinois, Urbana, 1993.
- [58] C. Aprea, A. Greco, G.P. Vanoli, Condensation heat transfer coefficients for R-22 and R407C in gravity driven flow regime within a smooth horizontal tube, *International Journal of Refrigeration*, 26, pp. 393-401 (2003).

- [59] J.R. Thome, J.E. Hajal, Two-phase flow pattern map for evaporation in horizontal tubes latest version, *Heat Transfer Engineering*, 24(6), pp. 3-10 (2003).
- [60] R. Suliman, L. Liebenberg, J.P. Meyer, Improved flow pattern map for accurate prediction of the heat transfer coefficients during condensation of R-134a in smooth horizontal tubes and within the low-mass flux range., *International Journal of Heat and Mass Transfer*, 52, pp. 5701-5711 (2009).
- [61] R. Suliman, M. Kyembe, J.P. Meyer, Experimental investigation and validation of heat transfer coefficients during condensation of R-134a at low mass fluxes, in: 7th International Conference on Heat Transfer, Fluid Mechanics and Thermodynamics, HEFAT2010, Antalya, pp. 1-7, 2010.
- [62] E.V. Rooyen, M. Christians, L. Liebenberg, J.P. Meyer, Probabilistic flow pattern-based heat transfer correlation for condensing intermittent flow of refrigerants in smooth horizontal tubes, *International Journal of Heat and Mass Transfer*, 53, pp. 1446-1460 (2010).
- [63] J.A. Olivier, L. Liebenberg, M.A. Kedzierski, J.P. Meyer, Pressure drop during refrigerant condensation inside horizontal smooth, helical microfin, and herringbone microfin tubes, *Journal of Heat Transfer*, 126, pp. 687-696 (2004).
- [64] L. Liebenberg, Condensation performance in smooth and enhanced tubes, Rand Afrikaans University, Johannesburg, 2002.
- [65] M.H. Kim, J.S. Shin, Condensation heat transfer of R-22 and R-410A in horizontal smooth and microfin tubes, *International Journal of Refrigeration*, 28, pp. 949-957 (2005).
- [66] D. Jung, K.H. Song, Y. Cho, S.J. Kim, Flow condensation heat transfer coefficients of pure refrigerants, *International Journal of Refrigeration*, 26, pp. 4-11 (2003).
- [67] D. Jung, Y. Cho, K. Park, Flow condensation heat transfer coefficient of R-22, R-134a, R407a and R-410A inside plain and microfin tubes, *International Journal of Refrigeration*, 27, pp. 25-32 (2004).
- [68] C.C. Wang, C.S. Chiang, D.C. Lu, Visual observation of two-phase flow pattern of R-22, R-134a, and R-407C in a 6.5-mm smooth tube, *Experimental Thermal and Fluid Science*, 15, pp. 395-405 (1997).
- [69] H. Lee, I. Mudawar, M.M. Hasan, Flow condensation in horizontal tubes, *International Journal of Heat and Mass Transfer*, 66, pp. 31-45 (2013).
- [70] O. Agra, I. Teke, Determination of heat transfer coefficient during annular flow condensation in smooth horizontal tubes, *Journal of Thermal Science and Technology*, 32(2), pp. 151-159 (2012).

- [71] H.-S. Lee, C.-H. Son, Condensation heat transfer and pressure drop characteristics of R-290, R-600a, R-134a and R-22 in horizontal tubes, *Heat and Mass Transfer*, 46, pp. 571-584 (2010).
- [72] H.M. Soliman, Mist-annular transition during condensation and its influence on the heat transfer mechanism, *International Journal of Heat and Mass Transfer*, 12(2), pp. 277-288 (1986).
- [73] J.E. Park, F. Vakili-Farahani, L. Consolini, J.R. Thome, Experimental study on condensation heat transfer in vertical minichannels for new refrigerant R-1234ze(E) versus R-134a and R-236fa, *Experimental Thermal and Fluid Science*, 35, pp. 442-454 (2011).
- [74] S. Koyama, K. Kuwahara, K. Yamamoto, Condensation of refrigerant in a multi-port channel, in: 1st International Conference of Microchannel and Minichannel, Rochester, USA, 2003.
- [75] M.M. Shah, An improved and extended general correlation for heat transfer during condensation in plain tubes, *HVAC&R Research*, 15(5), pp. 889-913 (2009).
- [76] X. Huang, G. Ding, H. Hu, Y. Zhu, H. Peng, Y. Gao, B. Deng, Influence of oil on flow condensation heat transfer of R-410A inside 4.18mm and 1.6mm inner diameter horizontal smooth tubes, *International Journal of Refrigeration*, 33, pp. 158-169 (2010).
- [77] A. Cavallini, R. Zecchin, A dimensionless correlation for heat transfer in forced convection condensation, in: 6th International Heat Transfer Conference, Tokyo, pp. 309-313, 1974.
- [78] S. Lips, J.P. Meyer, A review of two-phase flow in inclined tubes with specific reference to condensation, University of Pretoria, Pretoria, 2011.
- [79] S. Lips, J.P. Meyer, Effect of gravity forces on heat transfer and pressure drop during condensation of R-134a, *Microgravity Science Technology*, 24, pp. 157-164 (2012).
- [80] D.R.E. Ewim, J.P. Meyer, Condensation heat transfer coefficient of enhanced tubes, in: 3rd Southern African Solar Energy Conference, Kruger National Park, pp. 230-235, 2015.
- [81] Refprop, NIST thermodynamic properties of refrigerant and refrigerant mixtures, in, National Institute of Standards and Technology, Gaithersburg, MD, 2005.
- [82] A. Cavallini, G. Censi, D.D. Col, L. Doretto, L. Rossetto, G.A. Longo, Experimental investigation on condensation heat transfer and pressure drop of new HFC refrigerants (R-134a, R-125, R-32, R-410A, R-236ea) in a horizontal smooth tube, *International Journal of Refrigeration*, 24, pp. 73-87 (2001).

- [83] A.J. Ghajar, J.Y. Kim, A non-boiling two-phase flow heat transfer correlation for different flow patterns and pipe inclination angles, in: Proceedings of the Heat Transfer, ASME, San Francisco, 2005.
- [84] W.C. Wang, X.H. Ma, A.Z.D. Wei, P. Yu, Two-phase flow patterns and transition characteristics for in-tube condensation with different surface inclinations, International Journal of Heat and Mass Transfer, 41, pp. 4341-4349 (1998).
- [85] D. Barnea, A unified model for predicting flow-pattern transitions for the whole range of pipe inclinations, International Journal of Multiphase flow, 13(1), pp. 1-12 (1987).
- [86] T.J. Crawford, C.B. Weinberger, J. Weisman, Two-phase flow patterns and void fractions in downward flow - Part 1: Steady-state flow patterns, International Journal of Multiphase flow, 11, pp. 761-782 (1985).
- [87] S. Kline, F. McClintock, Describing uncertainties in single-sample experiments, 1953.
- [88] R.J. Moffat, Describing the uncertainties in experimental results, Experimental Thermal and Fluid Science, 1, pp. 3-17 (1985).

Appendix A. Uncertainty analysis

A.1. Introduction

There can never be an entirely accurate measurement of any physical quantity due to uncertainties in the measuring device or devices, human error, calculation error and calibration errors. In this experimental set-up, results were based on the input and the level of trust in the out-put results, which leaned heavily on the accuracy in the interpretation of those results. It was therefore very important that an uncertainty analysis be carried out for this study in order to determine the deviation of the experimental results from what could have been the true value. The uncertainty levels of the heat transfer area, tube length, internal diameter of the tube, wall temperature, saturation temperature of the refrigerant, mass flux, mass flow rate of the refrigerant, heat input and heat transfer coefficient were calculated in this appendix.

A.2. Uncertainty analysis methods

Kline and McClintock [87] specified that the uncertainty of an experimental value of a given value is the possible amount of error that value may have. When a variable X_1 is considered, the uncertainty is given by ∂X_1 . For the uncertainty calculations in this study, uncertainty is determined directly, like that of Christians [54] and Van Rooyen [39], unless otherwise stated. The bias error and the precision error are the two components of uncertainty. Bias error (B_1) is the fixed error of a measurement that arises due to an error in the measuring instrument. On the other hand, a precision (P_1) error is a random error in a data sample, the impact of which can be minimised by using large samples. The uncertainty is therefore calculated as the Euclidian norm of the two, as follows:

$$\partial X_1 = \left\{ (B_1)^2 + (P_1)^2 \right\}^{0.5} \quad \text{A.1}$$

The Euclidian norm of individual uncertainties is then given as the summation of the uncertainty of R with respect to the single variable, X_i , multiplied by the variable's uncertainty, ∂X_i , [39, 54]:

$$\partial R = \left\{ \sum_{i=1}^n \left(\frac{\partial}{\partial X_i} (R) \partial X_i \right)^2 \right\}^{0.5} \quad \text{A.2}$$

Where R is a quantity with a function of n variables of X_0 to X_n .

$$R = f(X_0, X_1, \dots, X_n) \quad \text{A.3}$$

Moffat [88], in his paper, stated that the equation applies only when the following is true:

- Each individual measurement is independent;
- A Gaussian distribution is displayed for repeated observations of each measurement;
- When the uncertainty in each individual measurement was initially exhibited at the same odds.

A.3. Uncertainty of the test section tube length

A measuring tape was used to determine the length of the tube. The tape had graduations of a millimeter. The uncertainty is therefore assumed as 1 mm.

$$\delta L = 1/1000 = 0.001 \text{ m} \quad \text{A.4}$$

A.4. Uncertainty in the test tube inner diameter

Diameter uncertainty is determined by the instrument used to measure the diameter, which was a vernier caliper with an accuracy of 0.02 mm. The uncertainty is therefore the following:

$$\delta D = 0.02/1000 = 0.00002 \text{ m} \quad \text{A.5}$$

A.5. Heat transfer area uncertainty

The heat transfer area uncertainty is calculated when uncertainties in diameter and tube length are determined.

$$\delta A = \left[\left(\frac{\partial A}{\partial D_{in}} \delta D_{in} \right)^2 + \left(\frac{\partial A}{\partial L} \delta L \right)^2 \right]^{0.5} \quad \text{A.6}$$

Where area $A = \pi DL$

$$\frac{\partial A}{\partial D_{in}} = \pi L \quad \text{and,} \quad \frac{\partial A}{\partial L} = \pi D_{in} \quad \text{A.7}$$

A.6. Refrigerant mass flow rate uncertainty

The flow meter that was used to capture flow rate was the coriolis flow meter and it had a measuring uncertainty of 0.001 of the indicated value.

A.7. Mass flux uncertainty

Since mass flux is a function of mass flow rate and the cross-sectional area of the tube, the uncertainty of mass flux is given as the following:

$$\delta G = \left[\left(\frac{\partial G}{\partial A_c} \delta A_c \right)^2 + \left(\frac{\partial G}{\partial \dot{m}} \delta \dot{m} \right)^2 \right]^{0.5} \quad \text{A.8}$$

$$\text{However } \frac{\partial G}{\partial A_c} = -\frac{\dot{m}}{A_c^2} \text{ and } \frac{\partial G}{\partial \dot{m}} = \frac{1}{A_c} \quad \text{A.9}$$

A.8. The uncertainty in saturation temperature (T_{sat})

A standard deviation was used to calculate the random errors in temperature measurements. A total of 121 data points were summed up and averaged (\bar{x}). Then the uncertainty in the temperature measurement was given as the following:

$$\delta T = \left(\frac{1}{n} \sum_{i=1}^n (\bar{x} - x_i)^2 \right)^{0.5} \quad \text{A.10}$$

Where n is the number of the data points.

$$T_{sat} = \delta \bar{T}$$

Finally, the uncertainty in the saturation temperature was taken as an average of the individual uncertainty in saturation temperature. Uncertainty in saturation temperature was found to be 0.04082 °C.

A.9. Uncertainty of the wall temperature

Uncertainty of the wall temperature was calculated in the same way as the uncertainty in the saturation temperature. See Equation A.10. In the same way, the uncertainty of the wall temperature was also an average of all the uncertainties of 28 thermocouples stations along the tube length, each with 121 samples. Uncertainty in the wall temperature was 0.03467 °C.

A.10. Uncertainty in temperature difference

The uncertainty in the temperature difference between the wall temperature and the saturation temperature was determined in the following way:

$$\delta \Delta T = \left(\delta T_{wall}^2 + \delta T_{sat}^2 \right)^{0.5} \quad \text{A.11}$$

A.11. Uncertainty in heat input

The heat gained by the water is the sum of the heat gained in each condenser: pre-condenser, test section and post-condenser. The heat lost by the refrigerant in the test condenser is taken as equal to the heat gained by the water in the annulus. The heat input is

a function of the specific heat of the water, temperature difference of the water from the inlet to the outlet, and the mass flow rate of the water in the annulus.

$$\dot{Q}_{ref_test} = \dot{m}_{ref} \Delta h \quad A.12$$

$$\dot{Q}_{water_test} = \dot{m}_{water} CP_{water} (T_{out_water} - T_{in_water}) \quad A.13$$

$$\dot{Q}_{ref} = \alpha A (T_{sat} - T_{wall}) \quad A.14$$

A.12. Heat transfer coefficient uncertainty

Finally, the heat transfer coefficient in the test section is given in equation uncertainty, and can be calculated as follows:

$$\alpha = \frac{\dot{Q}}{A(T_{sat} - T_{wall})} \quad A.15$$

$$\delta\alpha = \left[\left(\frac{1}{A(\Delta T)} \delta\dot{Q} \right)^2 + \left(-\frac{\dot{Q}}{A^2(\Delta T)} \delta A \right)^2 + \left(\left(-\frac{\dot{Q}}{A(\Delta T)} \delta\Delta T \right) \right)^2 \right]^{0.5} \quad A.16$$

A.13. Uncertainty in quality

The uncertainty in the mean quality of the refrigerant in the test section from the inlet and the outlet is calculated by first determining the uncertainty in the inlet vapour quality and then calculating the outlet vapour quality.

A.13.1. Uncertainty in inlet vapour quality

Inlet vapour quality is calculated by the enthalpies at the inlet to the test condenser and is given by the following equations:

$$x_{in} = \frac{h_{test_in} - h_f}{h_v - h_f} \quad A.17$$

The vapour and liquid enthalpies are determined from REFPROP [81] using the saturation point at the inlet to the test section. However, the test enthalpy at the inlet h_{test_in} is determined in the following way:

$$h_{test_in} = h_{pre_in} - \frac{|\dot{Q}_{pre}|}{\dot{m}_{ref}} \quad A.18$$

The enthalpy at the inlet to the pre-condenser is determined from REFPROP [81] at the saturation temperature and pressure.

The heat lost by the refrigerant in the pre-condenser can be determined from the heat gained by the water in the annulus of the pre-condenser.

$$\dot{Q}_{pre_water} = \dot{m}_{pre_water} c_{p_water} (\Delta T_{water}) \quad A.19$$

$$\delta Q_{pre_water} = \left[\left(\frac{\partial}{\partial \dot{m}} \dot{Q} \delta \dot{m} \right)^2 + \left(\frac{\partial}{\partial c_{p_water}} \dot{Q} \delta c_{p_water} \right)^2 + \left(\frac{\partial}{\partial \Delta T} \dot{Q} \delta \Delta T_{water} \right)^2 \right]_{pre_water}^{0.5} \quad A.20$$

The uncertainty of the vapour quality at the inlet to the test section is then given as follows:

$$\delta h_{test_in} = \left[\left(\frac{\partial}{\partial h_{pre_in}} (h_{test_in}) \delta h_{pre_in} \right)^2 + \left(\frac{\partial}{\partial \dot{Q}_{pre_water}} (h_{test_in}) \delta \dot{Q}_{pre_water} \right)^2 + \left(\frac{\partial}{\partial \dot{m}_{ref}} (h_{test_in}) \delta \dot{m}_{ref} \right)^2 \right]^{0.5} \quad A.21$$

The partial derivatives will then be the following:

$$\frac{\partial h_{test_in}}{\partial \dot{Q}_{pre_water}} = - \frac{1}{\dot{m}_{ref}} \quad A.22$$

$$\frac{\partial h_{test_in}}{\partial h_{pre_in}} = 1 \quad A.23$$

$$\frac{\partial h_{test_in}}{\partial \dot{m}_{ref}} = - \frac{\dot{Q}_{pre_water}}{\dot{m}_{ref}^2} \quad A.24$$

However, the uncertainty of the enthalpies from REFPROP has also been stated by researchers like Van Rooyen [39] and Christians [54]. Hence, uncertainty in the refrigerant enthalpy is given as 0.5% of the measured value.



$$\delta h_{test_in} = \left[\left(\frac{\partial}{\partial h_{pre_in}} (h_{test_in}) \delta h_{pre_in} \right)^2 + \left(\frac{\partial}{\partial \dot{Q}_{pre_water}} (h_{test_in}) \delta \dot{Q}_{pre_water} \right)^2 + \left(\frac{\partial}{\partial \dot{m}_{ref}} (h_{test_in}) \delta \dot{m}_{ref} \right)^2 \right]^{0.5} \quad A.25$$

Finally, uncertainty in quality can be calculated in the following way:

$$\partial x_{in} = \left[\left(\frac{\partial}{\partial h_{f,test_in}} (x_{in}) \delta h_{f,test_in} \right)^2 + \left(\frac{\partial}{\partial h_{water_in}} (h_{test_in}) \delta h_{test_in} \right)^2 + \left(\frac{\partial}{\partial h_{g,test_in}} (x_{in}) \delta h_{g,test_in} \right)^2 \right]^{0.5} \quad A.26$$

The partial derivatives will then be as follows:

$$\frac{\partial x_{in}}{\partial h_{test_in}} = \left[\left(\frac{1}{h_{g,test_in} - h_{f,test_in}} \right) \right] \quad A.27$$

$$\frac{\partial x_{in}}{\partial h_{g,test_in}} = \left[\left(\frac{h_f - h_{test_in}}{(h_g - h_f)^2} \right) \right] \quad A.28$$

$$\frac{\partial x_{in}}{\partial h_{test_in}} = \left[\left(\frac{1}{h_{g,test_in} - h_{f,test_in}} \right) - \frac{h_{test_in} - h_{f,test_in}}{(h_{g,test_in} - h_{f,test_in})^2} \right] \quad A.29$$

A.13.2. Uncertainty in outlet vapour quality

The outlet vapour quality is calculated by the enthalpies at the outlet from the test condenser and is given by the following equation:

$$x_{out} = \frac{h_{test_out} - h_f}{h_v - h_f} \quad A.30$$

The vapour and liquid enthalpies are determined from REFPROP using the saturation point at the outlet from the test section. However, the test enthalpy at the outlet h_{test_out} is determined by the following equations:

$$h_{test_out} = h_{test_in} - \frac{|\dot{Q}_{test}|}{\dot{m}_{ref}} \quad A.31$$

The heat lost by the refrigerant in the post-condenser can be determined from the heat gained by the water in the annulus of the post-condenser.

$$\dot{Q}_{post_water} = \dot{m}_{post_water} c_{p_water} (\Delta T_{post_water}) \quad A.32$$

$$\delta Q_{post_water} = \left[\left(\frac{\partial}{\partial \dot{m}} \dot{Q} \delta \dot{m} \right)^2 + \left(\frac{\partial}{\partial c_{p_water}} \dot{Q} \delta c_{p_water} \right)^2 + \left(\frac{\partial}{\partial \Delta T} \dot{Q} \delta \Delta T_{water} \right)^2 \right]_{post_water}^{0.5} \quad A.33$$

The uncertainty of the enthalpy at the outlet to the test section is then given as follows:

$$\delta h_{test_out} = \left[\left(\frac{\partial}{\partial h_{test_in}} (h_{test_out}) \delta h_{test_in} \right)^2 + \left(\frac{\partial}{\partial \dot{Q}_{test_water}} (h_{test_out}) \delta \dot{Q}_{test_water} \right)^2 + \left(\frac{\partial}{\partial \dot{m}_{ref}} (h_{test_out}) \delta \dot{m}_{ref} \right)^2 \right]^{0.5} \quad A.34$$

The partial derivatives will then be the following:

$$\frac{\partial h_{test_out}}{\partial \dot{Q}_{test_water}} = - \frac{1}{\dot{m}_{ref}} \quad A.35$$

$$\frac{\partial h_{test_out}}{\partial h_{test_in}} = 1 \quad A.36$$

$$\frac{\partial h_{test_out}}{\partial \dot{m}_{ref}} = - \frac{\dot{Q}_{test_water}}{\dot{m}_{ref}^2} \quad A.37$$

Now, the uncertainty in the enthalpy at the outlet to the test section is given as follows:



$$\delta h_{test_out} = \left[\left(\frac{\partial}{\partial h_{test_in}} (h_{test_out}) \delta h_{test_in} \right)^2 + \left(\frac{\partial}{\partial \dot{Q}_{test_water}} (h_{test_out}) \delta \dot{Q}_{test_water} \right)^2 + \left(\frac{\partial}{\partial \dot{m}_{ref}} (h_{test_out}) \delta \dot{m}_{ref} \right)^2 \right]^{0.5} \quad A.38$$

The partial derivatives will then be the following:

$$\frac{\partial x_{out}}{\partial h_{test_out}} = \left[\left(\frac{1}{h_{g,test_out} - h_{f,test_out}} \right) \right] \quad A.39$$

$$\frac{\partial x_{out}}{\partial h_{g,test_out}} = \left[\left(\frac{h_f - h_{test_out}}{(h_g - h_f)^2} \right) \right] \quad A.40$$

$$\frac{\partial x_{out}}{\partial h_{test_out}} = \left[\left(\frac{1}{h_{g,test_out} - h_{f,test_out}} \right) - \frac{h_{test_out} - h_{f,test_out}}{(h_{g,test_out} - h_{f,test_out})^2} \right] \quad A.41$$

A.14. Sample calculations of uncertainties

Sample calculations of uncertainty are shown for one data point of a mass flux of 100 kg/m².s, temperature difference of 5°C and quality of 0.5. The uncertainty includes the uncertainty temperature difference of the water side (inlet and outlet of the annulus), temperature difference between the wall temperature and the saturation temperature, heat transfer rate (\dot{Q}), heat transfer coefficient, mean quality and mass flux. The table below shows all the given values for the data point.

Table A.1: Parameters and values used in the sample calculation of uncertainty

Parameter	Value	Units
Length of test section tube	1.5	m
Internal diameter of tube	0.00838	m
Mass flow rate of refrigerant	$5801.17 \cdot 10^{-6}$	kg/s
Mass flow rate of water pre-condenser	$4714.68 \cdot 10^{-6}$	kg/s
Mass flow rate of water test condenser	$5487.5 \cdot 10^{-6}$	kg/s
Mass flow rate of water post-condenser	$8096.35 \cdot 10^{-6}$	kg/s
Refrigerant temperature pre-condenser inlet	90.37	°C
Refrigerant temperature test condenser inlet	39.69	°C
Refrigerant temperature test condenser outlet	39.5	°C
Saturation temperature (refrigerant)	39.58	°C
Wall temperature	34.66	°C
Temperature difference (wall and saturation temperatures)	4.92	°C
Inlet water temperature pre-condenser	21.87	°C
Outlet water temperature pre-condenser	51.82	°C
Inlet water temperature test condenser	20.95	°C
Outlet water temperature test condenser	36	°C
Inlet water temperature post-condenser	21.15	°C
Outlet water temperature post-condenser	34.03	°C
Inlet quality of refrigerant in test condenser	0.7	-
Outlet quality of refrigerant in test condenser	0.335	-
Inlet pressure pre-condenser	1039.55	kPa
Inlet pressure test condenser	1028	kPa

A.14.1. Heat transfer area uncertainty

The heat transfer area uncertainty is therefore calculated from Equations A.6 and A.7.

$$\frac{\partial A}{\partial D_{in}} = \pi L = \pi * 1.5 = 4.7124 \text{ m}$$

$$\frac{\partial A}{\partial L} = \pi D = \pi * 0.00838 = 0.02633 \text{ m}$$

$$\delta A = \left[(\pi \cdot L \cdot \delta D)^2 + (\pi \cdot D \cdot \delta L)^2 \right]^{0.5}$$

$$\delta A = [(\pi * 1.5 * 0.00002)^2 + (\pi * 0.00838 * 0.001)^2]^{0.5} \text{ m}^2$$

$$= 9.786 * 10^{-5} \text{ m}^2$$

A.14.2. Mass flux uncertainty

Mass flux is a function of mass velocity and the cross sectional area of the tube. Hence, the uncertainty is calculated from Equations A.8 and A.9.

$$A_c = \pi D^2 / 4 = \pi * 0.00838^2 / 4 = 5.5154 * 10^{-5} \text{ m}^2$$

$$\delta A_c = \pi \frac{D}{2} \delta D = \pi * \frac{0.00838}{2} * 0.00002 = 2.63 * 10^{-7}$$

$$\frac{\partial G}{\partial A} = \frac{\dot{m}}{A_c^2} = \frac{-5.80117 * 10^{-3}}{(5.5154 * 10^{-5})^2} = -1907047.73$$

$$\frac{\partial G}{\partial \dot{m}} = \frac{1}{A_c} = \frac{1}{5.5154 * 10^{-5}} = 18131.05$$

$$\delta G = \left[\left(\frac{\partial G}{\partial A_c} \delta A \right)^2 + \left(\frac{\partial G}{\partial \dot{m}} \delta \dot{m} \right)^2 \right]$$

$$\delta G = \left[(-1907047.73 * 2.63 * 10^{-7})^2 + (18131.051 * 5.80117 * 10^{-6})^2 \right]^{0.5}$$

The mass flux uncertainty is as follows:

$$\delta G = 0.513 \text{ kg/s}$$

A.14.3. Uncertainty in saturation temperature (T_{sat})

The uncertainty in the saturation temperature is taken as an average of the individual uncertainties in saturation temperature. See Equation A.10. Uncertainty in the saturation temperature was found to be 0.04082 °C.

A.14.4. Uncertainty of the wall temperature

Uncertainty of the wall temperature is calculated using Equation A.10. However, for the wall temperature, there are seven stations of four thermocouples per station along the length of the test tube. Hence, uncertainty is calculated per station and an average taken for the seven stations. Uncertainty in the wall temperature was then 0.05702 °C.

A.14.5. Uncertainty in temperature difference

The uncertainty in the temperature difference between the wall temperature and the saturation temperature was determined from Equation A.11.

$$\delta\Delta T = (0.057022^2 + 0.04082^2)^{0.5}$$

$$\delta\Delta T = 0.07013 \text{ } ^\circ\text{C}$$

A.14.6. Uncertainty in heat input

$$\dot{Q}_{ref_test} = \dot{m}_{ref} \Delta h$$

$$\dot{Q}_{ref_test} = 5.80117 * 10^{-3} * (310844 - 370306)$$

$$\dot{Q}_{ref_test} = -344.95 \text{ W}$$

$$\dot{Q}_{water_test} = \dot{m}_{water} C_{p_water} (T_{out_water} - T_{in_water})$$

$$\dot{Q}_{water_test} = 5.488 * 10^{-3} * 4180 * (35.992 - 20.954)$$

$$\dot{Q}_{water_test} = 344.97 \text{ W}$$

$$\dot{Q}_{water_test} \approx \dot{Q}_{ref_test}$$

$$\delta Q_{test_water} = \left[\left(\frac{\partial Q}{\partial \dot{m}} \delta \dot{m} \right)^2 + \left(\frac{\partial Q}{\partial C_{p_water}} \delta C_{p_water} \right)^2 + \left(\frac{\partial Q}{\partial \Delta T_{water}} \delta \Delta T_{water} \right)^2 \right]_{test_water}^{0.5}$$

$$\delta Q_{test_water} = \left[(C_p * \Delta T * \delta \dot{m})^2 + (\dot{m} * \Delta T * \delta c_{p_water})^2 + (\dot{m} * C_p * \delta \Delta T_{water})^2 \right]_{test_water}^{0.5}$$

$$\delta Q_{test_water} = \left[(0.345)^2 + (0.345)^2 + (1.874)^2 \right]^{0.5}$$

$$\delta Q_{test_water} = 1.94 \text{ W}$$

A.14.7. Heat transfer coefficient uncertainty

Lastly, the heat transfer coefficient uncertainty can be calculated from Equation A.16.

$$\alpha = \frac{Q}{A(T_{sat} - T_{wall})} \quad \text{A.1}$$

$$\delta\alpha = \left[\left(\frac{1}{A(\Delta T)} \delta Q \right)^2 + \left(-\frac{Q}{A^2(\Delta T)} \delta A \right)^2 + \left(\left(-\frac{Q}{A(\Delta T)} \delta \Delta T \right)^2 \right)^2 \right]^{0.5}$$

$$\delta\alpha = \left[\left(\frac{1}{0.03949(4.92)} 1.94 \right)^2 + \left(-\frac{345}{0.03949^2(4.92)} 9.786 * 10^{-5} \right)^2 + \left(\left(-\frac{345}{0.03949(4.92)} 0.07013 \right)^2 \right)^2 \right]^{0.5} \quad \text{A.2}$$

$$\delta\alpha = \left[(9.985)^2 + (-4.4003)^2 + ((25.31)^2)^2 \right]^{0.5}$$

$$\delta\alpha = 27.6 W$$

A.15. Summary of the uncertainties for this study

A short summary of uncertainties in the heat transfer coefficient, mass flux, heat transfer rate, quality and temperature difference is presented in this section. The data ranges from all the mass fluxes tested, and qualities of 0.25, 0.5 and 0.75. A comparison of uncertainty in temperature difference, heat transfer coefficients and quality for different mass fluxes was displayed.

A.15.1. Results of uncertainties

This section gives a summary of uncertainty results for qualities of 0.25, 0.5 and 0.75, temperature differences of 1 °C to 10 °C and mass fluxes from 25 kg/m².s to 100 kg/m².s. See the spread sheets on the attached CD for other qualities of 0.35 and 0.62.



G = 100 [kg/m².s]									
ΔT [3 °C]	<i>x</i> = 0.25			<i>x</i> = 0.5			<i>x</i> = 0.75		
	Value	Uncertainty		Value	Uncertainty		Value	Uncertainty	
		δ	%		δ	%		δ	%
α_{test}	1570	40.3	2.57	1838	45	2.45	1881	43.2	2.3
G	102	0.5	0.49	104	0.51	0.49	100	0.49	0.49
$\dot{Q}_{water-test}$	173.6	0.85	0.49	213	1.1	0.5	234	1.2	0.51
ΔT	2.8	0.07	2.51	2.94	0.07	2.38	3.2	0.07	2.2
x_{in}	0.35	0.015	4.2	0.62	0.041	2.3	0.88	0.014	1.6
x_{out}	0.16	0.0076	4.8	0.4	0.0078	2	0.62	0.0086	1.4
x_{avg}	0.25	0.0082	3.3	0.5	0.0081	1.6	0.75	0.0081	1.1

ΔT [5 °C]	<i>x</i> = 0.25		<i>x</i> = 0.5		<i>x</i> = 0.75				
	δ	%	δ	%	δ	%			
α_{test}	1446	22.4	1.55	1777	27.6	1.55	1919	30	1.57
G	103	0.5	0.49	105	0.5	0.49	103	0.5	0.49
$\dot{Q}_{water-test}$	280	1.5	0.54	345	1.9	0.56	368	2.03	0.55
ΔT	4.9	0.07	1.43	4.9	0.07	1.43	4.9	0.7	1.44
x_{in}	0.41	0.015	3.53	0.7	0.015	2.1	0.92	0.014	1.52
x_{out}	0.11	0.0073	6.7	0.33	0.0078	2.33	0.52	0.0088	1.7
x_{avg}	0.26	0.008	3.1	0.52	0.0083	1.6	0.72	0.0082	1.15

ΔT [8 °C]	<i>x</i> = 0.35		<i>x</i> = 0.5		<i>x</i> = 0.62				
	δ	%	δ	%	δ	%			
α_{test}	1472	16.5	1.12	1637	19	1.14	1776	20	1.13
G	101	0.49	0.49	101	0.49	0.49	104	0.51	0.49
$\dot{Q}_{water-test}$	463	3	0.65	508	3.4	0.7	563	3.83	0.68
ΔT	8	0.07	0.88	7.9	0.07	0.9	8	0.07	0.87
x_{in}	0.6	0.014	2.4	0.78	0.014	1.8	0.92	0.014	1.53
x_{out}	0.09	0.0075	8.2	0.22	0.0083	3.8	0.31	0.009	3
x_{avg}	0.35	0.0081	2.3	0.5	0.008	1.63	0.61	0.0084	1.37



ΔT [10 °C]	G = 100 [kg/m ² .s]			ΔT [1°C]	G = 25 [kg/m ² .s]		
	x = 0.5				x = 0.75		
	Value	Uncertainty			Value	Uncertainty	
		δ	%			δ	%
α_{test}	1621	20	1.22	α_{test}	1669	125	7.5
G	100	0.49	0.49	G	24.5	0.12	0.49
$\dot{Q}_{water-test}$	638	6.1	0.96	$\dot{Q}_{water-test}$	62	0.35	0.57
ΔT	9.96	0.07	0.7	ΔT	0.94	0.07	7.5
x_{in}	0.86	0.014	1.63	x_{in}	0.9	0.014	1.54
x_{out}	0.15	0.008	5.3	x_{out}	0.62	0.025	4
x_{avg}	0.5	0.008	1.6	x_{avg}	0.76	0.014	1.9

ΔT [3 °C]	G = 75 [kg/m ² .s]								
	x = 0.25			x = 0.5			x = 0.75		
	Value	Uncertainty		Value	Uncertainty		Value	Uncertainty	
		δ	%		δ	%		δ	%
α_{test}	1458	36	2.4	1685	42	2.5	1893	45	2.4
G	75	0.37	0.48	75	0.37	0.49	77	0.38	0.49
$\dot{Q}_{water-test}$	170	0.85	0.5	194	0.94	0.49	227	1.13	0.5
ΔT	2.95	0.07	2.4	2.9	0.07	2.4	3	0.07	2.3
x_{in}	0.37	0.014	3.9	0.65	0.014	2.2	0.91	0.014	1.53
x_{out}	0.12	0.007	6.6	0.36	0.0099	2.7	0.58	0.012	2
x_{avg}	0.25	0.008	3.34	0.51	0.0086	1.7	0.75	0.009	1.21

ΔT [5 °C]	x = 0.25			x = 0.5			x = 0.62		
		δ	%		δ	%		δ	%
α_{test}	1294	20	1.54	1577	23	1.48	1690	25.4	1.51
G	75	0.37	0.49	75	0.36	0.49	75	0.37	0.49
$\dot{Q}_{water-test}$	253	1.34	0.53	322	1.7	0.53	337	1.77	0.53
ΔT	4.9	0.07	1.42	5.2	0.07	1.36	5	0.07	1.4
x_{in}	0.44	0.014	3.3	0.75	0.014	1.86	0.86	0.014	1.63
x_{out}	0.07	0.0075	11.4	0.27	0.0082	3	0.36	0.0083	2.3
x_{avg}	0.25	0.0081	3.2	0.51	0.0081	1.59	0.61	0.0081	1.33



G = 50 [kg/m².s]									
ΔT [1 °C]	<i>x</i> = 0.25			<i>x</i> = 0.5			<i>x</i> = 0.75		
	Value	Uncertainty		Value	Uncertainty		Value	Uncertainty	
		δ	%		δ	%		δ	%
α_{test}	1428	97	6.8	1613	108	6.7	1673	112	6.7
<i>G</i>	50	0.24	0.49	49.7	0.24	0.49	52	0.25	0.49
$\dot{Q}_{water-test}$	58.5	0.32	0.55	67	0.33	0.49	69	0.33	0.48
ΔT	1	0.07	6.8	1	0.07	6.7	1	0.07	6.7
x_{in}	0.32	0.014	4.55	0.59	0.014	2.4	0.83	0.014	1.7
x_{out}	0.19	0.008	4.45	0.44	0.0078	1.78	0.68	0.01	1.53
x_{avg}	0.25	0.0083	3.3	0.51	0.008	1.56	0.75	0.0087	1.15

ΔT [3 °C]	<i>x</i> = 0.35			<i>x</i> = 0.5			<i>x</i> = 0.75		
		δ	%		δ	%		δ	%
α_{test}	1458	36	2.5	1523	37	2.42	1685	42	2.48
<i>G</i>	51	0.25	0.49	50.4	0.25	0.49	53	0.26	0.49
$\dot{Q}_{water-test}$	168	0.81	0.48	178	0.77	0.43	193	0.95	0.49
ΔT	2.92	0.07	2.4	2.96	0.07	2.37	2.9	0.07	2.42
x_{in}	0.53	0.014	2.66	0.71	0.014	1.96	0.96	0.014	1.44
x_{out}	0.17	0.0078	4.7	0.32	0.0091	2.86	0.55	0.0087	1.57
x_{avg}	0.35	0.008	2.3	0.51	0.0083	1.62	0.757	0.0081	1.08

ΔT [5 °C]	<i>x</i> = 0.25			<i>x</i> = 0.5		
		δ	%		δ	%
α_{test}	1350	21	1.55	1412	23	1.6
<i>G</i>	53	0.26	0.49	53	0.26	0.49
$\dot{Q}_{water-test}$	260	1.36	0.52	261	1.33	0.51
ΔT	4.9	0.07	1.44	4.7	0.070	1.5
x_{in}	0.54	0.014	2.62	0.77	0.014	1.84
x_{out}	0.0034	0.0076	224	0.22	0.0076	3.5
x_{avg}	0.27	0.008	2.96	0.49	0.008	1.63

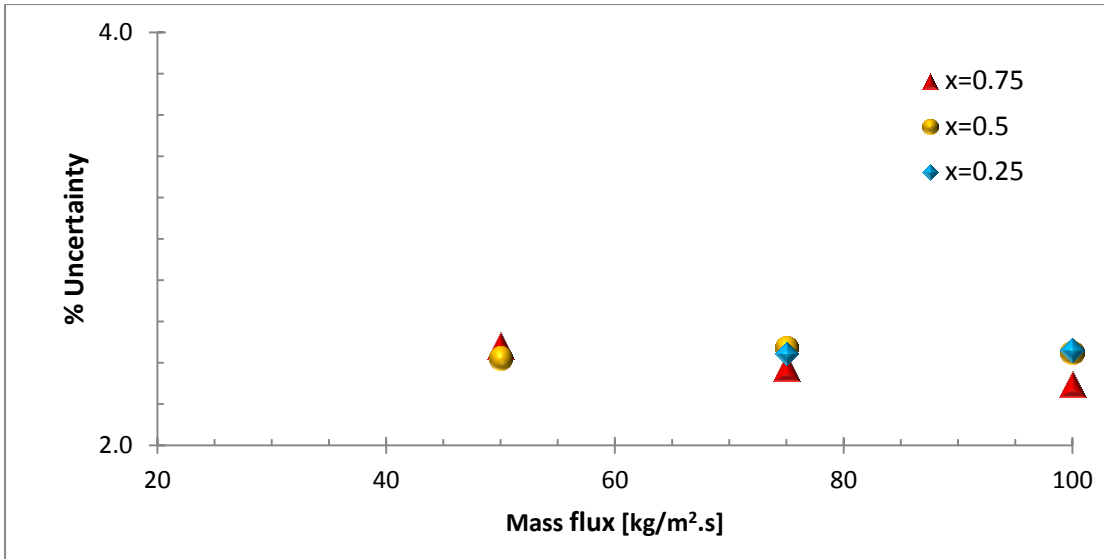


Figure A.1: Uncertainty in the heat transfer coefficients at a temperature difference of 3 °C

Figure A.1 shows uncertainty of the heat transfer coefficient as a function of mass flux. It shows that uncertainty in heat transfer coefficient is not a function of mass flux.

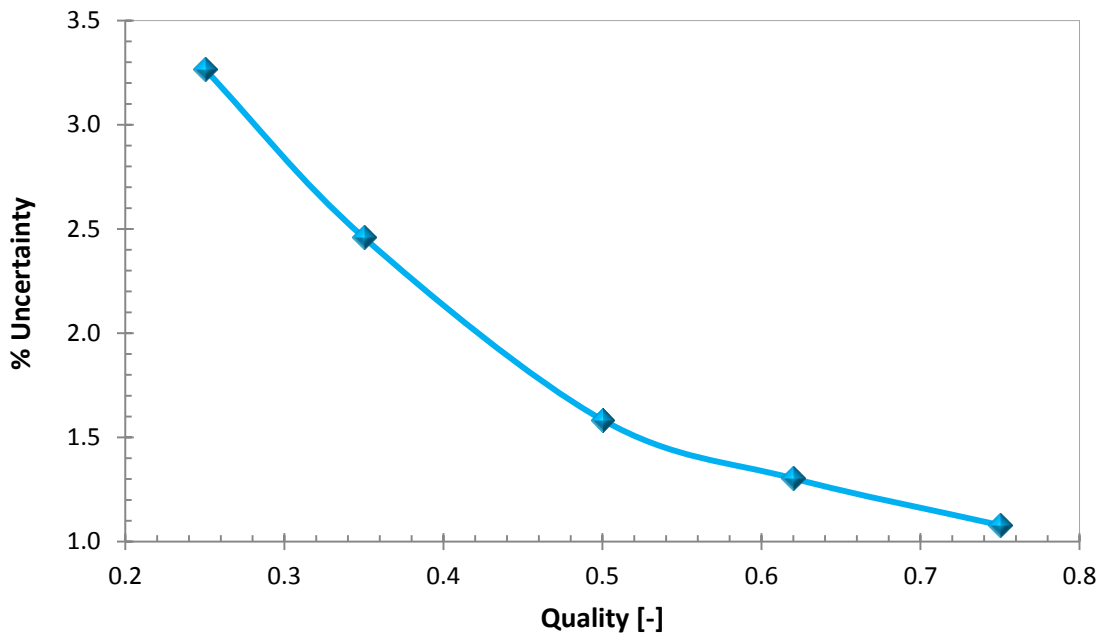


Figure A.2: Uncertainty of quality for a mass flux of 100 kg/m².s and a temperature difference of 3 °C.

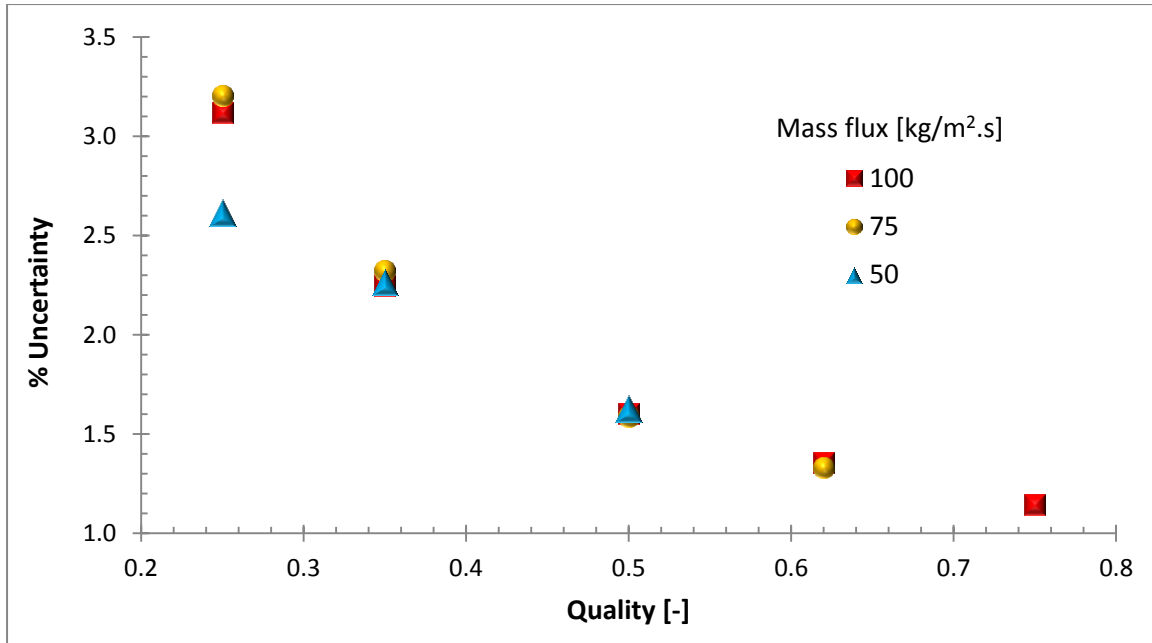


Figure A.3: Uncertainty in quality at different mass fluxes and temperature difference of 5 °C

Uncertainty in quality is presented in Figure A.2 and Figure A.3, with Figure A.2 being the uncertainty of quality at a mass flux of 100 kg/m².s at a temperature difference of 3 °C. The figure depicts quality as a function of quality, with uncertainty increasing with a decrease in quality. The same goes for Figure A.3 for different mass fluxes. However, as stated earlier, uncertainty is not a function of mass flux, hence the unchanging uncertainty for different mass fluxes.

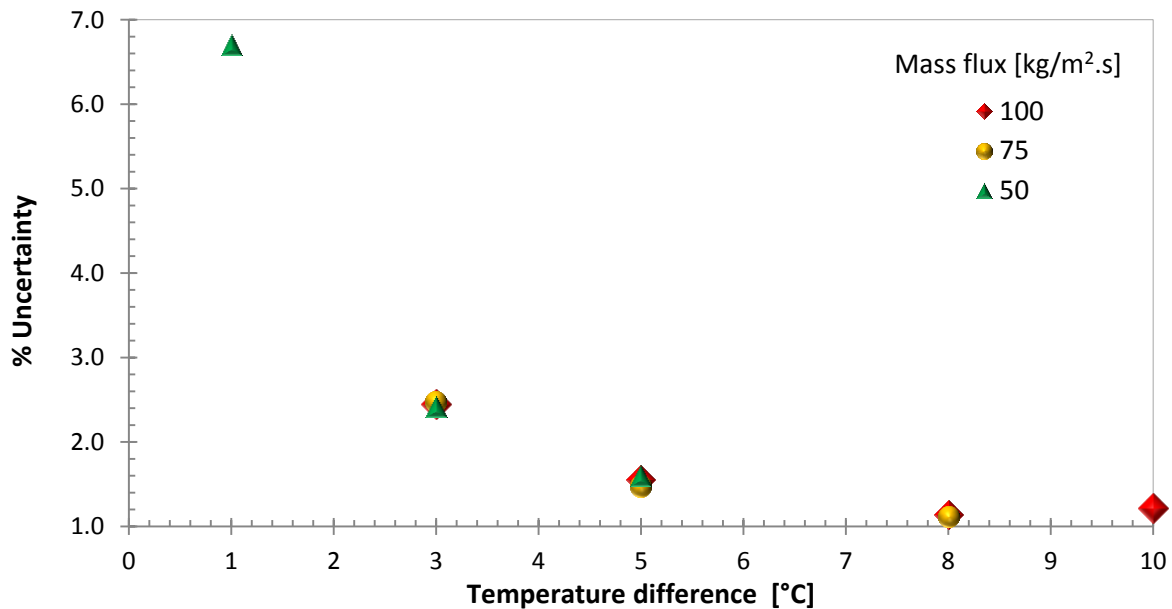


Figure A.4: Uncertainty in temperature difference at different mass fluxes

Uncertainty in the temperature difference at different mass fluxes is presented in Figure A.4. Uncertainty increases with a decrease in the temperature difference. Hence, uncertainty is also a function of the temperature difference.

A.16. Conclusion

In conclusion, uncertainty is a strong function of quality and temperature difference for this study. Uncertainty in mass flux remained constant for all the mass fluxes. On the other hand, uncertainty in quality at the outlet from the test condenser is higher than that on the inlet to the test condenser.

Appendix B. Heat transfer coefficients and flow patterns

B.1. Introduction

Appendix B summarises the effect of mass flux, quality and temperature difference on the heat transfer coefficient. This chapter follows the heat transfer coefficient summaries in Section 5.5.1 to Section 5.5.3. The summary in this section shows the prevailing flow patterns that were not shown previously. It is also an extension of Section 5.4. However the flow patterns are captured at the outlet from the test section and the following flow patterns were observed: - annular (*A*), stratified-wavy (*SW*), wavy (*W*), wavy-annular (*WA*), intermittent (*I*), wavy-churn (*WC*), churn (*C*) and stratified (*S*).

B.2. Effect of quality

The effect of quality on the heat transfer coefficient is shown for mass fluxes of 100 kg/m².s, 75 kg/m².s, 50 kg/m².s and 25 kg/m².s, and qualities of 0.25, 0.5 and 0.75 at temperature differences of 1 °C to 8 °C. For most of the mass fluxes and temperature differences, the heat transfer increases with an increase in quality for all inclination angles, except for ±90°, where the effect is insignificant.

The flow patterns transitions from stratified to stratified-wavy at 0° for high mass fluxes of 100 kg/m².s and 75 kg/m².s. On the other hand, at lower mass fluxes of 50 kg/m².s and below, the flow is stratified for all qualities. As temperature difference increases, the flow pattern becomes stratified. For the other negative inclination angles from -5° to -60°, the flow is stratified-wavy for all the mass fluxes and temperature differences.

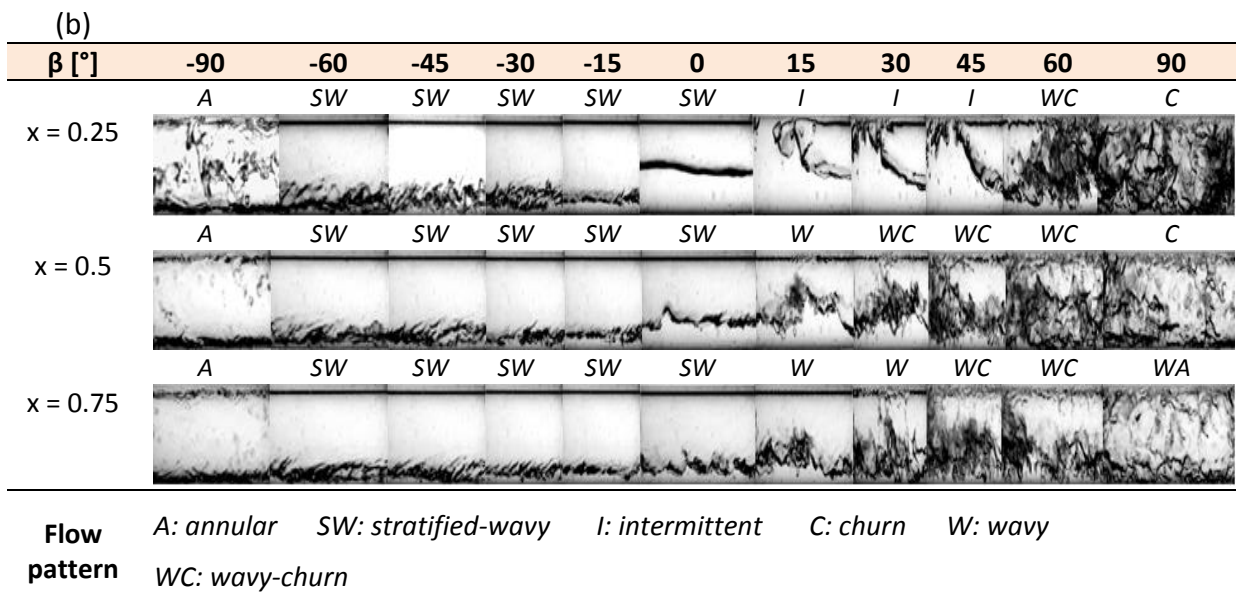
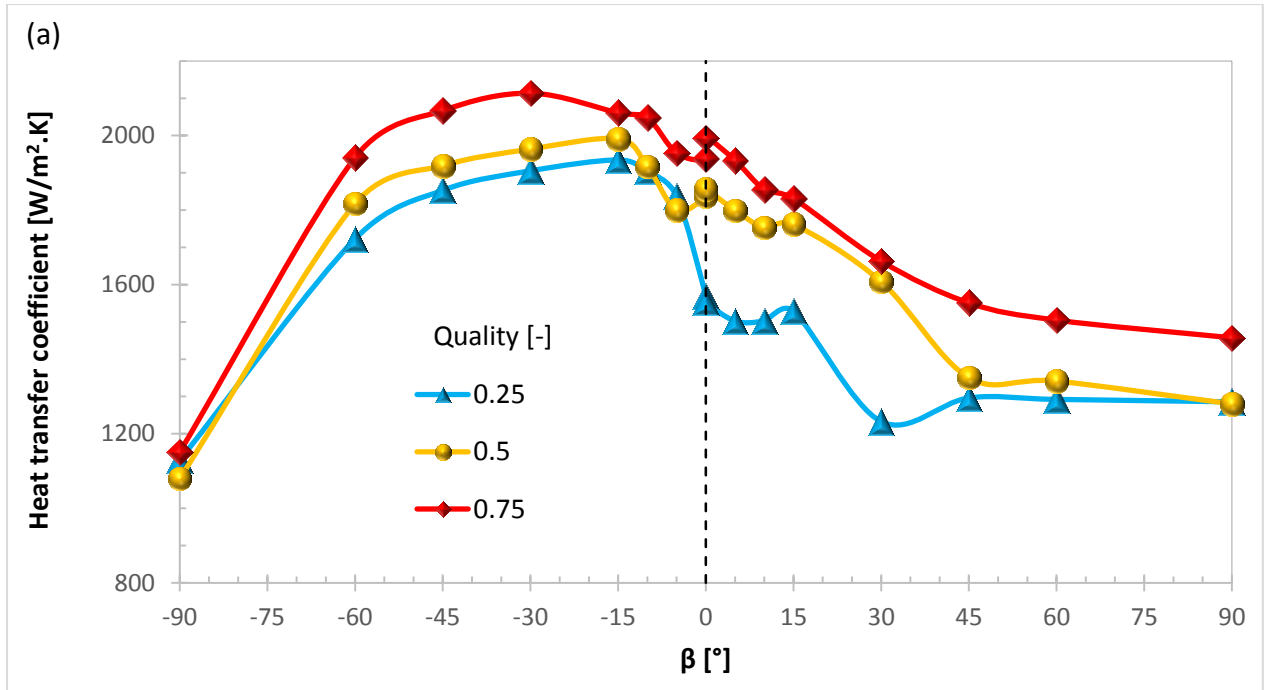
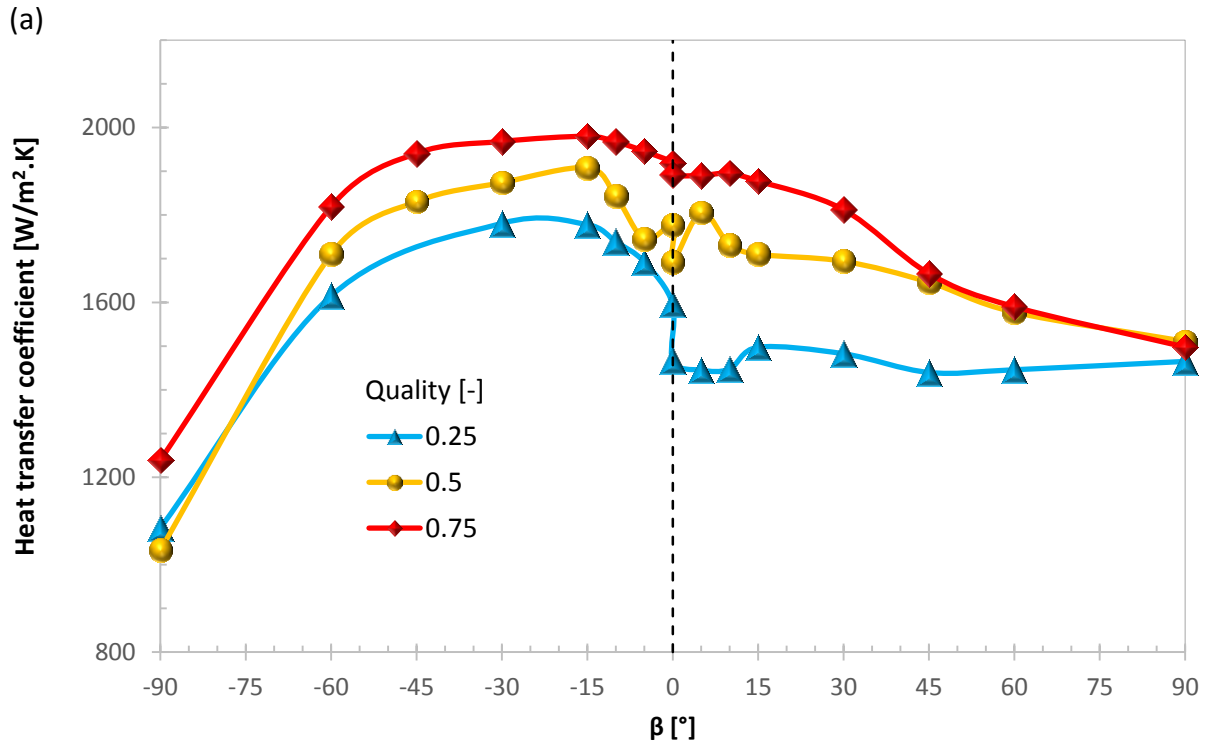


Figure B.1: Effect of quality for a mass flux $100 \text{ kg/m}^2\cdot\text{s}$ and a temperature difference of $3 \text{ }^\circ\text{C}$



(b)

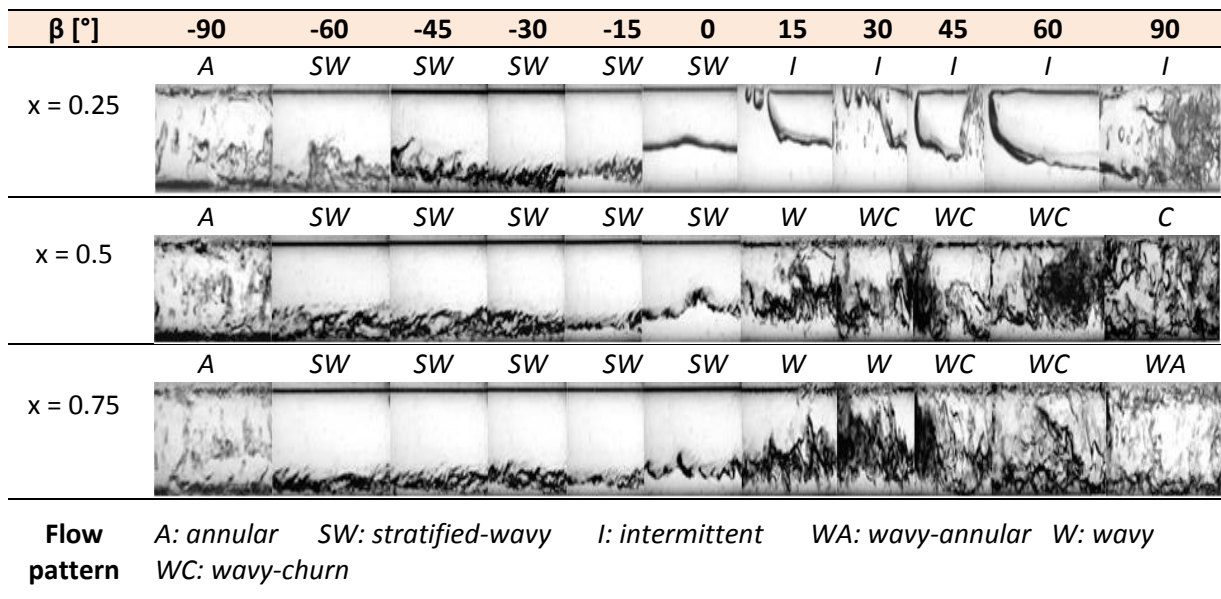
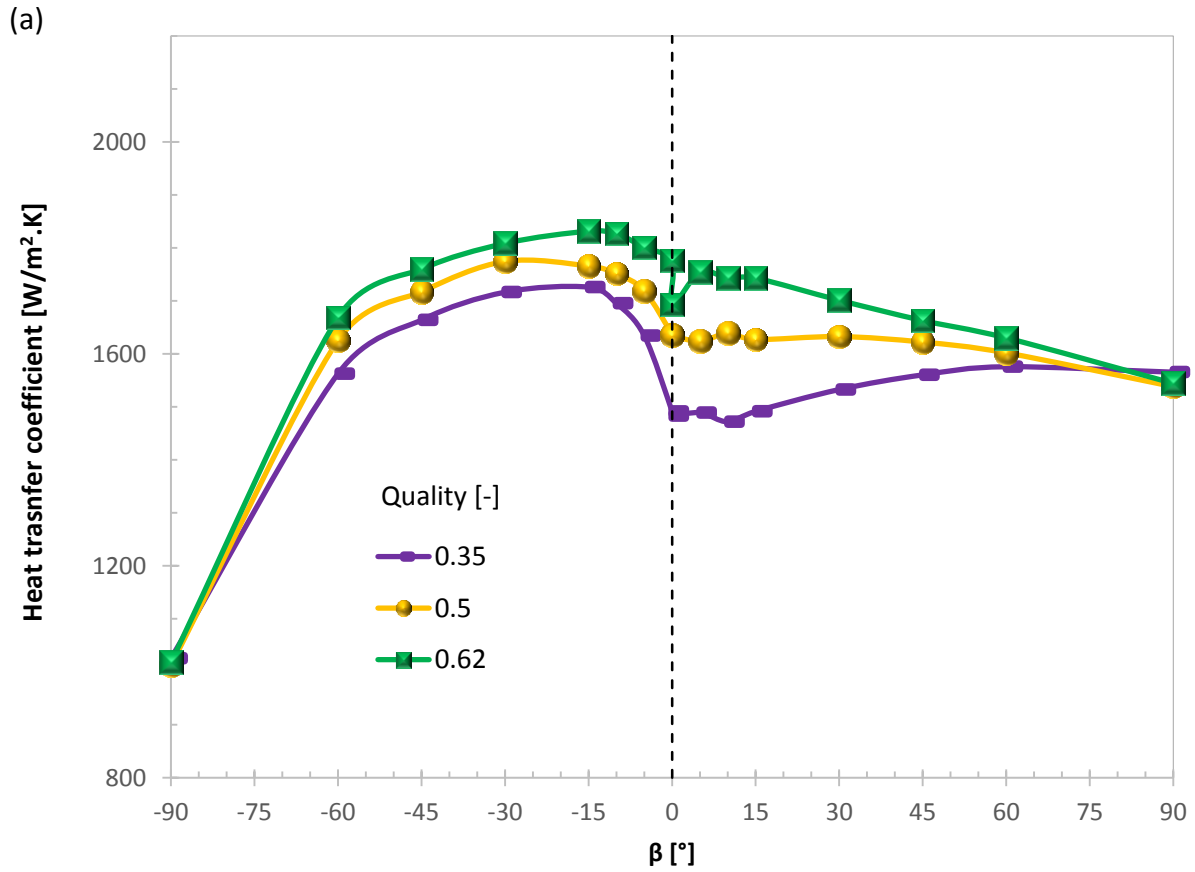


Figure B.2: Effect of quality for a mass flux 100 kg/m².s and a temperature difference of 5 °C



(b)

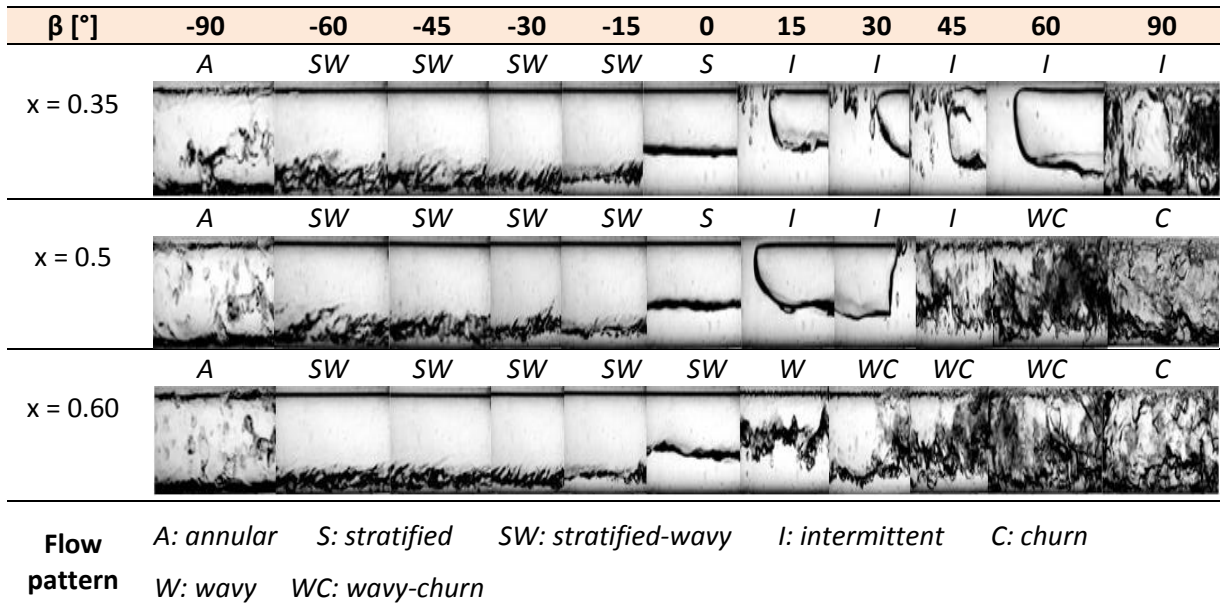
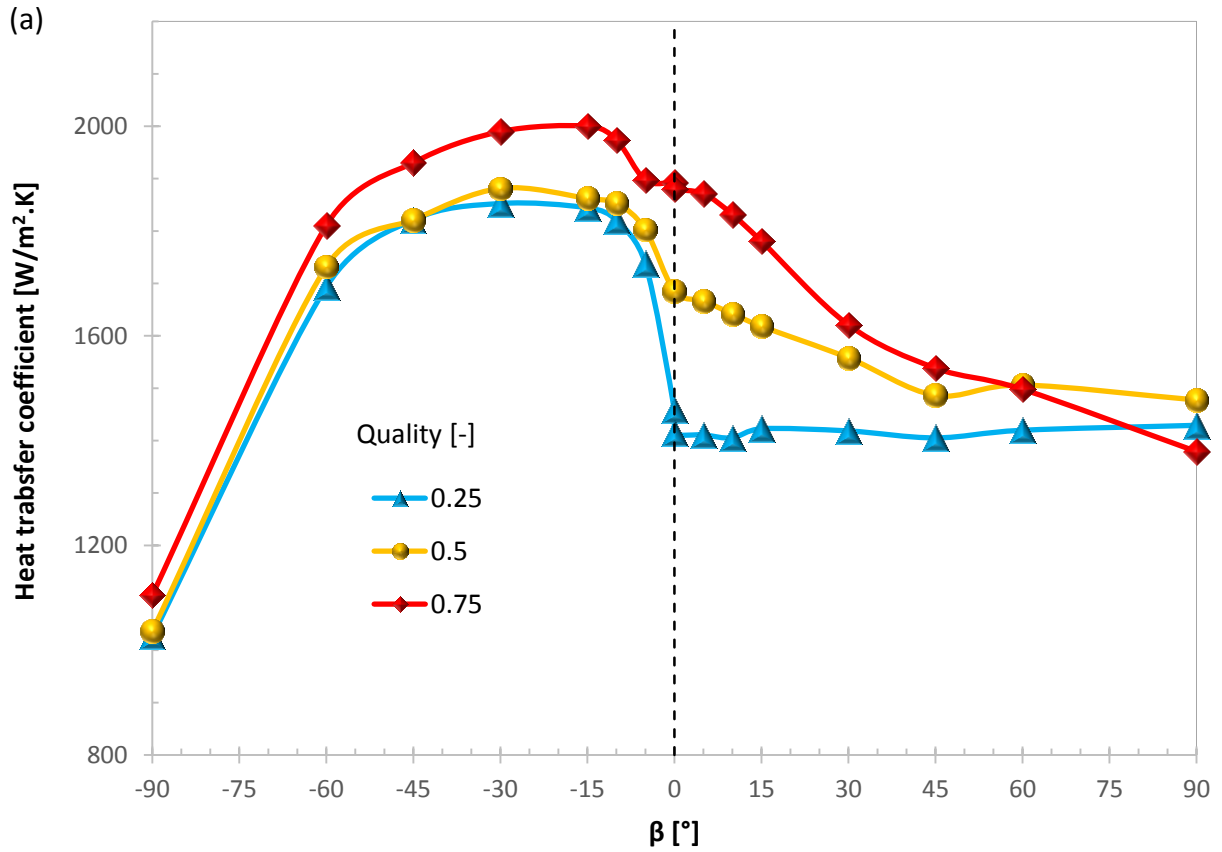


Figure B.3: Effect of quality for a mass flux 100 kg/m².s and a temperature difference of 8 °C



(b)

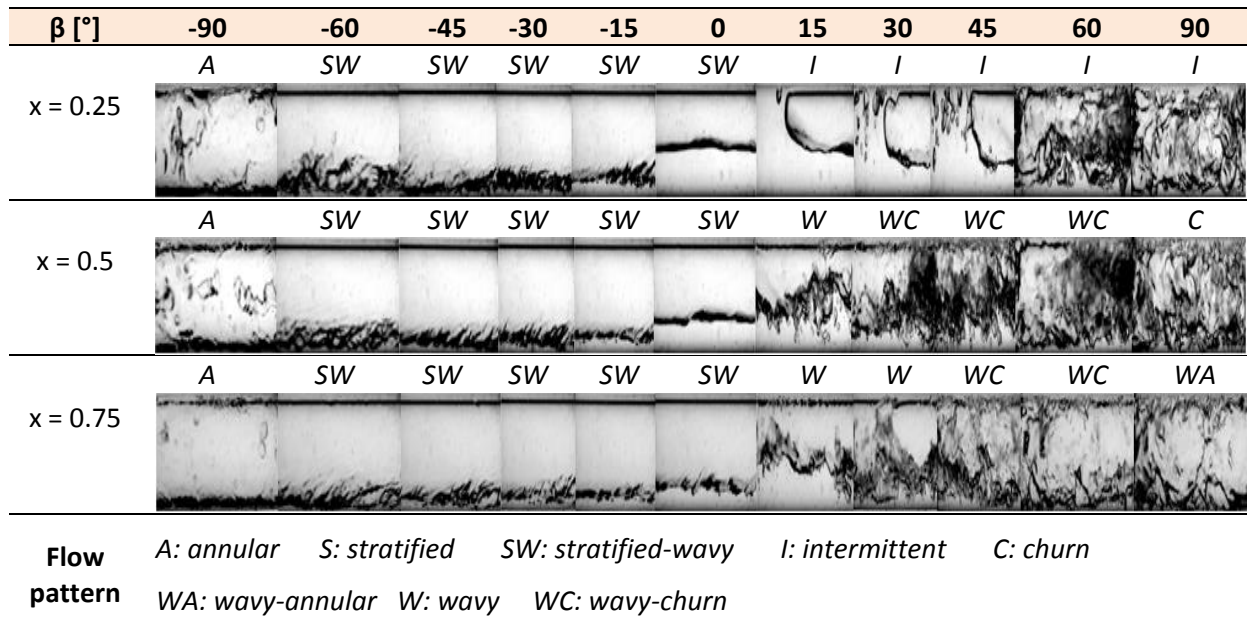
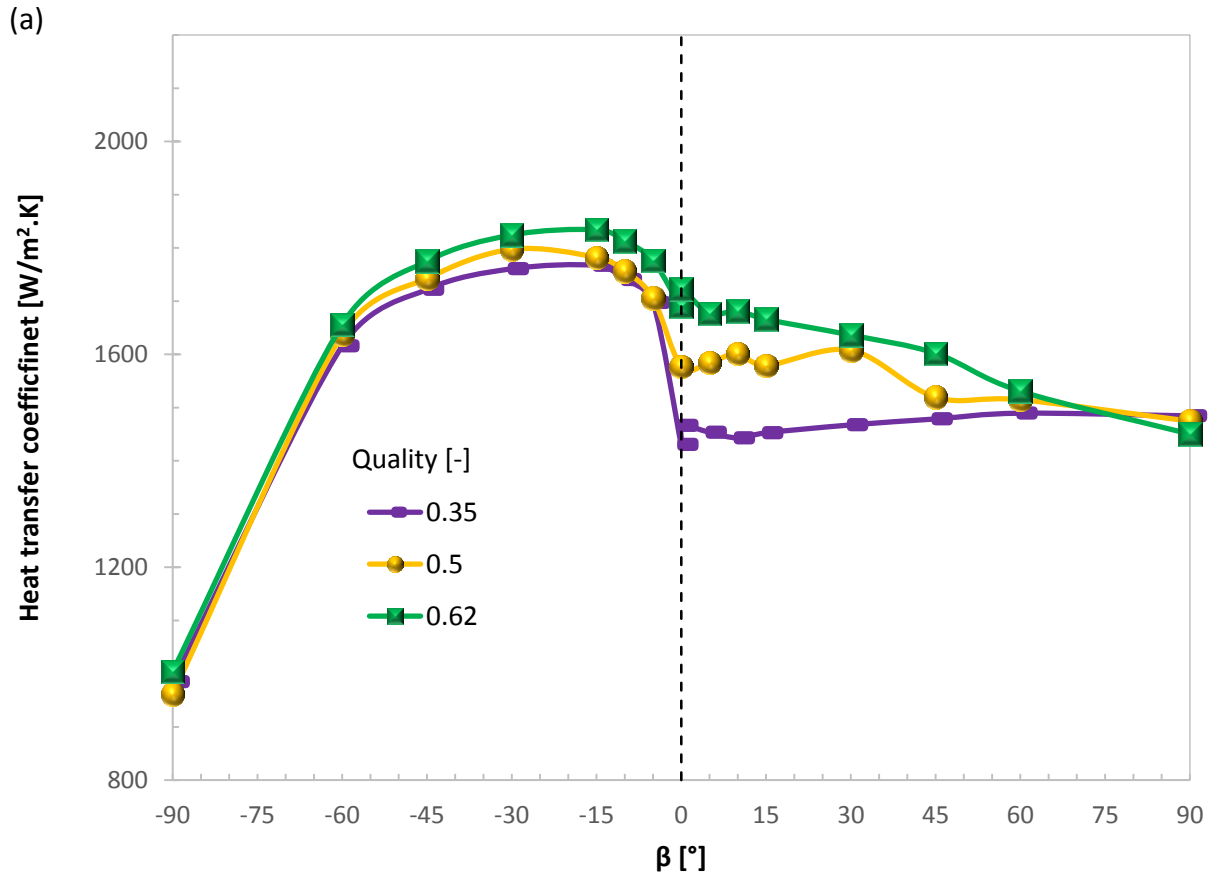


Figure B.4: Effect of quality for a mass flux $75 \text{ kg/m}^2\cdot\text{s}$ and a temperature difference of $3 \text{ }^\circ\text{C}$



(b)

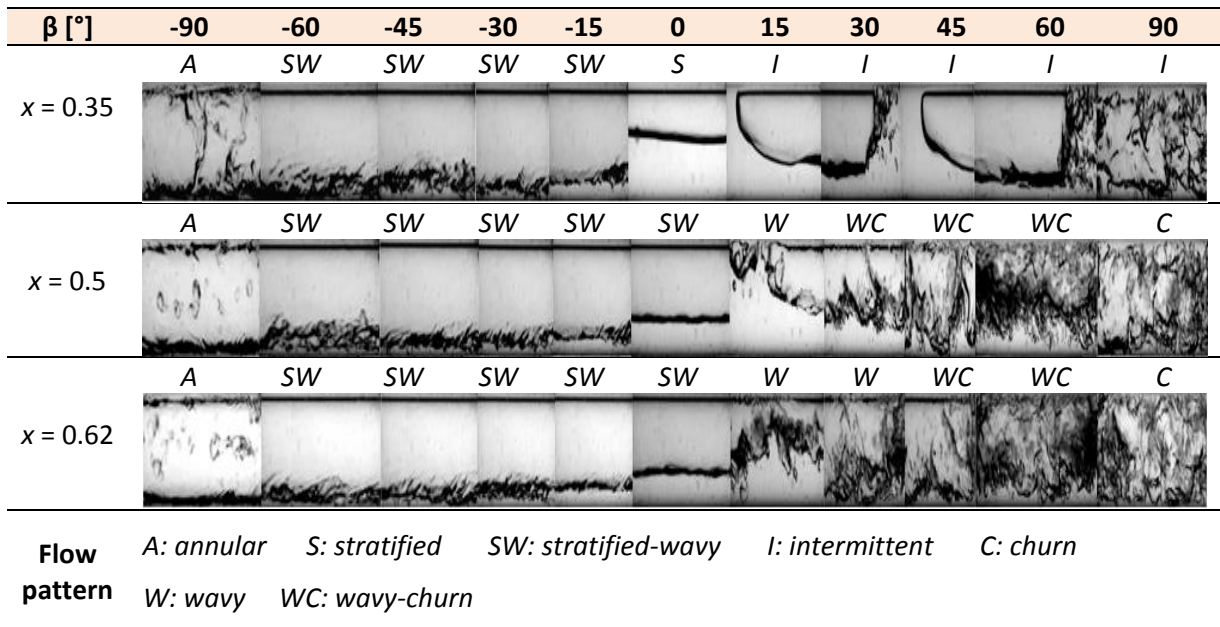
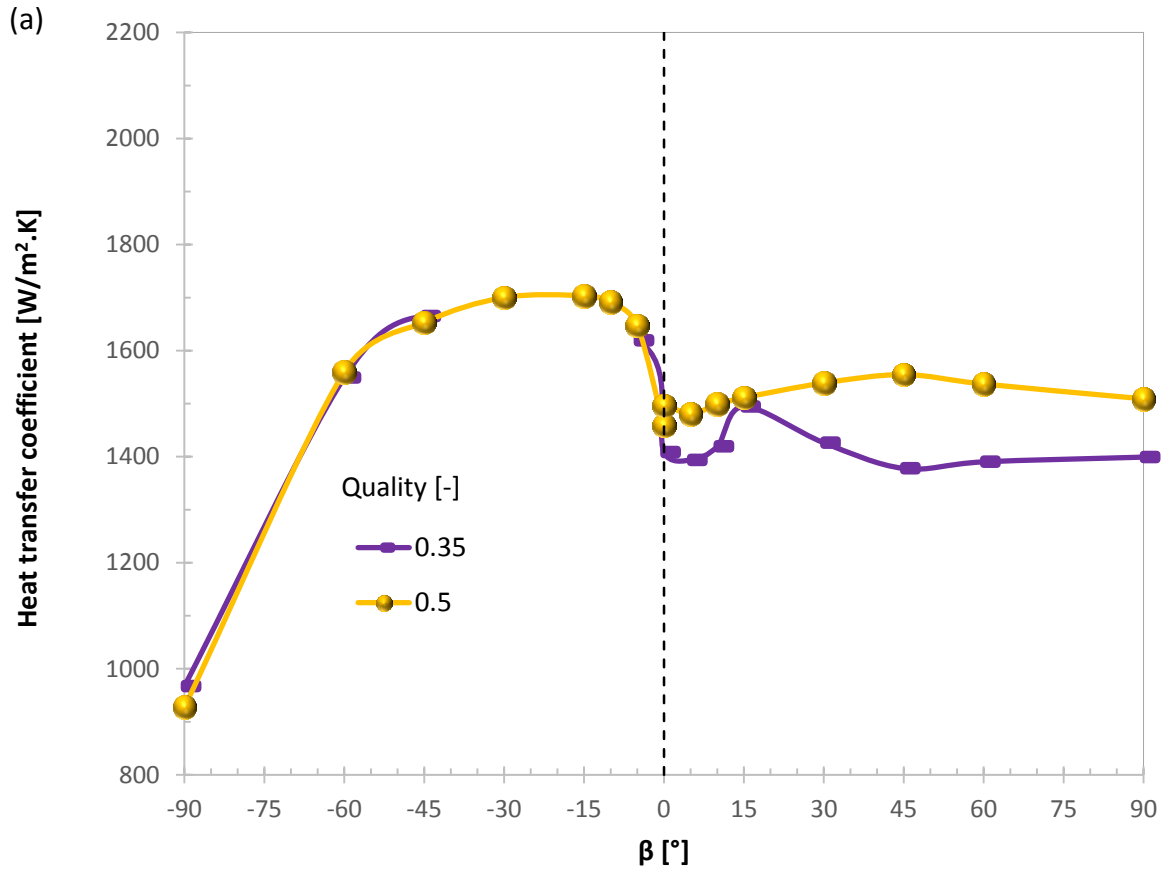


Figure B.5: Effect of quality for a mass flux $75 \text{ kg/m}^2 \cdot \text{s}$ and a temperature difference of $5 \text{ }^\circ\text{C}$



(a)

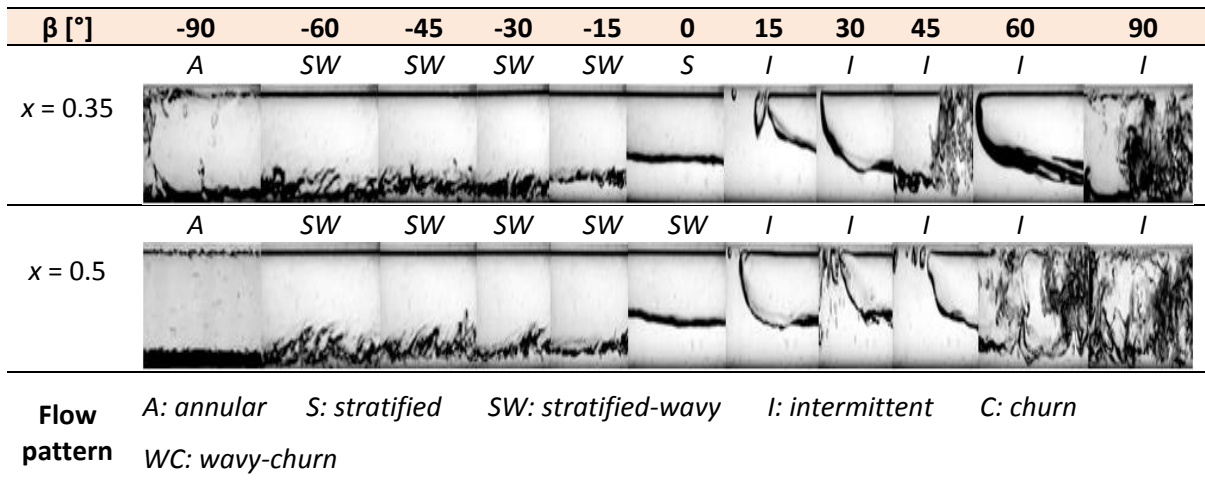
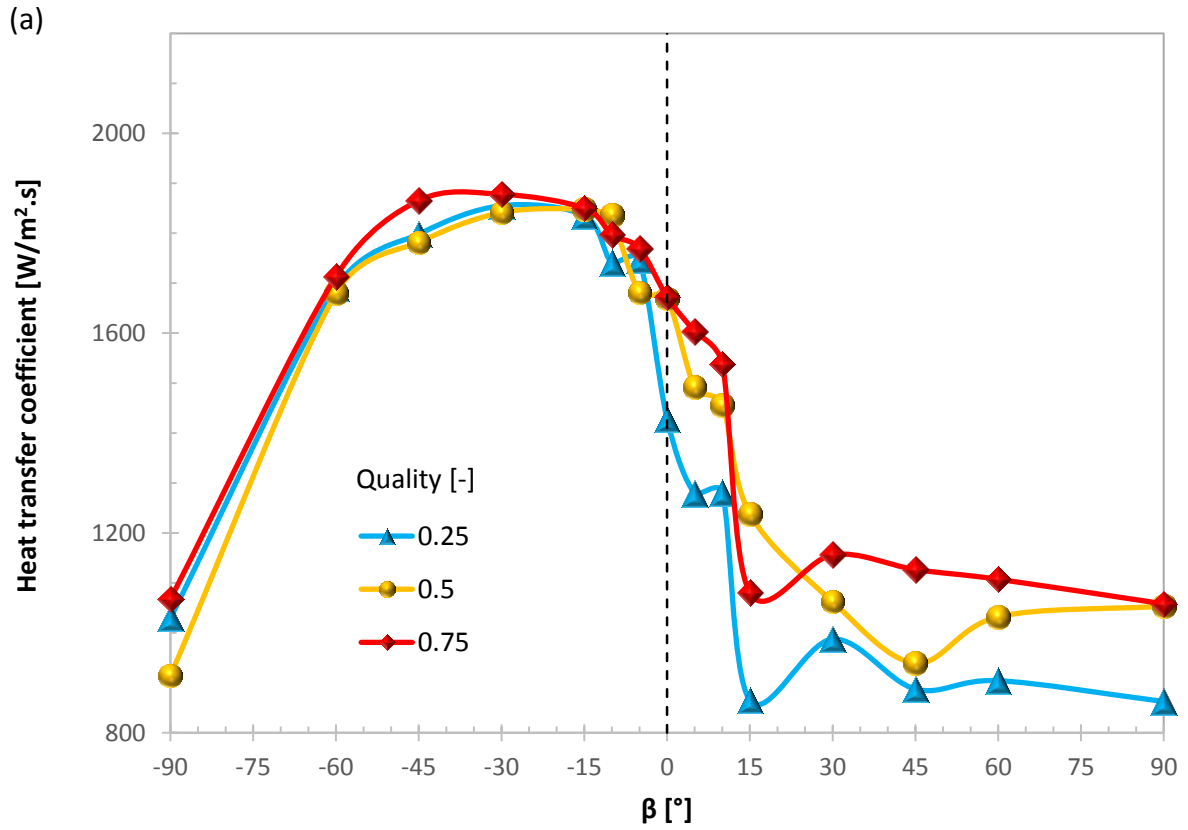


Figure B.6: Effect of quality for a mass flux $75 \text{ kg/m}^2 \cdot \text{s}$ and a temperature difference of $8 \text{ }^\circ\text{C}$



(b)

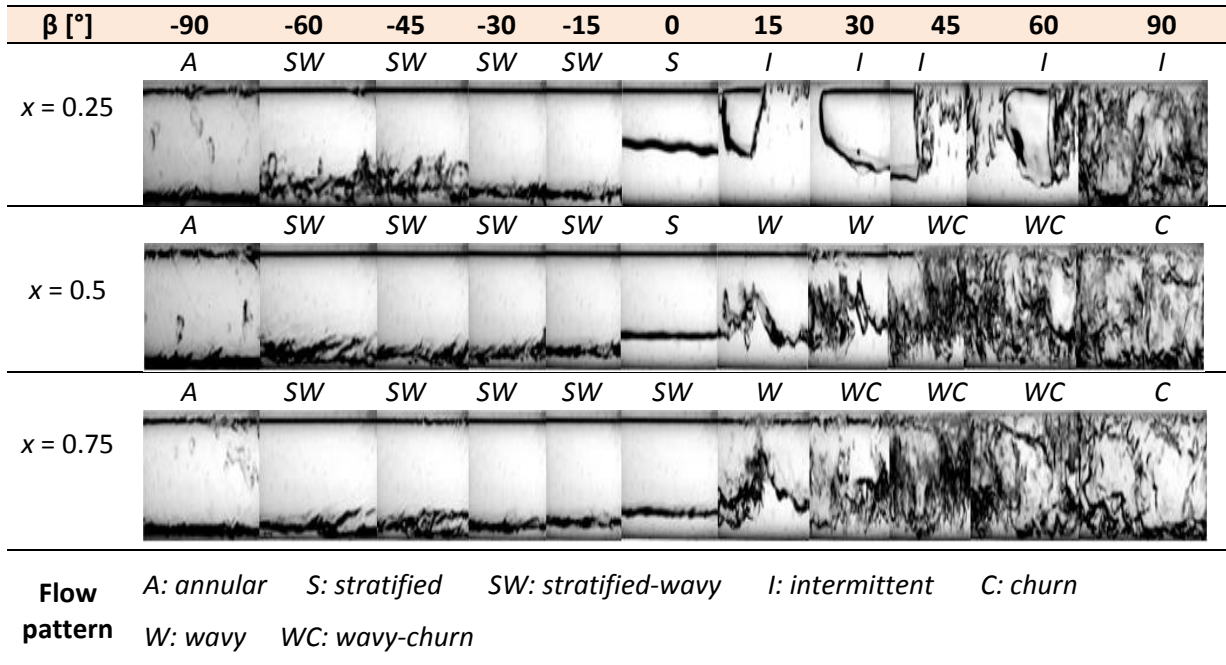
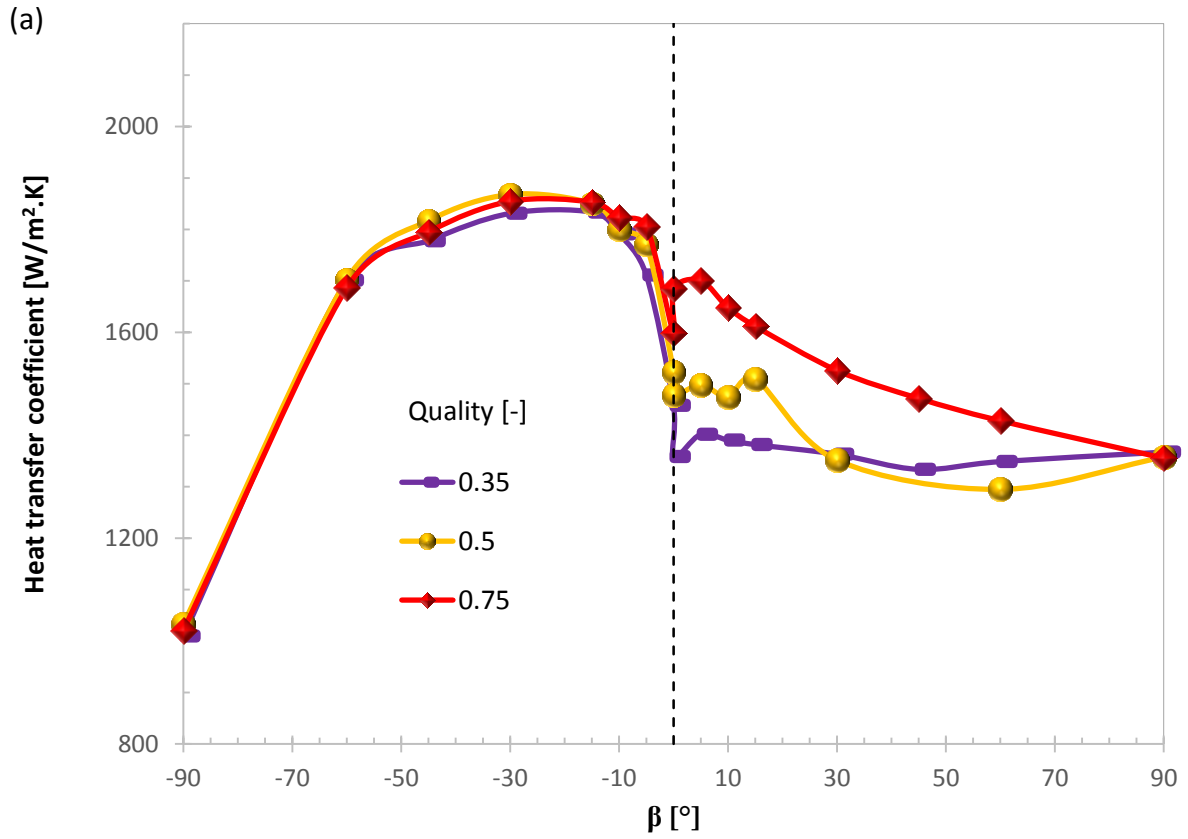


Figure B.7: Effect of quality for a mass flux $50 \text{ kg/m}^2\cdot\text{s}$ and a temperature difference of $1 \text{ }^\circ\text{C}$



(b)

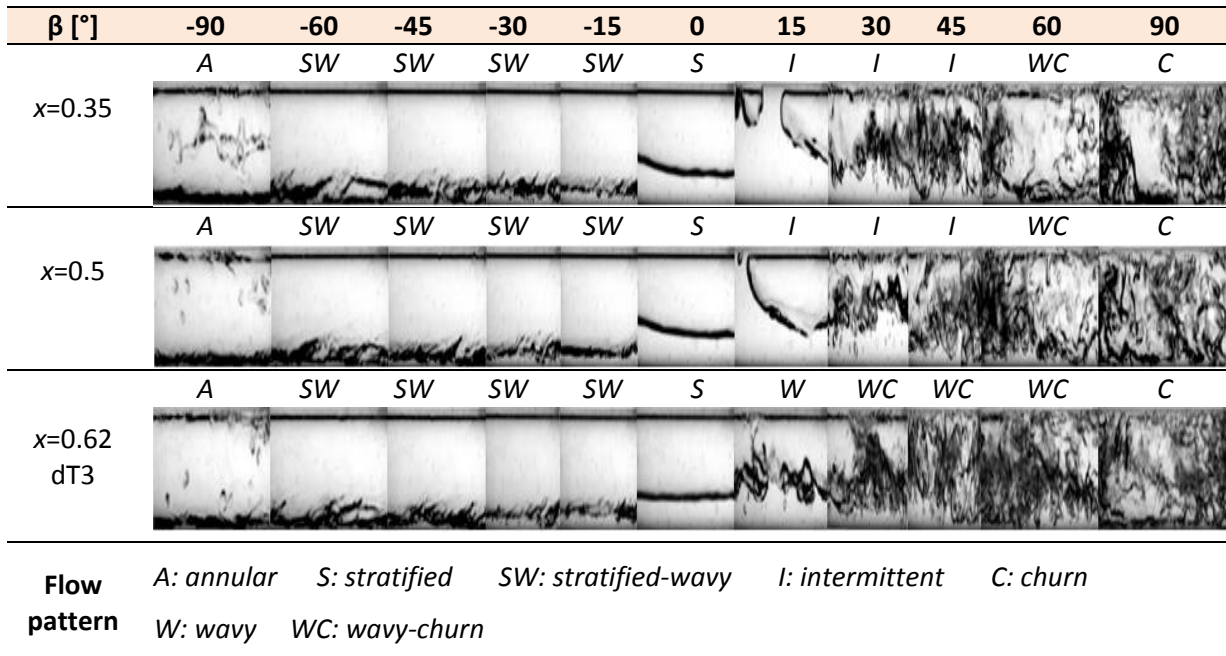
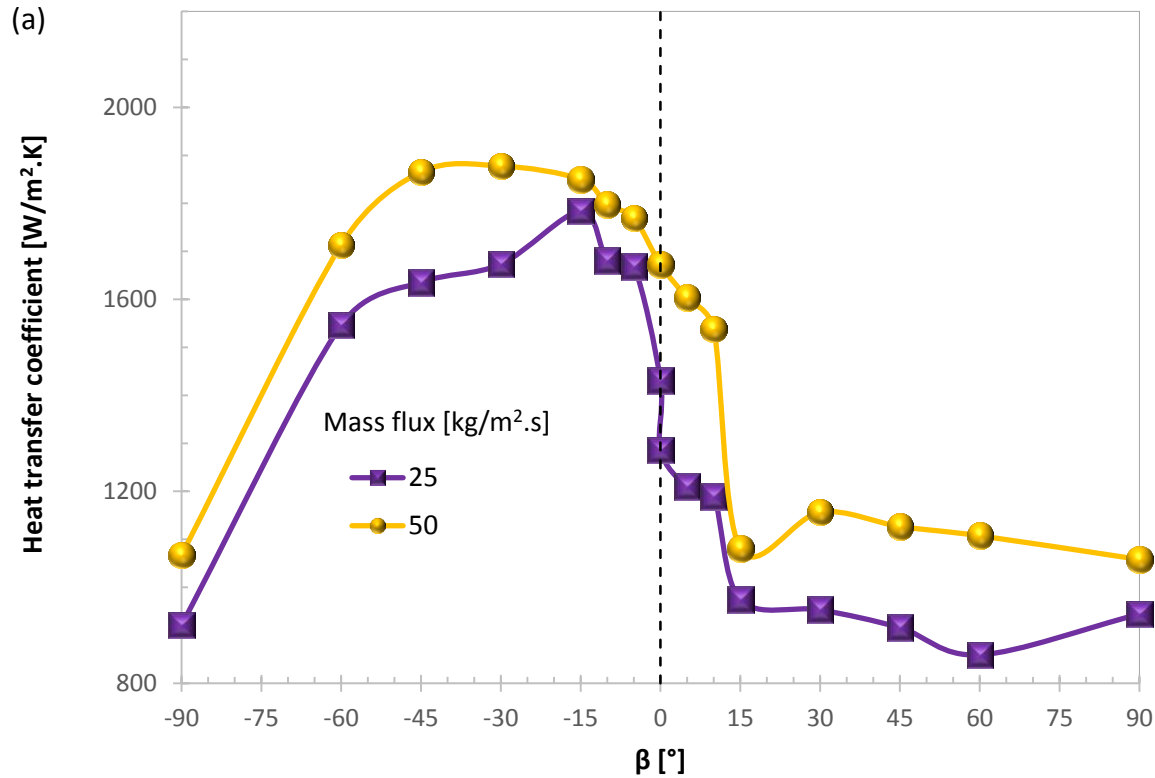


Figure B.8: Effect of quality for a mass flux $50 \text{ kg/m}^2 \cdot \text{s}$ and a temperature difference of $3 \text{ }^\circ\text{C}$

B.3. Effect of mass flux

The effect of mass flux on the heat transfer coefficient is discussed in the following sub-sections. The graphs and corresponding flow patterns are for different temperature differences from 1 °C to 8 °C at different qualities of 0.25 and 0.75.



(b)

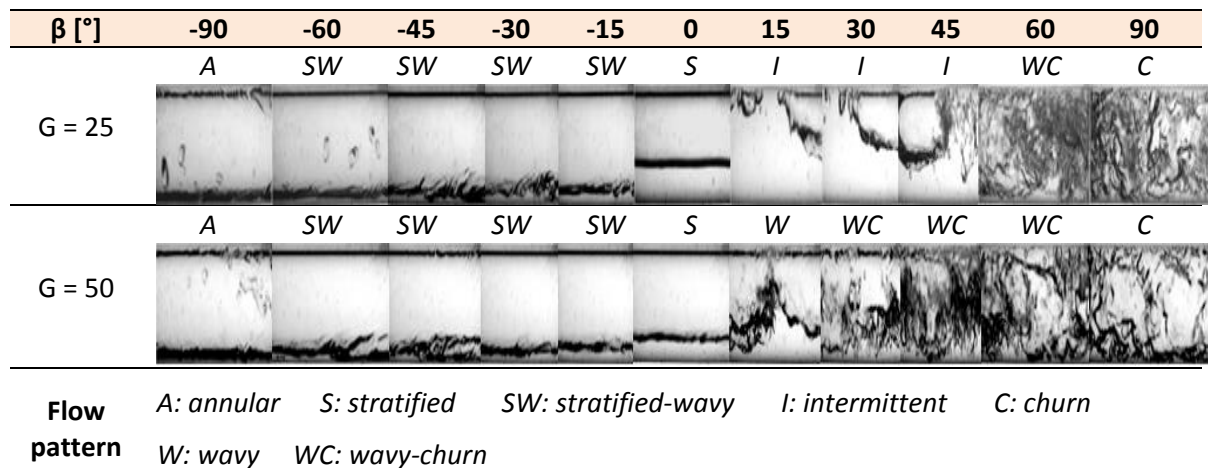
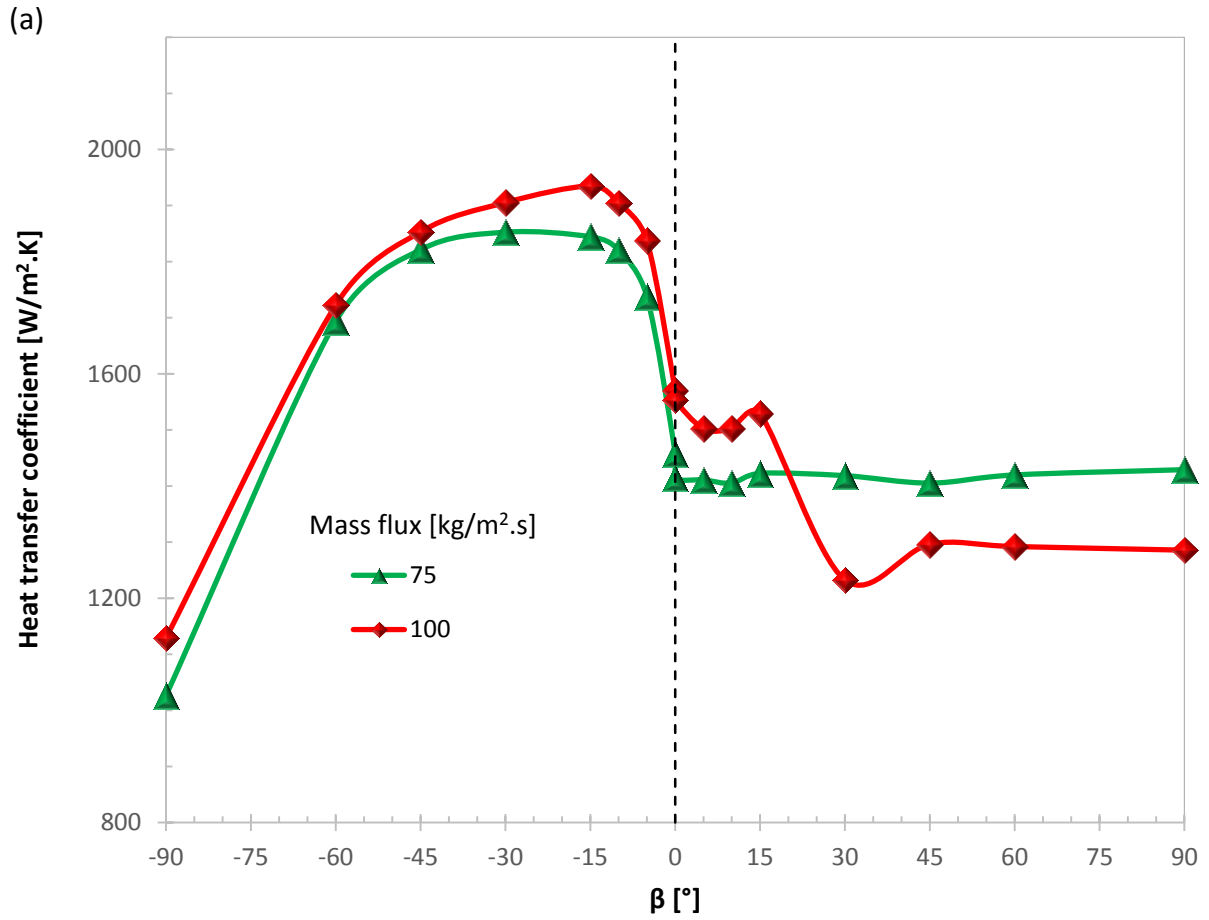


Figure B.9: Effect of mass flux for a temperature difference of 1 °C and a quality of 0.75



(b)

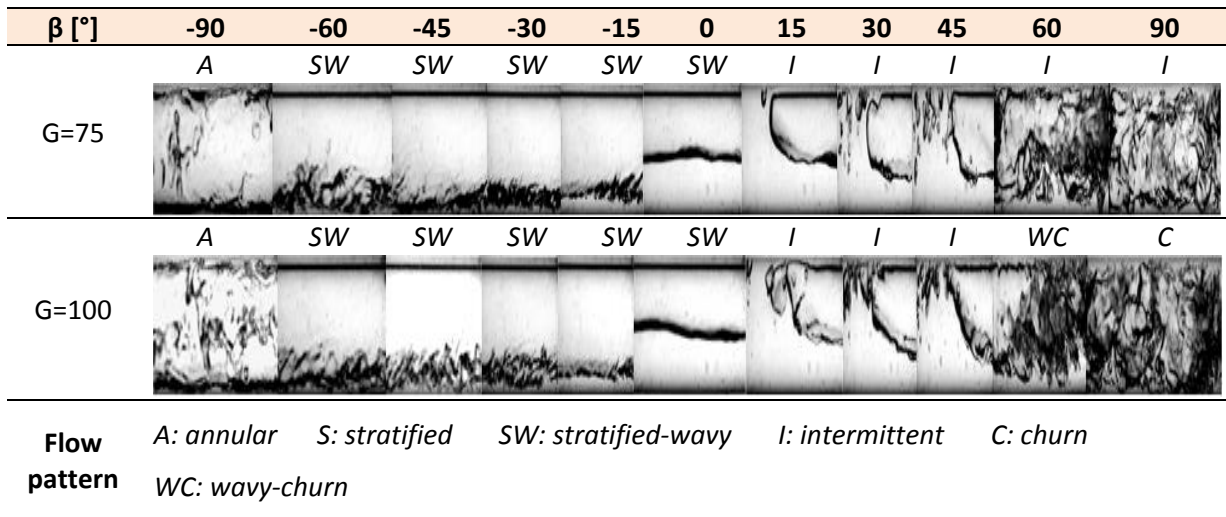
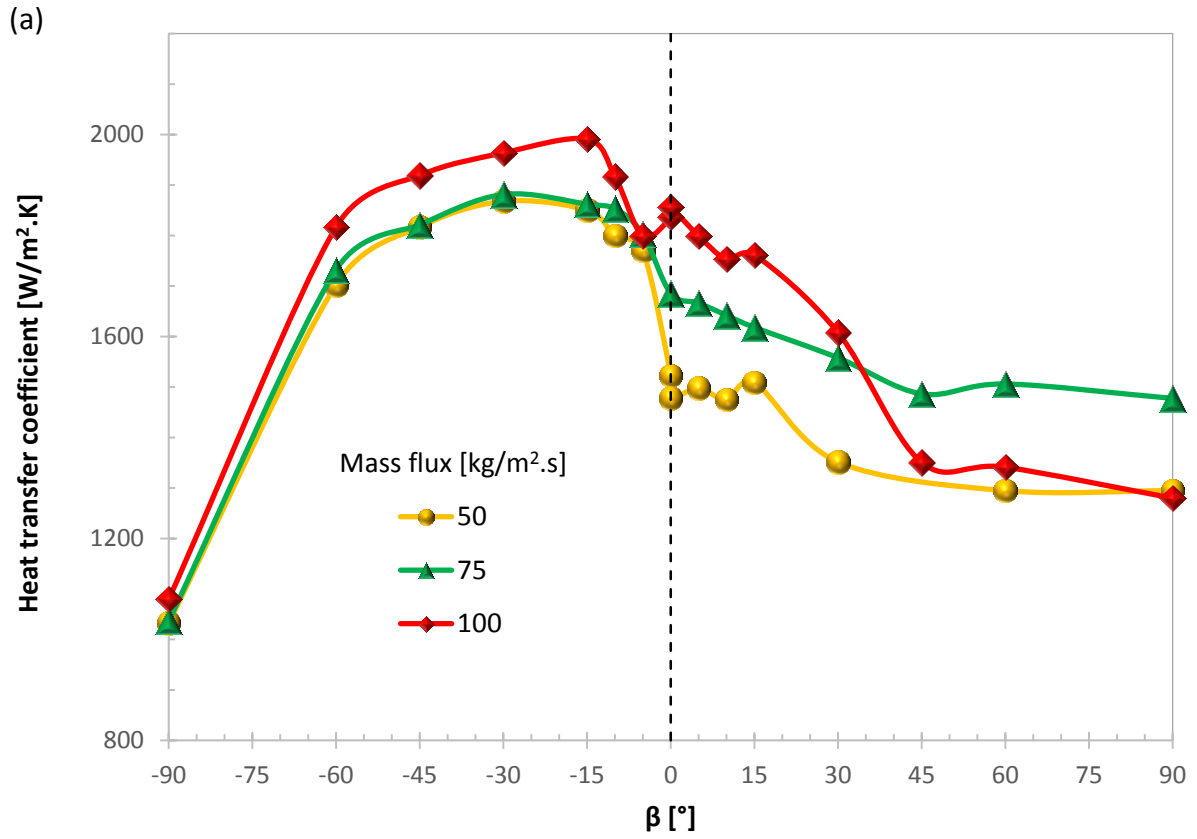


Figure B.10: Effect of mass flux for a temperature difference of 3 °C and a quality of 0.25



(b)

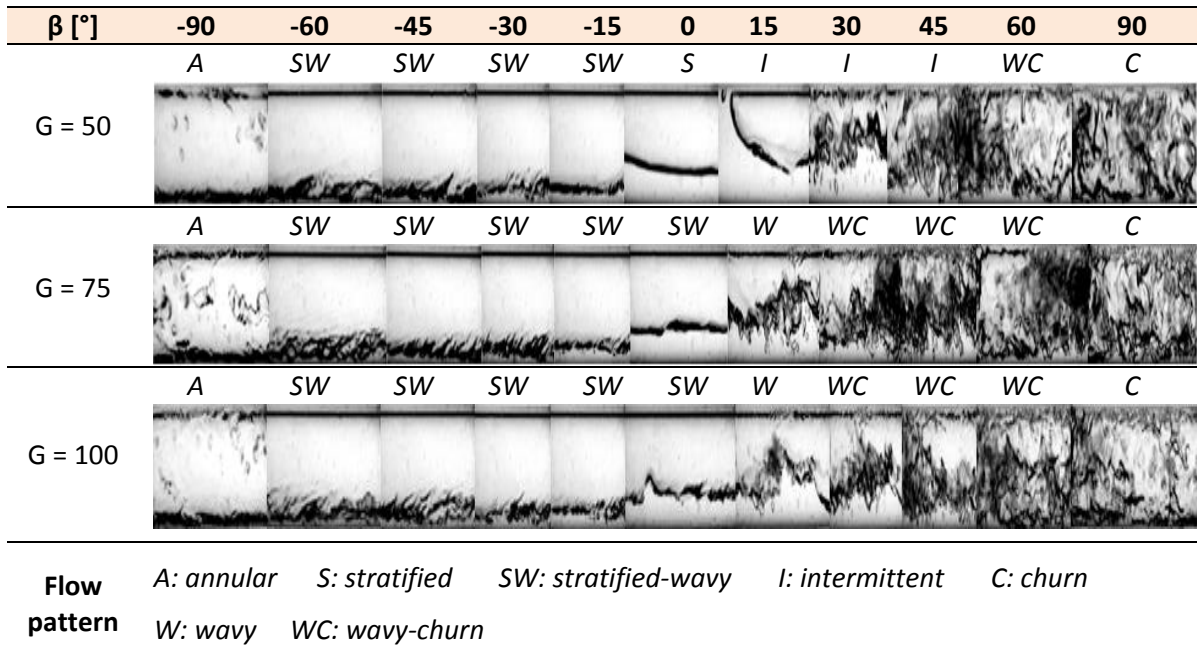
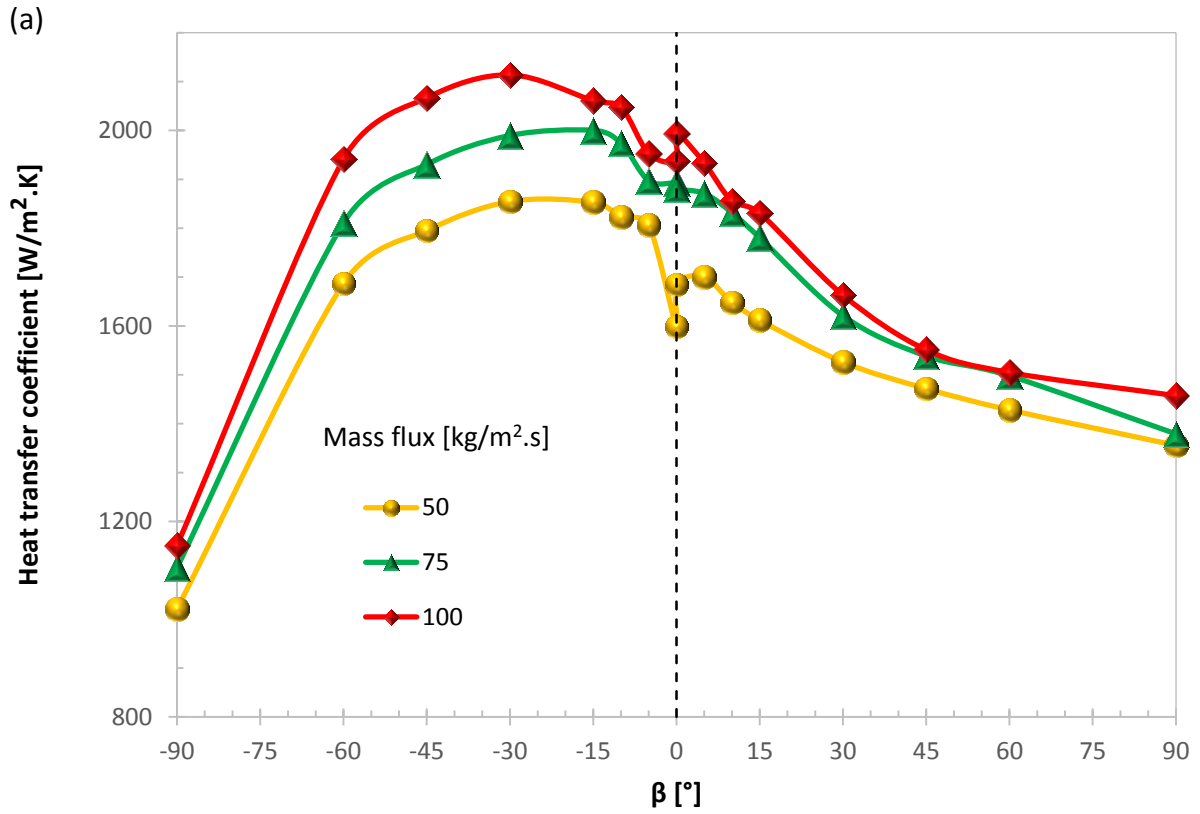


Figure B.11: Effect of mass flux for a temperature difference of 3 °C and a quality of 0.5



(b)

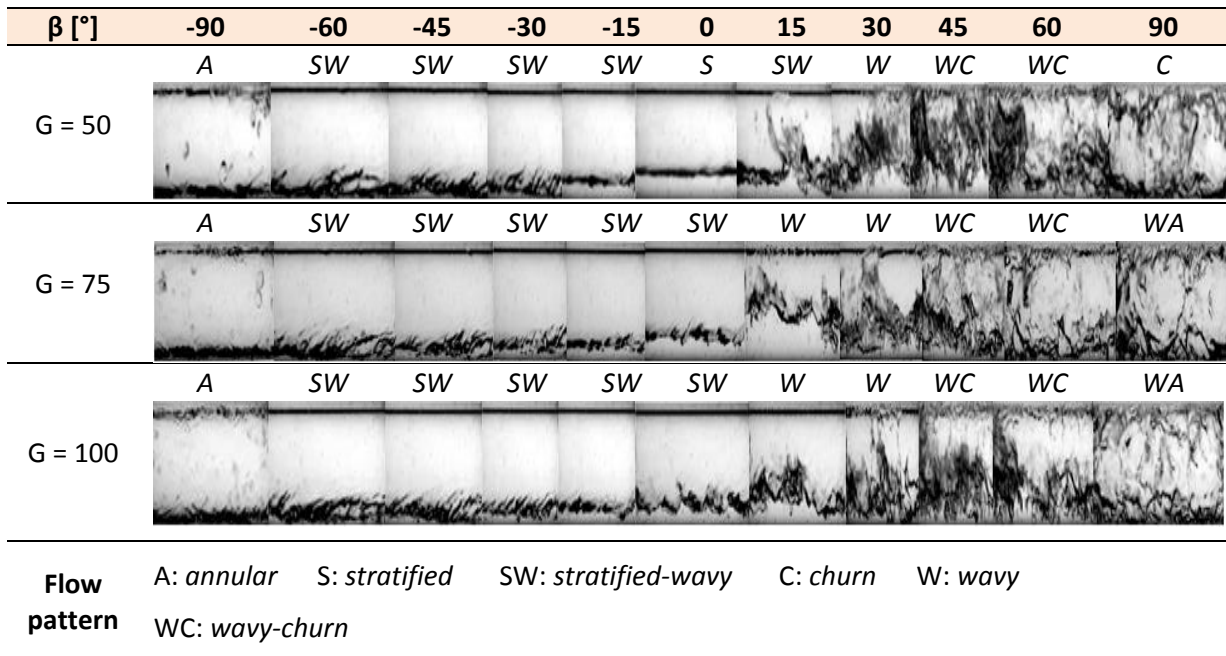
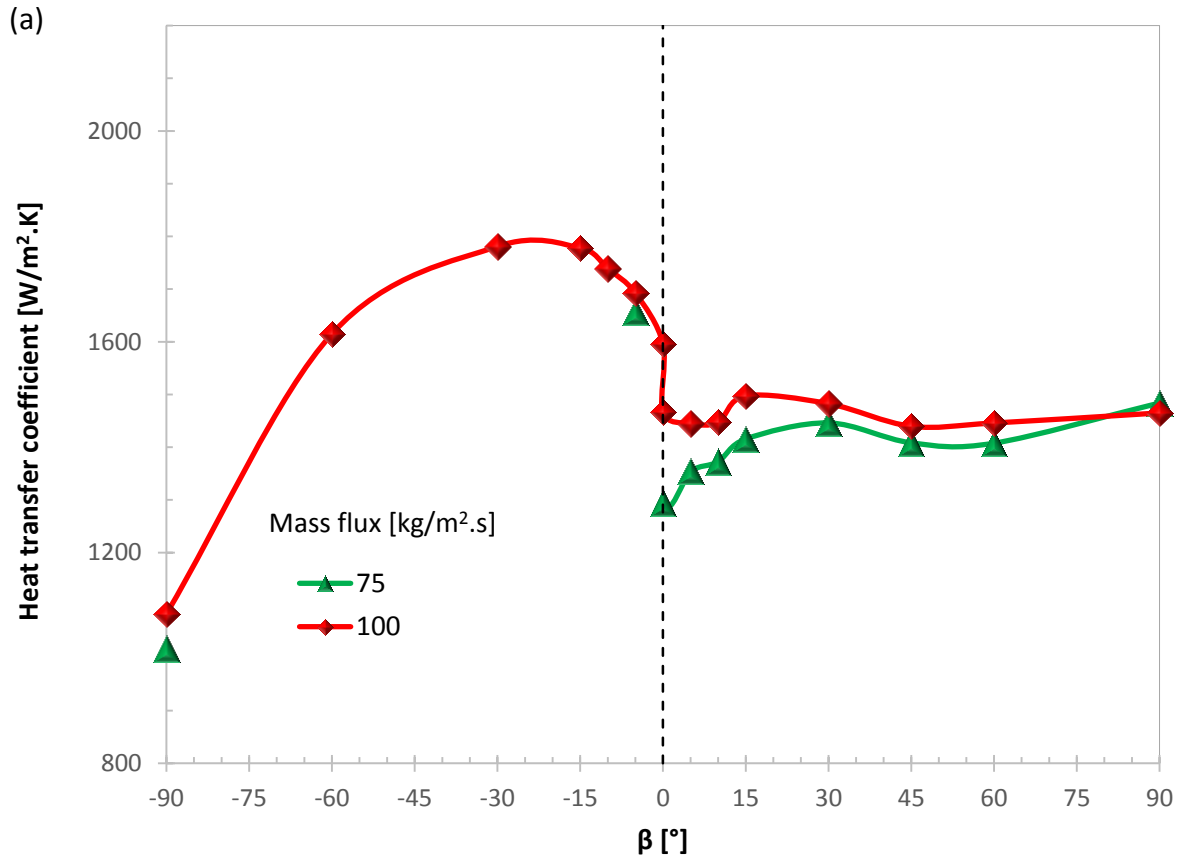


Figure B.12: Effect of mass flux for a temperature difference of 3 °C and a quality of 0.75



(b)

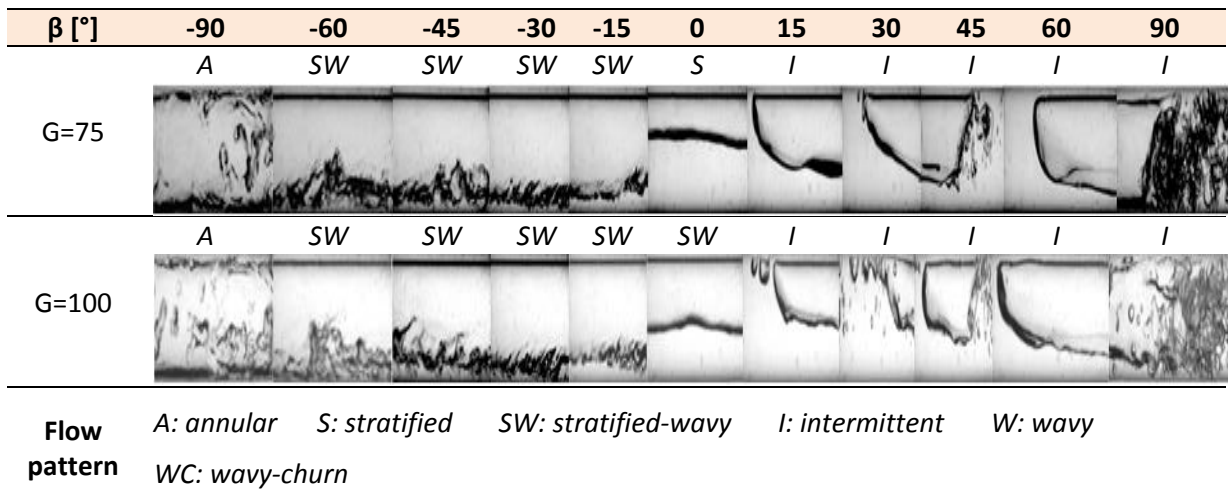
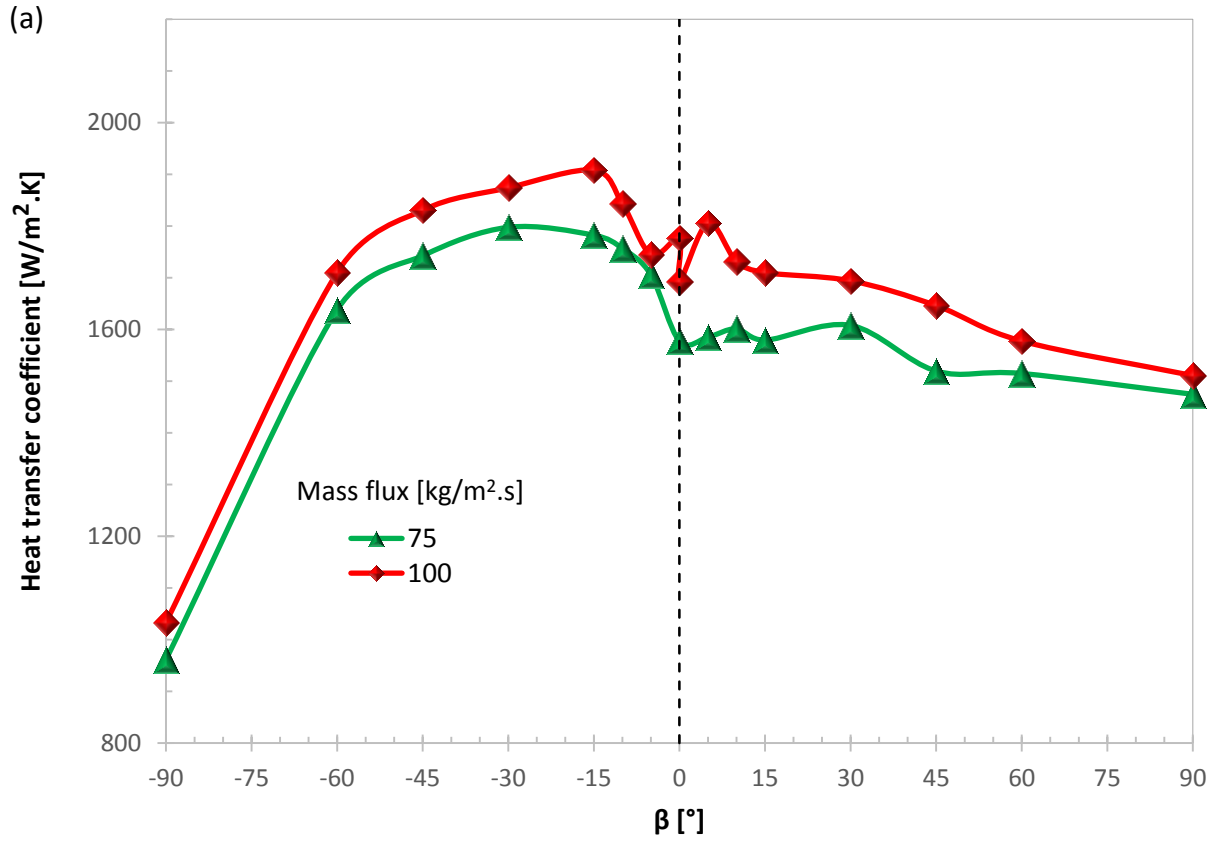


Figure B.13: Effect of mass flux for a temperature difference of 5 °C and a quality of 0.25



(b)

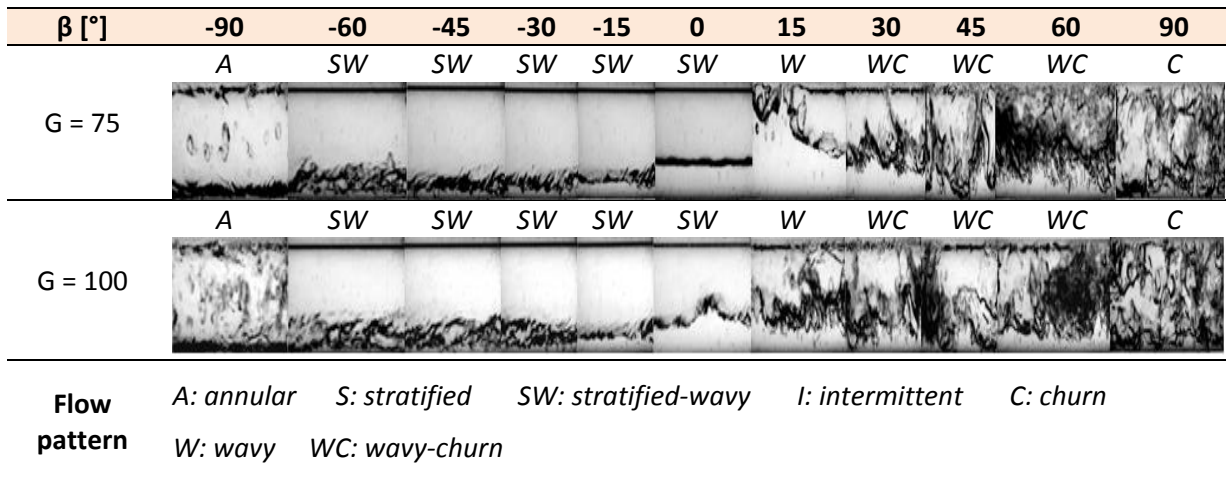
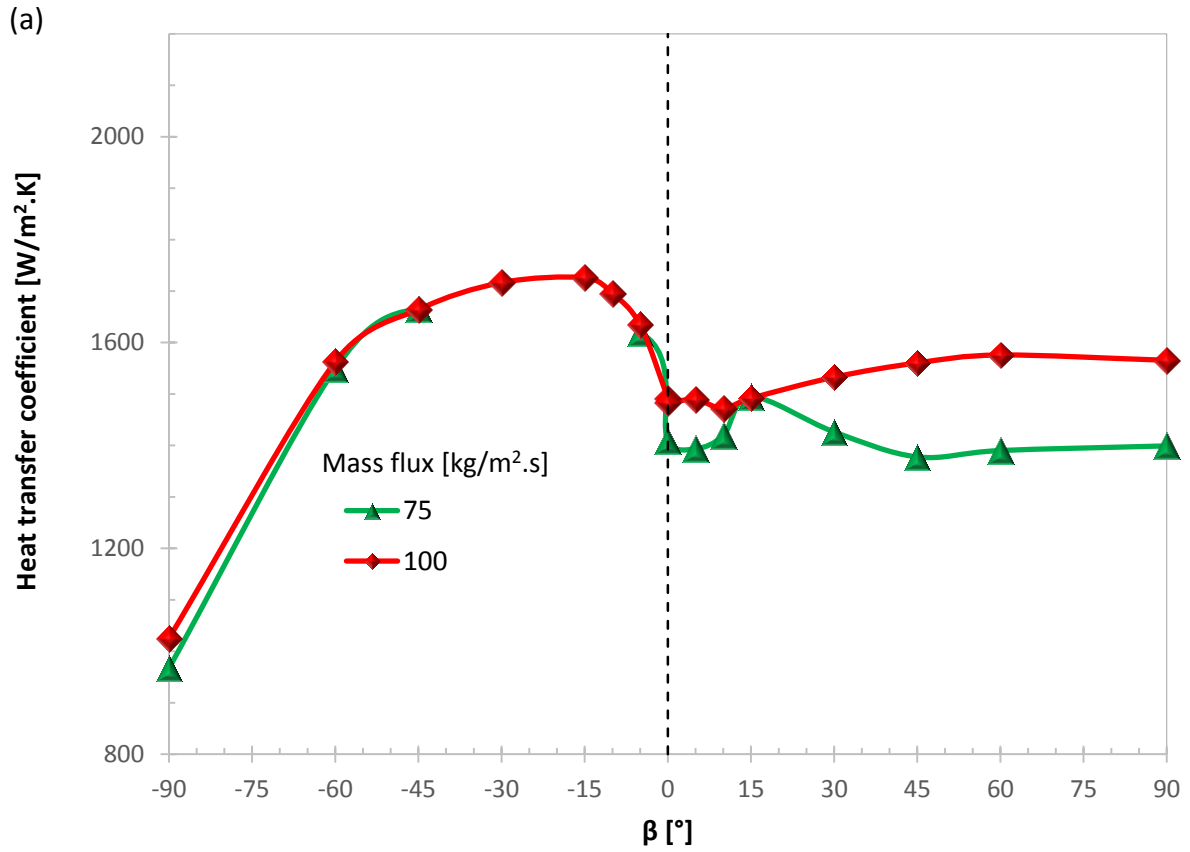


Figure B.14: Effect of mass flux for a temperature difference of 5 °C and a quality of 0.5



(b)

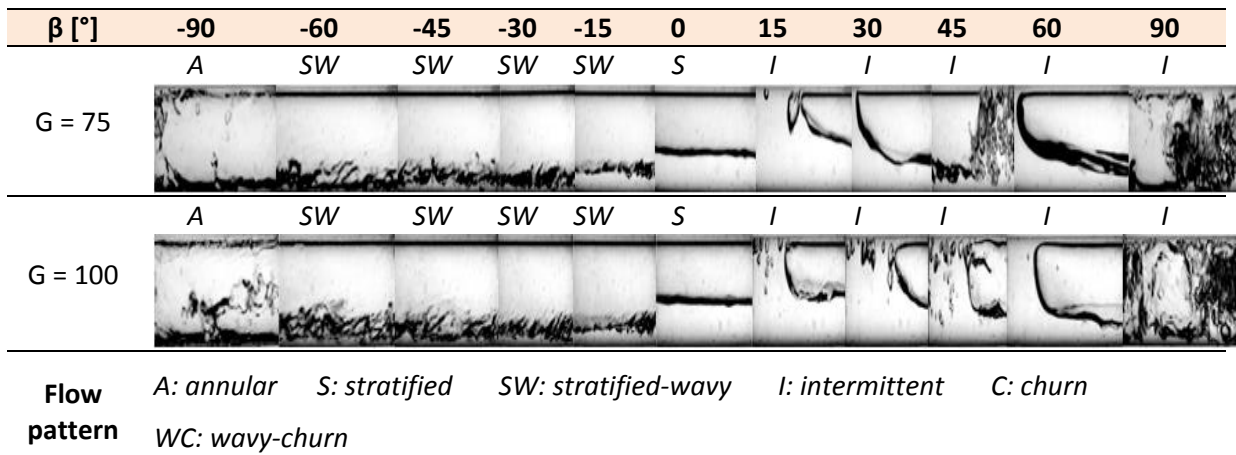
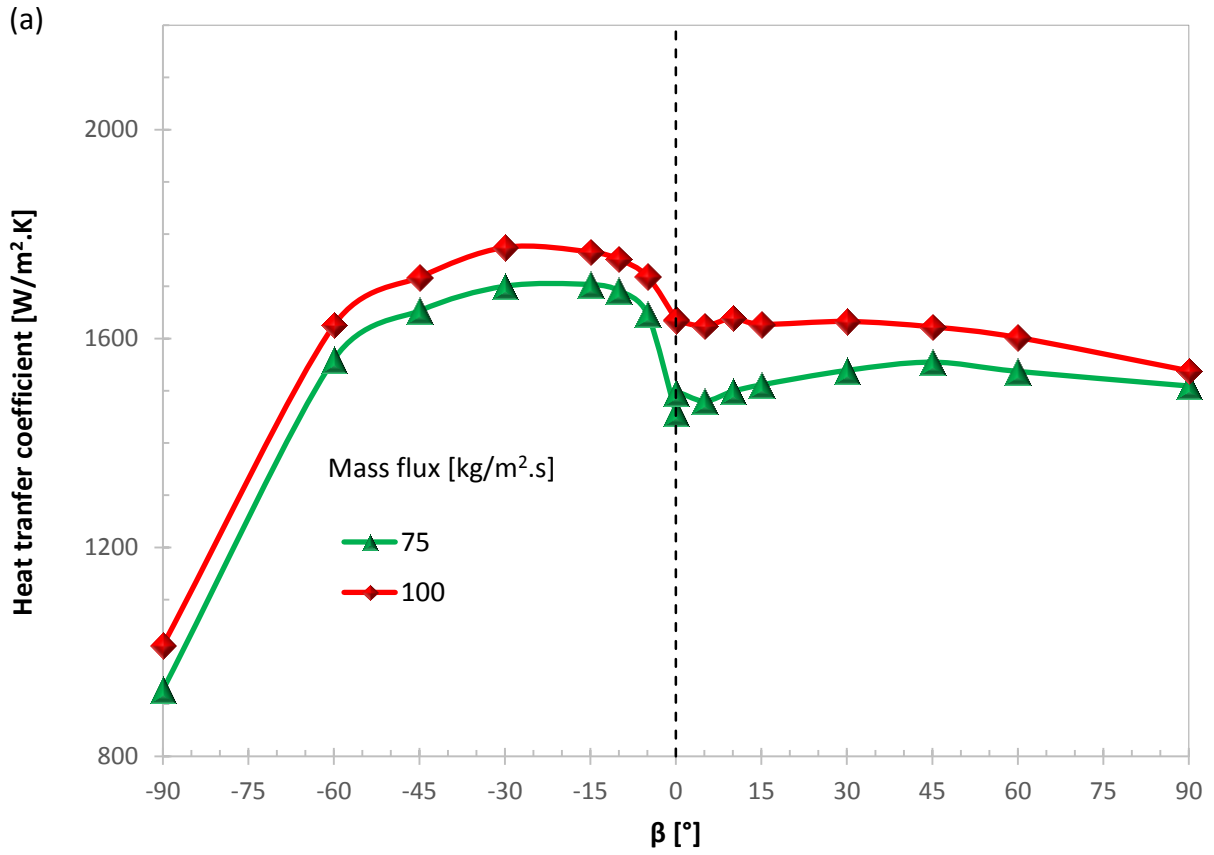


Figure B.15: Effect of mass flux for a temperature difference of 8 °C and a quality of 0.35



(b)

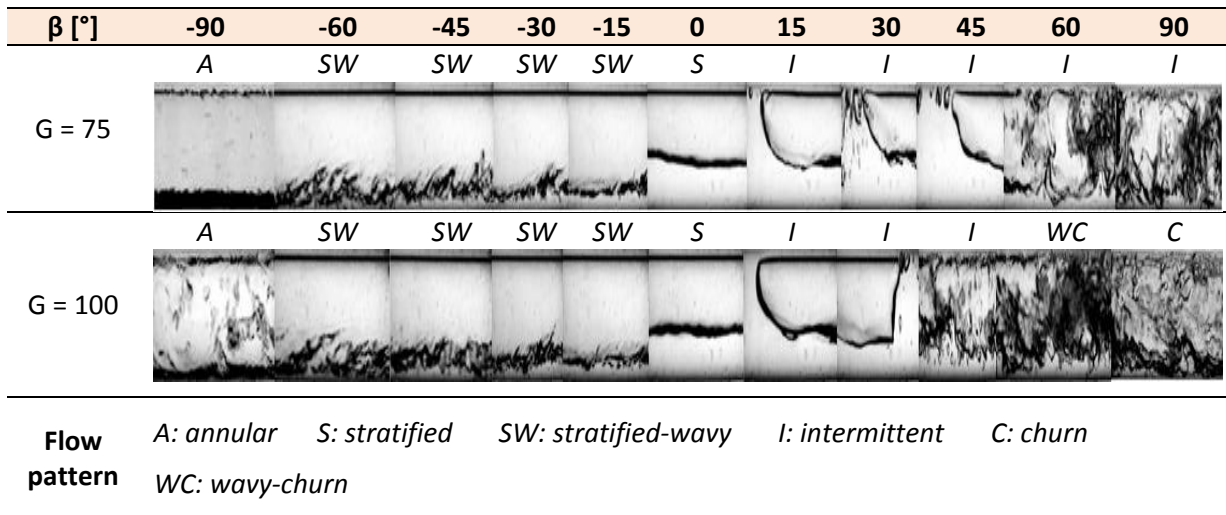
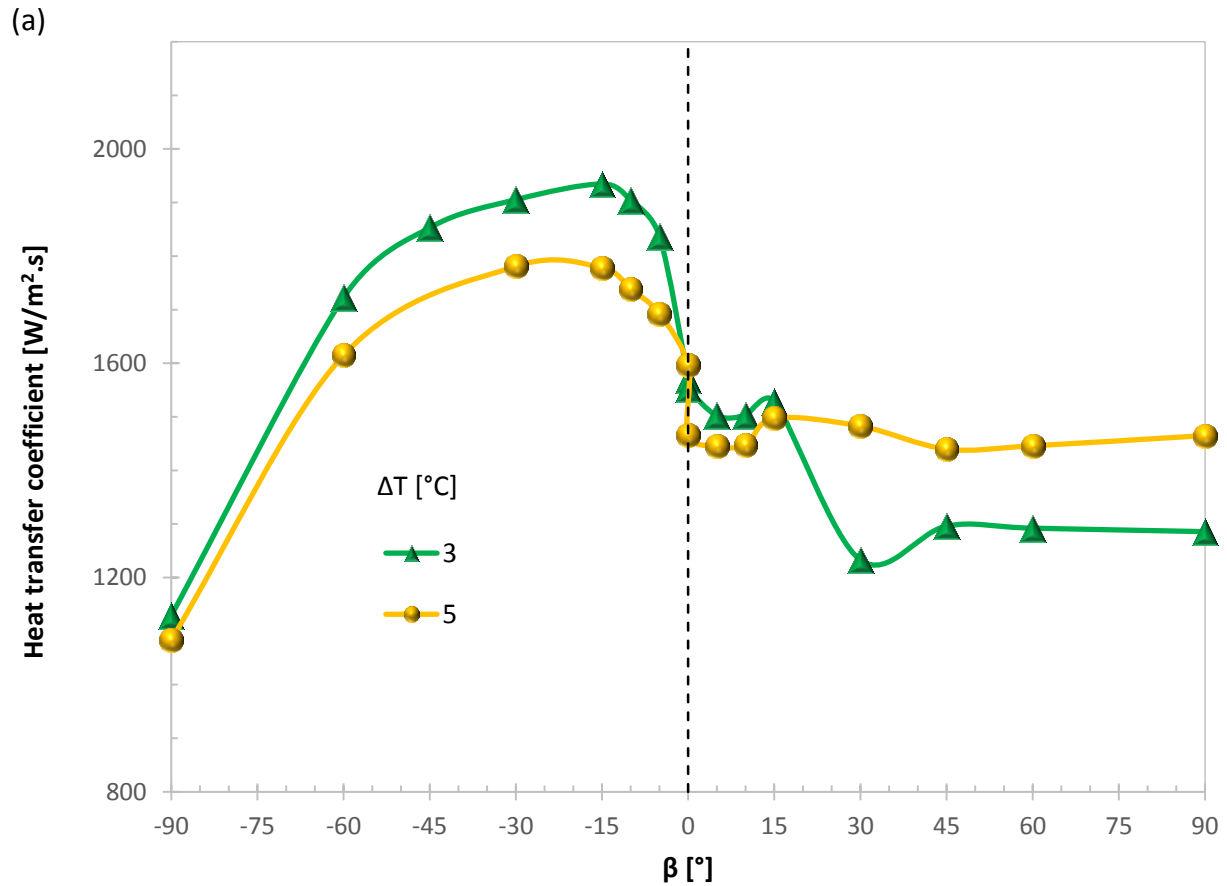


Figure B.16: Effect of mass flux for a temperature difference of 8 °C and a quality of 0.5

B.4. Effect of temperature difference

A comparison of the heat transfer coefficients and the prevailing flow patterns is shown in this section. For every mass flux and specific quality at different temperature differences, flow patterns on the outlet from the test section vary with changes in temperature difference.



(b)

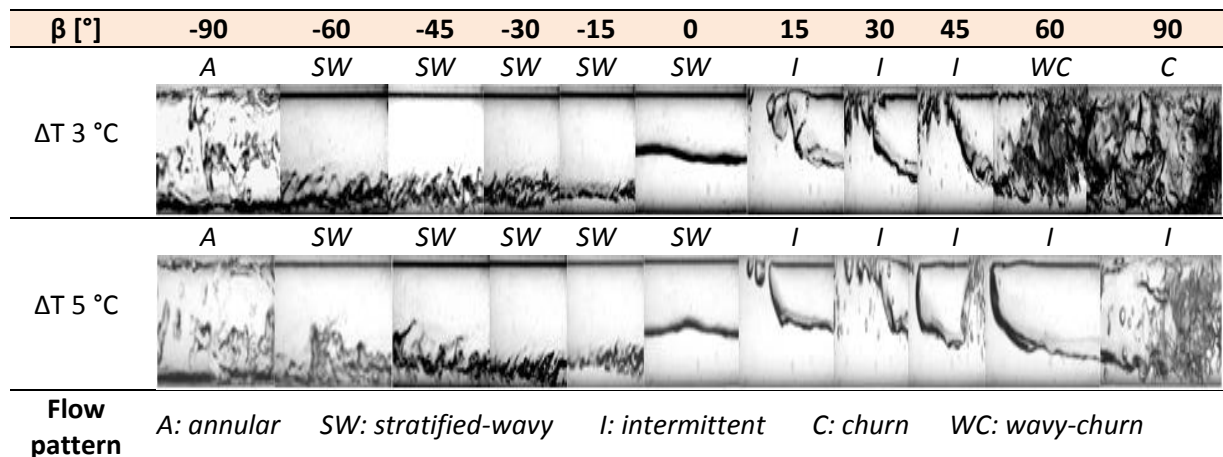
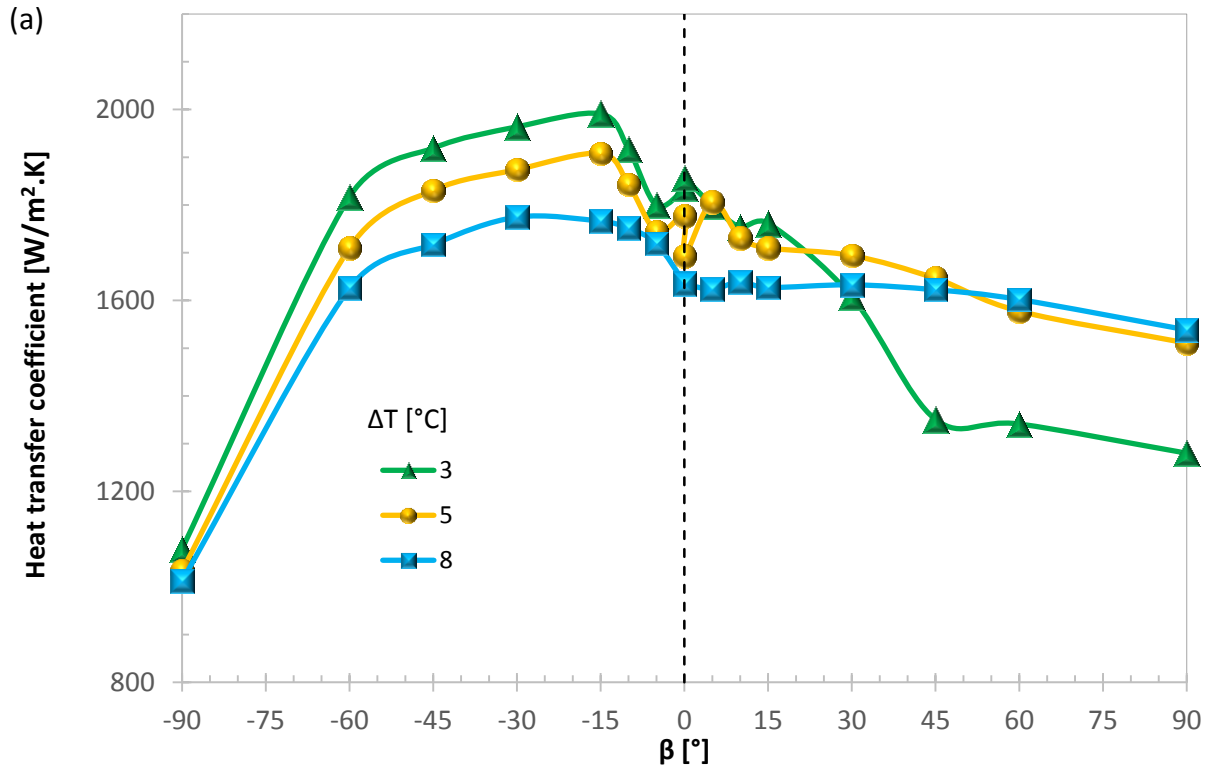


Figure B.17: Effect of temperature difference for a mass flux of 100 kg/m².s and a quality of 0.25



(b)

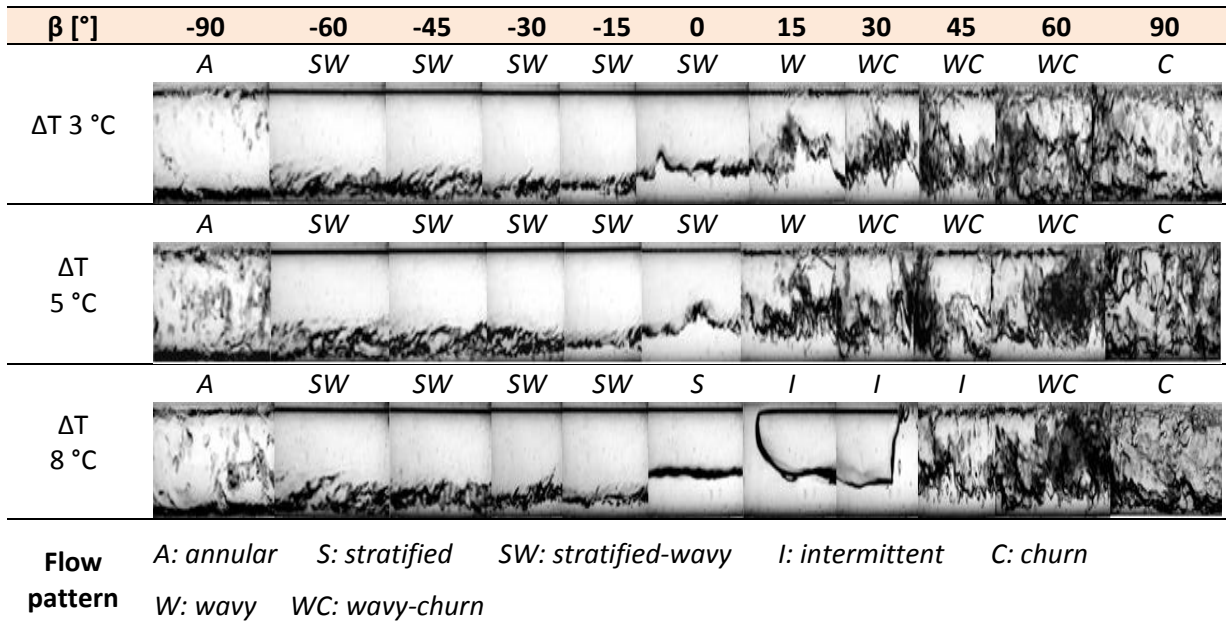
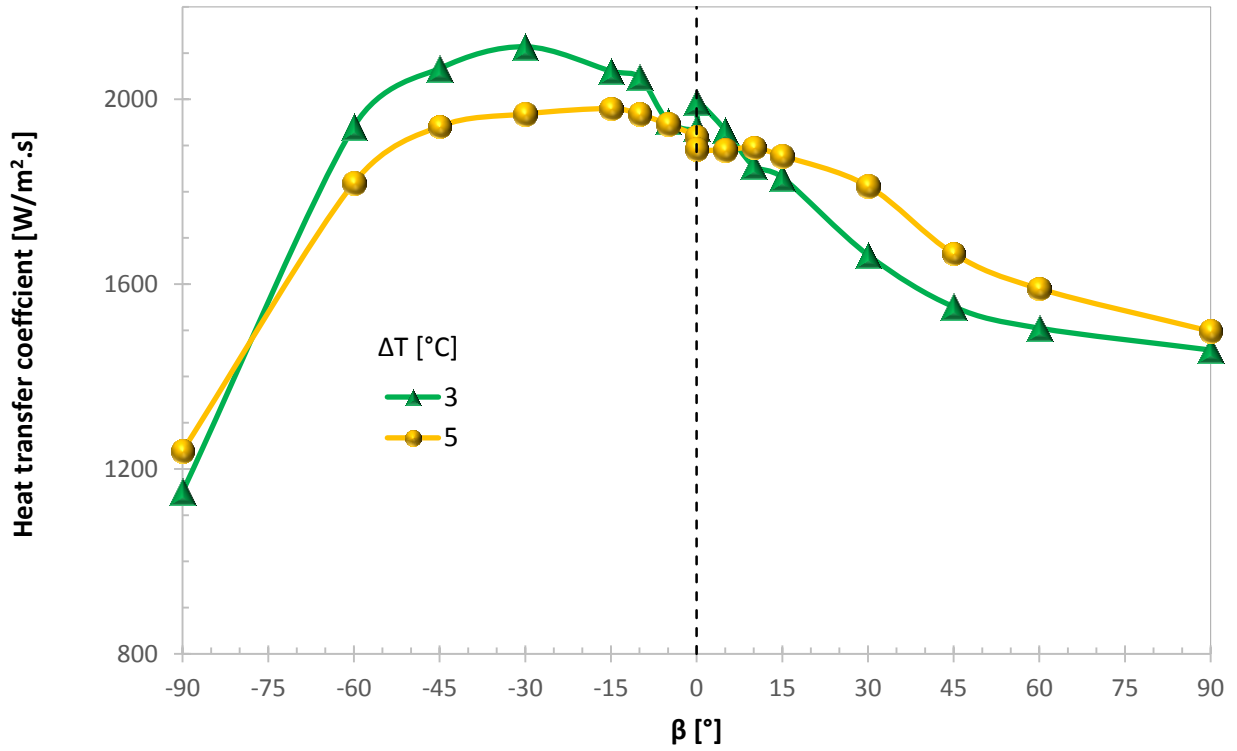


Figure B.18: Effect of temperature difference for a mass flux of $100 \text{ kg/m}^2 \cdot \text{s}$ and a quality of 0.5



(b)

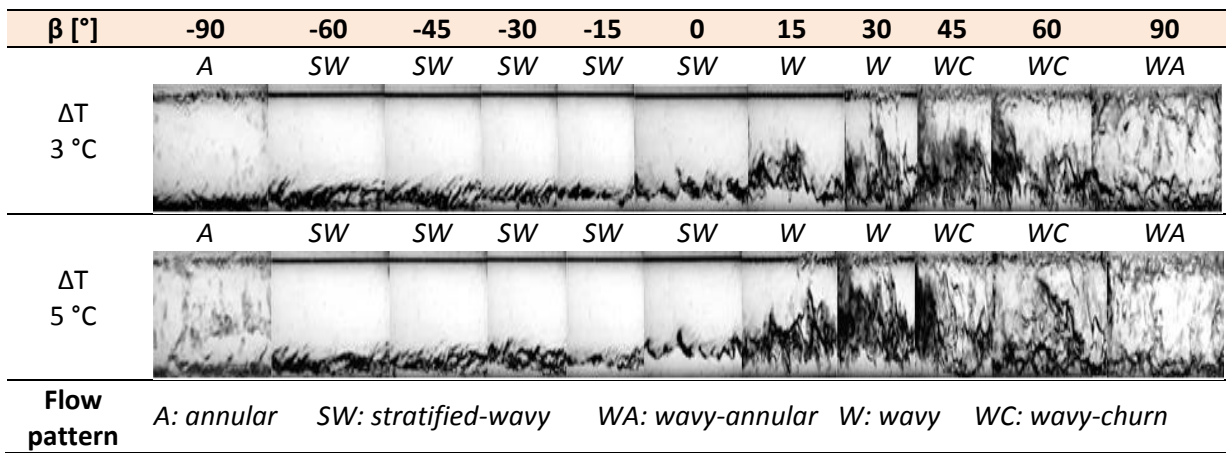
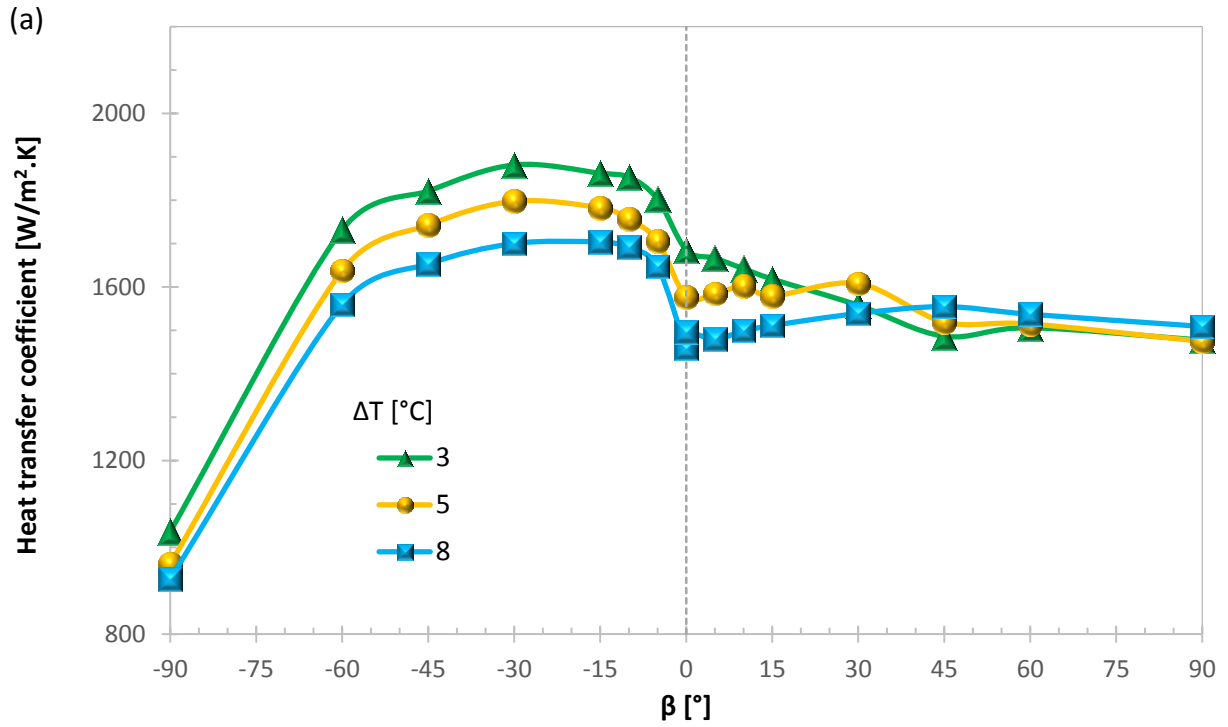


Figure B.19: Effect of temperature difference for a mass flux of 100 kg/m².s and a quality of 0.75



(b)

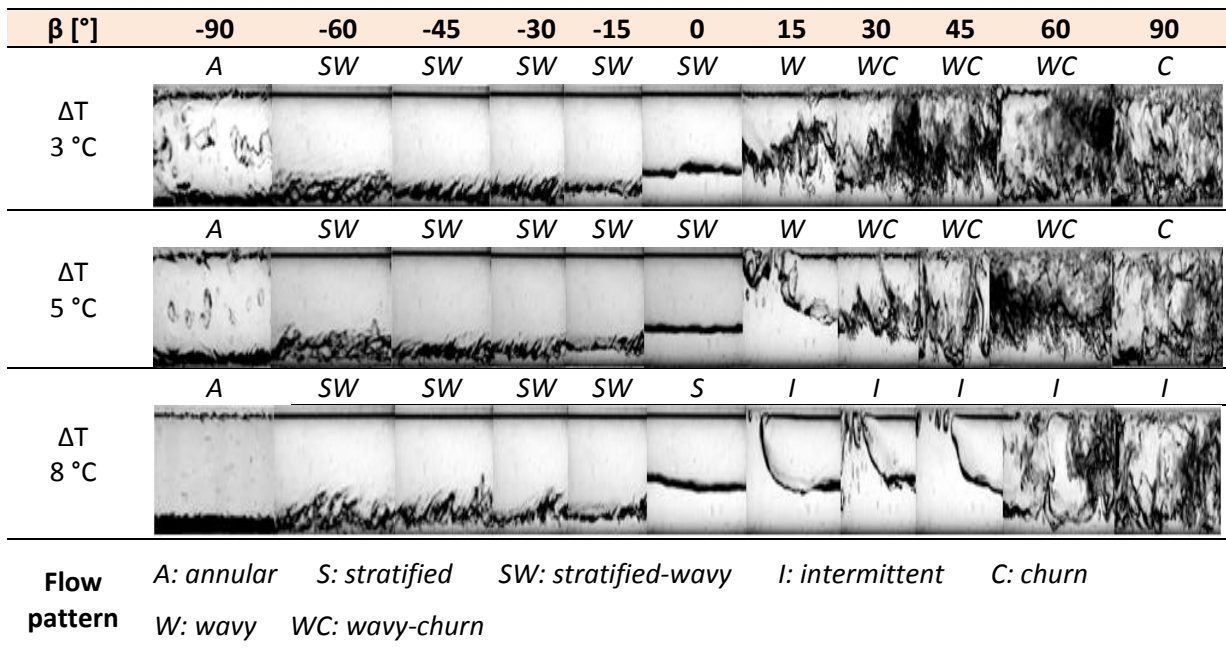
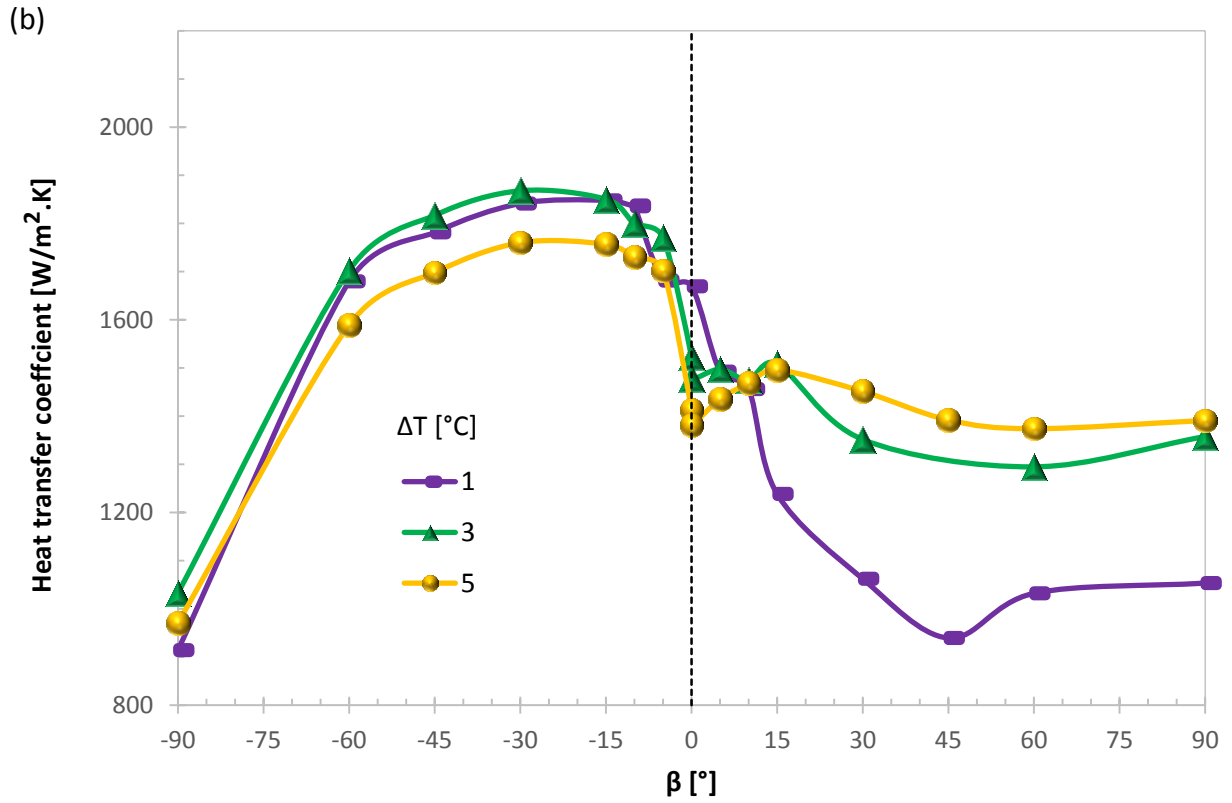


Figure B.20: Effect of temperature difference for a mass flux of 75 kg/m².s and a quality of 0.5



(b)

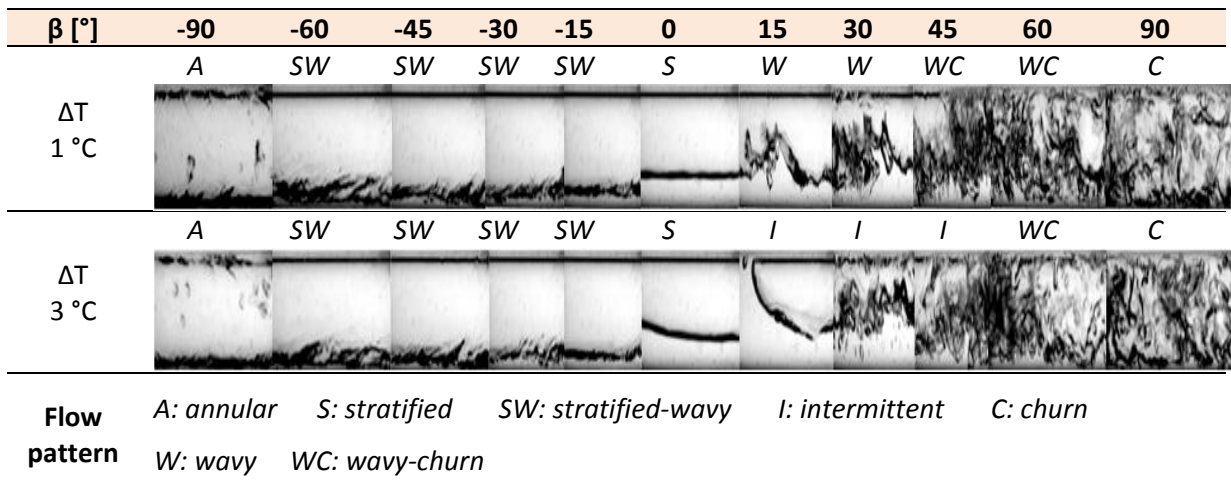
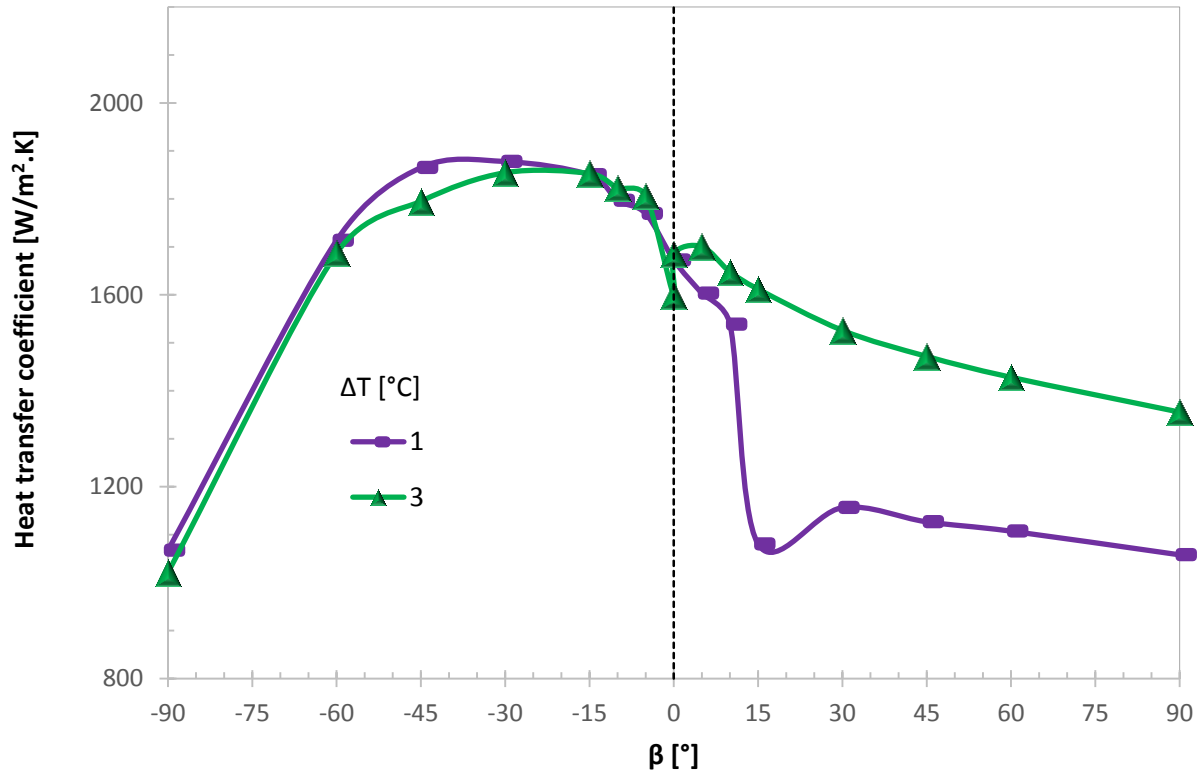
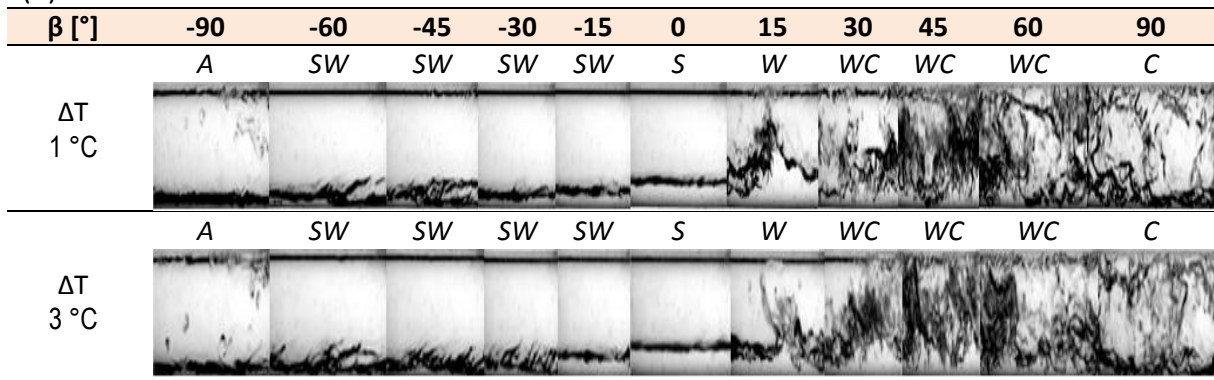


Figure B.21: Effect of temperature difference for a mass flux of 50 kg/m².s and a quality of 0.5



(b)



Flow pattern A: annular S: stratified SW: stratified-wavy C: churn WA: wavy-annular
 W: wavy WC: wavy-churn

Figure B.22: Effect of temperature difference for a mass flux of 50 kg/m².s and a quality of 0.75

B.5. Summary

Figure B.23 summarises the flow patterns for Appendix B, showing the effect quality, mass flux, temperature difference and inclination has on the flow pattern. The flow patterns are only for the outlet from the test section. Much more detailed flow pattern transitions are given in Appendix C and summarised in C.10 where the inlet and outlet flow patterns to and from the test condenser are discussed.

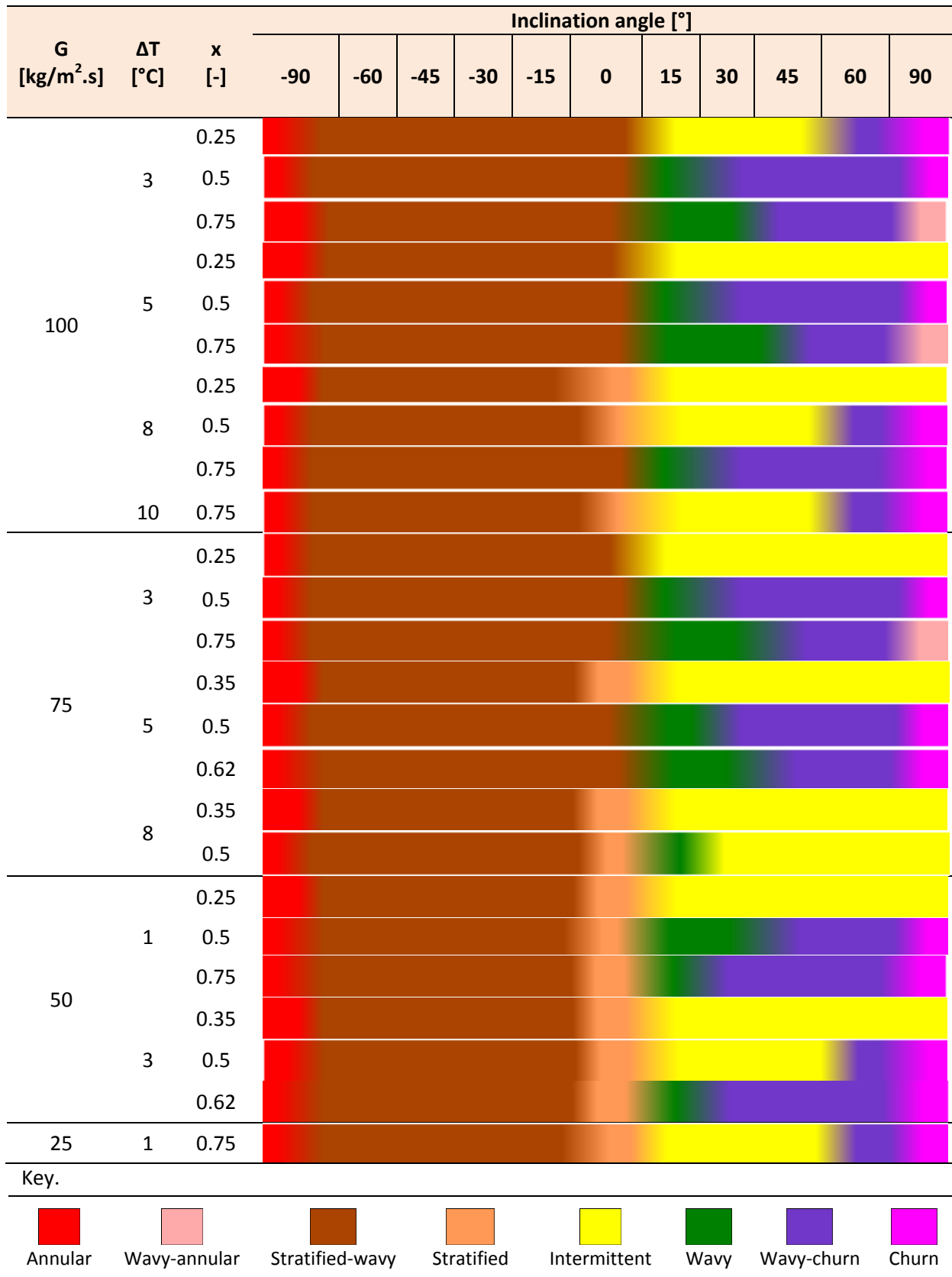


Figure B.23: Summary of flow pattern transitions

Two flow patterns are observed for all the negative inclined angles from -5° to -90°, which are annular and stratified flow. However, stratified flow is observed mainly at low mass

velocities and lower qualities. The intermittent flow pattern, on the other hand, is common at lower qualities, lower mass fluxes and high temperature differences. Wavy flow pattern in most cases would replace intermittent flow pattern at higher qualities 0.5 and above. The wavy-churn, churn and annular-wavy flow patterns are observed at higher inclination angles, with the annular and churn flow patterns being observed mostly at $+90^\circ$ angle. The wavy-churn flow pattern is always a result of flow pattern transition from either wavy or intermittent flow patterns as the inclination angle is increased. The wavy-annular flow pattern is only dominant at a high quality of 0.75 at $+90^\circ$.

Appendix C. Flow pattern transitions for a ΔT of 3 °C

C.1. Introduction

Appendix C to Appendix G summarise the transition of flow patterns from the inlet to the outlet of the test condenser, a lower quality of 0.25 to a higher quality of 0.75, mass flux of 100 kg/m².s to 50 kg/m².s, inclination angles of +90° to -90° and temperature differences of 3 °C, 5 °C, 8 °C and 10 °C. The analysis of flow pattern transitions will assist in the design of flow pattern maps that correctly predict flow patterns for different working parameters. Each sub-section consists of a different inclination angle for upward and downward flow. The flow patterns that were observed are indicated as stratified (*S*), stratified-wavy (*SW*), wavy (*W*), intermittent (*I*), churn (*C*), annular (*A*), wavy-annular (*WA*) and wavy-churn (*WC*). The flow patterns are somewhat subjective, hence some flow patterns might pose some differences in opinions, especially those close to the transition region, whereby they could fit on both sides. Sometimes, the stratified-wavy flow pattern might seem like a stratified flow, as the wave length increases and the amplitude of the waves are very small. In this case, one might observe the stratified-wavy pattern as stratified flow. A summary is given after every appendix from Appendix C to Appendix H of colour-coded flow patterns so that it becomes easy to show the transitions in brief.

C.2. Flow pattern transitions for the horizontal inclination 0°













Mass flux [kg/m ² .s]		Time [s]			Flow pattern
		0	0.25	0.5	
100	in				<i>SW</i>
	out				<i>SW</i>
75	in				<i>SW</i>
	out				<i>SW</i>

Figure C.1: Flow pattern transition at 0° inclination angle and a quality of 0.25

Mass flux [kg/m ² .s]		Time [s]			Flow pattern
		0	0.25	0.5	
100	in				SW
	out				SW
75	in				SW
	out				SW
50	in				SW
	out				S

Figure C.2: Flow pattern transition at 0° inclination angle and a quality of 0.5

Mass flux [kg/m ² .s]		Time [s]			Flow pattern
		0	0.25	0.5	
100	in				SW
	out				SW
75	in				SW
	out				SW
50	in				SW
	out				SW

Figure C.3: Flow pattern transition at 0° inclination angle and a quality of 0.75

C.3. Flow pattern transitions for the inclination angle of $\pm 5^\circ$


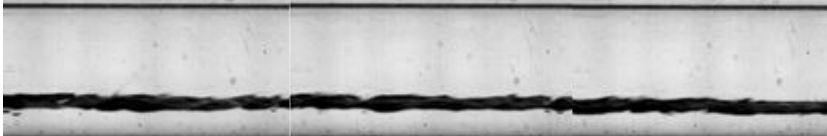


Mass flux [kg/m ² .s]	Time [s]			Flow pattern	
	0	0.25	0.5		
100	in				SW
	out				SW
75	in				S
	out				SW

Figure C.4: Flow pattern transition at -5° inclination angle and a quality of 0.25





Mass flux [kg/m ² .s]	Time [s]			Flow pattern	
	0	0.25	0.5		
100	in				SW
	out				I
75	in				SW
	out				I

Figure C.5: Flow pattern transition at $+5^\circ$ inclination angle and a quality of 0.25





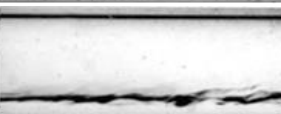













Mass flux [kg/m ² .s]		Time [s]			Flow pattern
		0	0.25	0.5	
100	in				SW
	out				SW
75	in				SW
	out				SW
50	in				S
	out				S

Figure C.6: Flow pattern transition at -5° inclination angle and a quality of 0.5


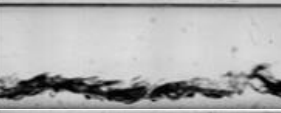













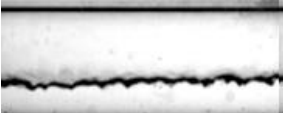


Mass flux [kg/m ² .s]		Time [s]			Flow pattern
		0	0.25	0.5	
100	in				SW
	out				SW
75	in				SW
	out				W
50	in				SW
	out				W

Figure C.7: Flow pattern transition at +5° inclination angle and a quality of 0.5

Mass flux [kg/m ² .s]		Time [s]			Flow pattern
		0	0.25	0.5	
100	in				SW
	out				SW
75	in				SW
	out				SW
50	in				S
	out				SW

Figure C.8: Flow pattern transition at -5° inclination angle and a quality of 0.75

Mass flux [kg/m ² .s]		Time [s]			Flow pattern
		0	0.25	0.5	
100	in				SW
	out				SW
75	in				SW
	out				SW
50	in				SW
	out				SW

Figure C.9: Flow pattern transition at +5° inclination angle and a quality of 0.75

C.4. Flow pattern transitions for the inclination angle of $\pm 10^\circ$





Mass flux [kg/m ² .s]		Time [s]			Flow pattern
		0	0.25	0.5	
100	in				SW
	out				SW
75	in				SW
	out				SW

Figure C.10: Flow pattern transition at -10° inclination angle and a quality of 0.25


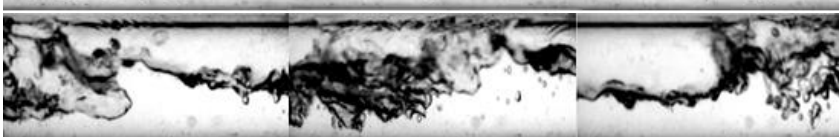


Mass flux [kg/m ² .s]		Time [s]			Flow pattern
		0	0.25	0.5	
100	in				W
	out				I
75	in				W
	out				I

Figure C.11: Flow pattern transition at $+10^\circ$ inclination angle and a quality of 0.25




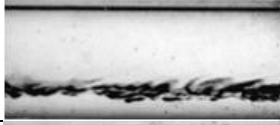
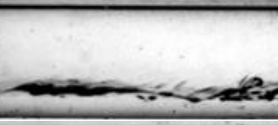

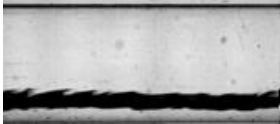
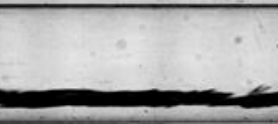
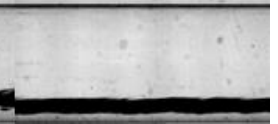








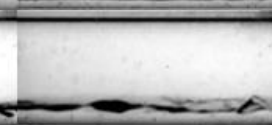
Mass flux [kg/m ² .s]		Time [s]			Flow pattern
		0	0.25	0.5	
100	in				SW
	out				SW
75	in				SW
	out				SW
50	in				S
	out				SW

Figure C.12: Flow pattern transition at -10° inclination angle and a quality of 0.5




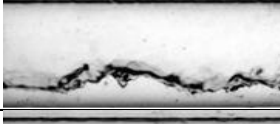
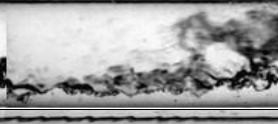





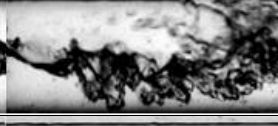







Mass flux [kg/m ² .s]		Time [s]			Flow pattern
		0	0.25	0.5	
100	in				SW
	out				W
75	in				SW
	out				W
50	in				SW
	out				I

Figure C.13: Flow pattern transition at +10° inclination angle and a quality of 0.5




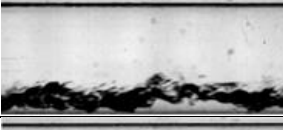




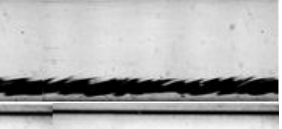
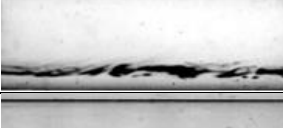
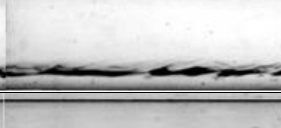
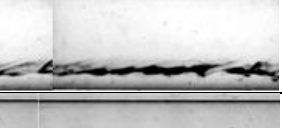






Mass flux [kg/m ² .s]		Time [s]			Flow pattern
		0	0.25	0.5	
100	in				SW
	out				SW
75	in				SW
	out				SW
50	in				S
	out				SW

Figure C.14: Flow pattern transition at -10° inclination angle and a quality of 0.75




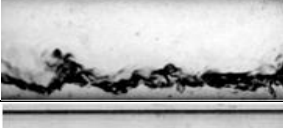
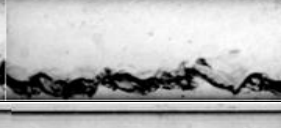




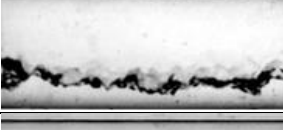
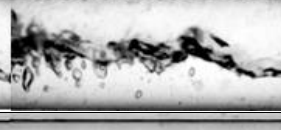

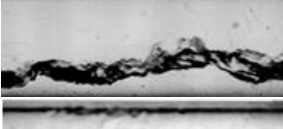

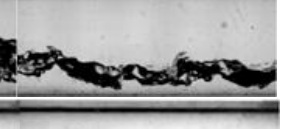



Mass flux [kg/m ² .s]		Time [s]			Flow pattern
		0	0.25	0.5	
100	in				SW
	out				SW
75	in				SW
	out				SW
50	in				SW
	out				SW

Figure C.15: Flow pattern transition at +10° inclination angle and a quality of 0.75

C.5. Flow pattern transitions for the inclination angle of $\pm 15^\circ$





Mass flux [kg/m ² .s]	Time [s]			Flow pattern	
	0	0.25	0.5		
100	in				SW
	out				SW
75	in				SW
	out				SW

Figure C.16: Flow pattern transition at -15° inclination angle and a quality of 0.25

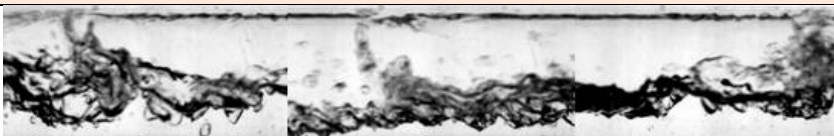

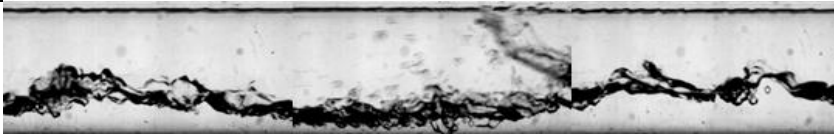

Mass flux [kg/m ² .s]	Time [s]			Flow pattern	
	0	0.25	0.5		
100	in				W
	out				I
75	in				W
	out				I

Figure C.17: Flow pattern transition at $+15^\circ$ inclination angle and a quality of 0.25



Mass flux [kg/m ² .s]		Time [s]			Flow pattern
		0	0.25	0.5	
100	in				SW
	out				SW
75	in				SW
	out				SW
50	in				S
	out				SW

Figure C.18: Flow pattern transition at -15° inclination angle and a quality of 0.5

Mass flux [kg/m ² .s]		Time [s]			Flow pattern
		0	0.25	0.5	
100	in				SW
	out				W
75	in				W
	out				W
50	in				W
	out				I

Figure C.19: Flow pattern transition at +15° inclination angle and a quality of 0.5













Mass flux [kg/m ² .s]		Time [s]			Flow pattern
		0	0.25	0.5	
100	in				SW
	out				
75	in				SW
	out				SW

Figure C.20: Flow pattern transition at -15° inclination angle and a quality of 0.75




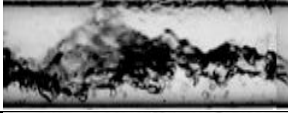
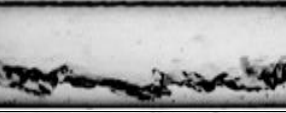






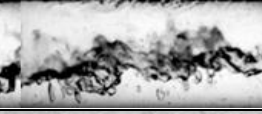

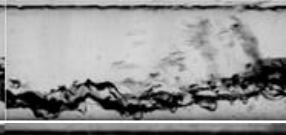




Mass flux [kg/m ² .s]		Time [s]			Flow pattern
		0	0.25	0.5	
100	in				SW
	out				
75	in				SW
	out				SW
50	in				SW
	out				W

Figure C.21: Flow pattern transition at +15° inclination angle and a quality of 0.75

C.6. Flow pattern transitions for the inclination angle of $\pm 30^\circ$









Mass flux [kg/m ² .s]	Time [s]			Flow pattern
	0	0.25	0.5	
100	in			SW
	out			
75	in			SW
	out			

Figure C.22: Flow pattern transition at -30° inclination angle and a quality of 0.25


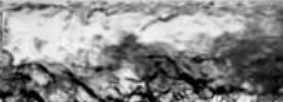

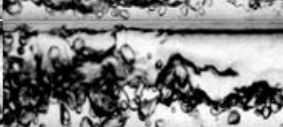
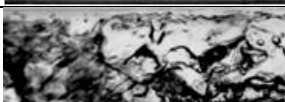
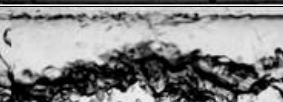
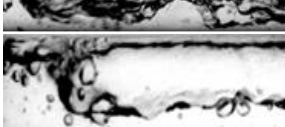
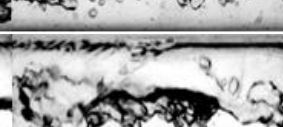
Mass flux [kg/m ² .s]	Time [s]			Flow pattern
	0	0.25	0.5	
100	in			W
	out			
75	in			W
	out			

Figure C.23: Flow pattern transition at $+30^\circ$ inclination angle and a quality of 0.25

Mass flux [kg/m ² .s]		Time [s]			Flow pattern
		0	0.25	0.5	
100	in				SW
	out				SW
75	in				SW
	out				SW
50	in				SW
	out				SW

Figure C.24: Flow pattern transition at -30° inclination angle and a quality of 0.5

Mass flux [kg/m ² .s]		Time [s]			Flow pattern
		0	0.25	0.5	
100	in				W
	out				WC
75	in				W
	out				WC
50	in				W
	out				I

Figure C.25: Flow pattern transition at +30° inclination angle and a quality of 0.5



















Mass flux [kg/m ² .s]		Time [s]			Flow pattern
		0	0.25	0.5	
100	in				SW
	out				SW
75	in				SW
	out				SW
50	in				S
	out				SW

Figure C.26: Flow pattern transition at -30° inclination angle and a quality of 0.75

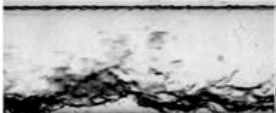








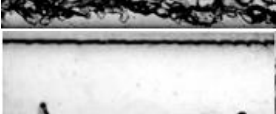

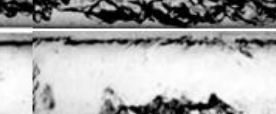


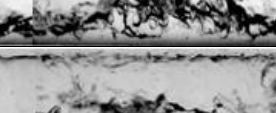
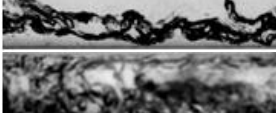

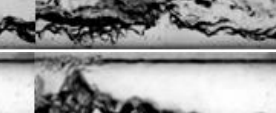
Mass flux [kg/m ² .s]		Time [s]			Flow pattern
		0	0.25	0.5	
100	in				SW
	out				W
75	in				SW
	out				SW
50	in				SW
	out				WC

Figure C.27: Flow pattern transition at +30° inclination angle and a quality of 0.75

C.7. Flow pattern transitions for the inclination angle of $\pm 45^\circ$









Mass flux [kg/m ² .s]	Time [s]			Flow pattern
	0	0.25	0.5	
100	in			SW
	out			
75	in			SW
	out			

Figure 7.28: Flow pattern transition at -45° inclination angle and a quality of 0.25





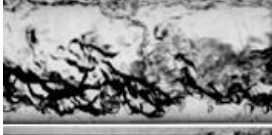
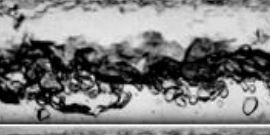

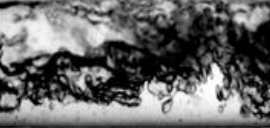
Mass flux [kg/m ² .s]	Time [s]			Flow pattern
	0	0.25	0.5	
100	in			W
	out			
75	in			W
	out			

Figure C.29: Flow pattern transition at $+45^\circ$ inclination angle and a quality of 0.25



















Mass flux [kg/m ² .s]		Time [s]			Flow pattern
		0	0.25	0.5	
100	in				SW
	out				SW
75	in				SW
	out				SW
50	in				SW
	out				SW

Figure C.30: Flow pattern transition at -45° inclination angle and a quality of 0.5

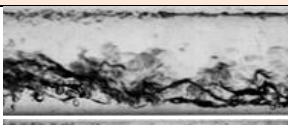
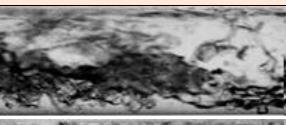
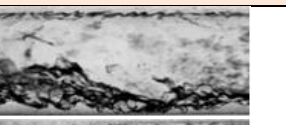

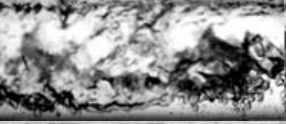
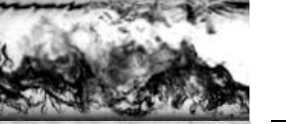

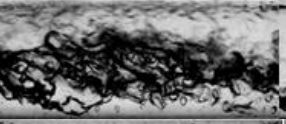

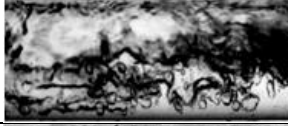
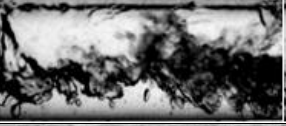
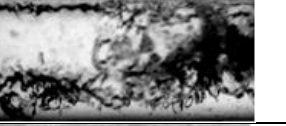
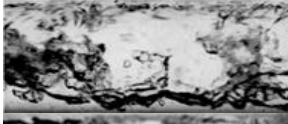
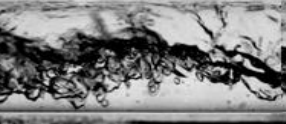




Mass flux [kg/m ² .s]		Time [s]			Flow pattern
		0	0.25	0.5	
100	in				W
	out				WC
75	in				W
	out				WC
50	in				WC
	out				I

Figure C.31: Flow pattern transition at +45° inclination angle and a quality of 0.5


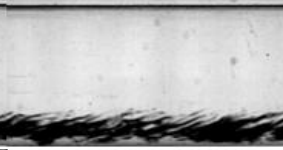


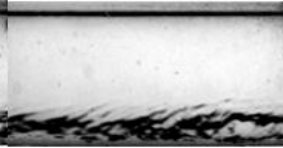


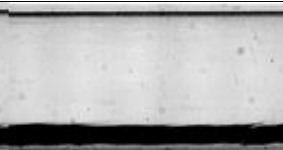
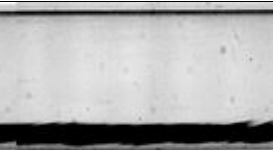



Mass flux [kg/m ² .s]		Time [s]			Flow pattern
		0	0.25	0.5	
100	in				SW
	out				
75	in				SW
	out				

Figure C.32: Flow pattern transition at -45° inclination angle and a quality of 0.75





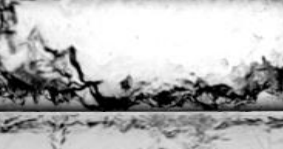

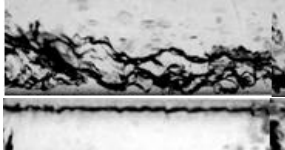
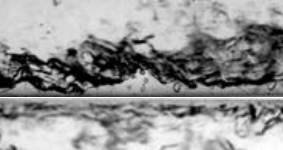
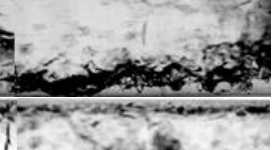
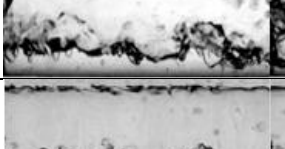
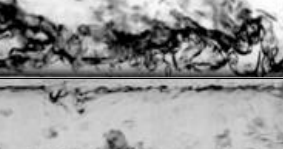
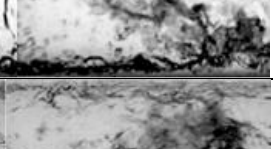
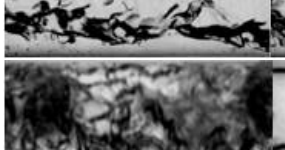
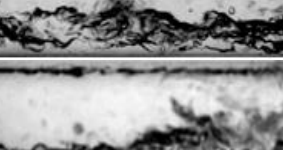
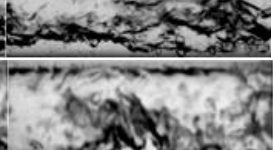


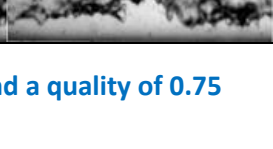
Mass flux [kg/m ² .s]		Time [s]			Flow pattern
		0	0.25	0.5	
100	in				W
	out				
75	in				W
	out				
50	in				W
	out				

Figure C.33: Flow pattern transition at +45° inclination angle and a quality of 0.75

C.8. Flow pattern transitions for the inclination angle of 60°









Mass flux [kg/m ² .s]	Time [s]			Flow pattern
	0	0.25	0.5	
100	in			SW
	out			
75	in			SW
	out			

Figure C.34: Flow pattern transition at -60° inclination angle and a quality of 0.25

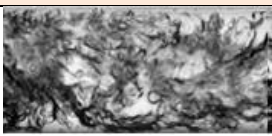
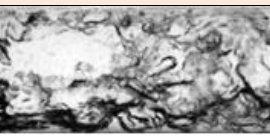
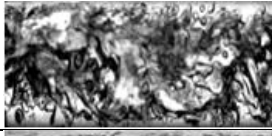
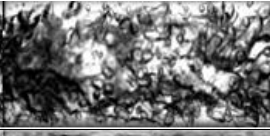
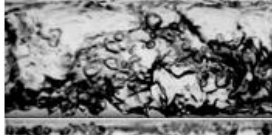
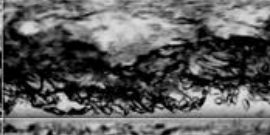
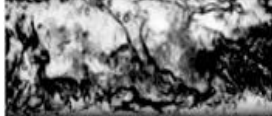

Mass flux [kg/m ² .s]	Time [s]			Flow pattern
	0	0.25	0.5	
100	in			WC
	out			
75	in			WC
	out			

Figure C.35: Flow pattern transition at +60° inclination angle and a quality of 0.25

Mass flux [kg/m ² .s]		Time [s]			Flow pattern
		0	0.25	0.5	
100	in				SW
	out				SW
75	in				SW
	out				SW
50	in				SW
	out				SW

Figure C.36: Flow pattern transition at -60° inclination angle and a quality of 0.5

Mass flux [kg/m ² .s]		Time [s]			Flow pattern
		0	0.25	0.5	
100	in				WC
	out				WC
75	in				WC
	out				WC
50	in				WC
	out				WC

Figure C.37: Flow pattern transition at +60° inclination angle and a quality of 0.5

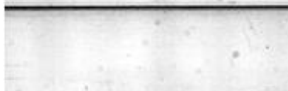

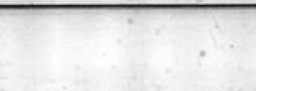



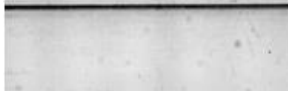
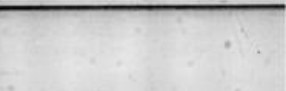
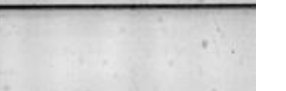
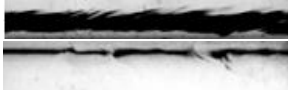
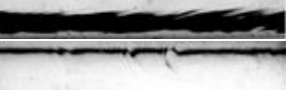
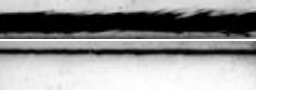
Mass flux [kg/m ² .s]		Time [s]			Flow pattern
		0	0.25	0.5	
100	in				SW
	out				
75	in				SW
	out				

Figure C.38: Flow pattern transition at -60° inclination angle and a quality of 0.75




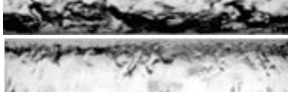
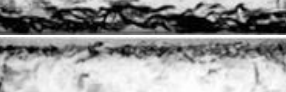
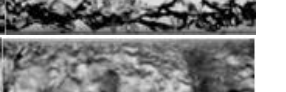

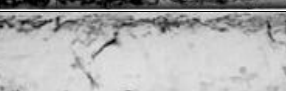

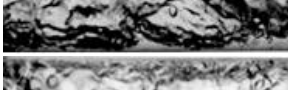
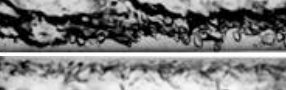
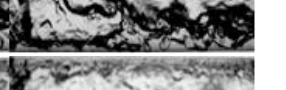



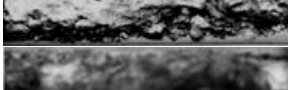
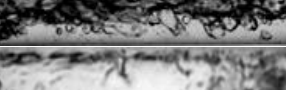
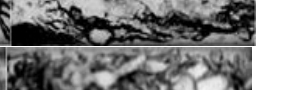
Mass flux [kg/m ² .s]		Time [s]			Flow pattern
		0	0.25	0.5	
100	in				W
	out				
75	in				WC
	out				
50	in				WC
	out				

Figure C.39: Flow pattern transition at +60° inclination angle and a quality of 0.75

C.9. Flow pattern transitions for the inclination angle of $\pm 90^\circ$


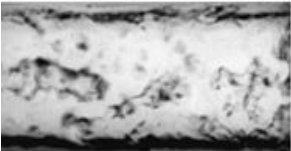

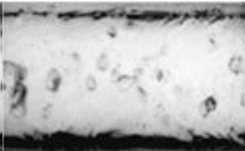
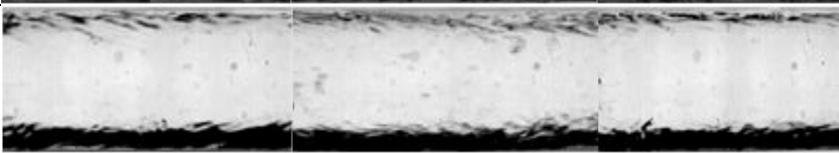



Mass flux [kg/m ² .s]	Time [s]			Flow pattern	
	0	0.25	0.5		
100	in				A
	out				A
75	in				A
	out				A

Figure C.40: Flow pattern transition at -90° inclination angle and a quality of 0.25

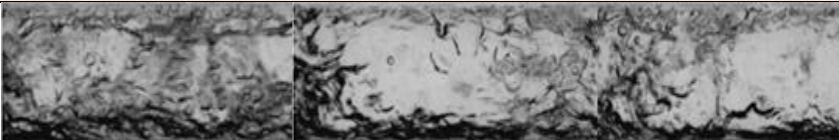

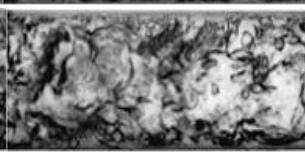
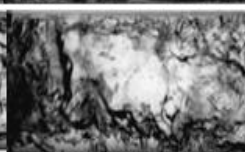
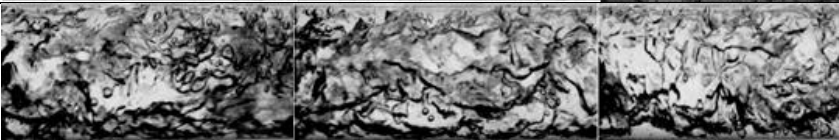
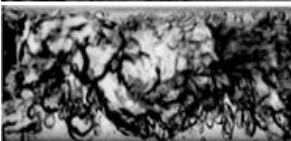
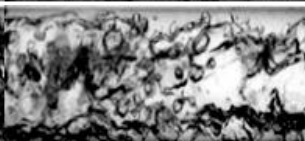
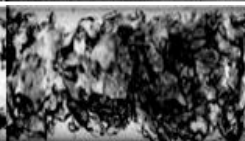
Mass flux [kg/m ² .s]	Time [s]			Flow pattern	
	0	0.25	0.5		
100	in				C
	out				C
75	in				C
	out				I

Figure C.41: Flow pattern transition at $+90^\circ$ inclination angle and a quality of 0.25

Mass flux [kg/m ² .s]		Time [s]			Flow pattern
		0	0.25	0.5	
100	in				A
	out				A
75	in				A
	out				A
50	in				A
	out				A

Figure C.42: Flow pattern transition at -90° inclination angle and a quality of 0.5

Mass flux [kg/m ² .s]		Time [s]			Flow pattern
		0	0.25	0.5	
100	in				WC
	out				C
75	in				C
	out				C
50	in				C
	out				C

Figure C.43: Flow pattern transition at +90° inclination angle and a quality of 0.5


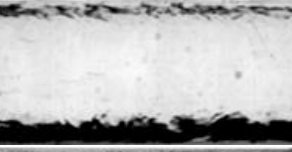


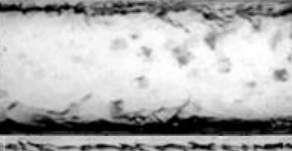
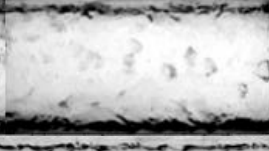






Mass flux [kg/m ² .s]		Time [s]			Flow pattern
		0	0.25	0.5	
100	in				A
	out				A
75	in				A
	out				A

Figure C.44: Flow pattern transition at -90° inclination angle and a quality of 0.75

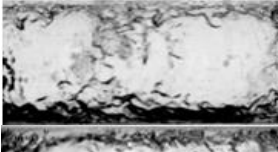
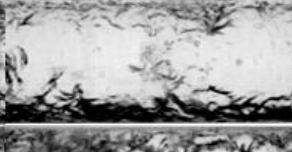
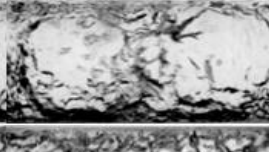
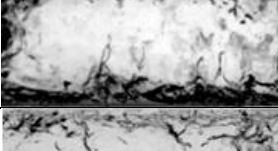
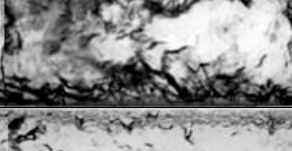
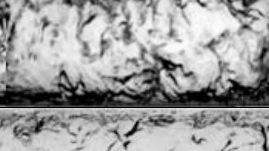
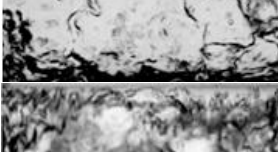
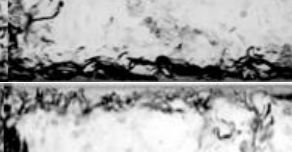
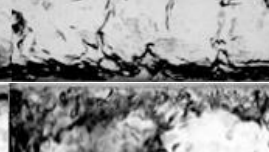
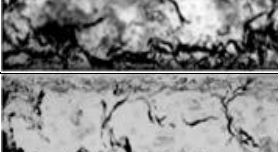
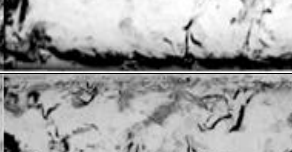
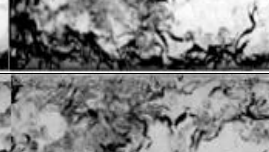
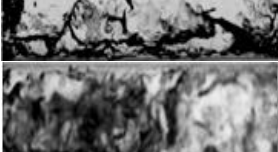
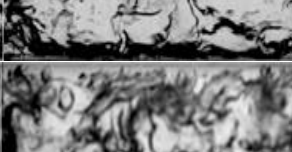
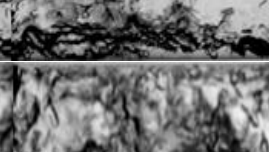


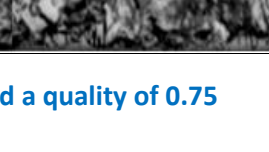
Mass flux [kg/m ² .s]		Time [s]			Flow pattern
		0	0.25	0.5	
100	in				WA
	out				WA
75	in				WA
	out				WA
50	in				C
	out				C

Figure C.45: Flow pattern transition at +90° inclination angle and a quality of 0.75

C.10. Summary

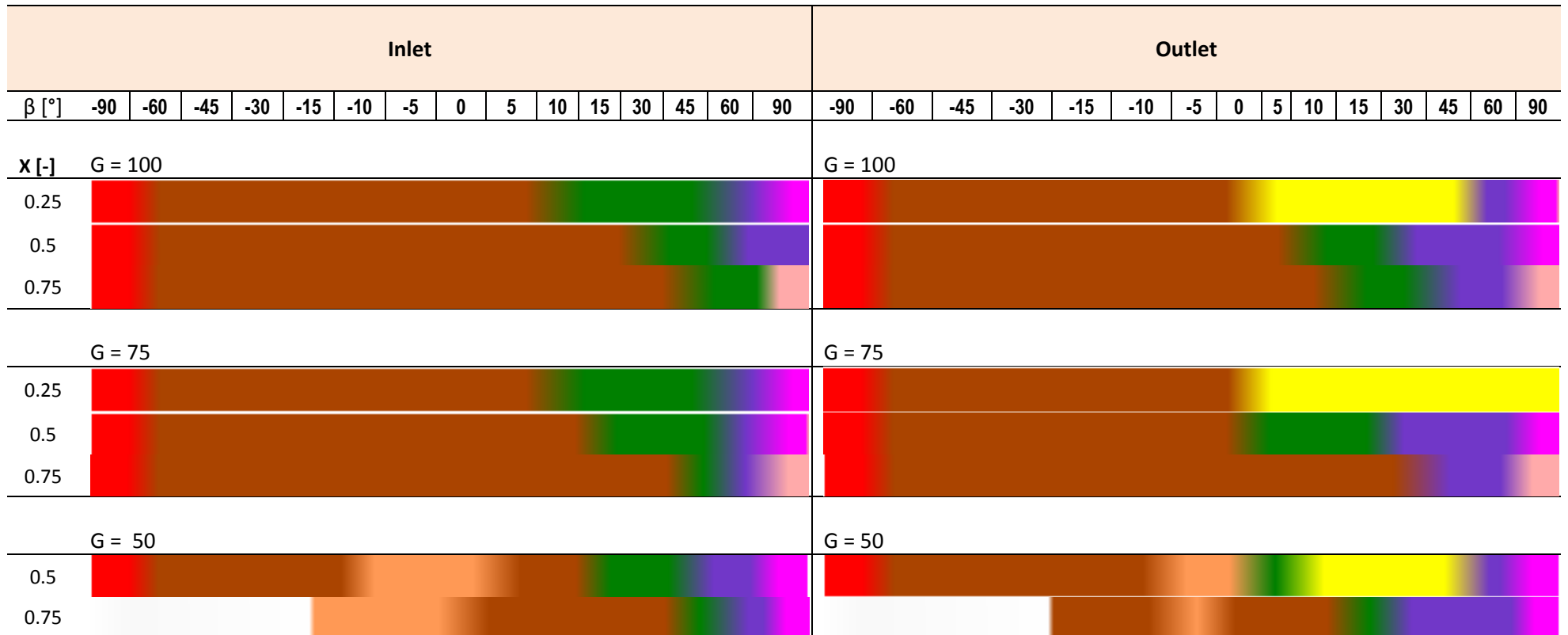
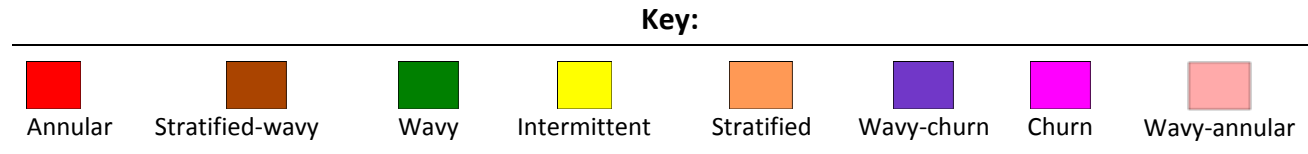


Figure C.46: Summary of flow pattern transitions



C.10.1. Comparing flow pattern transitions for negative and positive inclination angles

Figure C.46 shows the flow pattern transitions represented in colour-coding in order to simplify the analysis. For a temperature difference of 3 °C, it can be seen that the flow pattern transition on the inlet to the test condenser for the negative inclinations is from stratified-wavy to annular as the inclination angle is increased from 0° to -90° for mass fluxes of 75 kg/m².s and 100 kg/m².s. The two flow patterns are common for negative inclinations, with the annular flow pattern being confined to -90°. However, for very low qualities, at lower inclination angles from 0° to -60°, the flow transitions from stratified to stratified-wavy, and then to annular at -90°.

The effect of gravity acting against the flow of the condensing mixture and the velocities of the liquid and vapour creates an unstable interface between the vapour and the liquid, hence the variances in flow patterns as inclination angle is increased from 0° to +90°. Still on the inlet to the test section for the upward flow (positive inclination angles), it can be noted that the stratified-wavy flow pattern increases its prevalence with an increase in quality from negative to positive inclination angles. In contrast, the wavy flow pattern diminishes with an increase in quality and inclination. However, wavy-churn, churn and wavy-annular flow patterns are common from inclination angles close to +60° to +90°. From a wavy flow at inclination angles below +60°, the flow would transition to wavy-churn at 60° and then to churn at lower qualities or to wavy-annular at higher qualities from close to 0.75 and above and at mass fluxes of 75 kg/m².s to 100 kg/m².s.

Taking a look at the outlet, from the test condenser, it can be noted that the flow patterns for negative inclination angles are stratified-wavy and annular from 0° to -90°. Just like the inlet conditions, the stratified-wavy flow pattern increases in its appearance as quality increases from negative to positive inclination angles. The intermittent flow pattern, although not observed on the inlet, was most common at lower qualities of 0.25, replacing the wavy flow pattern. However, as quality increases, instead of the intermittent flow pattern, the stratified-wavy and wavy flow patterns take over, with wavy flow diminishing as quality continues to increase, making way for the wavy-churn flow pattern. The wavy-churn flow pattern appears regularly as quality increases. The stratified flow pattern was only prevalent at a lower mass flux of 50 kg/m².s decreasing in prevalence with an increase in quality.

C.10.2. Comparing test condenser inlet and outlet flow pattern transitions.

For all the negative inclination angles, the flow patterns remain constant from the inlet to the outlet. Hence, the annular flow pattern was also observed at -90° and the stratified-wavy flow pattern was observed from 0° to -60°, just like the inlet to the test condenser. The appearance of the stratified-wavy flow pattern declines with an increase in

the inclination angle from negative to positive. The wavy flow pattern transitions to the intermittent flow pattern from the inlet to the outlet at a quality of 0.25 to 0.5 for a mass flux of $50 \text{ kg/m}^2 \cdot \text{s}$. But for qualities of about 0.5 and above, the wavy flow decreases with an increase in quality. There is a general increase in the wavy-churn flow pattern from the inlet to the outlet as quality increases. Wavy-annular was not observed on the outlet from the test condenser at $+90^\circ$. Only the churn flow pattern that transitioned to the wavy-churn flow pattern at very high qualities of 0.75 was noted at $+90^\circ$.

Appendices D to H

Table of Contents

Appendix D. Flow pattern transitions for a ΔT of 5°C D-1

D.1	Introduction.....	D-1
D.2	Flow pattern transitions for the horizontal inclination 0°	D-1
D.3	Flow pattern transitions for the inclination angle of $\pm 5^\circ$	D-2
D.4	Flow pattern transitions for the inclination angle of $\pm 10^\circ$	D-5
D.5	Flow pattern transitions for the inclination angle of $\pm 15^\circ$	D-8
D.6	Flow pattern transitions for the inclination angle of $\pm 30^\circ$	D-11
D.7	Flow pattern transitions for the inclination angle of $\pm 45^\circ$	D-14
D.8	Flow pattern transitions for the inclination angle of 60°	D-17
D.9	Flow pattern transitions for the inclination angle of $\pm 90^\circ$	D-20
D.10	Summary	D-24
D.10.1	Comparing flow pattern transitions for negative and positive inclination angles	D-25

Appendix E. Flow pattern transitions for a ΔT of 8°C E-1

E.1	Introduction.....	E-1
E.2	Flow pattern transitions for the horizontal inclination 0°	E-1
E.3	Flow pattern transitions for the inclination angle of $\pm 5^\circ$	E-3
E.4	Flow pattern transitions for the inclination angle of $\pm 10^\circ$	E-5
E.5	Flow pattern transitions for the inclination angle of $\pm 15^\circ$	E-7
E.6	Flow pattern transitions for the inclination angle of $\pm 30^\circ$	E-10
E.7	Flow pattern transitions for the inclination angle of $\pm 45^\circ$	E-12
E.8	Flow pattern transitions for the inclination angle of 60°	E-15
E.9	Flow pattern transitions for the inclination angle of $\pm 90^\circ$	E-17
E.10	Summary	E-20
E.10.1	Comparing flow pattern transitions for negative and positive inclination angles	E-21

Appendix F. Flow pattern transitions for a ΔT of 10°C F-1

F.1	Introduction.....	F-1
F.2	Flow pattern transitions for the horizontal inclination 0°	F-1
F.3	Flow pattern transitions for the inclination angle of $\pm 5^\circ$	F-1
F.4	Flow pattern transitions for the inclination angle of $\pm 10^\circ$	F-2
F.5	Flow pattern transitions for the inclination angle of $\pm 15^\circ$	F-3
F.6	Flow pattern transitions for the inclination angle of $\pm 30^\circ$	F-3
F.7	Flow pattern transitions for the inclination angle of $\pm 45^\circ$	F-4
F.8	Flow pattern transitions for the inclination angle of 60°	F-5
F.9	Flow pattern transitions for the inclination angle of $\pm 90^\circ$	F-5
F.10	Summary	F-7
F.10.1	Comparing flow pattern transitions for negative and positive inclination angles ..	F-8

Appendix G. Flow pattern transitions for a ΔT of 1°C G-1

G.1	Introduction.....	G-1
G.2	Flow pattern transitions for the horizontal inclination 0°	G-1
G.3	Flow pattern transitions for the inclination angle of $\pm 5^\circ$	G-2
G.4	Flow pattern transitions for the inclination angle of $\pm 10^\circ$	G-4
G.5	Flow pattern transitions for the inclination angle of $\pm 15^\circ$	G-6
G.6	Flow pattern transitions for the inclination angle of $\pm 30^\circ$	G-8
G.7	Flow pattern transitions for the inclination angle of $\pm 45^\circ$	G-10
G.8	Flow pattern transitions for the inclination angle of 60°	G-12
G.9	Flow pattern transitions for the inclination angle of $\pm 90^\circ$	G-14
G.10	Summary	G-17
G.10.1	Comparing flow pattern transitions for negative and positive inclination angles	G-18

Appendix H. Summary of all the appendices: Appendix A to

Appendix G H-1

H.1	Conclusion	H-1
H.1.1	Annular flow pattern	H-1
H.1.2	Wavy-annular flow pattern	H-1
H.1.3	Stratified flow pattern	H-1
H.1.4	Stratified-wavy flow pattern	H-1
H.1.5	Intermittent flow pattern	H-2
H.1.6	Wavy flow pattern	H-2
H.1.7	Churn flow pattern	H-2
H.1.8	Wavy-churn flow pattern	H-2
H.2	Summary- Mass flux of $100 \text{ kg/m}^2 \cdot \text{s}$	H-3
H.3	Summary- Mass flux of $75 \text{ kg/m}^2 \cdot \text{s}$	H-4
H.4	Summary- Mass flux of $50 \text{ kg/m}^2 \cdot \text{s}$	H-5
H.5	Summary- Mass flux of $25 \text{ kg/m}^2 \cdot \text{s}$	H-6

List of figures

Figure D.1:	Flow pattern transition at 0° inclination angle and a quality of 0.25	D-1
Figure D.2:	Flow pattern transition at 0° inclination angle and a quality of 0.5	D-1
Figure D.3:	Flow pattern transition at 0° inclination angle and a quality of 0.75	D-2
Figure D.4:	Flow pattern transition at -5° inclination angle and a quality of 0.25	D-2
Figure D.5:	Flow pattern transition at +5° inclination angle and a quality of 0.25	D-3
Figure D.6:	Flow pattern transition at -5° inclination angle and a quality of 0.5	D-3
Figure D.7:	Flow pattern transition at +5° inclination angle and a quality of 0.5	D-4
Figure D.8:	Flow pattern transition at -5° inclination angle and a quality of 0.75	D-4
Figure D.9:	Flow pattern transition at +5° inclination angle and a quality of 0.75	D-5
Figure D.10:	Flow pattern transition at -10° inclination angle and a quality of 0.25	D-5
Figure D.11:	Flow pattern transition at +10° inclination angle and a quality of 0.25	D-6
Figure D.12:	Flow pattern transition at -10° inclination angle and a quality of 0.5	D-6
Figure D.13:	Flow pattern transition at +10° inclination angle and a quality of 0.5	D-7
Figure D.14:	Flow pattern transition at -10° inclination angle and a quality of 0.75	D-7
Figure D.15:	Flow pattern transition at +10° inclination angle and a quality of 0.75	D-8
Figure D.16:	Flow pattern transition at -15° inclination angle and a quality of 0.25	D-8
Figure D.17:	Flow pattern transition at +15° inclination angle and a quality of 0.25	D-9
Figure D.18:	Flow pattern transition at -15° inclination angle and a quality of 0.5	D-9
Figure D.19:	Flow pattern transition at +15° inclination angle and a quality of 0.5	D-10
Figure D.20:	Flow pattern transition at -15° inclination angle and a quality of 0.75	D-10
Figure D.21:	Flow pattern transition at +15° inclination angle and a quality of 0.75	D-11
Figure D.22:	Flow pattern transition at -30° inclination angle and a quality of 0.25	D-11
Figure D.23:	Flow pattern transition at +30° inclination angle and a quality of 0.25	D-12
Figure D.24:	Flow pattern transition at -30° inclination angle and a quality of 0.5	D-12
Figure D.25:	Flow pattern transition at +30° inclination angle and a quality of 0.5	D-13
Figure D.26:	Flow pattern transition at -30° inclination angle and a quality of 0.75	D-13
Figure D.27:	Flow pattern transition at +30° inclination angle and a quality of 0.75	D-14
Figure D.28:	Flow pattern transition at -45° inclination angle and a quality of 0.25	D-14
Figure D.29:	Flow pattern transition at +45° inclination angle and a quality of 0.25	D-15
Figure D.30:	Flow pattern transition at -45° inclination angle and a quality of 0.5	D-15
Figure D.31:	Flow pattern transition at +45° inclination angle and a quality of 0.5	D-16
Figure D.32:	Flow pattern transition at -45° inclination angle and a quality of 0.75	D-16
Figure D.33:	Flow pattern transition at +45° inclination angle and a quality of 0.75	D-17
Figure D.34:	Flow pattern transition at -60° inclination angle and a quality of 0.25	D-17
Figure D.35:	Flow pattern transition at +60° inclination angle and a quality of 0.25	D-18
Figure D.36:	Flow pattern transition at -60° inclination angle and a quality of 0.5	D-18
Figure D.37:	Flow pattern transition at +60° inclination angle and a quality of 0.5	D-19
Figure D.38:	Flow pattern transition at -60° inclination angle and a quality of 0.75	D-19
Figure D.39:	Flow pattern transition at +60° inclination angle and a quality of 0.75	D-20

Figure D.40:	Flow pattern transition at -90° inclination angle and a quality of 0.25	D-20
Figure D.41:	Flow pattern transition at $+90^\circ$ inclination angle and a quality of 0.25	D-21
Figure D.42:	Flow pattern transition at -90° inclination angle and a quality of 0.5	D-21
Figure D.43:	Flow pattern transition at $+90^\circ$ inclination angle and a quality of 0.5	D-22
Figure D.44:	Flow pattern transition at -90° inclination angle and a quality of 0.75	D-22
Figure D.45:	Flow pattern transition at $+90^\circ$ inclination angle and a quality of 0.75	D-23
Figure D.46:	Summary of flow pattern transitions	D-24
Figure E.1:	Flow pattern transition at 0° inclination angle and a quality of 0.35	E-1
Figure E.2:	Flow pattern transition at 0° inclination angle and a quality of 0.5	E-2
Figure E.3:	Flow pattern transition at 0° inclination angle and a quality of 0.75	E-2
Figure E.4:	Flow pattern transition at -5° inclination angle and a quality of 0.35	E-3
Figure E.5:	Flow pattern transition at $+5^\circ$ inclination angle and a quality of 0.35	E-3
Figure E.6:	Flow pattern transition at -5° inclination angle and a quality of 0.5	E-4
Figure E.7:	Flow pattern transition at $+5^\circ$ inclination angle and a quality of 0.5	E-4
Figure E.8:	Flow pattern transition at -5° inclination angle and a quality of 0.75	E-4
Figure E.9:	Flow pattern transition at $+5^\circ$ inclination angle and a quality of 0.75	E-5
Figure E.10:	Flow pattern transition at -10° inclination angle and a quality of 0.35	E-5
Figure E.11:	Flow pattern transition at $+10^\circ$ inclination angle and a quality of 0.35	E-5
Figure E.12:	Flow pattern transition at -10° inclination angle and a quality of 0.5	E-6
Figure E.13:	Flow pattern transition at $+10^\circ$ inclination angle and a quality of 0.5	E-6
Figure E.14:	Flow pattern transition at -10° inclination angle and a quality of 0.75	E-7
Figure E.15:	Flow pattern transition at $+10^\circ$ inclination angle and a quality of 0.75	E-7
Figure E.16:	Flow pattern transition at -15° inclination angle and a quality of 0.35	E-7
Figure E.17:	Flow pattern transition at $+15^\circ$ inclination angle and a quality of 0.35	E-8
Figure E.18:	Flow pattern transition at -15° inclination angle and a quality of 0.5	E-8
Figure E.19:	Flow pattern transition at $+15^\circ$ inclination angle and a quality of 0.5	E-9
Figure E.20:	Flow pattern transition at -15° inclination angle and a quality of 0.75	E-9
Figure E.21:	Flow pattern transition at $+15^\circ$ inclination angle and a quality of 0.75	E-9
Figure E.22:	Flow pattern transition at -30° inclination angle and a quality of 0.35	E-10
Figure E.23:	Flow pattern transition at $+30^\circ$ inclination angle and a quality of 0.35	E-10
Figure E.24:	Flow pattern transition at -30° inclination angle and a quality of 0.5	E-11
Figure E.25:	Flow pattern transition at $+30^\circ$ inclination angle and a quality of 0.5	E-11
Figure E.26:	Flow pattern transition at -30° inclination angle and a quality of 0.75	E-12
Figure E.27:	Flow pattern transition at $+30^\circ$ inclination angle and a quality of 0.75	E-12
Figure E.28:	Flow pattern transition at -45° inclination angle and a quality of 0.35	E-12
Figure E.29:	Flow pattern transition at $+45^\circ$ inclination angle and a quality of 0.35	E-13
Figure E.30:	Flow pattern transition at -45° inclination angle and a quality of 0.5	E-13
Figure E.31:	Flow pattern transition at $+45^\circ$ inclination angle and a quality of 0.5	E-14
Figure E.32:	Flow pattern transition at -45° inclination angle and a quality of 0.75	E-14
Figure E.33:	Flow pattern transition at $+45^\circ$ inclination angle and a quality of 0.75	E-14
Figure E.34:	Flow pattern transition at -60° inclination angle and a quality of 0.35	E-15

Figure E.35:	Flow pattern transition at +60° inclination angle and a quality of 0.35	E-15
Figure E.36:	Flow pattern transition at -60° inclination angle and a quality of 0.5	E-16
Figure E.37:	Flow pattern transition at +60° inclination angle and a quality of 0.5	E-16
Figure E.38:	Flow pattern transition at -60° inclination angle and quality of 0.75	E-17
Figure E.39:	Flow pattern transition at +60° inclination angle and a quality of 0.75	E-17
Figure E.40:	Flow pattern transition at -90° inclination angle and a quality of 0.35	E-17
Figure E.41:	Flow pattern transition at +90° inclination angle and a quality of 0.35	E-18
Figure E.42:	Flow pattern transition at -90° inclination angle and a quality of 0.5	E-18
Figure E.43:	Flow pattern transition at +90° inclination angle and a quality of 0.5	E-19
Figure E.44:	Flow pattern transition at -90° inclination angle and a quality of 0.75	E-19
Figure E.45:	Flow pattern transition at +90° inclination angle and a quality of 0.75	E-19
Figure E.46:	Summary of flow pattern transitions	E-20
Figure F.1:	Flow pattern transition at 0° inclination angle and a quality of 0.5	F-1
Figure F.2:	Flow pattern transition at -5° inclination angle and a quality of 0.5	F-1
Figure F.3:	Flow pattern transition at +5° inclination angle and a quality of 0.5	F-2
Figure F.4:	Flow pattern transition at -10° inclination angle and a quality of 0.5	F-2
Figure F.5:	Flow pattern transition at +10° inclination angle and a quality of 0.5	F-2
Figure F.6:	Flow pattern transition at -15° inclination angle and a quality of 0.5	F-3
Figure F.7:	Flow pattern transition at +15° inclination angle and a quality of 0.5	F-3
Figure F.8:	Flow pattern transition at -30° inclination angle and a quality of 0.5	F-3
Figure F.9:	Flow pattern transition at +30° inclination angle and a quality of 0.5	F-4
Figure F.10:	Flow pattern transition at -45° inclination angle and a quality of 0.5	F-4
Figure F.11:	Flow pattern transition at +45° inclination angle and a quality of 0.5	F-4
Figure F.12:	Flow pattern transition at -60° inclination angle and a quality of 0.5	F-5
Figure F.13:	Flow pattern transition at +60° inclination angle and a quality of 0.5	F-5
Figure F.14:	Flow pattern transition at -90° inclination angle and a quality of 0.5	F-5
Figure F.15:	Flow pattern transition at +90° inclination angle and a quality of 0.5	F-6
Figure F.16:	Summary of flow pattern transitions	F-7
Figure G. 1:	Flow pattern transition at 0° inclination angle and a quality of 0.25	G-1
Figure G.2:	Flow pattern transition at 0° inclination angle and a quality of 0.5	G-1
Figure G.3:	Flow pattern transition at 0° inclination angle and a quality of 0.75	G-2
Figure G.4:	Flow pattern transition at -5° inclination angle and a quality of 0.25	G-2
Figure G.5:	Flow pattern transition at +5° inclination angle and a quality of 0.25	G-2
Figure G.6:	Flow pattern transition at -5° inclination angle and a quality of 0.5	G-3
Figure G.7:	Flow pattern transition at +5° inclination angle and a quality of 0.5	G-3
Figure G.8:	Flow pattern transition at -5° inclination angle and a quality of 0.75	G-3
Figure G.9:	Flow pattern transition at +5° inclination angle and a quality of 0.75	G-4
Figure G.10:	Flow pattern transition at -10° inclination angle and a quality of 0.25	G-4
Figure G.11:	Flow pattern transition at +10° inclination angle and a quality of 0.25	G-4
Figure G.12:	Flow pattern transition at -10° inclination angle and a quality of 0.5	G-5
Figure G.13:	Flow pattern transition at +10° inclination angle and a quality of 0.5	G-5

Figure G.14:	Flow pattern transition at -10° inclination angle and a quality of 0.75	G-5
Figure G.15:	Flow pattern transition at $+10^\circ$ inclination angle and a quality of 0.75	G-6
Figure G.16:	Flow pattern transition at -15° inclination angle and a quality of 0.25	G-6
Figure G.17:	Flow pattern transition at $+15^\circ$ inclination angle and a quality of 0.25	G-6
Figure G.18:	Flow pattern transition at -15° inclination angle and a quality of 0.5	G-7
Figure G.19:	Flow pattern transition at $+15^\circ$ inclination angle and a quality of 0.5	G-7
Figure G.20:	Flow pattern transition at -15° inclination angle and a quality of 0.75	G-7
Figure G.21:	Flow pattern transition at $+15^\circ$ inclination angle and a quality of 0.75	G-8
Figure G.22:	Flow pattern transition at -30° inclination angle and a quality of 0.25	G-8
Figure G.23:	Flow pattern transition at $+30^\circ$ inclination angle and a quality of 0.25	G-8
Figure G.24:	Flow pattern transition at -30° inclination angle and a quality of 0.5	G-9
Figure G.25:	Flow pattern transition at $+30^\circ$ inclination angle and a quality of 0.5	G-9
Figure G.26:	Flow pattern transition at -30° inclination angle and a quality of 0.75	G-9
Figure G.27:	Flow pattern transition at $+30^\circ$ inclination angle and a quality of 0.75	G-10
Figure G.28:	Flow pattern transition at -45° inclination angle and a quality of 0.25	G-10
Figure G.29:	Flow pattern transition at $+45^\circ$ inclination angle and a quality of 0.25	G-10
Figure G.30:	Flow pattern transition at -45° inclination angle and a quality of 0.5	G-11
Figure G.31:	Flow pattern transition at $+45^\circ$ inclination angle and a quality of 0.5	G-11
Figure G.32:	Flow pattern transition at -45° inclination angle and a quality of 0.75	G-11
Figure G.33:	Flow pattern transition at $+45^\circ$ inclination angle and a quality of 0.75	G-12
Figure G.34:	Flow pattern transition at -60° inclination angle and a quality of 0.25	G-12
Figure G.35:	Flow pattern transition at $+60^\circ$ inclination angle and a quality of 0.25	G-12
Figure G.36:	Flow pattern transition at -60° inclination angle and a quality of 0.5	G-13
Figure G.37:	Flow pattern transition at $+60^\circ$ inclination angle and a quality of 0.5	G-13
Figure G.38:	Flow pattern transition at -60° inclination angle and a quality of 0.75	G-13
Figure G.39:	Flow pattern transition at $+60^\circ$ inclination angle and a quality of 0.75	G-14
Figure G.40:	Flow pattern transition at -90° inclination angle and a quality of 0.25	G-14
Figure G.41:	Flow pattern transition at $+90^\circ$ inclination angle and a quality of 0.25	G-15
Figure G.42:	Flow pattern transition at -90° inclination angle and a quality of 0.5	G-15
Figure G.43:	Flow pattern transition at $+90^\circ$ inclination angle and a quality of 0.5	G-15
Figure G.44:	Flow pattern transition at -90° inclination angle and a quality of 0.75	G-16
Figure G.45:	Flow pattern transition at $+90^\circ$ inclination angle and a quality of 0.62	G-16
Figure G.46:	Summary of flow pattern transitions	G-17
Figure H.1:	Summary of flow patterns for a mass flux of $100 \text{ kg/m}^2 \cdot \text{s}$	H-3
Figure H.2:	Summary of flow patterns for a mass flux of $75 \text{ kg/m}^2 \cdot \text{s}$	H-4
Figure H.3:	Summary of flow patterns for a mass flux of $50 \text{ kg/m}^2 \cdot \text{s}$	H-5
Figure H.4:	summary of flow patterns for a mass flux of $25 \text{ kg/m}^2 \cdot \text{s}$	H-6

Appendix D. Flow pattern transitions for a ΔT of 5°C

D.1 Introduction

Appendix D presents observed flow patterns for mass fluxes of 75 and 100 $\text{kg/m}^2\cdot\text{s}$ at a temperature difference of 5°C . In the same way as Appendix C, a brief summary will be given at the end of this section. The flow patterns were captured for qualities of 0.25, 0.5, 0.75 and 0.62.

D.2 Flow pattern transitions for the horizontal inclination 0°

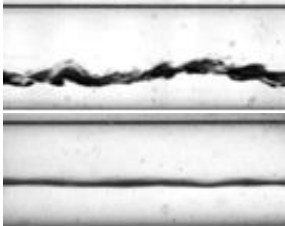
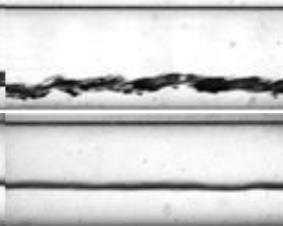
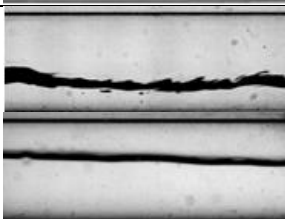
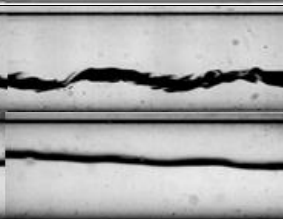
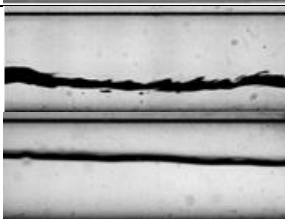
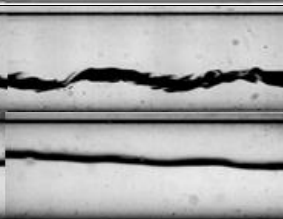
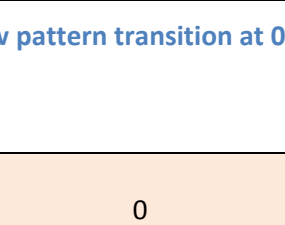
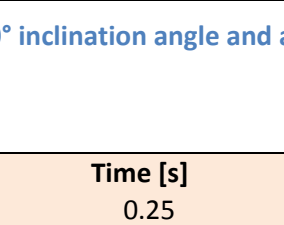
Mass flux [$\text{kg/m}^2\cdot\text{s}$]	Time [s]			Flow pattern
	0	0.25	0.5	
100	in			SW
	out			SW
75	in			SW
	out			S

Figure D.1: Flow pattern transition at 0° inclination angle and a quality of 0.25

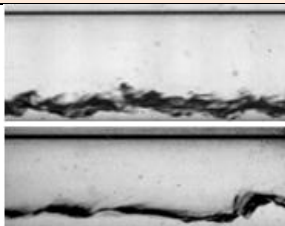
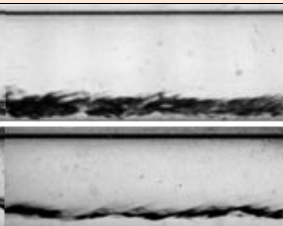
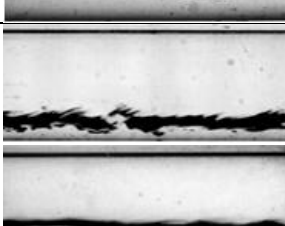


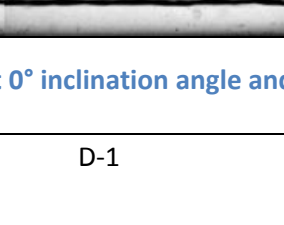


Mass flux [$\text{kg/m}^2\cdot\text{s}$]	Time [s]			Flow pattern
	0	0.25	0.5	
100	in			SW
	out			SW
75	in			SW
	out			SW

Figure D.2: Flow pattern transition at 0° inclination angle and a quality of 0.5




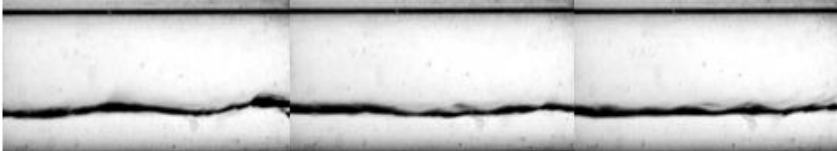
Mass flux [kg/m ² .s]	Time [s]			Flow pattern	
	0	0.25	0.5		
100	in				SW
	out				
75 x=0.62	in				SW
	out				

Figure D.3: Flow pattern transition at 0° inclination angle and a quality of 0.75

D.3 Flow pattern transitions for the inclination angle of ±5°

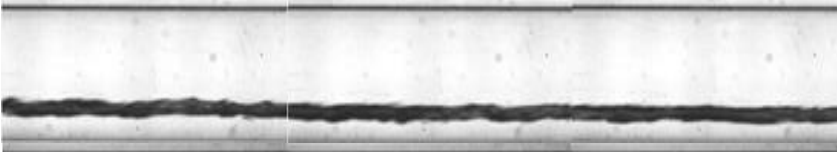
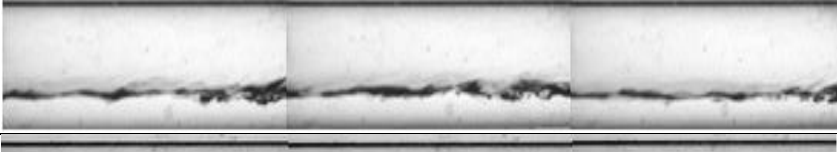
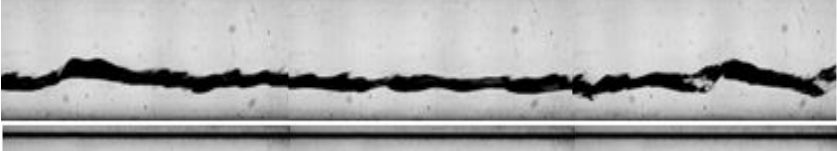

Mass flux [kg/m ² .s]	Time [s]			Flow pattern	
	0	0.25	0.5		
100	in				SW
	out				
75	in				SW
	out				

Figure D.4: Flow pattern transition at -5° inclination angle and a quality of 0.25

Mass flux [kg/m ² .s]		Time [s]			Flow pattern
		0	0.25	0.5	
100	in				SW
	out				
75	in				SW
	out				

Figure D.5: Flow pattern transition at +5° inclination angle and a quality of 0.25

Mass flux [kg/m ² .s]		Time [s]			Flow pattern
		0	0.25	0.5	
100	in				SW
	out				
75	in				SW
	out				

Figure D.6: Flow pattern transition at -5° inclination angle and a quality of 0.5

Mass flux [kg/m ² .s]	Time [s]			Flow pattern	
	0	0.25	0.5		
100	in				SW
	out				SW
75	in				SW
	out				W

Figure D.7: Flow pattern transition at +5° inclination angle and a quality of 0.5

Mass flux [kg/m ² .s]	Time [s]			Flow pattern	
	0	0.25	0.5		
100	in				SW
	out				SW
75 x=0.62	in				SW
	out				SW

Figure D.8: Flow pattern transition at -5° inclination angle and a quality of 0.75




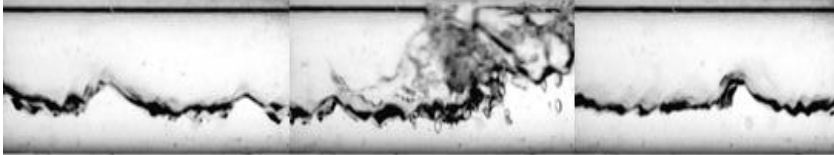



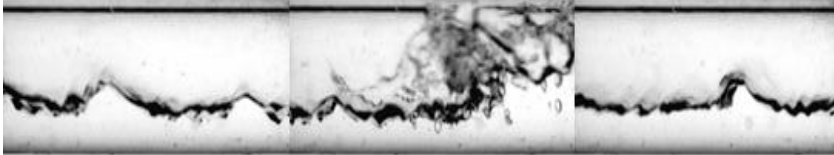



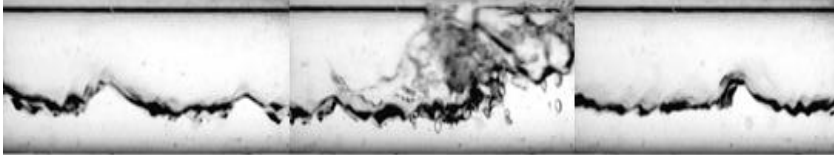
Mass flux [kg/m ² .s]	Time [s]			Flow pattern	
	0	0.25	0.5		
100	in				SW
	out				
75 x = 0.62	in				SW
	out				
100	in				SW
	out				
75 x = 0.62	in				W
	out				
100	in				SW
	out				
75 x = 0.62	in				W
	out				

Figure D.9: Flow pattern transition at +5° inclination angle and a quality of 0.75

D.4 Flow pattern transitions for the inclination angle of ±10°













Mass flux [kg/m ² .s]	Time [s]			Flow pattern	
	0	0.25	0.5		
100	in				SW
	out				
75	in				SW
	out				
100	in				SW
	out				
75	in				SW
	out				
100	in				SW
	out				
75	in				SW
	out				

Figure D.10: Flow pattern transition at -10° inclination angle and a quality of 0.25






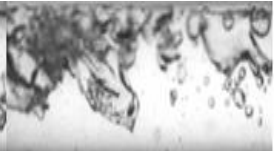





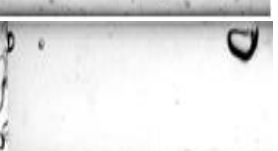
Mass flux [kg/m ² .s]	Time [s]			Flow pattern	
	0	0.25	0.5		
100	in				W
	out				
75	in				W
	out				

Figure D.11: Flow pattern transition at +10° inclination angle and a quality of 0.25


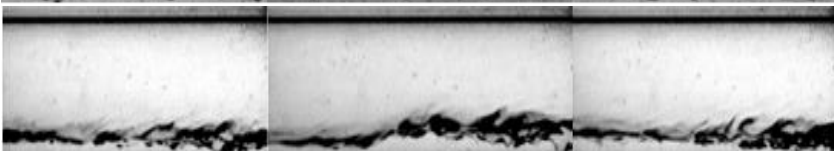


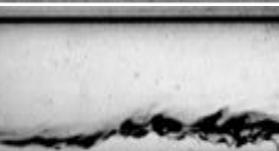



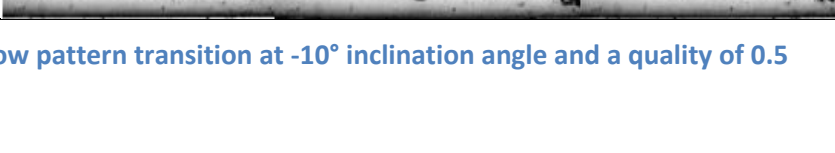


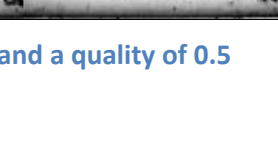
Mass flux [kg/m ² .s]	Time [s]			Flow pattern	
	0	0.25	0.5		
100	in				SW
	out				
75	in				SW
	out				

Figure D.12: Flow pattern transition at -10° inclination angle and a quality of 0.5



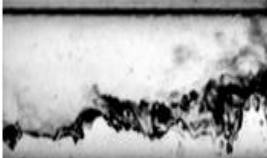



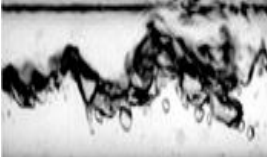

Mass flux [kg/m ² .s]	Time [s]			Flow pattern
	0	0.25	0.5	
100	in			SW
	out			
75	in			SW
	out			

Figure D.13: Flow pattern transition at +10° inclination angle and a quality of 0.5




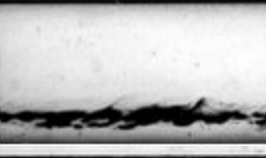




Mass flux [kg/m ² .s]	Time [s]			Flow pattern
	0	0.25	0.5	
100	in			SW
	out			
75 x=0.62	in			SW
	out			

Figure D.14: Flow pattern transition at -10° inclination angle and a quality of 0.75

Mass flux [kg/m ² .s]	Time [s]			Flow pattern	
	0	0.25	0.5		
100	in				SW
	out				
75 x = 0.62	in				SW
	out				
100	in				SW
	out				
75 x = 0.62	in				W
	out				
100	in				SW
	out				
75 x = 0.62	in				W
	out				

Figure D.15: Flow pattern transition at +10° inclination angle and a quality of 0.75

D.5 Flow pattern transitions for the inclination angle of ±15°

Mass flux [kg/m ² .s]	Time [s]			Flow pattern	
	0	0.25	0.5		
100	in				SW
	out				
75	in				SW
	out				
100	in				SW
	out				
75	in				SW
	out				
100	in				SW
	out				
75	in				SW
	out				

Figure D.16: Flow pattern transition at -15° inclination angle and a quality of 0.25

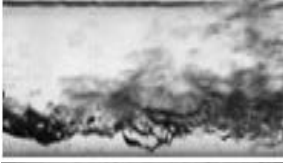

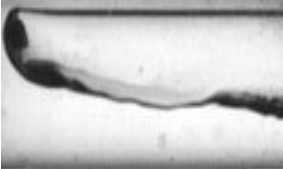




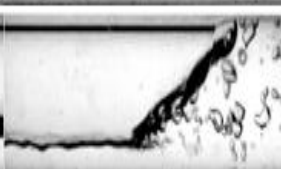
Mass flux [kg/m ² .s]	Time [s]			Flow pattern
	0	0.25	0.5	
100	in			W
	out			
75	in			W
	out			

Figure D.17: Flow pattern transition at +15° inclination angle and a quality of 0.25





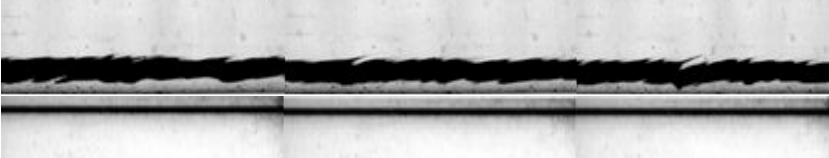

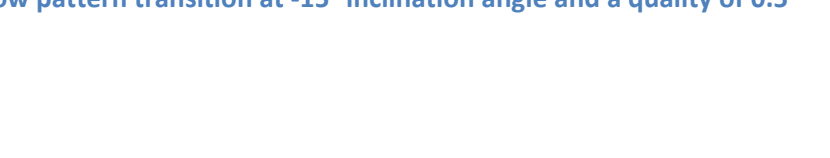
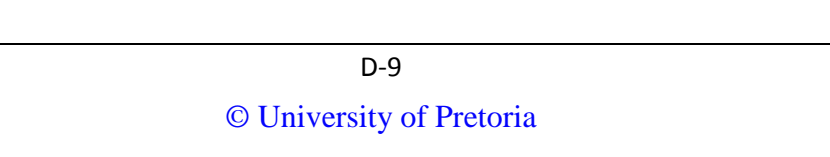
Mass flux [kg/m ² .s]	Time [s]			Flow pattern
	0	0.25	0.5	
100	in			SW
	out			
75	in			SW
	out			

Figure D.18: Flow pattern transition at -15° inclination angle and a quality of 0.5



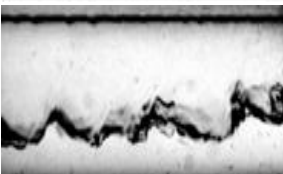



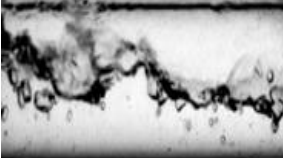
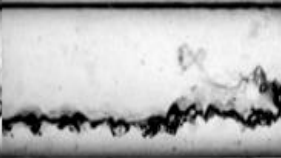
Mass flux [kg/m ² .s]	Time [s]			Flow pattern
	0	0.25	0.5	
100	in			SW
	out			
75	in			SW
	out			W

Figure D.19: Flow pattern transition at +15° inclination angle and a quality of 0.5









Mass flux [kg/m ² .s]	Time [s]			Flow pattern
	0	0.25	0.5	
100	in			SW
	out			SW
75 x = 0.62	in			SW
	out			SW

Figure D.20: Flow pattern transition at -15° inclination angle and a quality of 0.75

Mass flux [kg/m ² .s]	Time [s]			Flow pattern
	0	0.25	0.5	
100	in			SW
	out			
75 x = 0.62	in			SW
	out			
				W

Figure D.21: Flow pattern transition at +15° inclination angle and a quality of 0.75

D.6 Flow pattern transitions for the inclination angle of ±30°

Mass flux [kg/m ² .s]	Time [s]			Flow pattern
	0	0.25	0.5	
100	in			SW
	out			
75	in			SW
	out			
				SW

Figure D.22: Flow pattern transition at -30° inclination angle and a quality of 0.25

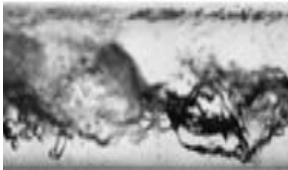
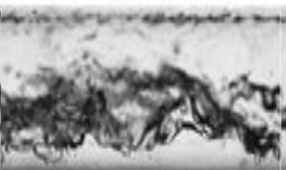
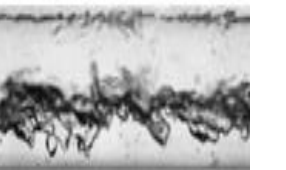

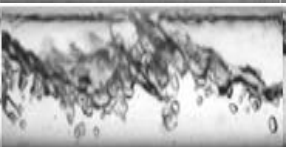

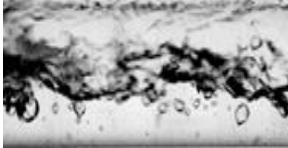



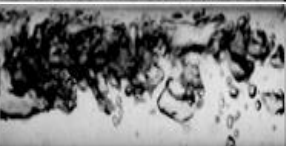

Mass flux [kg/m ² .s]	Time [s]			Flow pattern	
	0	0.25	0.5		
100	in				W
	out				
75	in				W
	out				

Figure D.23: Flow pattern transition at +30° inclination angle and a quality of 0.25













Mass flux [kg/m ² .s]	Time [s]			Flow pattern	
	0	0.25	0.5		
100	in				SW
	out				
75	in				SW
	out				

Figure D.24: Flow pattern transition at -30° inclination angle and a quality of 0.5

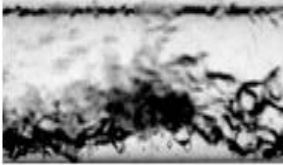





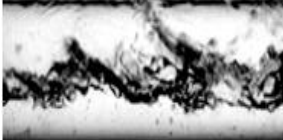

Mass flux [kg/m ² .s]	Time [s]			Flow pattern
	0	0.25	0.5	
100	in			W
	out			
75	in			W
	out			

Figure D.25: Flow pattern transition at +30° inclination angle and a quality of 0.5


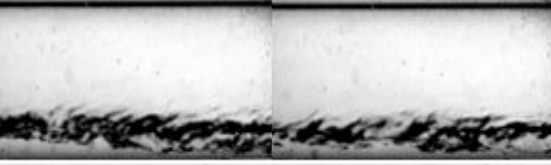



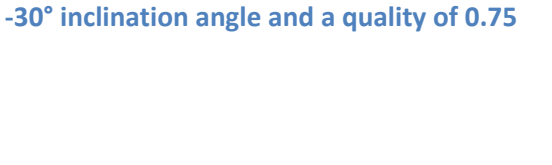

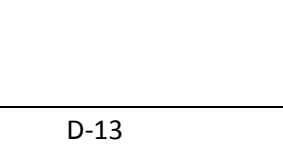
Mass flux [kg/m ² .s]	Time [s]			Flow pattern
	0	0.25	0.5	
100	in			SW
	out			
75	in			SW
	out			

Figure D.26: Flow pattern transition at -30° inclination angle and a quality of 0.75


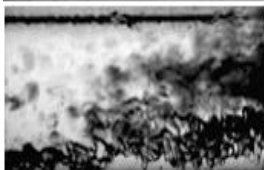
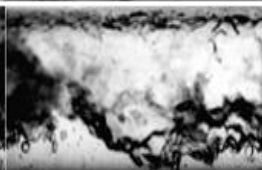
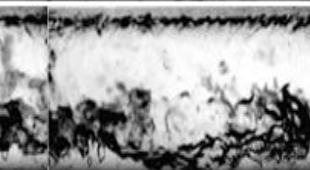
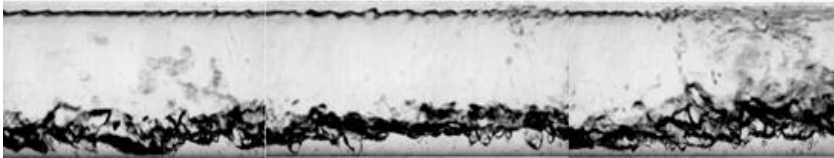
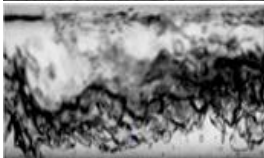
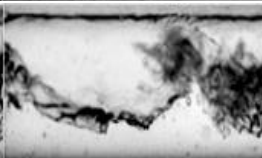
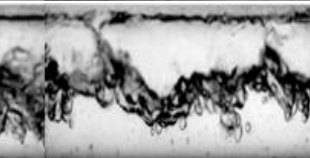
Mass flux [kg/m ² .s]	Time [s]			Flow pattern	
	0	0.25	0.5		
100	in				SW
	out				W
75	in				SW
	out				W

Figure D.27: Flow pattern transition at +30° inclination angle and a quality of 0.75

D.7 Flow pattern transitions for the inclination angle of ±45°









Mass flux [kg/m ² .s]	Time [s]			Flow pattern	
	0	0.25	0.5		
100	in				SW
	out				SW
75	in				SW
	out				SW

Figure D.28: Flow pattern transition at -45° inclination angle and a quality of 0.25




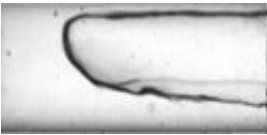

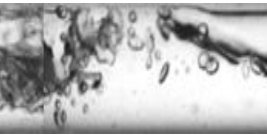
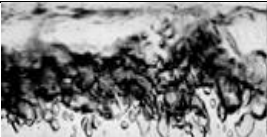
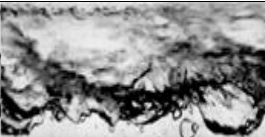




Mass flux [kg/m ² .s]		Time [s]			Flow pattern
		0	0.25	0.5	
100	in				W I
	out				
75	in				W I
	out				

Figure D.29: Flow pattern transition at +45° inclination angle and a quality of 0.25













Mass flux [kg/m ² .s]		Time [s]			Flow pattern
		0	0.25	0.5	
100	in				SW SW
	out				
75	in				SW SW
	out				

Figure D.30: Flow pattern transition at -45° inclination angle and a quality of 0.5

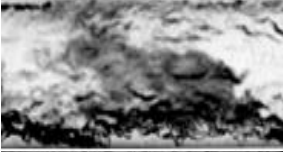






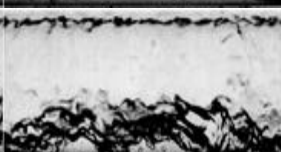




Mass flux [kg/m ² .s]		Time [s]			Flow pattern
		0	0.25	0.5	
100	in				W
	out				WC
75	in				W
	out				WC

Figure D.31: Flow pattern transition at +45° inclination angle and a quality of 0.5













Mass flux [kg/m ² .s]		Time [s]			Flow pattern
		0	0.25	0.5	
100	in				SW
	out				SW
75	in				SW
	out				SW

Figure D.32: Flow pattern transition at -45° inclination angle and a quality of 0.75

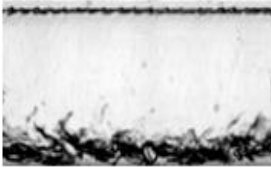

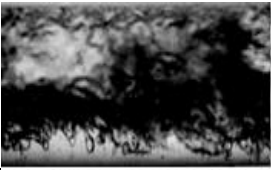
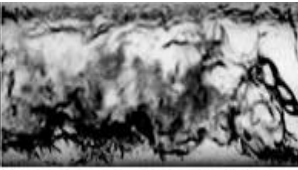

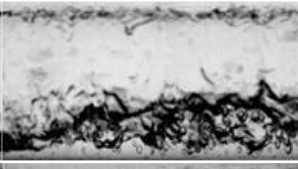
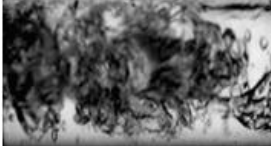

Mass flux [kg/m ² .s]	Time [s]			Flow pattern
	0	0.25	0.5	
100	in			SW
	out			
75	in			W
	out			

Figure D.33: Flow pattern transition at +45° inclination angle and a quality of 0.75

D.8 Flow pattern transitions for the inclination angle of 60°









Mass flux [kg/m ² .s]	Time [s]			Flow pattern
	0	0.25	0.5	
100	in			SW
	out			
75	in			SW
	out			

Figure D.34: Flow pattern transition at -60° inclination angle and a quality of 0.25







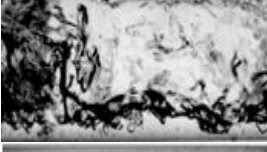
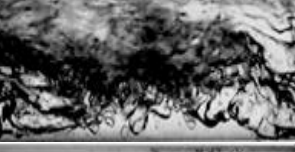
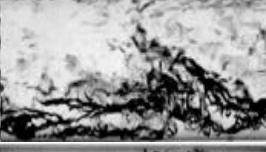



Mass flux [kg/m ² .s]	Time [s]			Flow pattern	
	0	0.25	0.5		
100	in				WC
	out				
75	in				WC
	out				

Figure D.35: Flow pattern transition at +60° inclination angle and a quality of 0.25










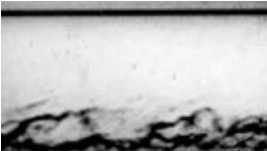


Mass flux [kg/m ² .s]	Time [s]			Flow pattern	
	0	0.25	0.5		
100	in				SW
	out				
75	in				SW
	out				

Figure D.36: Flow pattern transition at -60° inclination angle and a quality of 0.5




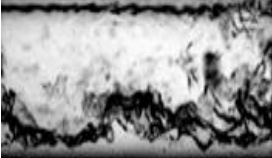
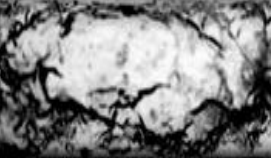
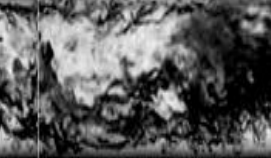
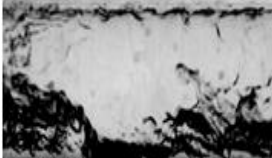
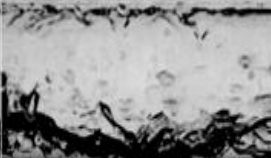

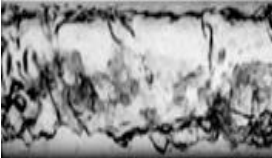


Mass flux [kg/m ² .s]	Time [s]			Flow pattern	
	0	0.25	0.5		
100	in				W
	out				WC
75	in				W
	out				WC

Figure D.37: Flow pattern transition at +60° inclination angle and a quality of 0.5







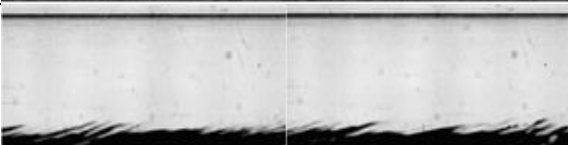

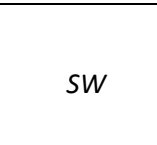
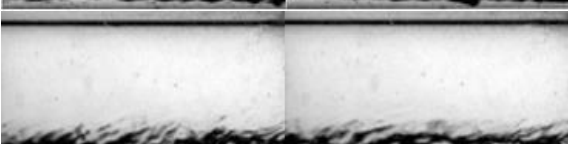


Mass flux [kg/m ² .s]	Time [s]			Flow pattern	
	0	0.25	0.5		
100	in				SW
	out				SW
75	in				SW
	out				SW

Figure D.38: Flow pattern transition at -60° inclination angle and a quality of 0.75

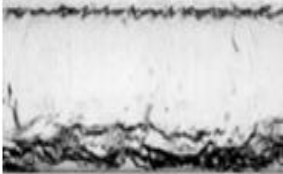

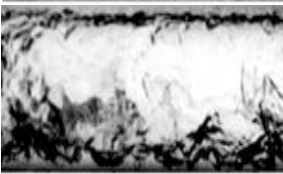
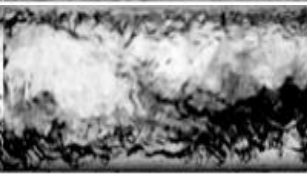
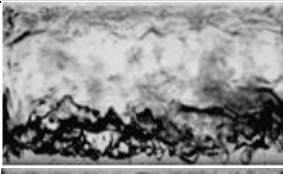
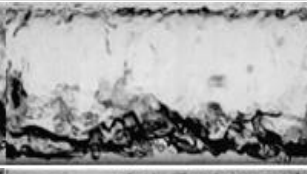
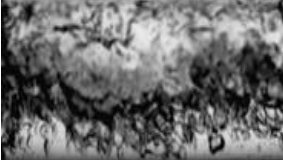

Mass flux [kg/m ² .s]	Time [s]			Flow pattern
	0	0.25	0.5	
100	in			SW
	out			
75	in			W
	out			WC

Figure D.39: Flow pattern transition at +60° inclination angle and a quality of 0.75

D.9 Flow pattern transitions for the inclination angle of ±90°



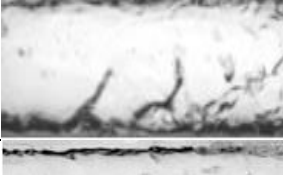
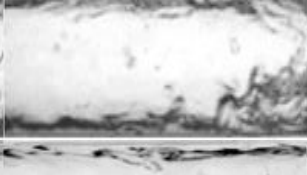
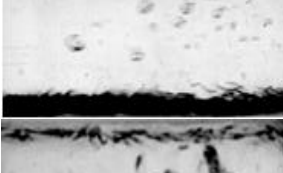
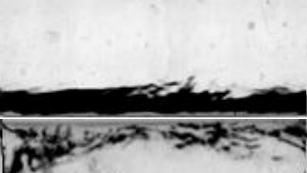


Mass flux [kg/m ² .s]	Time [s]			Flow pattern
	0	0.25	0.5	
100	in			A
	out			A
75	in			A
	out			A

Figure D.40: Flow pattern transition at -90° inclination angle and a quality of 0.25

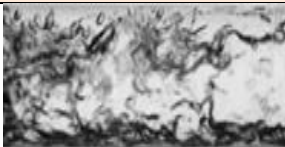
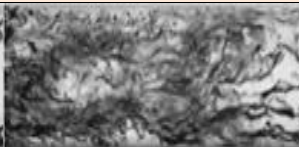










Mass flux [kg/m ² .s]		Time [s]			Flow pattern
		0	0.25	0.5	
100	in				C
	out				
75	in				C
	out				

Figure D.41: Flow pattern transition at +90° inclination angle and a quality of 0.25


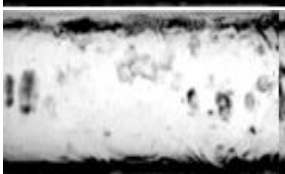

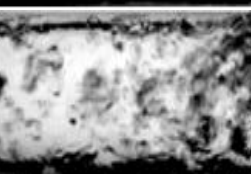

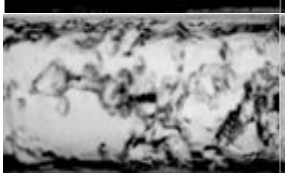


Mass flux [kg/m ² .s]		Time [s]			Flow pattern
		0	0.25	0.5	
100	in				A
	out				
75	in				A
	out				

Figure D.42: Flow pattern transition at -90° inclination angle and a quality of 0.5

Mass flux [kg/m ² .s]	Time [s]			Flow pattern
	0	0.25	0.5	
100	in			WA
	out			
75	in			WA
	out			

Figure D.43: Flow pattern transition at +90° inclination angle and a quality of 0.5

Mass flux [kg/m ² .s]	Time [s]			Flow pattern
	0	0.25	0.5	
100	in			A
	out			
75	in			A
	out			

Figure D.44: Flow pattern transition at -90° inclination angle and a quality of 0.75

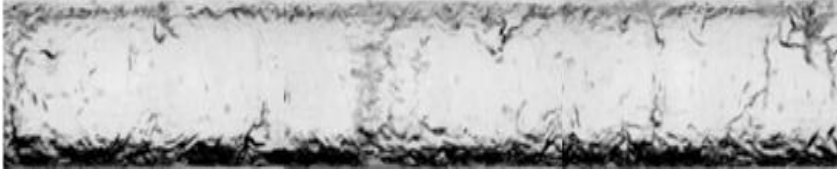
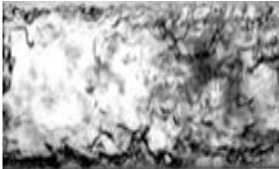

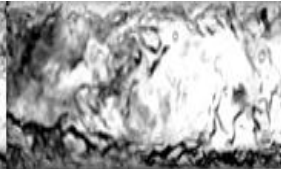
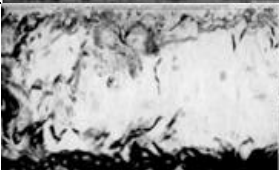

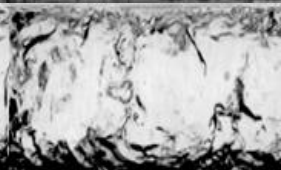
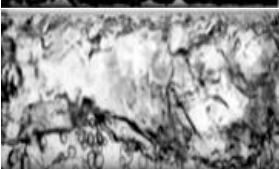
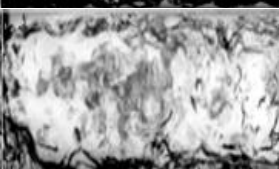
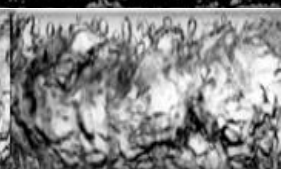
Mass flux [kg/m ² .s]		Time [s]			Flow pattern
		0	0.25	0.5	
100	in				WA
	out				WA
75	in				WA
	out				C

Figure D.45: Flow pattern transition at +90° inclination angle and a quality of 0.75

D.10 Summary

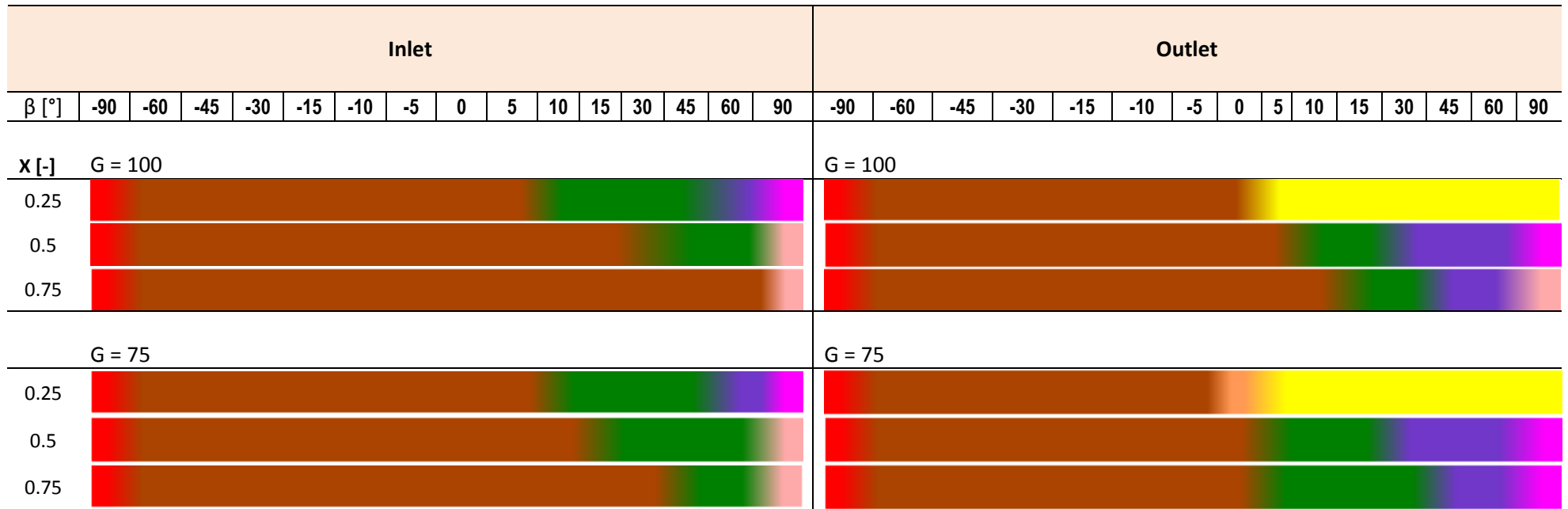
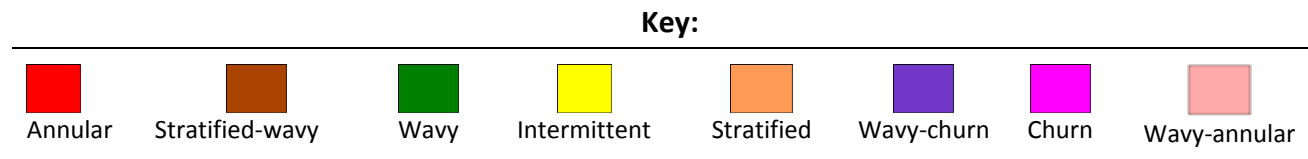


Figure D.46: Summary of flow pattern transitions



D.10.1 Comparing flow pattern transitions for negative and positive inclination angles

Figure D.46 shows flow pattern transitions for a temperature difference of 5°C. It can be seen that flow the pattern transition on the inlet to the test condenser for the negative inclinations is from stratified-wavy to annular as the inclination angle is increased from 0° to -90° for mass fluxes of 75 and 100 kg/m².s. The annular flow pattern is confined to -90°, while stratified-wavy spans from 0° to -60°.

For positive inclination angles at the inlet to the test condenser from 0° to +90° flow patterns transition from stratified-wavy to a wavy flow pattern from 0° to 45°. However, at a lower quality of 0.25, the flow transitions to wavy-churn at 60° then to churn at +90°. As quality is increased, wavy-churn is replaced by a wavy flow pattern which transitions to wavy-annular as the inclination angle is increased to +90°.

On the outlet from the test condenser, flow patterns for negative inclination angles are annular and stratified-wavy from 0° to -90°. Just like the inlet conditions, the stratified-wavy flow pattern increases in its prevalence as quality increases from negative to positive inclination angles. An intermittent flow pattern was common at lower qualities of 0.25 and from +5° to +90°. With an increase in quality, wavy, wavy-churn and churn flow patterns take over. A wavy-annular flow pattern was only observed at a higher quality of 100 kg/m².s and a high quality of 0.75. For all the negative inclination angles, the flow patterns remained constant from the inlet to the outlet. Hence, an annular flow pattern was also observed at -90° and a stratified-wavy flow pattern was observed from 0° to -60°.

Appendix E. Flow pattern transitions for a ΔT of 8°C

E.1 Introduction

This appendix shows observed flow patterns for the inlet and outlet to and from the test condenser for mass fluxes of $100 \text{ kg/m}^2\cdot\text{s}$ and $75 \text{ kg/m}^2\cdot\text{s}$ and temperature difference of 8°C . The qualities were for 0.35, 0.5 and 0.62 for all the inclination angles. Where flow patterns were not taken, another close quality will be used, for instance, if for a quality of 0.35, the flow pattern was not captured then a quality of 0.25 will be used. However, these instances were very few, as most of the flow patterns were captured.

E.2 Flow pattern transitions for the horizontal inclination 0°




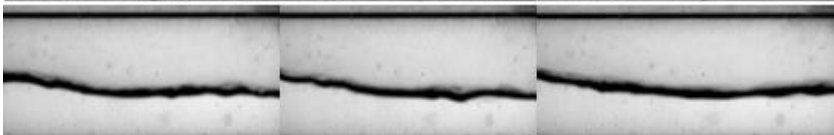
Mass flux [$\text{kg/m}^2\cdot\text{s}$]		Time [s]			Flow pattern
		0	0.25	0.5	
100	in				SW
	out				S
75	in				SW
	out				S

Figure E.1: Flow pattern transition at 0° inclination angle and a quality of 0.35





Mass flux [kg/m ² .s]	Time [s]			Flow pattern	
	0	0.25	0.5		
100	in				SW
	out				SW
75	in				SW
	out				SW

Figure E.2: Flow pattern transition at 0° inclination angle and a quality of 0.5



Mass flux [kg/m ² .s]	Time [s]			Flow pattern	
	0	0.25	0.5		
100	in				SW
	out				SW

Figure E.3: Flow pattern transition at 0° inclination angle and a quality of 0.75

E.3 Flow pattern transitions for the inclination angle of $\pm 5^\circ$

Mass flux [kg/m ² .s]		Time [s]			Flow pattern
		0	0.25	0.5	
100	in				SW
	out				SW
75	in				SW
	out				SW

Figure E.4: Flow pattern transition at -5° inclination angle and a quality of 0.35

Mass flux [kg/m ² .s]		Time [s]			Flow pattern
		0	0.25	0.5	
100	in				SW
	out				I
75	in				SW
	out				I

Figure E.5: Flow pattern transition at $+5^\circ$ inclination angle and a quality of 0.35













Mass flux [kg/m ² .s]		Time [s]			Flow pattern
		0	0.25	0.5	
100	in				SW
	out				SW
75	in				SW
	out				SW

Figure E.6: Flow pattern transition at -5° inclination angle and a quality of 0.5





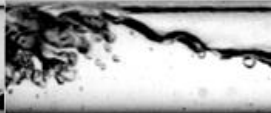







Mass flux [kg/m ² .s]		Time [s]			Flow pattern
		0	0.25	0.5	
100	in				SW
	out				W
75	in				SW
	out				I

Figure E.7: Flow pattern transition at +5° inclination angle and a quality of 0.5







Mass flux [kg/m ² .s]		Time [s]			Flow pattern
		0	0.25	0.5	
100	in				SW
	out				SW

Figure E.8: Flow pattern transition at -5° inclination angle and a quality of 0.75


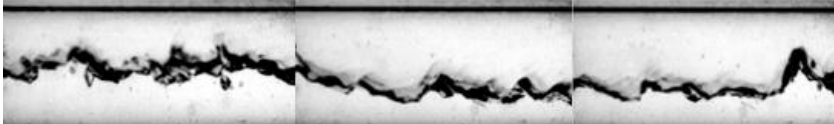
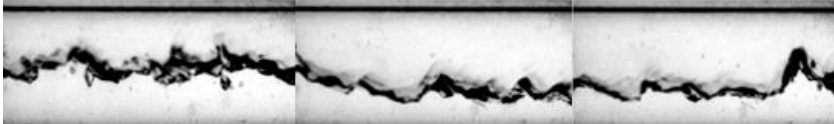
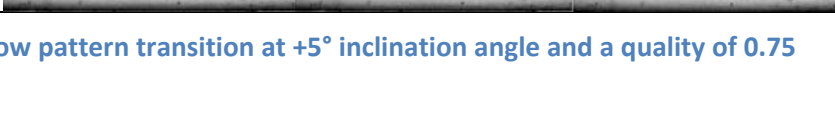


Mass flux [kg/m ² .s]		Time [s]			Flow pattern
		0	0.25	0.5	
100	in				SW
	out				
	in				SW
	out				
	in				SW
	out				

Figure E.9: Flow pattern transition at +5° inclination angle and a quality of 0.75

E.4 Flow pattern transitions for the inclination angle of ±10°


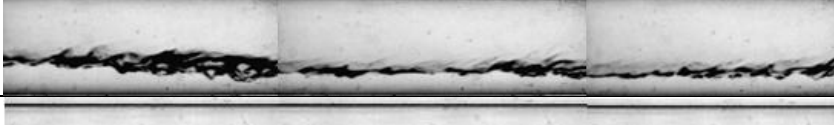


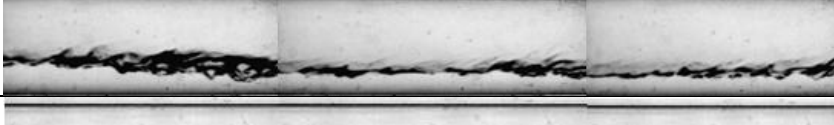


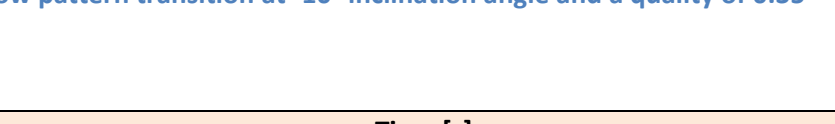
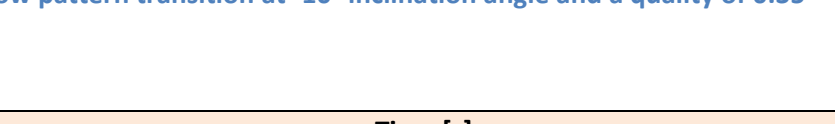
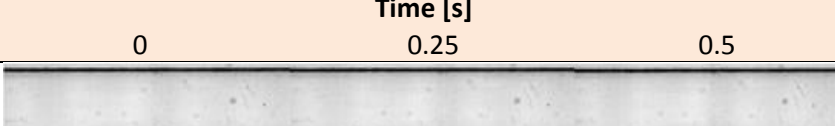
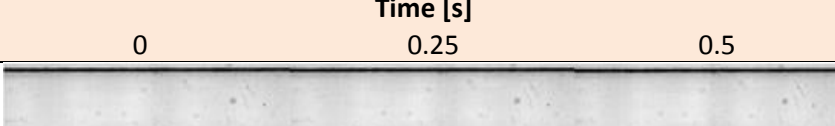

Mass flux [kg/m ² .s]		Time [s]			Flow pattern
		0	0.25	0.5	
100	in				SW
	out				
75	in				SW
	out				
	in				SW
	out				
	in				SW
	out				
	in				SW
	out				
	in				SW
	out				

Figure E.10: Flow pattern transition at -10° inclination angle and a quality of 0.35








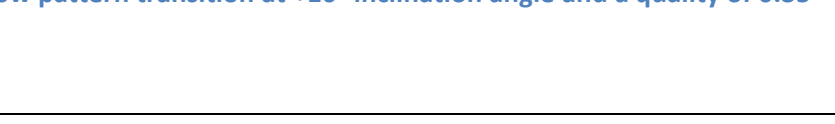
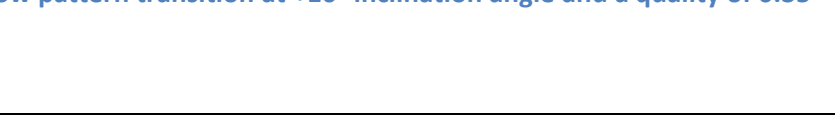
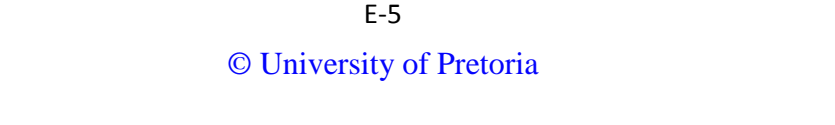
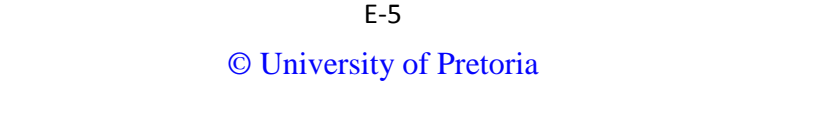
Mass flux [kg/m ² .s]		Time [s]			Flow pattern
		0	0.25	0.5	
100	in				W
	out				
75	in				W
	out				
	in				I
	out				
	in				I
	out				
	in				I
	out				
	in				I
	out				

Figure E.11: Flow pattern transition at +10° inclination angle and a quality of 0.35





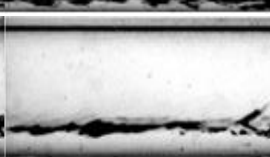




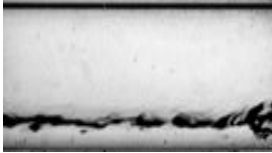

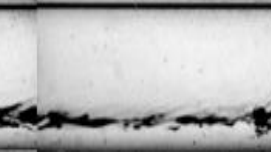
Mass flux [kg/m ² .s]		Time [s]			Flow pattern
		0	0.25	0.5	
100	in				SW
	out				
75	in				SW
	out				

Figure E.12: Flow pattern transition at -10° inclination angle and a quality of 0.5




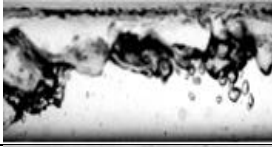
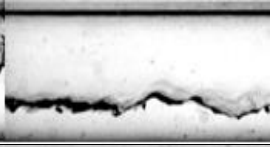
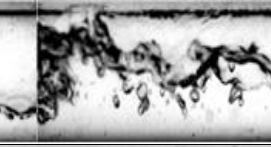




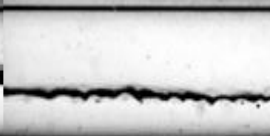
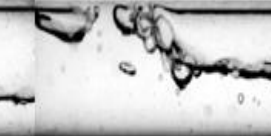
Mass flux [kg/m ² .s]		Time [s]			Flow pattern
		0	0.25	0.5	
100	in				SW
	out				
75	in				SW
	out				

Figure E.13: Flow pattern transition at +10° inclination angle and a quality of 0.5

Mass flux [kg/m ² .s]	Time [s]			Flow pattern	
	0	0.25	0.5		
100	In				SW
	out				

Figure E.14: Flow pattern transition at -10° inclination angle and a quality of 0.75

Mass flux [kg/m ² .s]	Time [s]			Flow pattern	
	0	0.25	0.5		
100	in				SW
	out				

Figure E.15: Flow pattern transition at +10° inclination angle and a quality of 0.75

E.5 Flow pattern transitions for the inclination angle of ±15°

Mass flux [kg/m ² .s]	Time [s]			Flow pattern	
	0	0.25	0.5		
100	In				SW
	out				
75	In				S
	out				

Figure E.16: Flow pattern transition at -15° inclination angle and a quality of 0.35




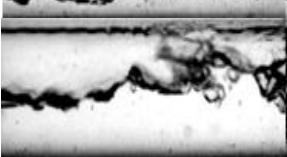
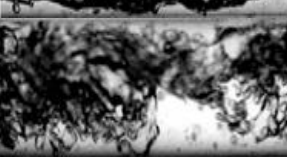







Mass flux [kg/m ² .s]		Time [s]			Flow pattern
		0	0.25	0.5	
100	in				<i>W</i>
	out				
75	in				<i>W</i>
	out				

Figure E.17: Flow pattern transition at +15° inclination angle and a quality of 0.35





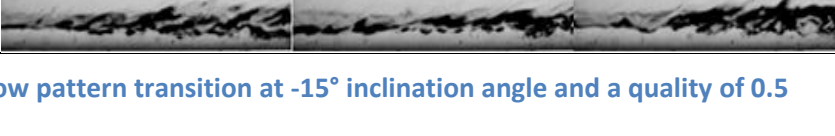



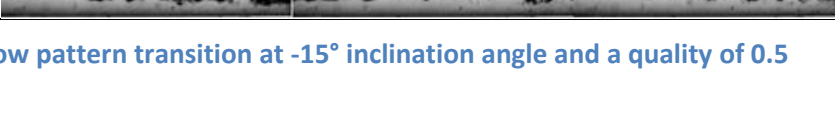


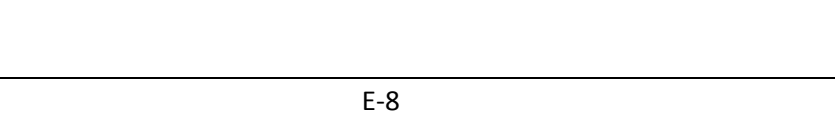
Mass flux [kg/m ² .s]		Time [s]			Flow pattern
		0	0.25	0.5	
100	in				<i>SW</i>
	out				
75	in				<i>SW</i>
	out				

Figure E.18: Flow pattern transition at -15° inclination angle and a quality of 0.5



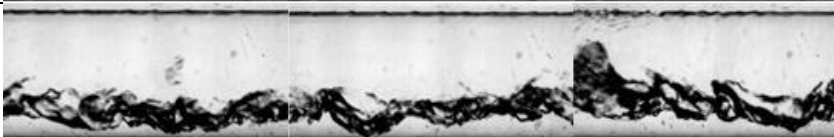

Mass flux [kg/m ² .s]	Time [s]			Flow pattern	
	0	0.25	0.5		
100	in				SW
	out				
75	in				W
	out				

Figure E.19: Flow pattern transition at +15° inclination angle and a quality of 0.5



Mass flux [kg/m ² .s]	Time [s]			Flow pattern	
	0	0.25	0.5		
100	in				SW
	out				

Figure E.20: Flow pattern transition at -15° inclination angle and a quality of 0.75



Mass flux [kg/m ² .s]	Time [s]			Flow pattern	
	0	0.25	0.5		
100	in				SW
	out				

Figure E.21: Flow pattern transition at +15° inclination angle and a quality of 0.75

E.6 Flow pattern transitions for the inclination angle of $\pm 30^\circ$



Mass flux [kg/m ² .s]	Time [s]			Flow pattern	
	0	0.25	0.5		
100	in				SW
	out				SW

Figure E.22: Flow pattern transition at -30° inclination angle and a quality of 0.35



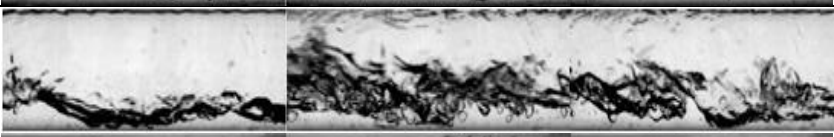
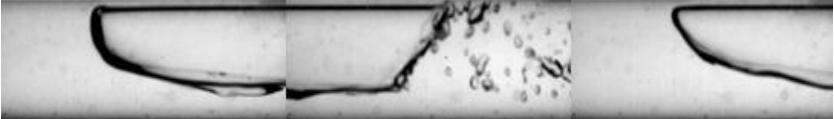
Mass flux [kg/m ² .s]	Time [s]			Flow pattern	
	0	0.25	0.5		
100	in				W
	out				WC
75	in				W
	out				I

Figure E.23: Flow pattern transition at $+30^\circ$ inclination angle and a quality of 0.35













Mass flux [kg/m ² .s]		Time [s]			Flow pattern
		0	0.25	0.5	
100	in				SW
	out				
75	in				SW
	out				

Figure E.24: Flow pattern transition at -30° inclination angle and a quality of 0.5



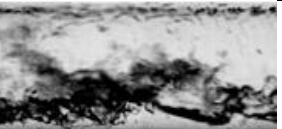

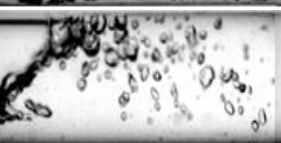



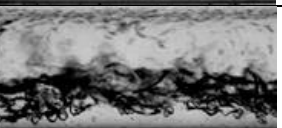
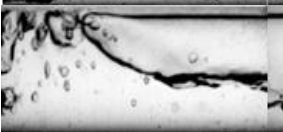


Mass flux [kg/m ² .s]		Time [s]			Flow pattern
		0	0.25	0.5	
100	in				W
	out				
75	in				W
	out				

Figure E.25: Flow pattern transition at +30° inclination angle and a quality of 0.5

Mass flux [kg/m ² .s]		Time [s]			Flow pattern
		0	0.25	0.5	
100	in				SW
	out				SW

Figure E.26: Flow pattern transition at -30° inclination angle and a quality of 0.75

Mass flux [kg/m ² .s]		Time [s]			Flow pattern
		0	0.25	0.5	
100	in				SW
	out				WC

Figure E.27: Flow pattern transition at +30° inclination angle and a quality of 0.75

E.7 Flow pattern transitions for the inclination angle of ±45°

Mass flux [kg/m ² .s]		Time [s]			Flow pattern
		0	0.25	0.5	
100	in				SW
	out				SW
75	in				SW
	out				SW

Figure E.28: Flow pattern transition at -45° inclination angle and a quality of 0.35

Mass flux [kg/m ² .s]		Time [s]			Flow pattern
		0	0.25	0.5	
100	in				W
	out				
75	in				W
	out				

Figure E.29: Flow pattern transition at +45° inclination angle and a quality of 0.35

Mass flux [kg/m ² .s]		Time [s]			Flow pattern
		0	0.25	0.5	
100	in				SW
	out				
75	in				SW
	out				

Figure E.30: Flow pattern transition at -45° inclination angle and a quality of 0.5


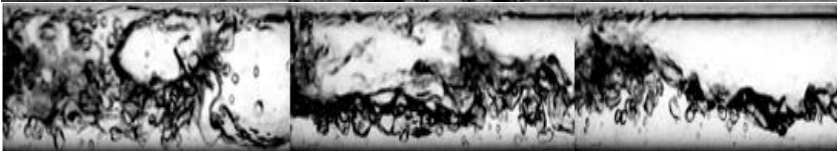
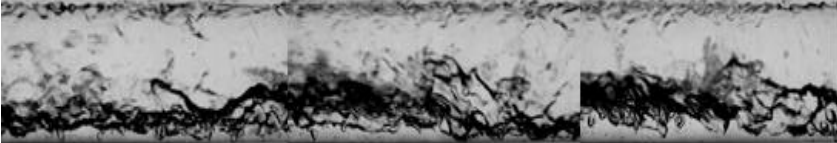

Mass flux [kg/m ² .s]		Time [s]			Flow pattern
		0	0.25	0.5	
100	in				W
	out				
75	in				W
	out				

Figure E.31: Flow pattern transition at +45° inclination angle and a quality of 0.5


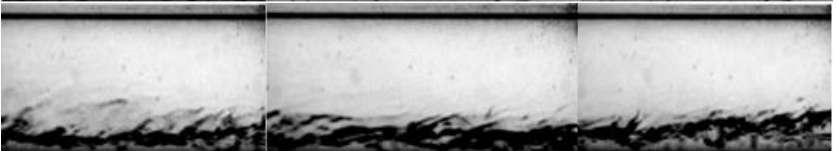
Mass flux [kg/m ² .s]		Time [s]			Flow pattern
		0	0.25	0.5	
100	In				SW
	out				

Figure E.32: Flow pattern transition at -45° inclination angle and a quality of 0.75


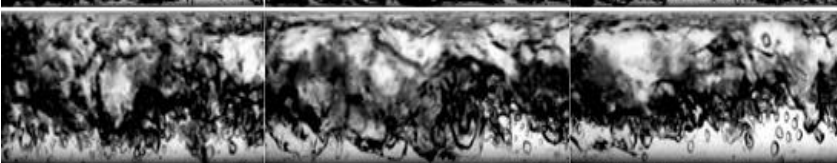
Mass flux [kg/m ² .s]		Time [s]			Flow pattern
		0	0.25	0.5	
100	in				W
	out				

Figure E.33: Flow pattern transition at +45° inclination angle and a quality of 0.75

E.8 Flow pattern transitions for the inclination angle of 60°













Mass flux [kg/m ² .s]	Time [s]			Flow pattern	
	0	0.25	0.5		
100	in				SW
	out				SW
75	in				SW
	out				SW

Figure E.34: Flow pattern transition at -60° inclination angle and a quality of 0.35

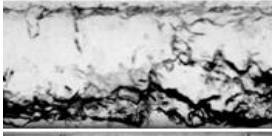
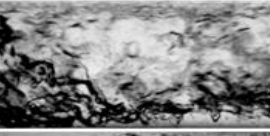
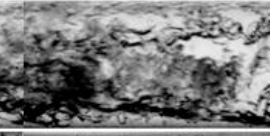




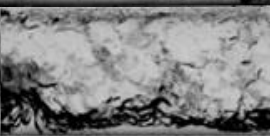


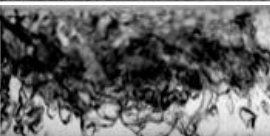

Mass flux [kg/m ² .s]	Time [s]			Flow pattern	
	0	0.25	0.5		
100	in				WC
	out				I
75	in				WC
	out				I

Figure E.35: Flow pattern transition at +60° inclination angle and a quality of 0.35













Mass flux [kg/m ² .s]		Time [s]			Flow pattern
		0	0.25	0.5	
100	in				SW
	out				
75	in				SW
	out				

Figure E.36: Flow pattern transition at -60° inclination angle and a quality of 0.5

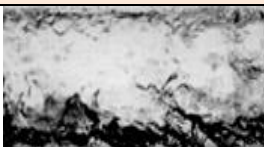
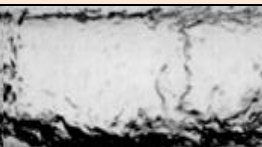
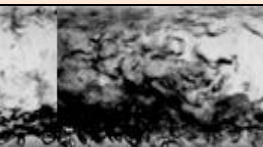

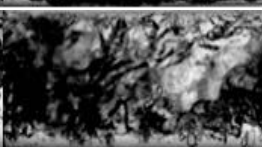

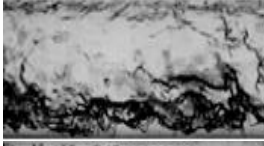
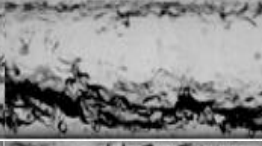
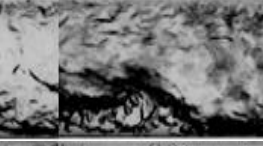

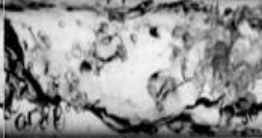

Mass flux [kg/m ² .s]		Time [s]			Flow pattern
		0	0.25	0.5	
100	in				WC
	out				
75	in				WC
	out				

Figure E.37: Flow pattern transition at +60° inclination angle and a quality of 0.5

Mass flux [kg/m ² .s]	Time [s]			Flow pattern	
	0	0.25	0.5		
100	in				SW
	out				

Figure E.38: Flow pattern transition at -60° inclination angle and quality of 0.75

Mass flux [kg/m ² .s]	Time [s]			Flow pattern	
	0	0.25	0.5		
100	in				SW
	out				

Figure E.39: Flow pattern transition at $+60^\circ$ inclination angle and a quality of 0.75

E.9 Flow pattern transitions for the inclination angle of $\pm 90^\circ$

Mass flux [kg/m ² .s]	Time [s]			Flow pattern	
	0	0.25	0.5		
100	in				A
	out				
75	in				A
	out				

Figure E.40: Flow pattern transition at -90° inclination angle and a quality of 0.35

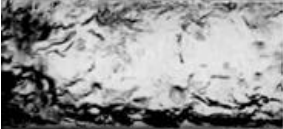
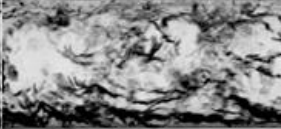
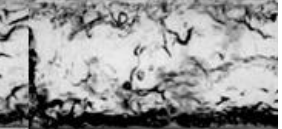


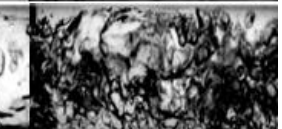
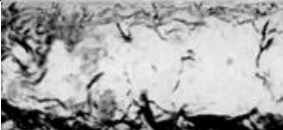





Mass flux [kg/m ² .s]		Time [s]			Flow pattern
		0	0.25	0.5	
100	in				C
	out				
75	in				C
	out				

Figure E.41: Flow pattern transition at +90° inclination angle and a quality of 0.35





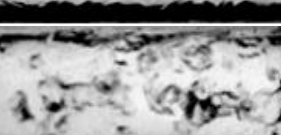
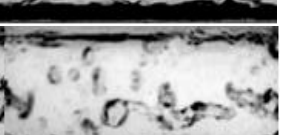

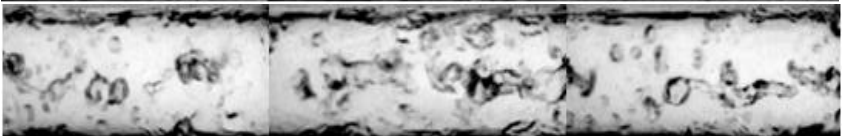
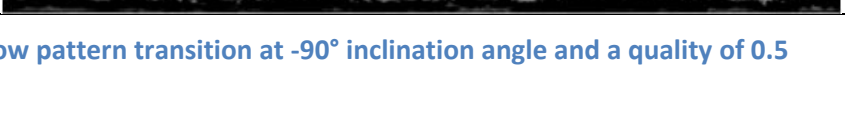



Mass flux [kg/m ² .s]		Time [s]			Flow pattern
		0	0.25	0.5	
100	in				A
	out				
75	in				A
	out				

Figure E.42: Flow pattern transition at -90° inclination angle and a quality of 0.5

Mass flux [kg/m ² .s]		Time [s]			Flow pattern
		0	0.25	0.5	
100	in				WA C
	out				
75	in				WA I
	out				

Figure E.43: Flow pattern transition at +90° inclination angle and a quality of 0.5

Mass flux [kg/m ² .s]		Time [s]			Flow pattern
		0	0.25	0.5	
100	in				A A
	out				

Figure E.44: Flow pattern transition at -90° inclination angle and a quality of 0.75

Mass flux [kg/m ² .s]		Time [s]			Flow pattern
		0	0.25	0.5	
100	in				WA C
	out				

Figure E.45: Flow pattern transition at +90° inclination angle and a quality of 0.75

E.10 Summary

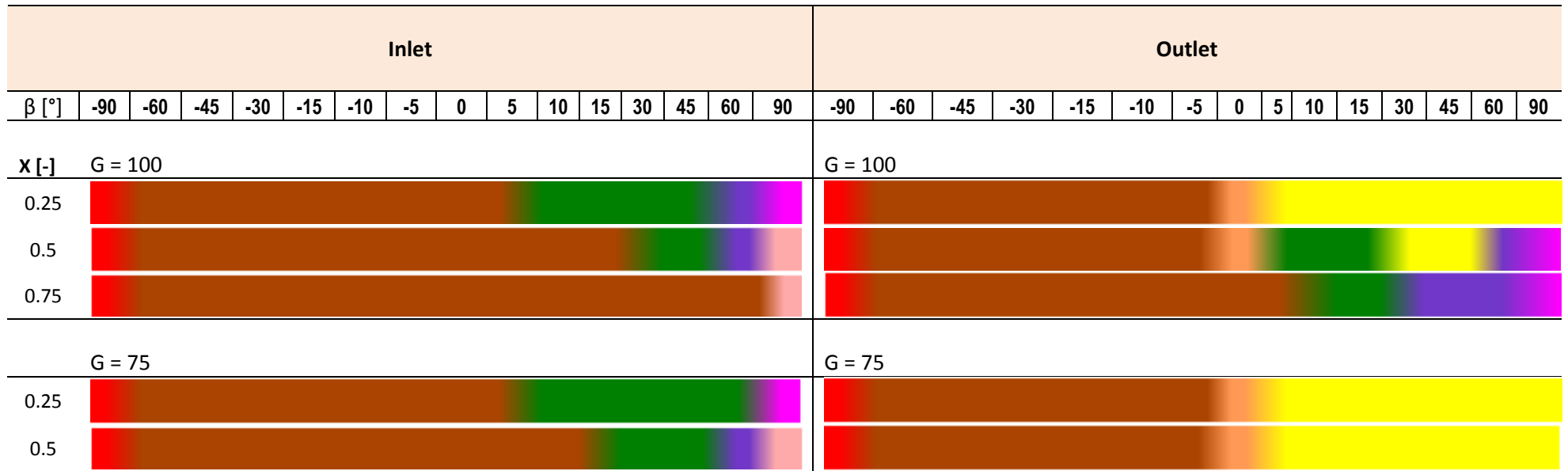
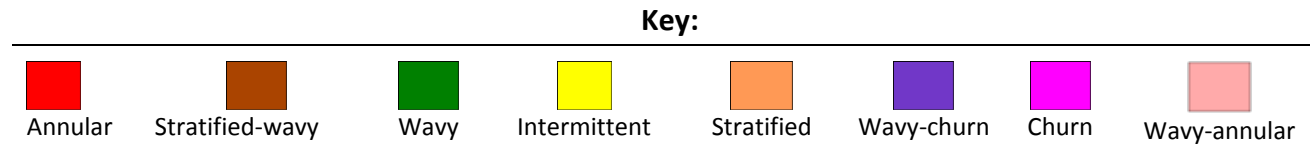


Figure E.46: Summary of flow pattern transitions



E.10.1 Comparing flow pattern transitions for negative and positive inclination angles

Figure E.46 presents flow pattern transitions for a temperature difference of 8 °C. The two observed flow patterns for the negative inclination angles for the inlet and outlet of the test condenser are stratified-wavy to annular. At 0° to -60° the flow pattern is stratified-wavy, while an annular flow pattern is only at -90°.

At the inlet to the test condenser from 0° to +90° (positive inclination angles), flow patterns transition from stratified-wavy to a wavy flow pattern from 0° to 45°. However, at a lower quality of 0.25, the flow transitions to wavy-churn at 60° then to churn at +90°. With an increase in quality, wavy-churn is replaced by a wavy flow pattern, which transitions to wavy-annular as the inclination angle is increased to +90°.

Flow patterns for negative inclination angles are annular and stratified-wavy from 0° to -90° on the outlet from the test condenser. An intermittent flow pattern is common at lower qualities of 0.25 and from +5° to +90°. With an increase in quality, wavy, wavy-churn and churn flow patterns take over. A wavy-annular flow pattern is only observed at a higher quality of 100 kg/m².s and a high quality of 0.75. For all the negative inclination angles, the flow patterns remained constant from inlet to outlet. A stratified flow pattern is common at lower qualities below 0.5 for the horizontal inclination.

Appendix F. Flow pattern transitions for a ΔT of 10°C

F.1 Introduction

In this appendix, only a mass flux of $100 \text{ kg/m}^2.\text{s}$ was used for a temperature difference of 10°C only for a quality of 0.5. The analysis was done to check the flow pattern transition from inlet to outlet of the test condenser, and the variation in flow pattern when the inclination angle was varied.

F.2 Flow pattern transitions for the horizontal inclination 0°


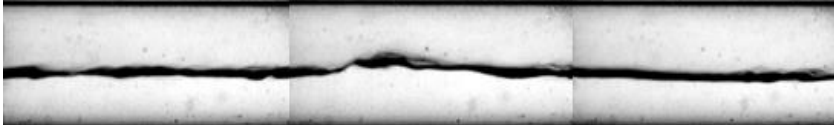
Mass flux [$\text{kg/m}^2.\text{s}$]	Time [s]			Flow pattern	
	0	0.25	0.5		
100	in				SW
	out				SW

Figure F.1: Flow pattern transition at 0° inclination angle and a quality of 0.5

F.3 Flow pattern transitions for the inclination angle of $\pm 5^\circ$



Mass flux [$\text{kg/m}^2.\text{s}$]	Time [s]			Flow pattern	
	0	0.25	0.5		
100	in				SW
	out				SW

Figure F.2: Flow pattern transition at -5° inclination angle and a quality of 0.5




Mass flux [kg/m ² .s]	0	Time [s] 0.25	0.5	Flow pattern
in				SW
100				
out				I

Figure F.3: Flow pattern transition at +5° inclination angle and a quality of 0.5

F.4 Flow pattern transitions for the inclination angle of ±10°


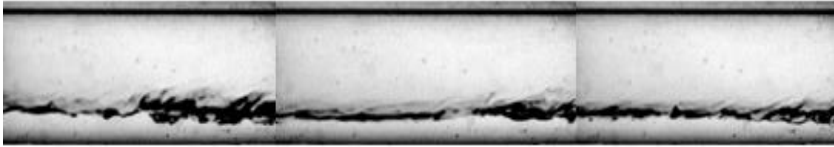
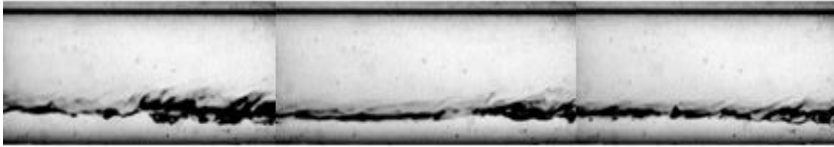
Mass flux [kg/m ² .s]	0	Time [s] 0.25	0.5	Flow pattern
in				SW
100				
out				SW

Figure F.4: Flow pattern transition at -10° inclination angle and a quality of 0.5


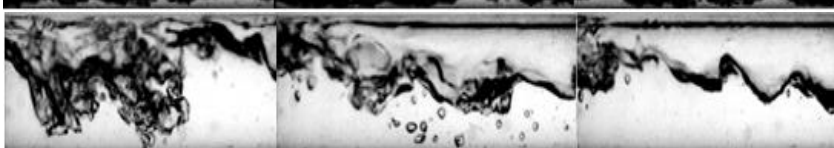
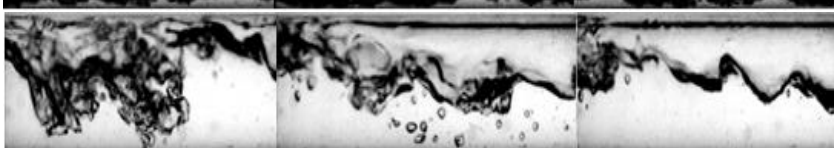
Mass flux [kg/m ² .s]	0	Time [s] 0.25	0.5	Flow pattern
in				SW
100				
out				I

Figure F.5: Flow pattern transition at +10° inclination angle and a quality of 0.5

F.5 Flow pattern transitions for the inclination angle of $\pm 15^\circ$






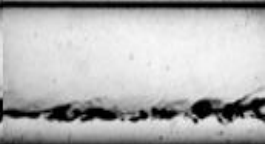
Mass flux [kg/m ² .s]	Time [s]			Flow pattern	
	0	0.25	0.5		
100	in				SW
	out				SW

Figure F.6: Flow pattern transition at -15° inclination angle and a quality of 0.5





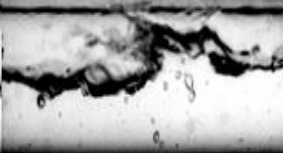

Mass flux [kg/m ² .s]	Time [s]			Flow pattern	
	0	0.25	0.5		
100	in				SW
	out				I

Figure F.7: Flow pattern transition at $+15^\circ$ inclination angle and a quality of 0.5

F.6 Flow pattern transitions for the inclination angle of $\pm 30^\circ$







Mass flux [kg/m ² .s]	Time [s]			Flow pattern	
	0	0.25	0.5		
100	in				SW
	out				SW

Figure F.8: Flow pattern transition at -30° inclination angle and a quality of 0.5

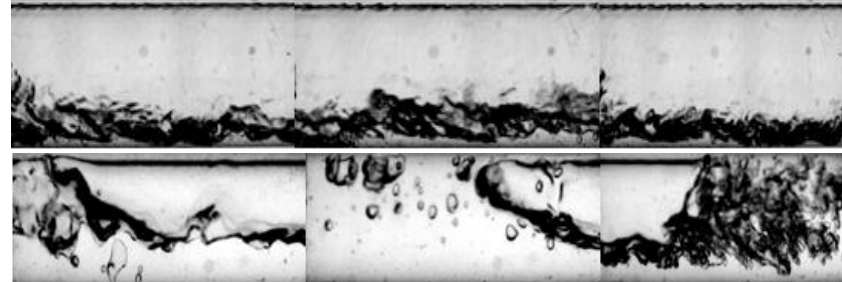
Mass flux [kg/m ² .s]	Time [s]			Flow pattern
	0	0.25	0.5	
in				SW
100				I
out				

Figure F.9: Flow pattern transition at +30° inclination angle and a quality of 0.5

F.7 Flow pattern transitions for the inclination angle of ±45°

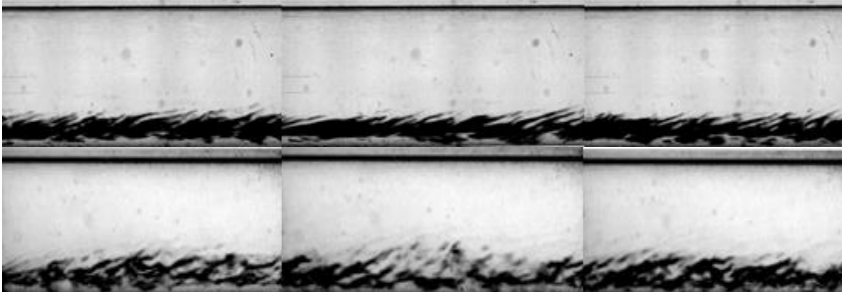
Mass flux [kg/m ² .s]	Time [s]			Flow pattern
	0	0.25	0.5	
in				SW
100				SW
out				

Figure F.10: Flow pattern transition at -45° inclination angle and a quality of 0.5

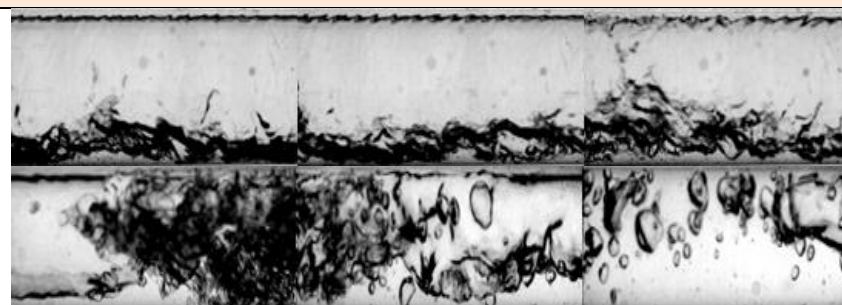
Mass flux [kg/m ² .s]	Time [s]			Flow pattern
	0	0.25	0.5	
in				SW
100				I
out				

Figure F.11: Flow pattern transition at +45° inclination angle and a quality of 0.5

F.8 Flow pattern transitions for the inclination angle of 60°



Mass flux [kg/m ² .s]	Time [s]			Flow pattern
	0	0.25	0.5	
in				SW
100				
out				SW

Figure F.12: Flow pattern transition at -60° inclination angle and a quality of 0.5


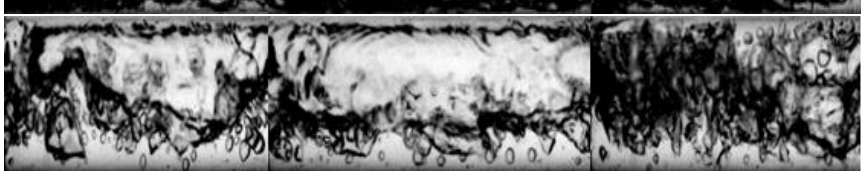
Mass flux [kg/m ² .s]	Time [s]			Flow pattern
	0	0.25	0.5	
in				W
100				
out				WC

Figure F.13: Flow pattern transition at +60° inclination angle and a quality of 0.5

F.9 Flow pattern transitions for the inclination angle of ±90°



Mass flux [kg/m ² .s]	Time [s]			Flow pattern
	0	0.25	0.5	
in				A
100				
out				A

Figure F.14: Flow pattern transition at -90° inclination angle and a quality of 0.5

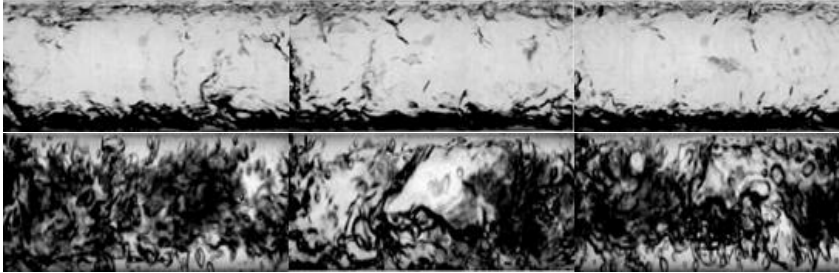
Mass flux [kg/m ² .s]	Time [s]			Flow pattern	
	0	0.25	0.5		
100	in				WA
	out				C

Figure F.15: Flow pattern transition at +90° inclination angle and a quality of 0.5

F.10 Summary

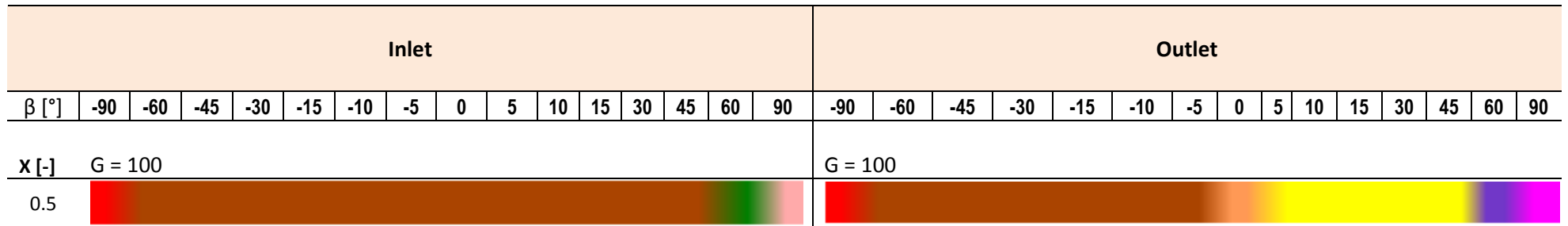
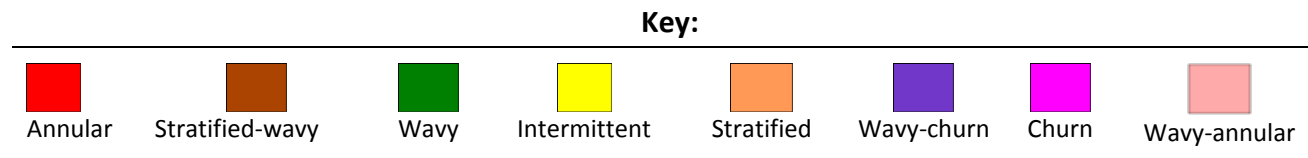


Figure F.16: Summary of flow pattern transitions



F.10.1 Comparing flow pattern transitions for negative and positive inclination angles

At a temperature difference of 10 °C, the flow is dominated by a stratified-wavy flow pattern on the inlet to the test condenser, with annular and wavy-annular flow pattern being observed at -90° and +90° respectively. On the outlet from the test condenser, intermittent flow pattern dominates the positive inclination angles with wavy-churn and churn flow pattern on the extreme angles of 60° and 90° respectively.

Overly, the annular flow pattern is confined to an inclination angle of -90° while wavy-annular and churn flow patterns are observed at +90°. A stratified-wavy flow pattern is common for most of the inclination angles disappearing at higher inclinations to give way for stratified, wavy-churn and wavy-annular. However at low qualities, low mass fluxes and higher temperature differences, an intermittent flow pattern dominates for the upward inclination angles.

Appendix G. Flow pattern transitions for a ΔT of 1°C

G.1 Introduction

Appendix G summarises observed flow patterns for the inlet and the outlet to and from the test condenser for mass fluxes of $50 \text{ kg/m}^2.\text{s}$ and $25 \text{ kg/m}^2.\text{s}$ and temperature difference of 1°C . The qualities are for 0.25; 0.5 and 0.75 for all the inclination angles for a mass flux of $50 \text{ kg/m}^2.\text{s}$. A quality of 0.75 was captured for a mass flux of $20 \text{ kg/m}^2.\text{s}$. In instances where flow patterns were not captured, other flow patterns were used close to the same quality range. For instance, if for a quality of 0.35 the flow pattern was not captured then a quality of 0.25 will be used. However, these instances were very few, as most of the flow patterns were captured.

G.2 Flow pattern transitions for the horizontal inclination 0°


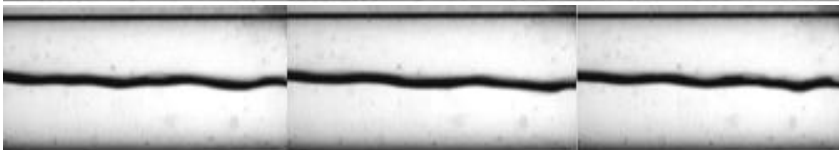
Mass flux [$\text{kg/m}^2.\text{s}$]	Time [s]			Flow pattern	
	0	0.25	0.5		
50	in				S
	out				S

Figure G. 1: Flow pattern transition at 0° inclination angle and a quality of 0.25



Mass flux [$\text{kg/m}^2.\text{s}$]	Time [s]			Flow pattern	
	0	0.25	0.5		
50	in				SW
	out				S

Figure G.2: Flow pattern transition at 0° inclination angle and a quality of 0.5


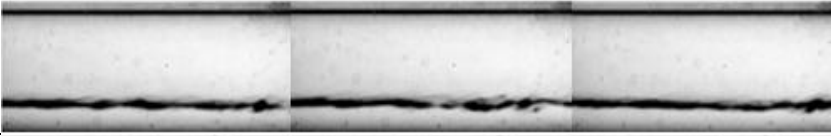


Mass flux [kg/m ² .s]		Time [s]			Flow pattern
		0	0.25	0.5	
50	in				SW
	out				S
25	in				SW
	out				S

Figure G.3: Flow pattern transition at 0° inclination angle and a quality of 0.75

G.3 Flow pattern transitions for the inclination angle of ±5°

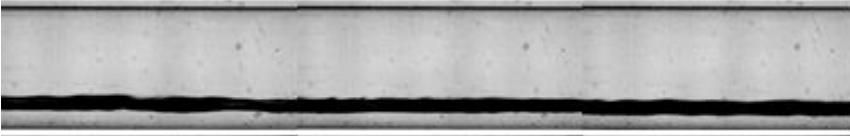
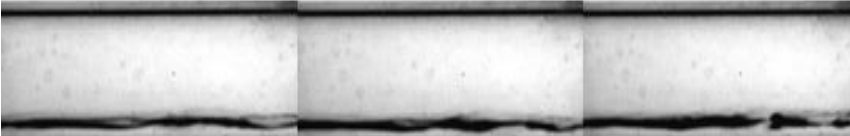
Mass flux [kg/m ² .s]		Time [s]			Flow pattern
		0	0.25	0.5	
50	in				S
	out				S

Figure G.4: Flow pattern transition at -5° inclination angle and a quality of 0.25


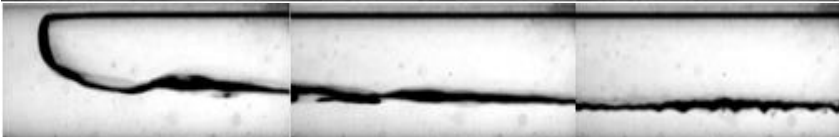
Mass flux [kg/m ² .s]		Time [s]			Flow pattern
		0	0.25	0.5	
50	in				I
	out				I

Figure G.5: Flow pattern transition at +5° inclination angle and a quality of 0.25






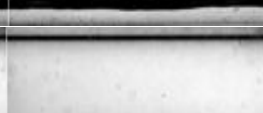
Mass flux [kg/m ² .s]	Time [s]			Flow pattern
	0	0.25	0.5	
50	in			S
	out			
				

Figure G.6: Flow pattern transition at -5° inclination angle and a quality of 0.5







Mass flux [kg/m ² .s]	Time [s]			Flow pattern
	0	0.25	0.5	
50	in			SW
	out			
				

Figure G.7: Flow pattern transition at +5° inclination angle and a quality of 0.5










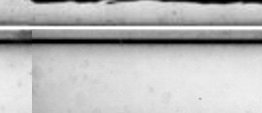

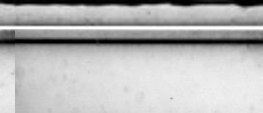
Mass flux [kg/m ² .s]	Time [s]			Flow pattern
	0	0.25	0.5	
50	in			S
	out			
				
25	in			S
	out			
				

Figure G.8: Flow pattern transition at -5° inclination angle and a quality of 0.75

Mass flux [kg/m ² .s]		Time [s]			Flow pattern
		0	0.25	0.5	
100	in				SW
	out				
25	in				SW
	out				

Figure G.9: Flow pattern transition at +5° inclination angle and a quality of 0.75

G.4 Flow pattern transitions for the inclination angle of ±10°

Mass flux [kg/m ² .s]		Time [s]			Flow pattern
		0	0.25	0.5	
50	in				S
	out				

Figure G.10: Flow pattern transition at -10° inclination angle and a quality of 0.25

Mass flux [kg/m ² .s]		Time [s]			Flow pattern
		0	0.25	0.5	
50	in				I
	out				

Figure G.11: Flow pattern transition at +10° inclination angle and a quality of 0.25

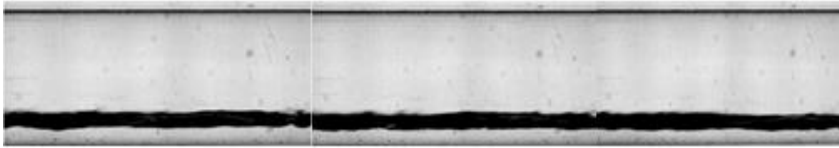
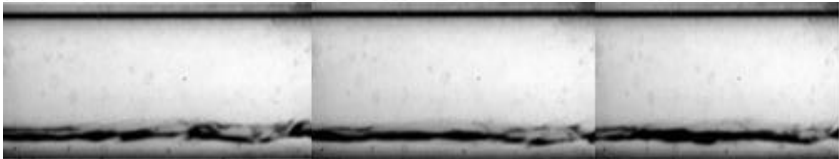
Mass flux [kg/m ² .s]	Time [s]			Flow pattern
	0	0.25	0.5	
50	in			S
	out			S

Figure G.12: Flow pattern transition at -10° inclination angle and a quality of 0.5

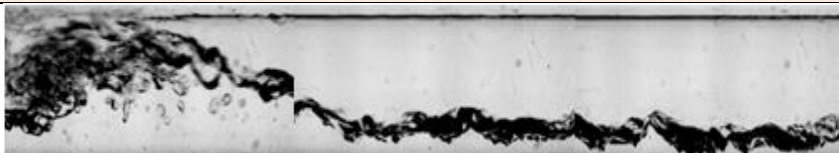

Mass flux [kg/m ² .s]	Time [s]			Flow pattern
	0	0.25	0.5	
50	in			W
	out			W

Figure G.13: Flow pattern transition at +10° inclination angle and a quality of 0.5





Mass flux [kg/m ² .s]	Time [s]			Flow pattern
	0	0.25	0.5	
50	in			S
	out			S
25	in			S
	out			S

Figure G.14: Flow pattern transition at -10° inclination angle and a quality of 0.75

Mass flux [kg/m ² .s]		Time [s]			Flow pattern
		0	0.25	0.5	
50	in				SW
	out				W
25	in				W
	out				W

Figure G.15: Flow pattern transition at +10° inclination angle and a quality of 0.75

G.5 Flow pattern transitions for the inclination angle of ±15°

Mass flux [kg/m ² .s]		Time [s]			Flow pattern
		0	0.25	0.5	
50	in				S
	out				S

Figure G.16: Flow pattern transition at -15° inclination angle and a quality of 0.25

Mass flux [kg/m ² .s]		Time [s]			Flow pattern
		0	0.25	0.5	
50	in				I
	out				I

Figure G.17: Flow pattern transition at +15° inclination angle and a quality of 0.25

Mass flux [kg/m ² .s]	Time [s]			Flow pattern
	0	0.25	0.5	
50	in			S
	out			

Figure G.18: Flow pattern transition at -15° inclination angle and a quality of 0.5

Mass flux [kg/m ² .s]	Time [s]			Flow pattern
	0	0.25	0.5	
50	in			W
	out			

Figure G.19: Flow pattern transition at +15° inclination angle and a quality of 0.5

Mass flux [kg/m ² .s]	Time [s]			Flow pattern
	0	0.25	0.5	
50	in			S
	out			
25	in			SW
	out			

Figure G.20: Flow pattern transition at -15° inclination angle and a quality of 0.75

Mass flux [kg/m ² .s]		Time [s]			Flow pattern
		0	0.25	0.5	
50	in				W
	out				
25	in				W
	out				

Figure G.21: Flow pattern transition at +15° inclination angle and a quality of 0.75

G.6 Flow pattern transitions for the inclination angle of ±30°

Mass flux [kg/m ² .s]		Time [s]			Flow pattern
		0	0.25	0.5	
50	in				S
	out				

Figure G.22: Flow pattern transition at -30° inclination angle and a quality of 0.25

Mass flux [kg/m ² .s]		Time [s]			Flow pattern
		0	0.25	0.5	
50	in				I
	out				

Figure G.23: Flow pattern transition at +30° inclination angle and a quality of 0.25

Mass flux [kg/m ² .s]		Time [s]			Flow pattern
		0	0.25	0.5	
50	in				SW
	out				

Figure G.24: Flow pattern transition at -30° inclination angle and a quality of 0.5

Mass flux [kg/m ² .s]		Time [s]			Flow pattern
		0	0.25	0.5	
50	in				W
	out				

Figure G.25: Flow pattern transition at +30° inclination angle and a quality of 0.5

Mass flux [kg/m ² .s]		Time [s]			Flow pattern
		0	0.25	0.5	
50	in				S
	out				
25	in				SW
	out				

Figure G.26: Flow pattern transition at -30° inclination angle and a quality of 0.75

Mass flux [kg/m ² .s]		Time [s]			Flow pattern
		0	0.25	0.5	
50	in				W
	out				
25	in				W
	out				

Figure G.27: Flow pattern transition at +30° inclination angle and a quality of 0.75

G.7 Flow pattern transitions for the inclination angle of ±45°

Mass flux [kg/m ² .s]		Time [s]			Flow pattern
		0	0.25	0.5	
50	in				S
	out				

Figure G.28: Flow pattern transition at -45° inclination angle and a quality of 0.25

Mass flux [kg/m ² .s]		Time [s]			Flow pattern
		0	0.25	0.5	
50	in				WC
	out				

Figure G.29: Flow pattern transition at +45° inclination angle and a quality of 0.25

Mass flux [kg/m ² .s]	Time [s]			Flow pattern
	0	0.25	0.5	
50	in			SW
	out			
50	in			SW
	out			

Figure G.30: Flow pattern transition at -45° inclination angle and a quality of 0.5

Mass flux [kg/m ² .s]	Time [s]			Flow pattern
	0	0.25	0.5	
50	in			W
	out			
50	in			WC
	out			

Figure G.31: Flow pattern transition at +45° inclination angle and a quality of 0.5

Mass flux [kg/m ² .s]	Time [s]			Flow pattern
	0	0.25	0.5	
50	in			SW
	out			
50	in			SW
	out			
25	in			SW
	out			
25	in			SW
	out			

Figure G.32: Flow pattern transition at -45° inclination angle and a quality of 0.75

Mass flux [kg/m ² .s]		Time [s]			Flow pattern
		0	0.25	0.5	
50	in				W
	out				
25	in				WC
	out				

Figure G.33: Flow pattern transition at +45° inclination angle and a quality of 0.75

G.8 Flow pattern transitions for the inclination angle of 60°

Mass flux [kg/m ² .s]		Time [s]			Flow pattern
		0	0.25	0.5	
50	in				SW
	out				

Figure G.34: Flow pattern transition at -60° inclination angle and a quality of 0.25

Mass flux [kg/m ² .s]		Time [s]			Flow pattern
		0	0.25	0.5	
50	in				WC
	out				

Figure G.35: Flow pattern transition at +60° inclination angle and a quality of 0.25





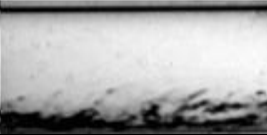

Mass flux [kg/m ² .s]		Time [s]			Flow pattern
		0	0.25	0.5	
50	in				SW
	out				

Figure G.36: Flow pattern transition at -60° inclination angle and a quality of 0.5

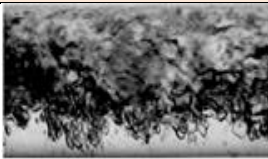
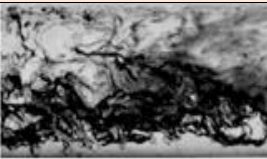


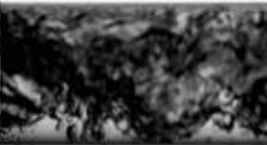

Mass flux [kg/m ² .s]		Time [s]			Flow pattern
		0	0.25	0.5	
50	in				WC
	out				

Figure G.37: Flow pattern transition at +60° inclination angle and a quality of 0.5













Mass flux [kg/m ² .s]		Time [s]			Flow pattern
		0	0.25	0.5	
50	in				SW
	out				
25	in				SW
	out				

Figure G.38: Flow pattern transition at -60° inclination angle and a quality of 0.75

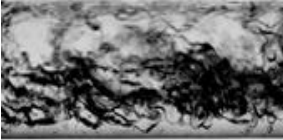
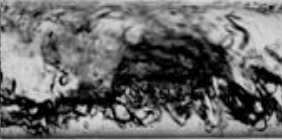

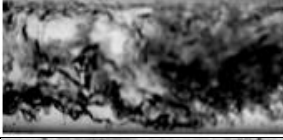

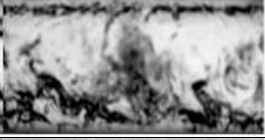
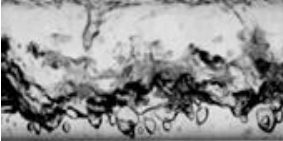





Mass flux [kg/m ² .s]		Time [s]			Flow pattern
		0	0.25	0.5	
50	in				WC
	out				
25	in				WC
	out				

Figure G.39: Flow pattern transition at +60° inclination angle and a quality of 0.75

G.9 Flow pattern transitions for the inclination angle of ±90°







Mass flux [kg/m ² .s]		Time [s]			Flow pattern
		0	0.25	0.5	
50	in				A
	out				

Figure G.40: Flow pattern transition at -90° inclination angle and a quality of 0.25





Mass flux [kg/m ² .s]	Time [s]			Flow pattern
	0	0.25	0.5	
50	In			C
	out			

Figure G.41: Flow pattern transition at +90° inclination angle and a quality of 0.25





Mass flux [kg/m ² .s]	Time [s]			Flow pattern
	0	0.25	0.5	
50	in			A
	out			

Figure G.42: Flow pattern transition at -90° inclination angle and a quality of 0.5



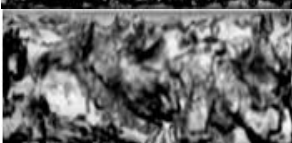
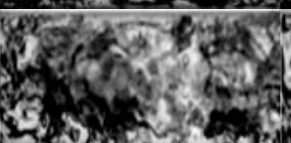
Mass flux [kg/m ² .s]	Time [s]			Flow pattern
	0	0.25	0.5	
50	in			C
	out			

Figure G.43: Flow pattern transition at +90° inclination angle and a quality of 0.5






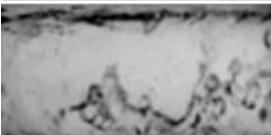
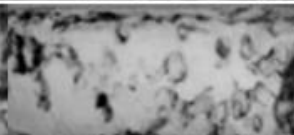

Mass flux [kg/m ² .s]		Time [s]			Flow pattern
		0	0.25	0.5	
50	in				A
	out				
25	in				A
	out				

Figure G.44: Flow pattern transition at -90° inclination angle and a quality of 0.75

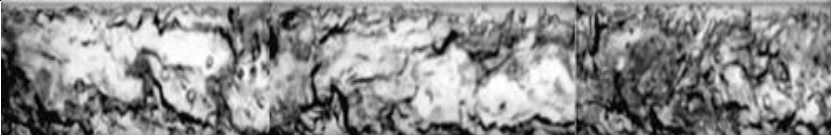

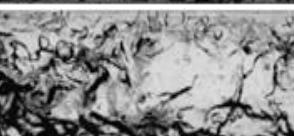

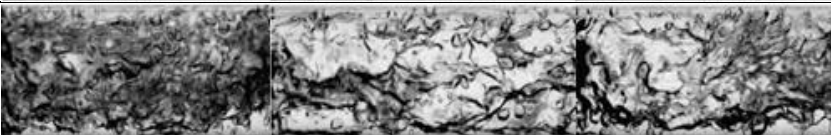



Mass flux [kg/m ² .s]		Time [s]			Flow pattern
		0	0.25	0.5	
50	in				C
	out				
25	in				C
	out				

Figure G.45: Flow pattern transition at +90° inclination angle and a quality of 0.62

G.10 Summary

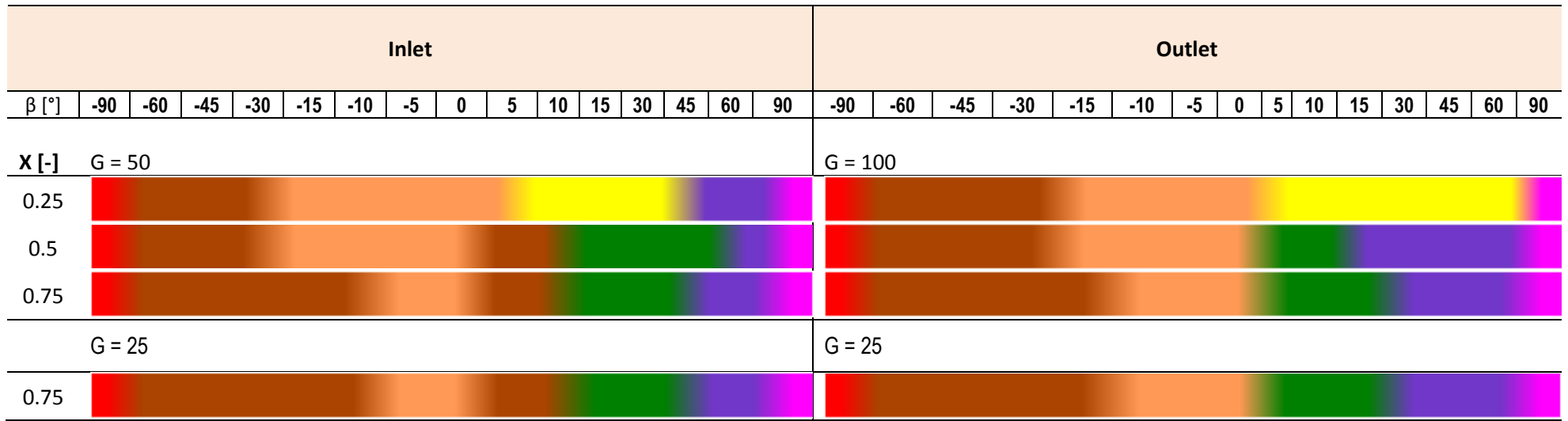
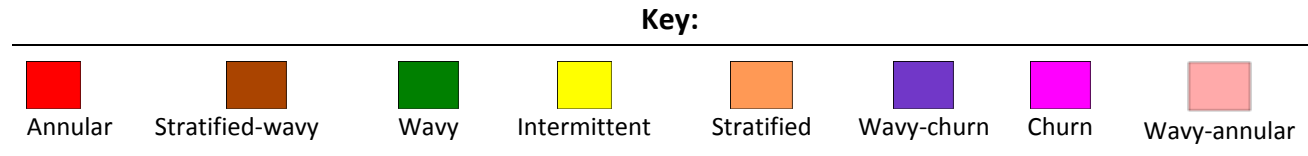


Figure G.46: Summary of flow pattern transitions



G.10.1 Comparing flow pattern transitions for negative and positive inclination angles

At the lowest temperature difference of 1°C, it can be seen that stratified flow pattern is very common at lower inclination angles on both the inlet and the outlet of the test section. This is evident for the horizontal orientation and for lower negative inclination angles. The stratified-wavy is confined to the higher negative inclination angles except for the -90° inclination angle. The wavy, churn and wavy-churn are common at qualities higher than 0.25. At a quality of 0.25, intermittent flow pattern replaces the wavy flow pattern for the positive inclination angles.

Appendix H. Summary of all the appendices: Appendix A to Appendix G

H.1 Conclusion

The purpose of this appendix is to summarise all the other appendices for flow pattern transitions from Appendix A to Appendix G. Colour charts of flow patterns were presented as seen in Figure H.1 to Figure H.4 as functions of mass flux, quality, inclination angle and temperature difference. Each flow patterns observed in the study is discussed as it varies with the above parameters.

H.1.1 Annular flow pattern

An annular flow pattern was only observed for the -90° inclination angle for all the qualities, mass fluxes and temperature differences. Hence, it can be concluded that an annular flow pattern is prevalent for only an inclination angle of -90° for low mass fluxes below $100 \text{ kg/m}^2.\text{s}$.

H.1.2 Wavy-annular flow pattern

The wavy-annular flow pattern was prevalent for the $+90^\circ$ inclination angle but mainly on the inlet to the test condenser at higher mass fluxes of $75 \text{ kg/m}^2.\text{s}$ and $100 \text{ kg/m}^2.\text{s}$ and higher qualities of 0.5 and above and also higher temperature differences of 5°C and above. The flow pattern diminishes as condensation continues to take place along the test tube such that it was only observed at the outlet from the test condenser, at a quality of 0.75 and only for the higher mass fluxes of $75 \text{ kg/m}^2.\text{s}$ and $100 \text{ kg/m}^2.\text{s}$.

H.1.3 Stratified flow pattern

A stratified flow pattern was common at very low mass fluxes of $50 \text{ kg/m}^2.\text{s}$ and below. It was frequent on the inlet and outlet of the test condenser. However, it was confined to lower inclination angles from 0° to between -15° and -30° . Stratified flow pattern was not observed at positive inclination angles but for the horizontal orientation (0°) at high temperature differences of 5°C and above, and low qualities of 0.5 and below at higher mass fluxes of $75 \text{ kg/m}^2.\text{s}$ and $100 \text{ kg/m}^2.\text{s}$.

H.1.4 Stratified-wavy flow pattern

Stratified-wavy was the most common flow pattern observed on the inlet and the outlet of the test condenser at low mass fluxes. The flow pattern apart from annular flow pattern at -90° was the only observed flow pattern for the negative inclination angles from 0° to 60° at higher mass fluxes of $75 \text{ kg/m}^2.\text{s}$ and $100 \text{ kg/m}^2.\text{s}$. As the mass fluxes decrease, then the flow pattern was replaced by a stratified flow pattern at lower inclination angles from 0° to

15°. On the other hand for positive inclination angles, stratified-wavy strongly depend on quality and also on the temperature difference. The prevalence of stratified-wavy flow pattern increases with increase in quality from 0° to small inclination angles of +10° and below. However as temperature difference increases, the flow pattern stopped to depend on quality hence at qualities of 0.5 and below and temperature differences of 5 °C to 10 °C stratified-wavy gave way to stratified flow.

H.1.5 Intermittent flow pattern

The one major factor that can be concluded from the intermittent flow pattern was that it was only observed for the positive inclination angles only, and only on the outlet from the test condenser. The flow pattern depended heavily on quality where by it was common at low qualities of 0.25 and was non-existent at high qualities of 0.75 despite the mass flux. As quality increased, the flow pattern depended mainly on the temperature difference only spotted at higher temperature differences of 8°C and 10°C. However, at lower mass fluxes it was observed at a temperature difference of 3°C and quality 0.5. At low qualities, intermittent flow pattern was mainly not depended on the inclination angle. The gravity effect that aided the flow by suppressing it to the bottom as the liquid condensate moved along the tube for the negative inclination angles acted on the opposite, opposing the flow for the positive inclination hence giving rise to liquid slugs.

H.1.6 Wavy flow pattern

Wavy flow pattern resulted from the transition from stratified-wavy or stratified flow pattern. It was observed on both the inlet and outlet of the test section but much more pronounced on the inlet at low qualities and diminishing as quality increased. This was due to the high vapour flow rate on the inlet to the test section. Just like intermittent flow pattern, wavy flow pattern was only observed for positive inclination angles only.

H.1.7 Churn flow pattern

A Churn flow pattern was confined to the +90° inclination angle and mainly at low qualities. The flow pattern was dependent on quality and mass flux. The flow pattern was evident when quality increased and mass flux decreased on the outlet from the test condenser. However on the inlet to the test condenser, churn flow pattern was common at low qualities increasing with decrease in the mass flux. At higher qualities on the other hand, due to the much increase in vapour flow rate, wavy-annular was dominant.

H.1.8 Wavy-churn flow pattern

Wavy-churn flow pattern was prevalent for both the inlet and the outlet of the test condenser. The flow would transition from wavy flow or stratified-wavy flow to wavy-churn flow pattern as the vapour-liquid mixture condenses along the tube.

H.2 Summary- Mass flux of 100 kg/m².s

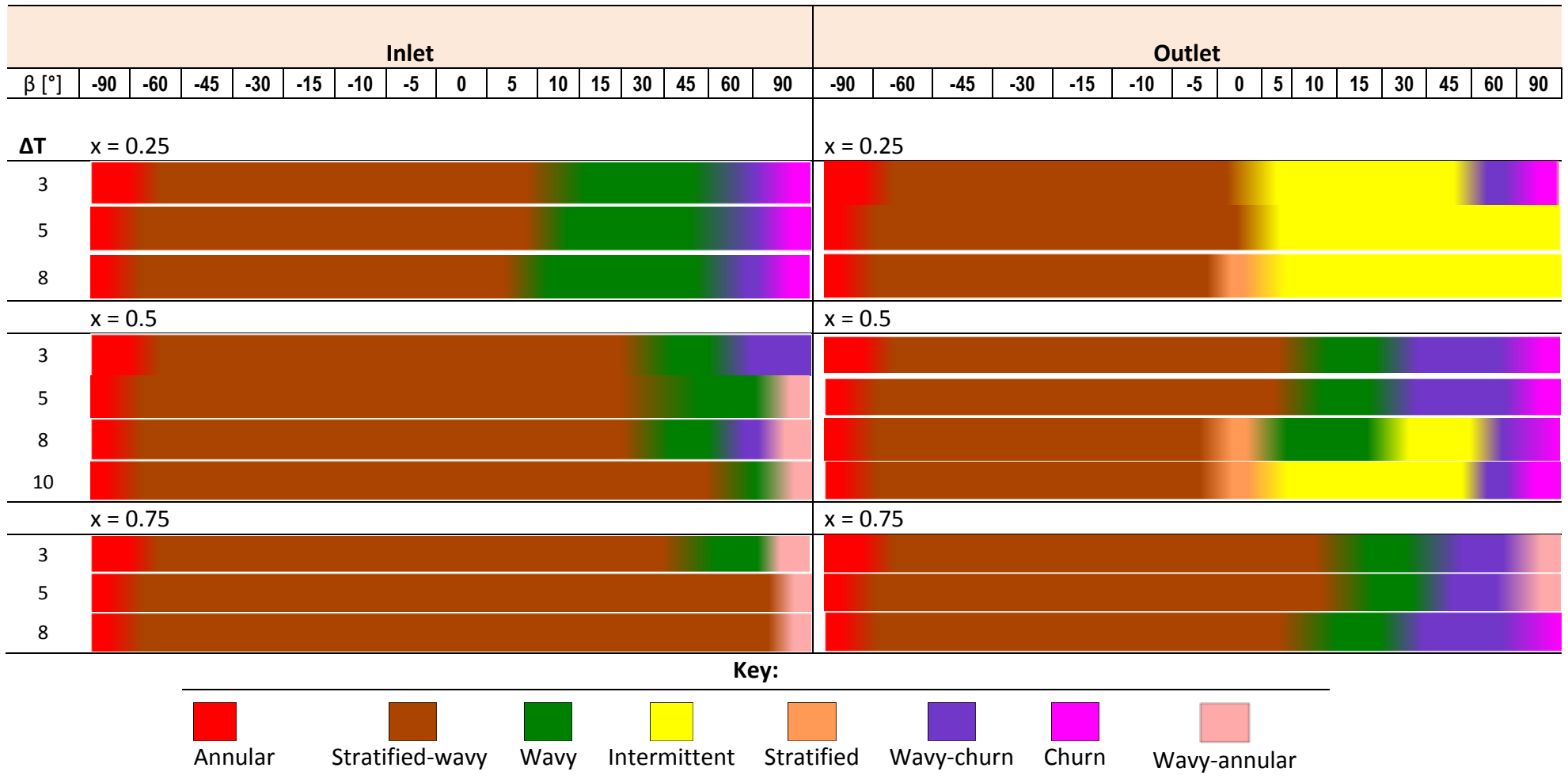


Figure H.1: Summary of flow patterns for a mass flux of 100 kg/m².s

H.3 Summary- Mass flux of 75 kg/m².s

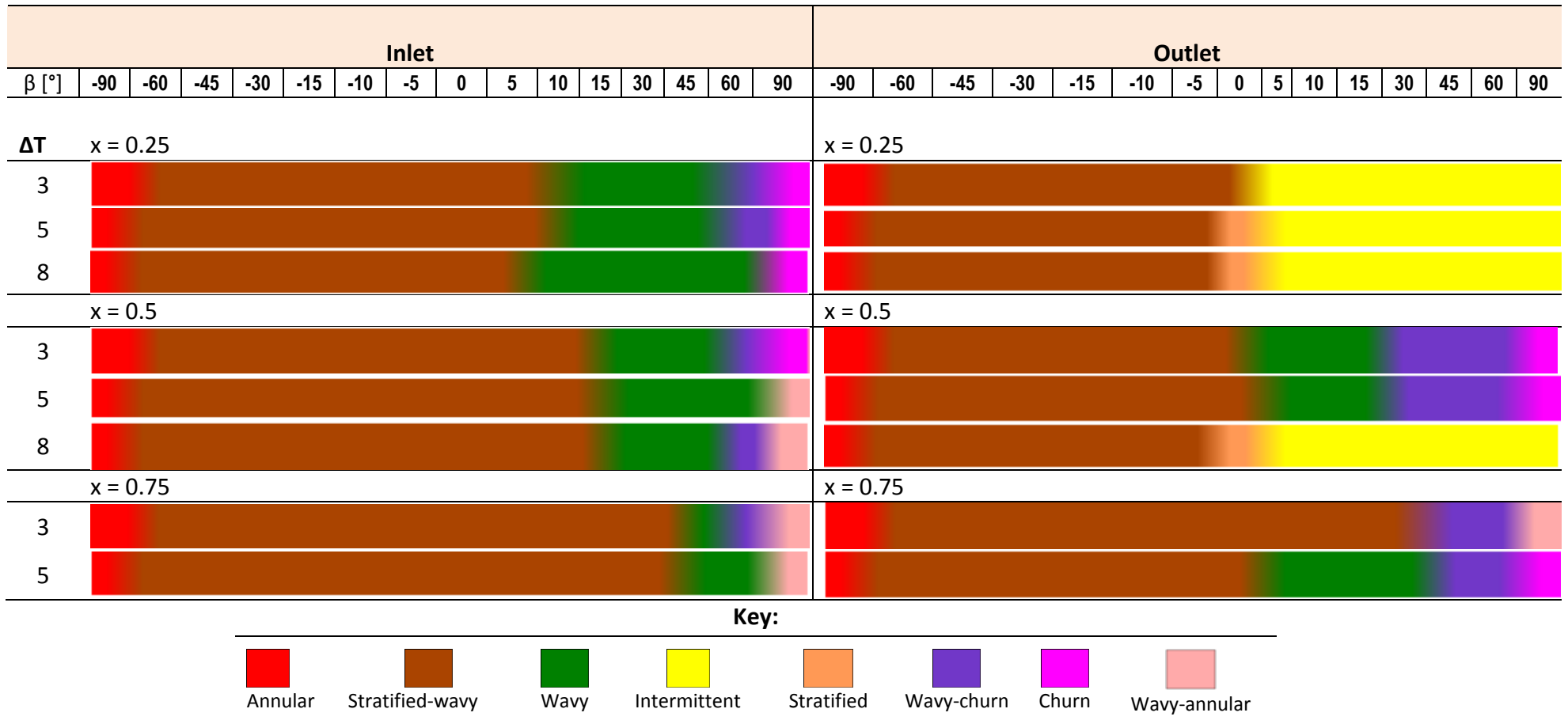


Figure H.2: Summary of flow patterns for a mass flux of 75 kg/m².s

H.4 Summary- Mass flux of 50 kg/m².s

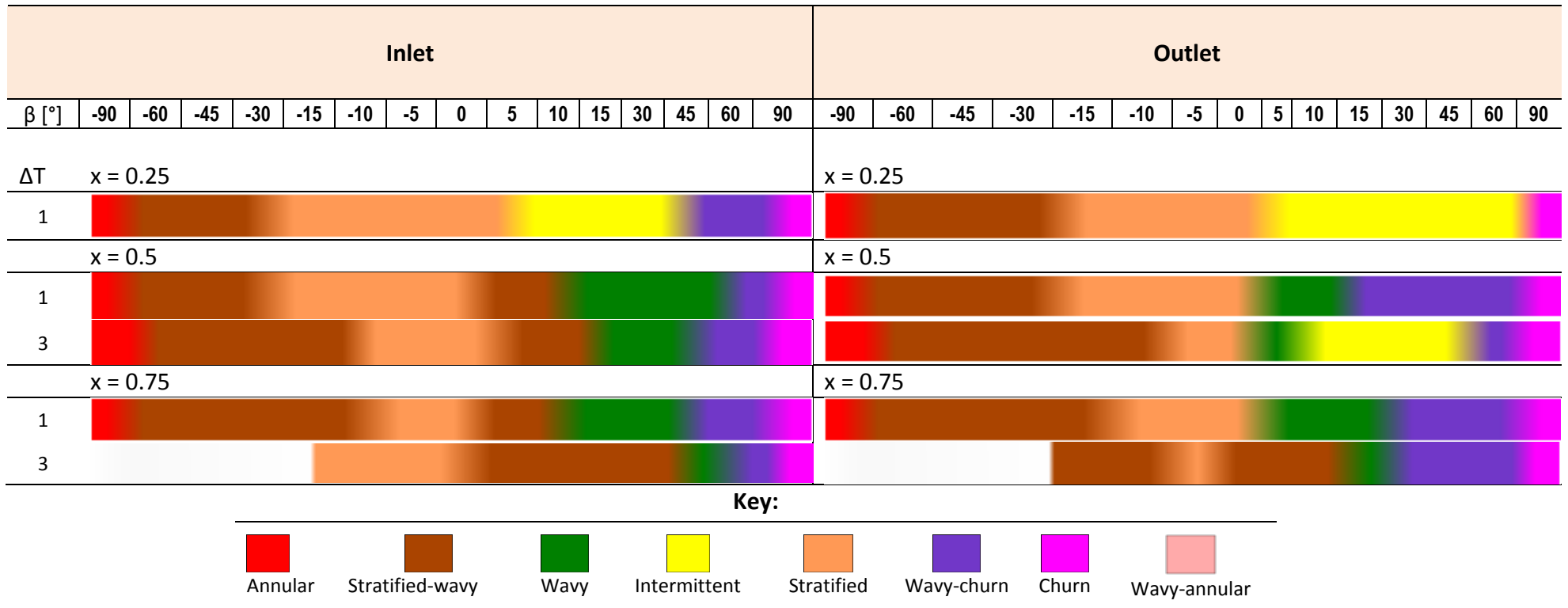


Figure H.3: Summary of flow patterns for a mass flux of 50 kg/m².s

H.5 Summary- Mass flux of 25 kg/m².s

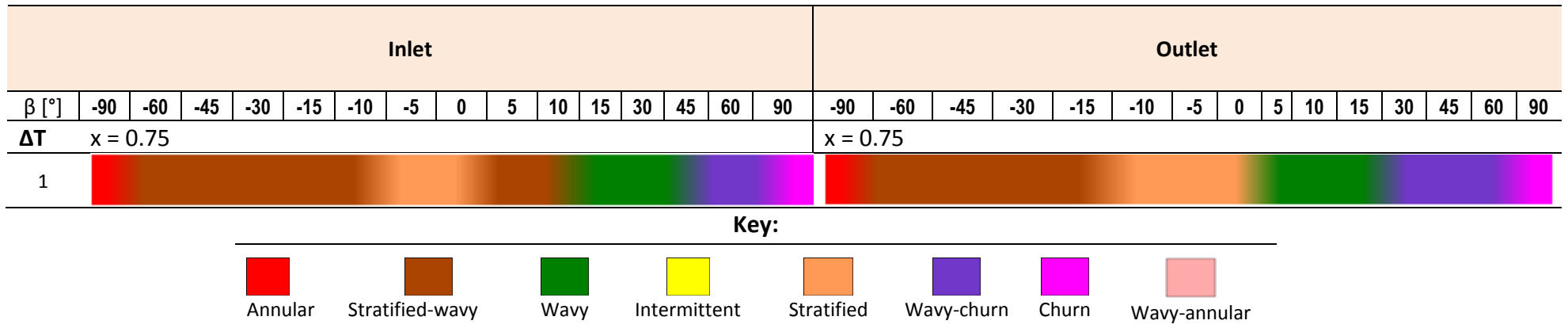


Figure H.4: Summary of flow patterns for a mass flux of 25 kg/m².s